THÈSE DE DOCTORAT

Etude multi-échelle de films minces photomécaniques basés sur l'assemblage supramoléculaire de photochromes bistables et d'élastomère thermoplastique

Présentée et soutenue publiquement à

L'UNIVERSITE DE LILLE

École doctorale Sciences de la matière, du rayonnement et de l'environnement

Pour obtenir le grade de

Docteur

Par

Maroua LOUATI

Soutenue le 07 Novembre 2019 devant la Commission d'Examen composée de :

Dr. Rémi METIVIER	ENS Paris-Saclay	Président du jury
Pr. Dominique HOURDET	ESPCI Paris	Rapporteur
Pr. Eléna ISHOW	Université de Nantes	Rapporteur
Pr. Michinori TAKESHITA	Université de Saga	Examinateur
Dr. Stéphane ALOISE	Université de Lille	Directeur de thèse
Dr. Sophie BARRAU	Université de Lille	Co-Encadrante de thèse

PhD THESIS

Multiscale approach of photomechanical thin films based on the supramolecular assembly of bistable photoswitch and thermoplastic elastomer

PhD defended at

THE UNIVERSITY OF LILLE

Doctoral School for Materials, Radiation and Environmental Sciences

To obtain the grade of

Doctor

By

Maroua LOUATI

Defended the 7th of November, 2019 in front of the following dissertation committee :

Dr. Rémi METIVIER	ENS Paris-Saclay	Committee chair
Pr. Dominique HOURDET	ESPCI Paris	Referee
Pr. Eléna ISHOW	University of Nantes	Referee
Pr. Michinori TAKESHITA	University of Saga	Examiner
Dr. Stéphane ALOISE	University of Lille	Thesis supervisor
Dr. Sophie BARRAU	University of Lille	Thesis co-supervisor

Acknowledgements

This thesis becomes a reality thanks to the support, help and encouragements of many people. I would like to extend my sincere thanks to all of them here.

All above, the present work within this manuscript has been carried out in both laboratories: UMET (CNRS UMR-8207) headed by Pr. Patrice Woisel in ISP team and LASIR (CNRS UMR-8516) headed by Dr. Hervé Vezin in PCS team. I would like to express my sincere gratitude to them for giving me the opportunity to join their laboratories and working on this innovative project.

Foremost, I would like to thank my supervisor Stéphane Aloise for his advices, patience, enthusiasm and motivation throughout this thesis, which helped the advancing of my thesis. Besides, this thesis would not have been possible without the help of my co-supervisor, Sophie Barrau. The support and friendship are invaluable on both academic and personal level. You believed in me and you taught me a lot, and for this, I will forever be grateful.

I would like to thank the rest of my thesis committee. I am very grateful to Dr. Rémi Métivier who accepted to chair the jury, Pr. Eléna Ishow, Pr. Dominique Hourdet and Pr. Michinori Takeshita who accepted to be part of the jury to bring their expertise as reviewers of this manuscript.

I would like to acknowledge my team in UMET: Jean-Marc Lefebvre, Valérie Gaucher, Tiana Deplancke, Gregory Stoclet, Corinne Binet, Jean-Francois Brun, Adeline Marin and Jean-Francois Tahon. Thank you Jean-Marc for your good suggestions, ideas and constructive remarks that helped me move forward. Valérie, your spontaneity and your sincerity have always made a good ambience during the group meetings. Thank you a lot for your insightful comments regarding my oral presentation preparation. Thank you Gregory, Corinne and Jean-Francois B. for your expertise and scientific knowledge shared every meeting. Tiana, your kindness and encouragements throughout the preparation of my oral presentation certainly helped me to express myself that is why I want to thank you. Adeline, you were present whenever needed. Your encouragements and smiles when we meet in UMET corridor mean a lot to me. Jean-Francois T., my preferred engineer!!. I really appreciate the time we spent in UMET. The sleepless nights we were working in Soleil and ESRF. Your advices and propositions to help whenever needed. Your support was unbeatable.

Furthermore, I would like to thank Ahmed Haddad for his good humor and our little daily teasing, Alexandre Fadel for the funny time spent, I will never forget that «Chez-tati-t'as-tout ♫» and Anne-Marie Blanchenet for support and small talks in UMET corridor and metro!. I am truly indebted to Alexandre Mussi for good time we spent and talk we had about research and zest of life «in office 107». You tried to listen to me when I needed to decompress. Thank you for giving me advices and encouragements throughout this thesis. I am most grateful to Benoit Hue for providing me any information or software, which have been always valuable for my advancing. Corinne Henry, you are the kindest secretary I have ever met. Moreover, it was a pleasure to interact with people always available to provide support and help as Frederic Cazaux, David Fournier, Nicolas Tabary, Jérémie Bouquerel and Joël Lyskawa.

In addition to this, special thanks goes out to LASIR and especially to Guy Buntinx and Vincent de Waele, who were always there to response or help me. I cannot also forget the day when, despite the fact that you were busy you tried to help me measuring the power of my Lamp. I would like to acknowledge Jérémy Gaillard for his expertise on absorption-spectroscopy technique. Furthermore, I would like to thanks Cécile Willems for her kindness whenever I go to her office for papers signature.

My sincere thanks also goes to Région Haut-de-France for offering me the internship fund opportunity «Bourse MERMOZ» leading me working and staying for some time in Japan. Without this help, this thesis would not have been the same. For that, I am really grateful.

Within this logic, I express my heartfelt thanks to Michinori Takeshita who welcomed me to his research laboratory in order to work with his team members in Saga University. I had the pleasure to stay in Japan. Their hospitality, kindness, help when needed and talk we had to tell me more about Japanese lifestyle will stay forever stuck in my memory. By the way, thank you Marumi Takao for all your syntheses efforts. Waiting see you again!

I would like to thank Rémi Métiver for the second time herein as collaborator, who welcomed me with open-arms in PPSM laboratory. He and Arnaud Brosseau were always ready to help me during my stay; without them, this thesis would not have been the same.

I would also like to thank Isabelle Morfin, our contact at the ESRF (D2AM beamline) for her welcome, her kindness, and her great availability including the weekend and during our experiments in March 2018.

My tutoring in IUT «Département mesures physiques» for two successive years surely enriched me. Mathieu Beaucamp, thank you for accepting and offering me the chance to work in your department. The pleasant moments, we had with Aude Bouchet and David Leroy, mean a lot to me.

I would like to thank everyone with whom I shared or share the office 210, the best office I had ever been. Pierre Marie, your enthusiasm, your dynamism and your kindness whenever needed will be memorable. Shanshan, thank you for the time-shared every day to discuss, to have your/my opinion in science, experience and lifestyle. By the way, I will never forget our trip to Amesterdam!. I will not forget your warm care, our teasing from time-to-time, it is you, Estelle!. Ah, the melted cheese was a good idea to try ;-). Cuong and Ahmad, even if your presence was not as frequent, but sharing your adventures, breaks were really appreciable. Sharing time after work was possible with the coming of Tommaso, Konstantinos, Jeffrey to our lab, which will be unforgettable even after ten years ;-)). Thank you for the easy-going atmosphere we shared in the lab or after work. Gabriel, whenever we meet, we tried to encourage each other and for this, I am really grateful.

When I arrived to the lab, Christopher, Audrey and Adélina, who already left two years ago, were my mentors when needed, for which I am grateful. Christopher, you were always there to help. The funny discussion breaks were unforgettable. Adélina, your presence was as important to me. You continued believing in me, supporting my choices, and providing advices within the difficult moments. Thank you for motivating me and for being more than a friend.

From the other hand, Quentin, I really appreciate your encouragements and whenever I came to LASIR and your support even when I printed my manuscript :-). Am sure you will do it in two years, fighting!!. Lucas, we shared funny time when talked about Alhambra and sharing your adventures. Thank you for inviting me to your housewarming party!

It was a pleasure to share moments with people from the lab who were available to share their experience and providing help. Thanks to their good humor, they made coming to the lab always a pleasure even during difficult periods!. I wish you all the best in the future.

Last but not least, I would not have come this far without the support, love and patience of my parents. Seeing in your eyes how much you are proud is the most reward that I can receive. My little brother, Marouane, you were always proud of me and for this am grateful. I also thank all the members of my family as my grandfather for always believing in me and my aunties Sarah and Nadia for allowing me to decompress when the need arose. Aunty Hayet, you followed my progress from time-to-time without hesitating encouraging and believing in me. Thank you all!

To conclude, Aymen, your presence by my side has always been precious. You have always supported my choices. You transmit usually vibes of love, energy and goodness when needed. My expression of thanks likewise does not suffice how much I will always be grateful.

Maroua Louati

Table of Content

ABBREVIATIONS XI

GENERAL INTRODUCTION 1

REFERENCES 7

CHAPTER I. FROM MONOCRYSTAL TO SUPRAMOLECULAR SELF-ASSEMBLY: AN OVERVIEW OF PHOTORESPONSIVE DTE BASED MATERIALS 9

I.1. INTRODUCTION ABOUT PHOTOCHROMISM 12
  I.1.1. General definitions 12
  I.1.2. Photochromic parameters. 12
  I.1.3. The different families of photochromes 13
  I.1.4. Photochromic dithienylethenes (DTEs) 15
I.2. PHOTOMECHANICAL EFFECT OF DTES CRYSTALS 17
  I.2.1. Preliminary findings: Crystal surface changes 17
  I.2.2. Photoinduced changes of crystal shape 18
    I.2.2.1. Contraction and expansion behaviors 19
    I.2.2.2. Bending behavior 20
    I.2.2.3. Jumping behavior 23
    I.2.2.4. Fragmentation behavior 24
I.3. PHOTORESPONSIVE COVALENT BONDED POLYMERS 25
  I.3.1. Introduction on polymers 25
  I.3.2. DTEs polymerization 26
I.4. SUPRAMOLECULAR ASSEMBLIES BASED ON UPY UNITS 28
  I.4.1. UPy units: presentation 28
  I.4.2. UPy telechelic supramolecular polymers 29
  I.4.3. UPy telechelic PEB 30
    I.4.3.1. Physical properties 30
    I.4.3.2. Thermal properties 31
    I.4.3.3. Structure and morphology 32
  I.4.4. The DTE-UPy supramolecular assembly 34
I.5. PHOTOMECHANICAL EFFECT OF DTE/THERMOPLASTIC ELASTOMER SYSTEM 35
REFERENCES 37

CHAPTER II. BASIC MATERIALS, SAMPLES PREPARATION AND CHARACTERIZATION TECHNIQUES.......45

II.1. MOLECULES SYNTHESIS PATHWAYS 47
II.1.1. DTE-UPy photoswitch 47
II.1.2. PEB-UPy thermoplastic elastomer 50
II.2. SAMPLE PREPARATIONS 51
II.2.1. DTE recrystallization.......51
II.2.2. DTE-UPy precipitation.......51
II.2.3. Thin film preparation.......52
II.2.3.1. PEB-UPy thin film.......52
II.2.3.2. PEB-UPy/DTE-UPy thin film.......53
II.3. CHARACTERIZATION METHODS.......55
II.3.1. Irradiation system 55
II.3.2. Photochromic properties.......56
II.3.3. Photomechanical measurements.......58
II.3.3.1. Macro-scaled measurements.......58
II.3.3.2. Micro-scaled measurements.......59
II.3.4. Chemical characterization 61
II.3.5. Thermal properties.......61
II.3.5.1. Thermogravimetric Analysis (TGA).......61
II.3.5.2. Differential Scanning Calorimetry (DSC) 62
II.3.6. Viscoelastic properties (DMA).......64
II.3.7. Structural properties 65
II.3.7.1. Wide angle X-ray scattering (WAXS).......65
II.3.7.2. Small angle X-ray scattering (SAXS).......67
II.3.7.3. Synchrotron radiation 68
II.3.8. Morphological observations 70
REFERENCES 71

CHAPTER III. NEW INSIGHTS TOWARD REVERSIBLE DYNAMIC MOTIONS OF DITHIENYLETHENE SUPRAMOLECULAR ASSEMBLY.......73

III.1. PHOTOCHROMISM OF DTE.......75
III.2. THERMAL ANALYSIS OF DTE.......77
III.3. STRUCTURAL PROPERTIES OF DTE MADE BY DIFFERENT PROCESS METHOD 79
III.3.1. DTE powder (noted DTE-pwd).......79
III.3.2. Recrystallized DTE (noted DTE-recrys) 80
III.3.3. Amorphous DTE (noted DTE-am).......81
III.4. PHOTORESPONSIVE DTE – JUMPING VS BENDING PHENOMENON 81
III.4.1. DTE powder 82
III.4.1.1. Presentation of the photomechanical effect 82
III.4.1.2. Under UV irradiation.......83
III.4.1.3. Visible irradiation and reversibility 86

III.4.1.4. Summary about DTE-pwd....87
III.4.2. Recrystallized DTE 87
III.4.2.1. Presentation for UV/Visible irradiation....88
III.4.2.2. Reversibility – UV/visible illumination cycles....89
III.4.2.3. Summary about DTE-recrys....91
III.4.3. Amorphous DTE 91
III.4.3.1. Under UV/visible irradiation....92
III.4.3.2. Bending behavior 93
III.4.3.3. Summary about DTE-am....94
III.4.4. Physical Interpretation of the Photo-Mechanical effect 94
III.4.4.1. Jumping of crystals....94
III.4.4.2. Bending of DTE crystals 96
III.4.4.3. Bending of amorphous DTE....97
III.4.5. CONCLUSION 97
REFERENCES 98

CHAPTER IV. PHOTOMECHANICAL EFFECT OF THE DTE-UPY SUPRAMOLECULAR SELF-ASSEMBLY 101

IV.1. PHOTOCHROMIC PROPERTIES OF DTE-UPY IN SOLUTION 105
IV.1.1. Absorption spectra 105
IV.1.2. Photochromic parameters 105
IV.1.2.1. Extinction coefficients....105
IV.1.2.2. Quantum yields 106
IV.2. EVIDENCE FOR DTE-UPY SUPRAMOLECULAR ASSEMBLY IN THE SOLID STATE 108
IV.3. DTE-UPY SUPRAMOLECULAR SYSTEM: THERMAL ANALYSIS 109
IV.3.1. Degradation kinetics.... 109
IV.3.2. Thermal transitions.... 110
IV.4. DTE-UPY SUPRAMOLECULAR SYSTEM: STRUCTURAL ANALYSIS.... 111
IV.4.1. Evidence for quadruple hydrogen bonds by WAXS 111
IV.4.2. Long range distances.... 111
IV.4.3. Light effect on structure 115
IV.4.4. Schematic representation of the structure.... 116
IV.5. PHOTOMECHANICAL EFFECT OF DTE-UPY SUPRAMOLECULAR SYSTEMS: PRESENTATION 118
IV.5.1. Small oligomers for DTE-UPypwd (OF) 118
IV.5.2. Large supramolecular assembly for DTE-UPy$_{prp}$ (CF) 120
IV.5.2.1. Aggregation Induced Emission upon visible light....120
IV.5.2.2. Photomechanical effect upon visible light....122
IV.5.2.3. Photomechanical effect upon UV light 123
IV.6. PHOTOMECHANICAL EFFECT OF DTE-UPY SUPRAMOLECULAR SYSTEMS: RATIONALIZATION 124
IV.7. CONCLUSION 125
REFERENCES 127

CHAPTER V. TELECHELIC UREIDOPYRIMIDONONE FUNCTIONALIZED THERMOPLASTIC ELASTOMER SUPRAMOLECULAR PROPERTIES 129

V.1. STRUCTURE AND MORPHOLOGY OF PEB 131
V.1.1. Chemical content analysis 131
V.1.2. Thermal behavior 132
V.1.2.1. Degradation of PEB 132
V.1.2.2. Thermal transitions 133
V.1.3. Mechanical relaxation of PEB 135
V.1.4. Crystal phase analysis of PEB 136
V.1.5. Morphology of PEB 138
V.1.6. Summary on PEB 140
V.2. STRUCTURE AND MORPHOLOGY OF PEB-UPY 141
V.2.1. Thermal behavior of PEB-UPy 141
V.2.1.1. Degradation kinetics 141
V.2.1.2. Thermal transitions 142
V.2.1.3. Crystallinity 143
V.2.2. Mechanical relaxation of PEB-UPy 144
V.2.3. Polymorphic crystalline structure of PEB-UPy 145
V.2.4. Morphology of PEB-UPy - correlation distances 146
V.2.4.1. Process impact 146
V.2.4.2. Temperature evolution 147
V.2.5. Summary on PEB-UPy 149
V.3. CONCLUSION 150
REFERENCES 152

CHAPTER VI. PHOTOMECHANICAL EFFECT: VARIOUS SUPRAMOLECULAR SYSTEMS (DTE-UPY, PEB-UPY) – FIRST EVIDENCES 155

VI.1. PHOTOMECHANICAL EFFECT AT MACROSCOPIC SCALE 158
VI.1.1. Photoinduced morphological changes 158
VI.1.1.1. DC-thin films 159
VI.1.1.1.1. DC-NR thin film 159
VI.1.1.1.2. DC-R thin film 162
VI.1.1.2. MM thin film 164
VI.1.1.3. Discussion about the macroscopic bending behavior 167
VI.1.2. Summary on macroscopic photo-induced changes 168
VI.2. PHOTOMECHANICAL EFFECT AT MICROSCOPIC SCALE 169
VI.2.1. DC-thin films 170
VI.2.1.1. DC-NR thin film 170
VI.2.1.2. DC-R thin film 174
VI.2.2. MM thin films 178
VI.2.3. Comprehensive mechanism to explain the microscopic bending behavior 183
VI.2.4. Summary on microscopic photo-induced changes 184

VI.3. CONCLUSION 185
REFERENCES 189

CHAPTER VII. PHOTOMECHANICAL EFFECT: STRUCTURAL AND MORPHOLOGICAL RELEVANT PARAMETERS 191

VII.1. STRUCTURE OF DTE-UPY/PEB-UPY THIN FILMS 194
VII.1.1. Thermal behavior 194
VII.1.2. Crystal phase analysis 196
VII.1.3. Arrangements of DTE-UPy/PEB-UPy self-assemblies 197
VII.1.3.1. Signature of DTE-UPy 197
VII.1.3.2. Molecular arrangements of assemblies at room temperature 199
VII.1.3.3. Molecular arrangements of UPy-Assemblies upon heating 200
VII.1.3.4.1. DC-NR thin films (OF) 201
VII.1.3.4.2. DC-NR thin film (CF) 203
VII.1.3.4.3. DC-R thin film (CF) 204
VII.1.3.4.4. MM-NR thin films (CF) 206
VII.1.3.4.5. Structure discussion 207
VII.2. SURFACE TOPOGRAPHY OF THIN FILM SUPRAMOLECULAR POLYMERS 209
VII.2.1. Process effect on self-assemblies 209
VII.2.1.1. First insights about surface morphology 209
VII.2.1.2. Surface analysis 210
VII.2.1.2.1. MM-NR thin film (OF) surface topography 211
VII.2.1.2.2. MM-NR thin film (CF) 212
VII.2.1.2.3. DC-NR thin film (OF) surface topography 213
VII.2.1.2.4. DC-NR thin film (CF) 214
VII.2.1.2.5. DC-R thin film (CF) 215
VII.2.1.2.6. Summary about morphology 216
VII.2.2. Morphology discussion 218
VII.3. FIRST INSIGHT TO EXPLAIN PHOTOMECHANICAL EFFECT 219
VII.3.1. Effect of light on structure 219
VII.3.2. Correlation morphology/structure with photoactuation 220
VII.3.2.1. Importance of DTE-UPy domains 220
VII.3.2.2. Importance of long period (Lp) 222
VII.4. CONCLUSION 223

GENERAL CONCLUSION 225

APPENDICES I

Abbreviations

Azo	Azobenzene
AZOs	Azobenzenes
CF	Closed Form
DAEs	diarylethenes
DC-NR	Drop casting thin film without reflux
DC-R	Drop casting thin film with reflux
DMA	Dynamic mechanical analysis
DSC	Differential Scanning Calorimetry
DTE or DTEcore	1,2-bis(2,4-dimethyl-5-phenyl-3 thienyl) perfluorocyclopentane
DTE-1	1,2-bis(2-ethyl-5-phenyl-3-thienyl) perfluorocyclopentene
DTE-2	1,2-bis(5-methyl-2-phenyl-4-thiazolyl) perfluorocyclopentene
DTEam	Amorphous DTE
DTEpwd	Commercially available DTE raw powder
DTErecrys	Recrystallized DTE raw powder
DTEs	Dithienylethenes
DTE-UPy	1,2-bis(2,4-dimethyl-5-phenyl-3 thienyl) perfluorocyclopentane functionalized UPy
DTE-UPy$_{prp}$	Precipitate of DTE-UPy high aggregation
DTE-UPy$_{pwd}$	Raw powder of DTE-UPy small oligomers
LC	liquid-crystalline polymers
LCE	Liquid crystal elastomer
MM-NR	Melt molded thin film without reflux
NMR	Nuclear Magnetic Resonance
OF	Open Form
PDLLA	non-crystallizable PLA
PDMS	Polydimethylsiloxane polymer
PEB	poly(ethylene-butylenes) diol

PEB-T-UPy	Telechelic poly(ethylene-butylenes) functionalized UPy and urethane motifs (T)
PEB-UPy	Telechelic poly(ethylene-butylenes) functionalized UPy
PEB-U-UPy	Telechelic poly(ethylene-butylenes) functionalized UPy and urea motifs (U)
PEP	poly(ethylene-co-propylene) diol
PLA	poly(lactic acid)
PLLA	crystallizable PLA
PMMA	poly(methyl methacrylate)
PSS	Photo Stationary State
SAXS	Small angle X-ray scattering
SEM	Scanning electron microscopy
Tg	Glass transition temperature
TGA	Thermogravimetric Analysis
Tm	Melting temperature
TPEs	Thermoplastic elastomers
UPy	2-ureido-4[1H]-pyrimidinone
WAXS	Wide angle X-ray scattering

General Introduction

Smart Organic Actuators. Nowadays, actuation materials that effectively convert external controllable stimuli into mechanical energy are of particularly interest in the fields of soft robotics [1], biomedicine [2], biomimetic systems [3], and molecular machines [4]. Different kinds of actuations were reported involving twisting, bending, swimming, and elongation/contraction [5] stimulated by external physical or chemical stimuli (for example heat [6], electricity [7], magnetism [8], humidity [9], or light [10]). Among all those recent innovations, photoactuators are particularly attractive for energy conversion, as they can be triggered externally in a non-invasive, non-contact manner for practical applications [11]. Two main types of photoactuators can be distinguished: (i) systems based on photothermal effects [12] or (ii) incorporating a molecular photoswitch [13]. The actuation mechanism for photoinduced motion is well established for photoresponsive molecules, including anthracene [14], schiff-bases [15], diarylethene [16] and azobenzene [17], which undergoes reversible shape deformations upon photoirradiation. Because of very distinct actuation mechanism (photothermal effect will be ignored in this manuscript), photoactuators incorporating an organic photoswitch deserves to be focus on.

Azobenzene/LCE materials. Azobenzenes are photochromic molecules in which the light induced switch based on trans-cis isomerization. Driven actuators, most of them host azobenzene derivatives (AZOs) as light responsive units [18]. In order to reach good mechanical flexibility, Finkelmann et al. have elaborated a monodomain nematic elastomer by crosslinking an azobenzene-substituted polymer into a liquid crystal state (LC). Upon irradiation, this system reveals photoinduced expansion/contraction behaviors [19, 20]. Further improvement was obtained by Ikeda group through the synthesis of polydomain LCE (liquid crystal elastomer) for which both thermal polymerization LC monomer and crosslinker are associated to azobenzene derivatives [21].

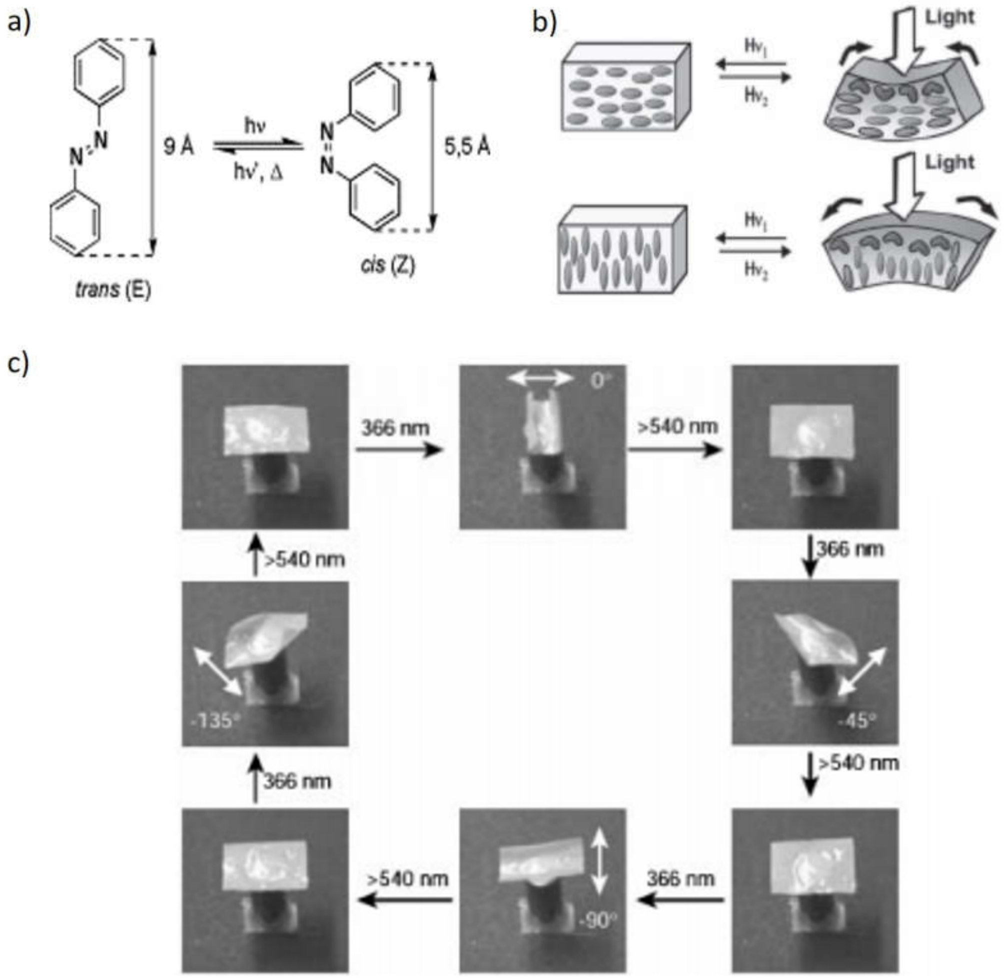

Figure 0-1: a) Cis-trans isomerization photochromism of azobenzene. b) Photomechanical effect in LCEs: the homogenous alignment of LCs produces bending towards the actinic light, whereas the homeotropic alignment of LCs causes bending away from the light source [22]. c) Control of the bending direction of a azobenzene with LCs film by linearly polarized light [23].

Since then, extensive number of photoactuators based on AZO/LCE systems were published with different kind of photoactuators (plastic motor, oscillator) [24, 25]. The hegemonic use of azobenzene derivatives is due to the large geometrical change caused by its photoisomerization (Figure 0-1a), inducing a LC-isotropic phase transition at the origin of the macroscopic film bending. Even in the absence of such LC phase transition, weak changes of AZOs (1% of AZOs molar fraction is sufficient) can allow photomodulating photoinert mesogens via inherent molecular cooperative motion effects. Macroscopically (Figure 0-1b), the light penetrates at first the LC film surface inducing an efficient gradient of isomerization along the film thickness. As result, the film bends toward or away from the incident light depending on the initial - homogenous or homeotropic - LC alignment. In Figure 0-1c, the film bending direction was controlled via lineary polarized light. As response to different angles of polarization, different bending directions were reported upon UV and visible lights. However, two major inconveniences still arise for azobenzene-based actuators: i) the response of these systems is relatively slow; ii) the deformed states are thermally unstable because the cis isomer relaxes spontaneously to the trans-isomer. A decisive step in view of applications is thus the use of true bistable photochromic systems.

Photoactuators using Dithienylethene. In this framework, dithienylethenes (DTEs), which are known to be thermally bi-stable photoswitches, constitute promising actuator candidates. Indeed, Irie et al. have shown few years ago that the photocyclization reaction of the DTE derivative induces a 7% volume contraction of the monocrystal, the latter being reversible using visible light, which could be used as a potential photomechanical effect [26-28]. However, in view of application, this effect observable for a single monocrystal would probably be lost if the diarylethene molecule is surrounded by a polymeric film. Another key issue when dealing with photomechanical effect is related to the capacity of the material to sustain reversible deformation from the molecular scale up to the macroscopic scale. This implies a careful monitoring of intermolecular interactions and more specifically of the photoactive units organization in order to achieve their cooperative response. Combining DAEs with a flexible thermoplastic elastomer would be a perfect alternative to DAEs monocrystals.

Prof. TAKESHITA System. In order to bring flexibility to a DTE based device, professor Takeshita (Saga University) has elaborated few years ago a new system combining a DTE and a thermoplastic elastomer through non-covalent supramolecular approach. The main idea was to take advantage of an efficient recognition units based on quadruple hydrogen bonds through a well-known ureidopyrimidinone units (UPy) reported by professor Meijer (Eindhoven University) in 2000. Together with the DTE, its leads to structural difference between the flexible open form (OF) and the rigid close form (CF) [29]. To obtain a photoactuator, the procedure was based on combining in chloroform a functionalized DTE (noted DTE-UPy) with an UPy-functionalized poly(ethylene-1,2-butylene) thermoplastic elastomer [30] (noted noted PEB-UPy) as illustrated in Figure 0-2a. The DTE in its closed form (blue solution), large supramolecular assemblies occur: UPy-DTE-UPy-UPy-PEB-UPy-…-UPy-PEB-UPy-UPy-DTE-UPy.

After spin-coating process, an 80 µm thin film was obtained and illuminated by either UV (CF film) or Visible (OF film) lights. Upon visible irradiation, the initially bent blue film (CF) is instantaneously flattened and as long as light penetrates into the material (inducing a CF/OF gradient), slow bending back motion is observed as shown on Figure 0-2b and on youtube video https://www.youtube.com/watch?v=IVrt9k7rLOQ. Upon UV irradiation, only moderate flattening is reported for the case of transparent film (OF) as illustrated in

Figure 0-2b (video not shown). Note that photo-thermal effect cannot be responsible for such observations because mechano-active behaviour were reported for the film immersed in water.

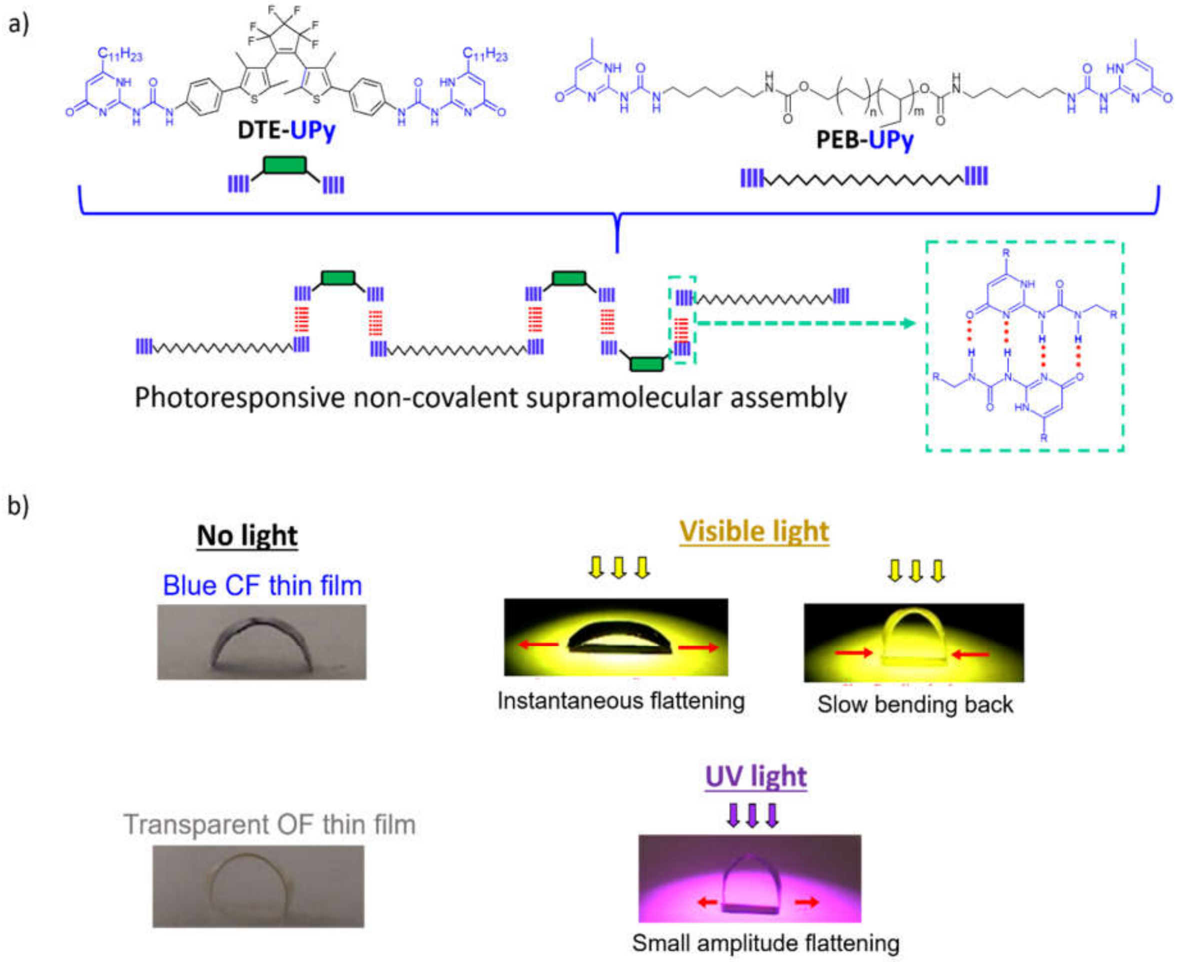

Figure 0-2: DTE-UPy/PEB-UPy supramolecular approach. a) DTE-UPy and PEB-UPy molecules and issued photoresponsive non-covalent self-assembly via quadruple hydrogen bonds. b) Photomechanical effects of thin film (film size: 1.5 cm×0.3 cm×80 μm) elaborated with spin coating under visible (blue film) and UV (transparent film) lights.

The main objective of this PhD thesis is thus to not only rationalize the described photomechanical effect (Figure 0-2) for DTE-UPy/PEB-UPy system reported by professor Takeshita but exploring new elaboration process distinct from the matter consuming spin-coating routes. Furthermore, in the case of visible irradiation, two steps movements occurred (initial flattening and then bending back motion) which is not a straightforward phenomenon. Rationalizing the various photomechanical effects in either Vis or UV excitation, from microscopic to macroscopic scale, is a very difficult task knowing that the supramolecular interactions of DTE-UPy/PEB-UPy system are propagated into the entire thin film (in contrast, AZO/LCE systems get a sandwich structure).

To reach some rationalization, we have decided to focus our attention on structural and morphological features responsible (or not) for the photomechanical effects. In particular, we have decided to answer the following questions: Is the choice of the photochromic core (without UPy) a good one? Is the DTE-UPy compound already a photoactive material? Among all structural parameters, is the crystallinity of either DTE-UPy or PEB-UPy a prerequisite for photoactuations? Can the thin elaboration process influence the photomechanical effect? Will microscopic and macroscopic investigation lead to exactly the same photoinduced motions? If photomechanical effect exists, which are the relevant parameters responsible of such photoactuations?

To answer those questions, the strategy was to undertake morphological/structural study to individual component (or precursors) of the thin films, i.e. PEB, PEB-UPy, DTE, DTE-UPy through DSC, TGA, WAXS, SAXS, SEM and DMTA. Then, different thin films PEB-UPy/DTE-UPy were prepared and photomechanical effects were explored (if any) at microscopic and macroscopic scales.

This manuscript is organized into seven chapters.

Chapter I gives an overview concerning DTE based photoactuators from monocrystals to recent DTE/LCE system. As an evidence, fundamentals about photochromism, polymers and UPy supramolecular systems will be gathered in this chapter.

Chapter II is devoted to describe materials and methods. The first part deals with the synthesis of DTE-UPy and PEB-UPy. Then, samples preparations (second part) including thin film elaboration protocols were detailed. In order to exhibit photocontrollable characteristics that could extend the field of the materials science applications with simple, economic and tunable process, two different elaboration methods are applied: drop cast (DC) and melt molding (MM) thin films. Furthermore, the third part is dedicated to investigate methods in relationships with photochemical, thermal, structural properties, morphological observations and the multi-scale photomechanical measurements.

Chapter III is dedicated to explore the photomechanical potentiality of the nude photochromic core (before UPy functionalization) noted DTE. Through applying different ways of elaborations, properties including photoinduced motions upon UV/visible illuminations have been investigated.

Chapter IV is a thoughtful structural and morphological study of DTE-UPy with a comparison with the previous chapter (influence of specific UPy motifs on DTE_{core}). The question of the (non) crystallinity of DTE-UPy is of prime importance. The photochromic properties of DTE-UPy (in solution) will be reviewed as well remaining the supramolecular activities different for the OF and CF. In solid state and for distinct morphological samples (powder from synthesis, crystals, dried precipitate…), a particular attention has been paid to reveal UPy signature through the supramolecular assembly of DTE-UPy and their direct effect on the investigated photoinduced motions.

Chapter V is dedicated to structural/morphological and rheological properties of PEB-UPy thermoplastic elastomer. The main chapter is based on two parts. The first part deals with the polymeric matrix core before functionalization noted PEB. The second part describes the modifications exhibited through UPy-motifs on thermoplastic elastomer features in order to better rationalize the UPy-UPy connection through quadruple hydrogen bonds.

Chapter VI deals with the photomechanical characterization of DTE-UPy/PEB-UPy thin films (OF or CF) under illuminations UV or Visible irradiations. Distinct elaborations protocols were tested (drop-casting and melt molding) to assess the influence of the elaboration process on possible photoactuation. Furthermore, according to a multiscale approach including in-situ illumination, photomechanical effects were assessed at microscopic scale (wild-field microscope) and macroscopic scales (camera). Concurrently, the reversibility and relaxation behaviors were examined as well.

Chapter VII deals with the understanding of the existant photomechanical effects through combining structural propeties into morphological studies. Instructive comparison between the different thin films pave the way to a future control of the photomechanical effects. Furthermore, a first comprehensive approach is developed about reversible light-controlled systems linking molecular organization (microscopic) to the material itself (macroscopic).

To complete the manuscript, a general conclusion is drawn and proposals about future studies on the subject are given.

References

[1] Mingming, M., et al., Bio-Inspired Polymer Composite Actuator and Generator Driven by Water Gradients, Science 2013, 339, 186 – 189.

[2] Mendes, P.M., Stimuli-responsive surfaces for bio-applications. Chemical Society Reviews, 2008. 37(11): p. 2512-2529.

[3] Xiao, K., et al., A Biomimetic Multi-Stimuli-Response Ionic Gate Using a Hydroxypyrene Derivation-Functionalized Asymmetric Single Nanochannel. Advanced Materials, 2014. 26(38): p. 6560-6565.

[4] Daniela, R. and T.T. Michael, Design, fabrication and control of soft robots. Nature, 2015. 521(7553): p. 467.

[5] Jiawen, C., et al., Artificial muscle-like function from hierarchical supramolecular assembly of photoresponsive molecular motors. Nature Chemistry, 2017. 10(2): p. 132.

[6] William, A.P., Thermal-energy conversion: Under pressure. Nature Energy, 2016. 1(7).

[7] Cheng, C. and A.H.W. Ngan, Reversible electrochemical actuation of metallic nanohoneycombs induced by pseudocapacitive redox processes. ACS nano, 2015. 9(4): p. 3984.

[8] Islam, M.R., et al., Polymer-Based Muscle Expansion and Contraction. Angewandte Chemie International Edition, 2013. 52(39): p. 10330-10333.

[9] Hu, Y., et al., Photoactuators for Direct Optical-to-Mechanical Energy Conversion: From Nanocomponent Assembly to Macroscopic Deformation. Advanced Materials, 2016. 28(47): p. 10548-10556.

[10] Deng, J., et al., Tunable Photothermal Actuators Based on a Pre-programmed Aligned Nanostructure. Journal of the American Chemical Society, 2016. 138(1): p. 225.

[11] Han, D.-D., et al., Light-Mediated Manufacture and Manipulation of Actuators. Advanced Materials, 2016. 28(38): p. 8328-8343.

[12] Kumazaki, H., S. Inaba, and K. Hane, Pressure Sensor Using Photothermal Vibration of Optical Fiber Core. SHINKU, 1995. 38(3): p. 176-178.

[13] Pianowski, Z.L., Recent Implementations of Molecular Photoswitches into Smart Materials and Biological Systems. Chemistry - A European Journal, 2019. 25(20): p. 5128-5144.

[14] Tong, F., et al., Photomechanical motion of diarylethene molecular crystal nanowires. Nanoscale, 2018. 10(7): p. 3393-3398.

[15] Kumar, K., et al., A chaotic self-oscillating sunlight driven polymer actuator. Nature Communications, 2016. 7: p. urn:issn:2041-1723.

[16] Medishetty, R., et al., Photosalient Behavior of Photoreactive Crystals. Chemistry of Materials, 2015. 27(5): p. 1821-1829.

[17] Uchida, E., R. Azumi, and Y. Norikane, Light-induced crawling of crystals on a glass surface. Nature Communications, 2015. 6(1): p. 7310.

[18] Agolini, F. and F.P. Gay, Synthesis and Properties of Azoaromatic Polymers. Macromolecules, 1970. 3(3): p. 349-351.

[19] Finkelmann, H., et al., A New Opto-Mechanical Effect in Solids. Physical Review Letters, 2001. 87(1).

[20] Sanchez-Ferrer, A., A. Merekalov, and H. Finkelmann, Opto-mechanical effect in photoactive nematic side-chain liquid-crystalline elastomers. Macromolecular Rapid Communications, 2011. 32(8): p. 671.

[21] Yanlei, Y., et al., Photomechanics: Directed bending of a polymer film by light. Nature, 2003. 425(6954): p. 145.

[22] Yamada, M., et al., Photomobile polymer materials: Towards light-driven Plastic motors. Angewandte Chemie - International Edition, 2008. 47(27): p.4986-4988.

[23] Barrett, C. J., et al., Photomechanical effects in azobenzene-containing soft materials. Soft Matter, 2007, 3, 1249-1261.

[24] Yu, H., et al., Dancing with Light: Advances in Photofunctional Liquid-Crystalline Materials; Jenny Stanford Publishing, 2015

[25] Zhao, Y.; Ikeda, T. Smart Light-Responsive Materials: Azobenzene-Containing Polymers and Liquid Crystals; Wiley, 2009

[26] Irie, M., Photochromism of diarylethene molecules and crystals. Proceedings of the Japan Academy. Series B, Physical and biological sciences, 2010. 86(5): p. 472.

[27] Irie, M., et al., Reversible surface morphology changes of a photochromic diarylethene single crystal by photoirradiation. Science, 2001, 291(5509), 1769-72.

[28] Seiya, K., et al., Rapid and reversible shape changes of molecular crystals on photoirradiation. Nature, 2007. 446(7137): p. 778.

[29] Takeshita, M., et al., Photoreversible supramolecular polymer formation. Chemical Communications, 2005(6): p. 761-763.

[30] Folmer, B.J.B., et al., Supramolecular Polymer Materials: Chain Extension of Telechelic Polymers Using a Reactive Hydrogen-Bonding Synthon. Advanced Materials, 2000. 12(12): p. 874-878.

Chapter I.

From monocrystal to supramolecular self-assembly: an overview of photoresponsive DTE based materials

Within the large frameworks of the organic smart materials, [1,2] the general scope of the present manuscript deals with photomechanical materials or organic photoactuators based on the following definition: photomechanical effect represents the change in the shape of a material when exposed to light. Over the time, several types of physical mechanisms were reported as being able to generate a significant photomechanical effect: photothermal mechanism [4], mechanism of photostriction[1] [5] and mechanism of molecular reorientation in the presence of polarized light [6]. It is worth to precise that this manuscript will only concern photoactuators incorporating a molecular photoswitch. Indeed, the present bibliographic chapter deals with photomechanical effect induced by photochromic molecules themselves (monocrystals) or photochromic molecules combined with a polymer through covalent approach (a photochromic molecule being inside a polymeric sequence) or supramolecular approach (typically, a photochromic molecule and a polymer interacting to each-others through hydrogen bonding). However, it is worth to remind that since the discovery of professor Ikeda in 2007 (see introduction), there is an extensive literature dealing with neighboring azobenzene-LCE photoactuators [7, 8] for which light induced bending/flattening are explained by advanced mechanical models [9]. As an evidence, those kinds of systems (LCE-Azo-LCE) represent a special category of organic photoactuators that will not be fully detailed in this chapter (special reviews or books [7, 8]). Despite the impressive academic performances of azobenzene systems, a drawback will always affect such system: azobenzene photochromic molecules are not bistable in the sense they underwent a thermal back reaction with time when light is switch off (a bended photoactuators will return spontaneously at the initial flat position). As already evoked previously, a good alternative to azobenzene systems is based on combining an actual bistable photochromic molecules: the dithienylethenes (DTEs).

The present manuscript focuses on professeur Takeshita supramolecular photoactuator combining a dithienylethene (DTE) and thermoplastic elastomer (PEB) both functionalized by UPy motifs. As consequence, the present bibliographic chapter deals with neighboring systems through a special focus on DTEs. After the fundamental notions about photochromism, the general properties of DTEs will be emphasized and the photomechanical effect of DTEs monocrystals will be presented. In the following, introducing the basics concepts of supramolecular approach in polymer science through the special case of UPy supramolecular polymer developed by professor Meijer will be reviewed.

---

[1] Involves two phenomena: the photovoltaic effect, which transforms light energy into electrical energy, and the piezoelectric effect, which transforms light energy into mechanical energy.

I.1. Introduction about Photochromism

I.1.1. General definitions

Photochromism is defined as a photoinduced reversible transformation between two isomers A and B of a chemical species having different absorption spectra [10]. Generally, the photochromic reaction is characterized by a color change during the phototransformation between both states A and B. As shown in Figure I-1a, the thermodynamic stable form A (λ_A) can be transformed by irradiation to a less stable form B (λ_B) according to the forward reaction (denoted A → B). The reverse reaction, i.e. from isomer B to isomer A, is designed back reaction (denoted B → A) and can occur thermally and/or photochemically.

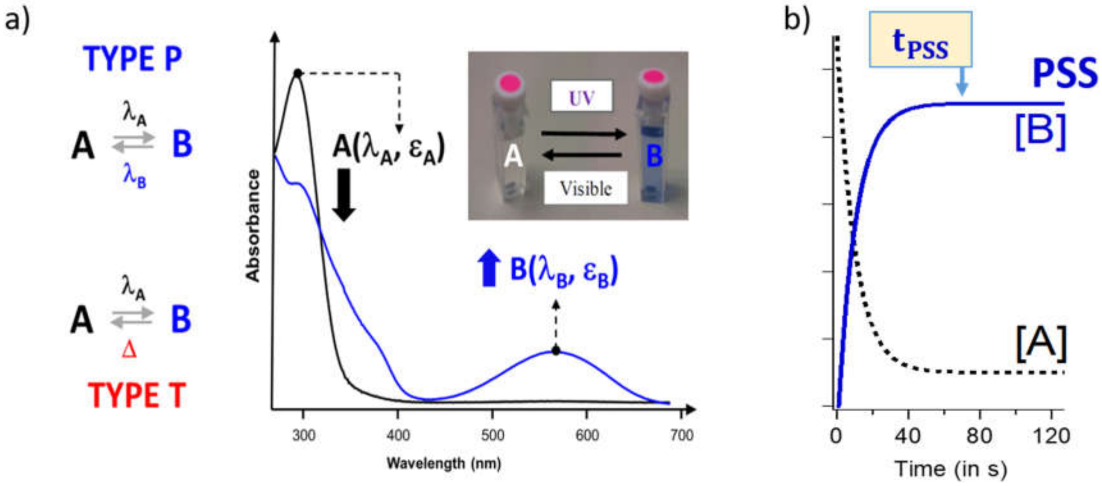

Figure I-1: a) Principle and definitions of photochromism: T- and P-type photochromic reactions and absorption spectra. b) Reached Photo-Stationary State (PSS).

Two types of photochromic materials can then be distinguished when light is switched off: (i) **T-type** for which the color of the isomer B does not persist and the compound returns thermally to its original color; (ii) **P-type** for which the color of isomer B persists and the return reaction B → A can only be achieved through exciting the isomer B in its absorption band (λ_B).

I.1.2. Photochromic parameters.

Photochemical parameters. To evidence the color change, the absorption spectroscopy is classically used in order to identify the spectroscopic parameters of A and B isomers including the wavelength of absorption maxima (λ_A and λ_B) and the absorption coefficients (ε_A and ε_B) as mentioned in Figure I-1a. Besides these classical photochemical parameters, it is substantial to evaluate the quantum yield of B formation after the excitation of A, $\phi_{A\rightarrow B}$ (or reverse process) according to the equations (I.1) and (I.2).

$$\phi_{A\rightarrow B} = \frac{number\ of\ B - formed\ molecules}{number\ of\ absorbed\ photons\ by\ A} \qquad (I.1)$$

$$\phi_{B\rightarrow A} = \frac{number\ of\ A - formed\ molecules}{number\ of\ absorbed\ photons\ by\ B} \qquad (I.2)$$

The experimental determination of quantum yields is detailed in Chapter II.

Photo-Stationary State. Both processes A→B and B→A can be induced with different quantum yields efficiency at the some excitation wavelength. After sufficient time of exposure into light, the converted molecules reach a state of thermodynamic equilibrium denoted Photo-Stationary State (denoted PSS). Through typically photoconversion kinetic of absorbance (Abs) as a function of time Abs_B= f(t), it is important to defined the time for which PSS is reached, t_{PSS}, as defined on Figure I-1b.

Fatigue resistance. In view of the achieved reversible photochromic transformations, secondary reactions may occur upon long exposure time into light and can be attributed to photodegradation phenomenon responsible for the progressive loss of photochromic properties. This loss of performance can be quantified through determining the number of illulination cycles, photoconversion - photoreversion reactions, that the material can undergo without significant photodegradation of isomer A.

I.1.3. The different families of photochromes

Different families of photochromic molecules can be classified according to the type of chemical reaction: proton transfer, homolytic cleveage, cycle opening reaction …etc. For further informations, it is possible to refer to journals [10] and books [11, 12] dedicated for photochromism. Concerning smart organic photoactuators, the most important families are azobenzenes (AZOs) and Diarylethenes (DAEs) compounds.

AZOs. The photochromism of AZOs is based on cis-trans isomerization around the N=N bond as illustrated in Figure I-2. The thermally stable trans-isomer is converted to cis-isomer via light irradiation. The reverse reaction is thermally spontaneous (T-type molecules) induced by light as well. One of the great advantages of AZOs is the large geometrical change between the isomers.

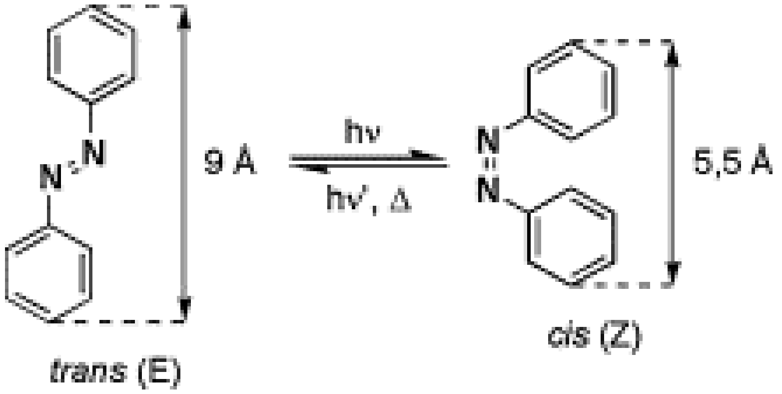

Figure I-2: Azobenzene photoisomerization.

Nowadays, azobenzene derivatives represent the most promising photochromic molecules widely used in polymers matrices, thin films, functionalized nanoparticles or liquid crystals [13-15]. The materials not only show a switching of the dichroism and birefringence properties but also matter displacements [16, 17].

DAEs. The photochromic properties of DAEs are based on pericyclic reaction [18]. Irie et al. report the photochromism of diarylethene in 1988 [19]. Since then, the study of these molecules has occurred a fast growing because of their improved performance.

First, the most stable isomer corresponds to open form isomer (OF). Under UV irradiation, the photochromic reaction consists on the ring-closing of OF according to the electro-cyclization reaction of a 1,3,5-hexatriene unit that involves 3 electron π-pairs and 6 atoms (red-colored bonds and atoms in Figure I-3) and is called photocyclization reaction. The photoinduced electronic rearrangement generates the closing of the ring. The resulting molecule is noted close form isomer (CF). The reverse ring-opening reaction, called photocycloreversion reaction, is carried out upon irradiation in the visible range in general. Unlike AZOs, diarylethenes are thermally bistable P-type photochromic molecules [20, 21]. The bistability of the two isomers makes these molecules interesting for various applications.

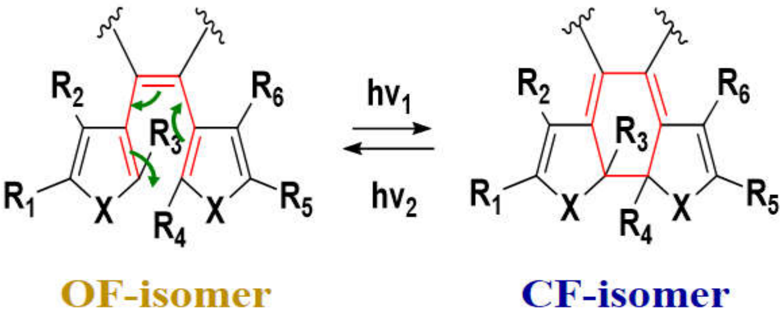

Figure I-3: Photoisomerization of diarylethenes (X=S: dithienylethenes).

I.1.4. Photochromic dithienylethenes (DTEs)

Among all the diarylethenes, dithienylethenes for which aryl nuclei are thiophene, are one of the most efficient bistable photochromic molecules with negligible thermal back reaction, good quantum yields, high fatigue resistance and rapid photochromic response [18, 22-23]. In general, the C=C is substituted with a perfluorocyclopentene bridge in order to prevent cis-trans isomerisation. The general mechanism for both cyclization and reversion have been reviewed recently by our groups [24, 25].

OF conformers properties. Generally, the dithienylethene OF isomer is thermodynamically more stable than the closed form. The initial colorless OF has an absorption band at shorter wavelength in the UV range as illustrated in Figure I-5 whereas no absorption band appears in the visible range. The OF exhibits two stable conformations as shown in Figure I-3 [53]:

- **Parallel conformer (P)** having a plane of symmetry with the aryl groups in mirror symmetry.
- **Antiparallel conformer (AP)** having a C2 symmetry axis where both aryl groups on either side of the central double bond plane.

In solution, the photoinactive P and the photoreactive AP conformers are in approximately equal amounts [19]. In solid state, when the DTEs is placed in a confined space, the AP proportion can be increased [27]. Whereas, the parallel conformation keeps unreactive regardless in solution or in solid state. By the way, when the DTEs molecules exist in pure AP conformation and the distance between the reactive carbons is less than 4.2 Å, the single-crystals can undergo a photochromic reaction with an efficient photocyclization quantum yield nearly a unit.

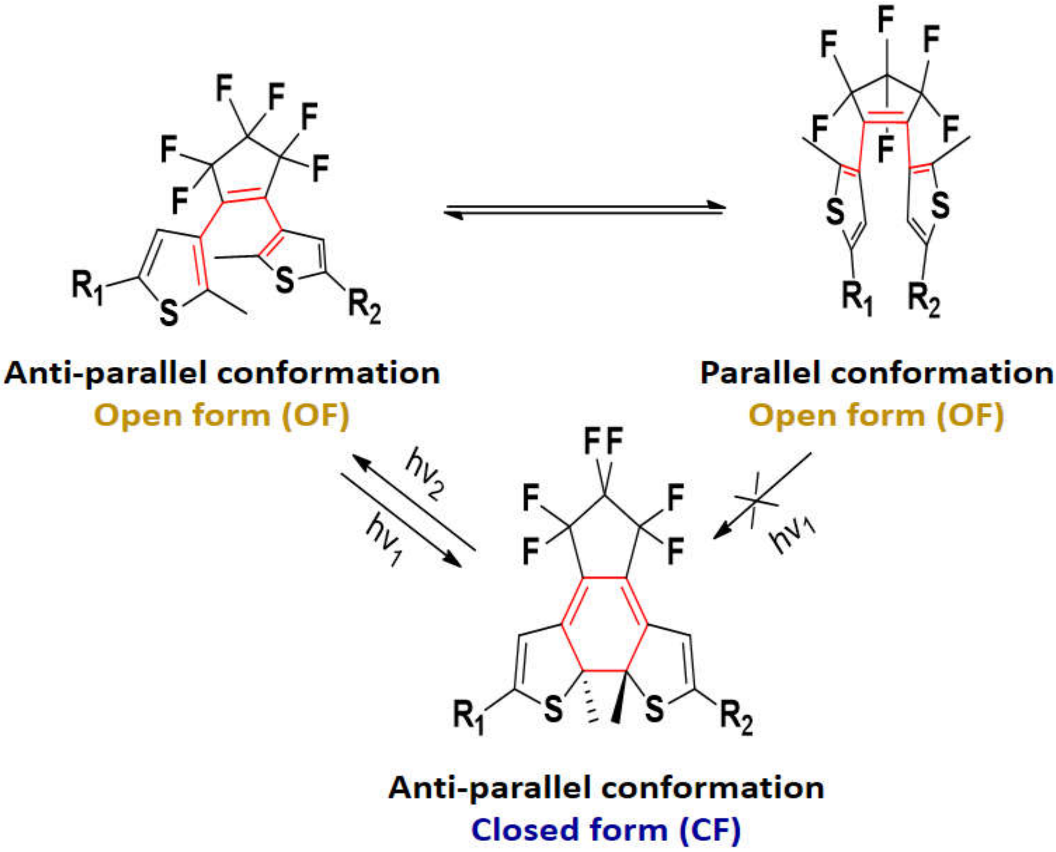

Figure I-4: Antiparallel and parallel conformations of the dithienylethene open and closed forms. [26]

CF conformer properties. Starting from OF isomer, its irradiation with UV light induces a color change due to the formation of CF isomer. This light induced reaction is observed not only in solution but also in solid state. Under irradiation, DTEs crystals can undergo to a photochromic reaction exhibiting multi-colored changes related to structural modification and conjugation evolution as illustrated in Figure I-5 [28]. Indeed, upon UV light irradiation, the colorless crystals change within the absorption visible range to yellow, purple, red, blue, or green, depending on the molecular structure of the DTEs. In darkness, these colors remain stable at room temperature. Upon exposure to visible light, the crystals recover the first colorless state recovery.

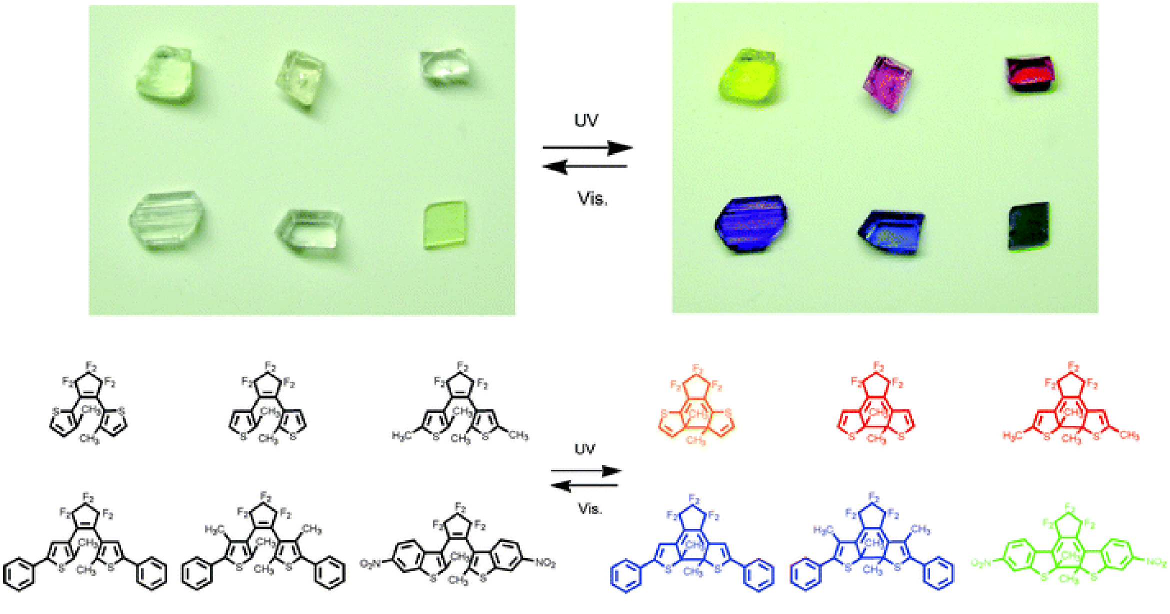

Figure I-5: Color changes of single-crystals of diarylethene derivatives upon irradiation. [28]

The coloration/decoloration cycles can be repeated more than 10^4 times without any noticeable destruction of the crystal shape [29].

I.2. Photomechanical effect of DTEs crystals

The photomechanical effects of photoresponsive molecules have attracted much attention because of their ability to convert energy light into mechanical work without applying any direct contact and electronic wires. Organic molecular crystals present a particular interest as they play a key role in nano- and micro- technological applications using photon energy to drive molecular displacements including miniaturization of gear-wheel rotation and molecular machines [30-32].

I.2.1. Preliminary findings: Crystal surface changes

Besides the typical color change, the light can induce surface morphological changes. Irie et al. reported morphology changes of 1,2-bis(2,4-dimethyl-5-phenyl-3 thienyl) perfluorocyclopentane (designed DTE) upon UV and visible irradiations as mentioned in Figure I-6 [33].

Upon UV light exposure, the crystal undergoes a color change from colorless into blue. To confirm the photoconversion, the crystal was partially irradiated and then observed from the top and side views. The photographs proved that the light penetrated the crystal bulk and border as shown in Figure I-6a.i and Figure I-6a.ii. The parallelepiped shaped crystal was obtained from the huge crystal via a razor blade (Figure I-6a.iii). The surface changes were then underlined via AFM measurements. Before irradiation, the crystal had a flatten surface (Figure I-6c). The UV light exposure induced two different surface features (Figure I-6d). From the (100) surface side, steps of 1 nm in height were noticed. From the (010) surface side, the appearance of valleys as deep as 10-50 nm range were observed. After subsequent irradiation with visible light, both surface features disappeared (Figure I-6e). The photoinduced changes were then reversible.

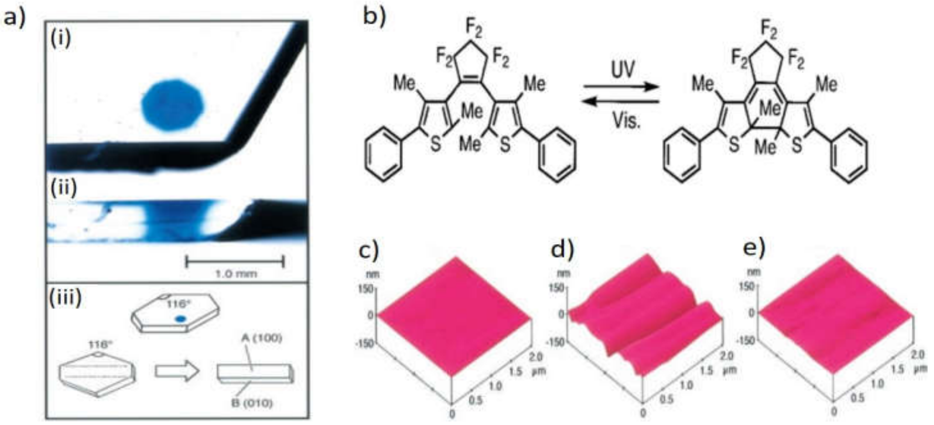

Figure I-6: Chemical structures and reversible surface morphological changes of DTE single-crystal; a) photographs of crystal (i-Top, ii-side views and iii-crystal shape); b) photochemical reaction of DTE; c) before irradiation, d) after UV irradiation and e) after visible irradiation. [64]

Under irradiation, the decrease of the distance between the two reactive carbons due to the cyclization reaction induces a shorter distance between the phenyl substituent. Thus, this implies the decrease of the whole molecule length. Therefore, in DTEs single-crystals where molecules are organized in successive layers, several nanometer changes occur within each layer from the crystal. The accumulation of these nanoscaled changes implies the morphological modifications of the surface at macroscopic scale.

I.2.2. Photoinduced changes of crystal shape

Various types of photomechanical motions in diarylethene crystals based on the geometrical change of the molecules were reported in literature. Generally, a crystal is defined as a highly ordered microscopic arrangement of molecules, forming a crystalline lattice that extends in all directions. The macroscopic crystal growth leads to identify the geometrical shape (length, width and thickness) of single crystal.

The mechanism of the photo-transformation reaction caused by the crystal high absorbance can be described through (i) the photoreaction of the surface and then (ii) its propagation in the crystal volume. As result, the crystal undergoes a photodeformation such as contraction, bending, fragmentation and/or jumping.

I.2.2.1. Contraction and expansion behaviors

Materials classically expand or contract if they are subjected to stimulus such as the temperature. Indeed, most of materials expand (increase in volume) when they are heated and contract (decrease in volume) when they are cooled. In the case of thermally stable molecules such as DAEs, light stimulus is also found to induce the deformation of the materials [34-36].

Figure I-7 illustrates the first reported examples of DTEs in literature that induce contraction-expansion phenomena [34]. Upon UV light, the photocyclization reaction of two DTEs single crystals leads the transformation from OF isomers into CF isomers. Thus, the materials color change from colorless into violet and blue, respectively. As consequence, each crystal exhibits a contraction behavior.

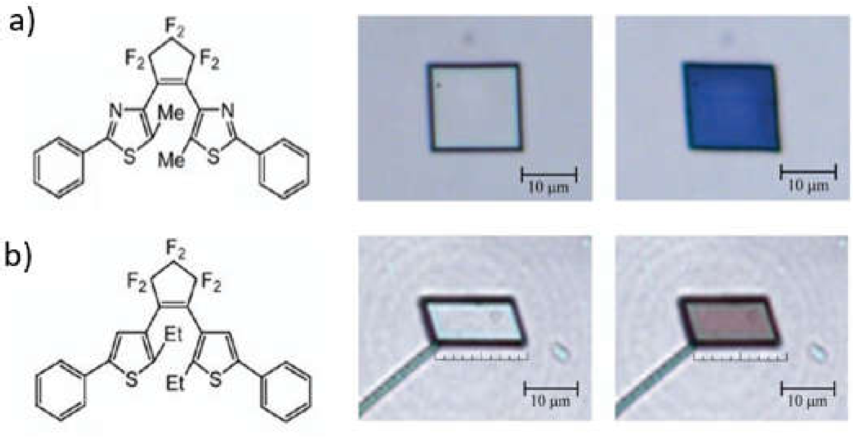

Figure I-7: Molecular DTEs structures with images illustrating the deformation of their single crystals upon UV light excitation. a) Reversible DTE-1 changes from square with corner angles of 88° and 92° to a lozenge shape with corner angles of 82° and 98°. b) Reversible DTE-2 contraction and expansion by as much as 7%. [34]

Indeed, the single crystal shaped lozenge of 1,2-bis(2-ethyl-5-phenyl-3-thienyl) perfluorocyclopentene noted DTE-1 changes its corner angles from 88° and 92° into 82° and 98° respectively, and hence its shape from a colorless square to a blue (Figure I-7a). The colorless rectangular plate-like crystal of 1,2-bis(5-methyl-2-phenyl-4-thiazolyl) perfluorocyclopentene noted DTE-2 contracts upon UV irradiation. The long axis length in the crystal decreases by about 5–7 % within its violet color (Figure I-7b). Both crystals revert their initial color and expand following the same trajectory on irradiation with visible light.

However, the irradiation of individual crystal changes the geometrical structure of molecule and then affects the molecular packing. The intermolecular interaction between the photogenerated isomers thus plays a significant role in inducing deformation within the crystal.

It is there noteworthy to notice that by recrystallizing DTE-2 within a rod-like crystal shape, the crystal interestingly bends upon UV light exposure and regains its straightened form upon visible light exposure. Despite their same crystalline structure revealed by X-ray crystallographic analysis, DTE-2 rectangular plate-like crystal and DTE-2 rod-like crystal exhibit different shape changes. In order to assess the second photomechanical effect, the next section is devoted to carefully explain the bending behavior.

I.2.2.2. Bending behavior

In photoresponsive single crystal case, the bending is a typical photomechanical response reported for various photochromic diarylethene crystals **[37-42]**. Upon irradiation, two types of bending directions can be investigated: bending away or toward the incident light. The bending away from the light source is initiated by the expansion of the photoirradiated crystal layer. Whereas, the crystal bending toward the source light is due to the contraction of the first photoreacted crystal layer.

Figure I-8 illustrates some examples of DTEs derivatives crystals with symmetric and asymmetric structures bending away (Figure I-8a, Figure I-8c) or toward (Figure I-8b, Figure I-8d) the UV light source. The occurred different directions depend on various parameters such as the illumination parameters **[43-44]**, the crystal thickness **[48-50]** and the molecular stacking **[45-47].**

To evaluate the crystal bending efficiency, quantitative analysis of photoinduced bending was required. Naumov and Bardeen have reported independently sophisticated mathematical treatments where the concentration of the photoreacted compounds throughout the crystal changes continuously as a function of the gradient between the reactant molecules and other photoactive compounds **[51, 52]**.

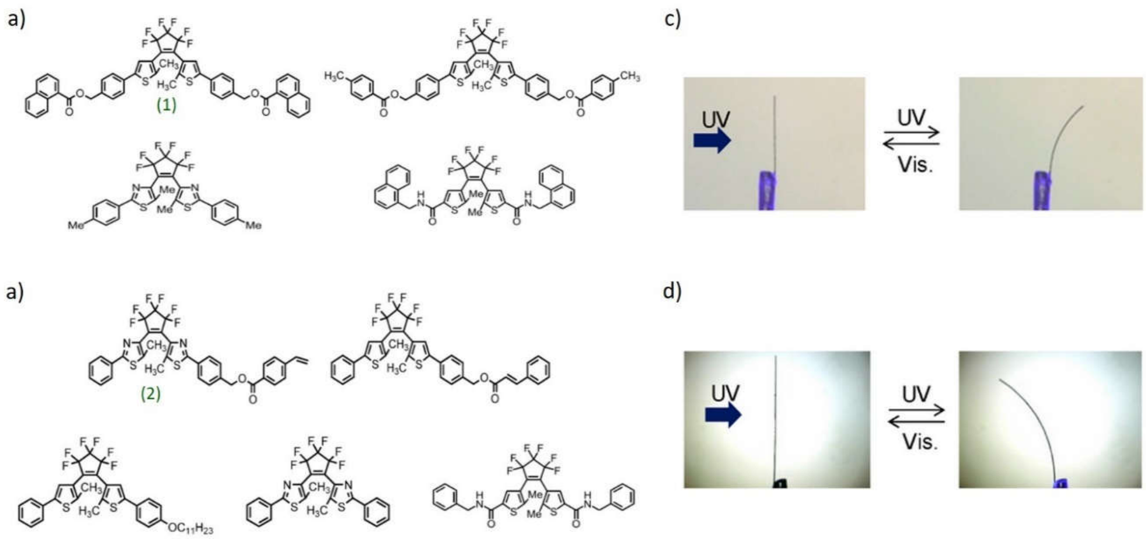

Figure I-8: DTEs derivative crystals showing bending behavior: a) bending away from UV light source and b) bending toward UV light source. c) illustrations of molecule (1) bending away and d) of molecule (2) bending toward UV light source. [47]

Kitagawa et al. have reported more simplified bimetal model associated to Timoshenko's equation [53] where the bending speedness depends essentially on the crystal thickness. As example, the authors proposed a bending mechanism for DTEs derivative crystals [54] prepared by recrystallization from n-hexane as mentioned in Figure I-9a. When irradiated with 365 nm light from the left side, the crystal bent toward the incident light. Upon irradiation with visible light from the right side, the crystal returned straight through the same bending trajectory, as shown in Figure I-9b.

To describe briefly the observed bending behavior, a mechanism for photoinduced crystal bending was proposed and illustrated in Figure I-9c. The irradiation of rod-like crystal with UV light induces at first a random electrocyclization from the OF isomer into the CF isomer. Thus, the repulsion between both isomers may induce at first an expansion of the photoreacted layer. By the increase of photogenerated CF within this layer under UV light, the photogenerated repulsion disappears and Van der Waals interaction between the CF isomers occurs leading the contraction of the photoreacted layer (Figure I-9c).

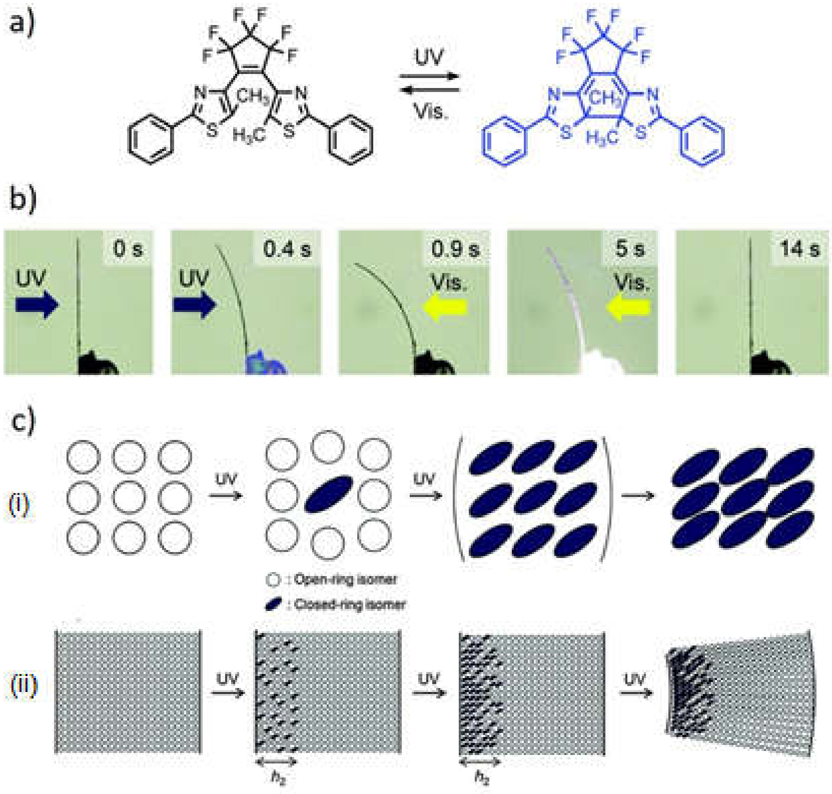

Figure I-9: Photoinduced bending behavior of crystal; a) dithienylethene derivative; b) UV and visible irradiations; c) Schematic illustration of the bending mechanism. A- Model for bending of the crystal when the crystal was irradiated with 365 nm light. [54]

Photoinduced bending behavior of DTEs can be explained by the Timoshenko's bimetal model where the depth reaction of photoconversion from the crystal surface (h_2) plays a very important role in the crystal bending behavior. Relatively to the crystal thickness (h), the crystal cannot significantly bend if h_2 is very small ($h_2 << h$). Contrarily, significant bending occurs when h_2 is approximately half of the crystal thickness ($h_2 \approx h/2$).

Upon UV light irradiation, the photoconversion reaction (OF → CF) of rod-like crystal occurs firstly at the crystal surface because of the high absorbance of the dense crystal. If h_2 is small enough, the conversion of the photoreacted layer increases quickly and the layer macroscopically contracts. Due to the CF/OF gradient in the thickness, the bending toward the incident light occurs immediately as shown in Figure I-9c.i. Subsequent irradiation with visible light induces the photocycloreversion (CF → OF) within the photoreacted layer, which expands. The bent crystal returns to its original straight shape.

I.2.2.3. Jumping behavior

Crystals of diarylethene derivatives were also reported to undergo jumping upon UV irradiation [55, 56]. Relevant parameters such as jump length, jump direction and time evolution were investigated.

Colombier et al. have observed microcrystals unidirectional hopping within few seconds under UV light [56]. Figure I-10 shows the associated optical microscopy images: before irradiation, photoconversion of the microcrystal when turning into red and the crystal jumping. This jumping was characterized by absorption micro-spectroscopy with time jumping of about 17s. The jump lengths are in the millimeter range. It is important to note that crystal size play a key role in allowing the jumping. Big-sized crystal does not jump. If crystal is sized of tens microns (<200µm), the jumping occurs as irreversible phenomenon. These photomechanical effects could result from a Grinfeld surface instability [57] where the uniaxial stress induced in the crystal lattice relaxes through directional jumps.

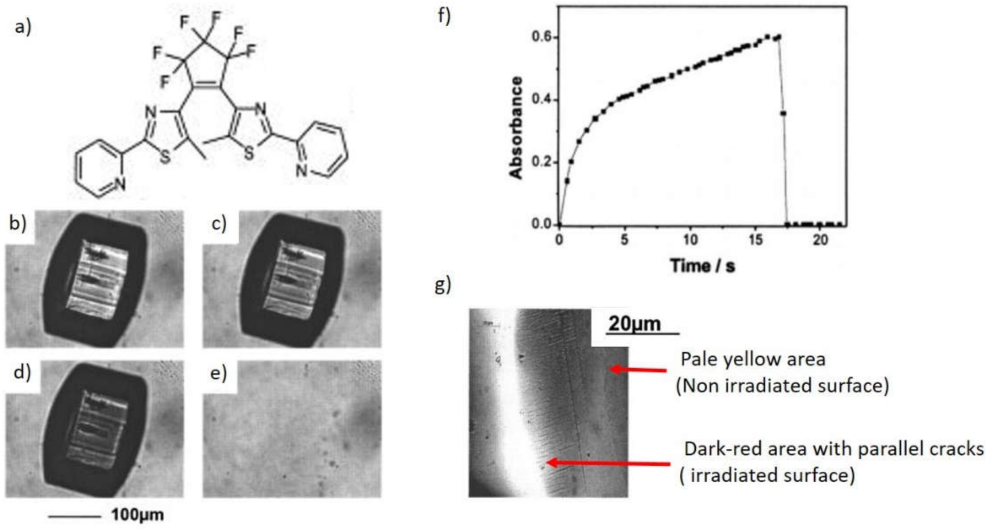

Figure I-10: Optical microscopy images of a microcrystal when irradiated with UV light: a) example of dithienylethene derivative. b) before irradiation. c)–d) the crystal turns red because of the photoreaction. e) the crystal has jumped. f) time evolution of the absorbance at 550 nm. g) crystal surface with dark-red partially irradiated area presenting parallel cracks and pale yellow non irradiated area. [56]

If the microcrystal is prevented from jumping, cracks appear on the crystal surface as shown in Figure I-10g. When a part of the pale-yellow crystal is exposed to UV light, the photoconversion occurs within the irradiated part and the color of the irradiated area becomes dark-red due to photocoloration reaction. This reaction is accompanied with the appearance of irreversible equidistant parallel cracks due to the accumulation of local stress in the crystal surface. Furthermore, the distance between cracks depends on UV light wavelength i.e. the crack distance decreases while decreasing the UV light wavelength.

I.2.2.4. Fragmentation behavior

The explosively scattering of crystals into fragments induced by light stimulus is a phenomenon called photosalient effect. In 1834, Trommsdorff was the first to report an organic crystal explosion of α-santonin after its color change into yellow when exposed into sunlight [58]. This phenomenon was reinvestigated over the recent years. Many groups such as Naumov et al. have intensively studied the crystal fragmentation obtained through complexation using a light irradiation [59-62].

The crystals of dithienylethene derivatives were also reported to undergo photosalient effect. Examples of DTEs are presented in Figure I-11a: diarylethenes with a five-membered perfluorocyclopentene ring [63, 64] and other derivative with a perfluorocyclohexene ring [65]. The explosively fragmentation of the photochromic molecule having urethane units numerated (2) is illustrated as shown in Figure I-11b.

Such strong phenomenon is ascribed to the presence of intermolecular hydrogen bonding between the urethane groups. The strong intermolecular interactions are considered to cause a large strain when the photoconversion reaction occurs. As consequence, a rapid and explosive crystal fragmentation takes place.

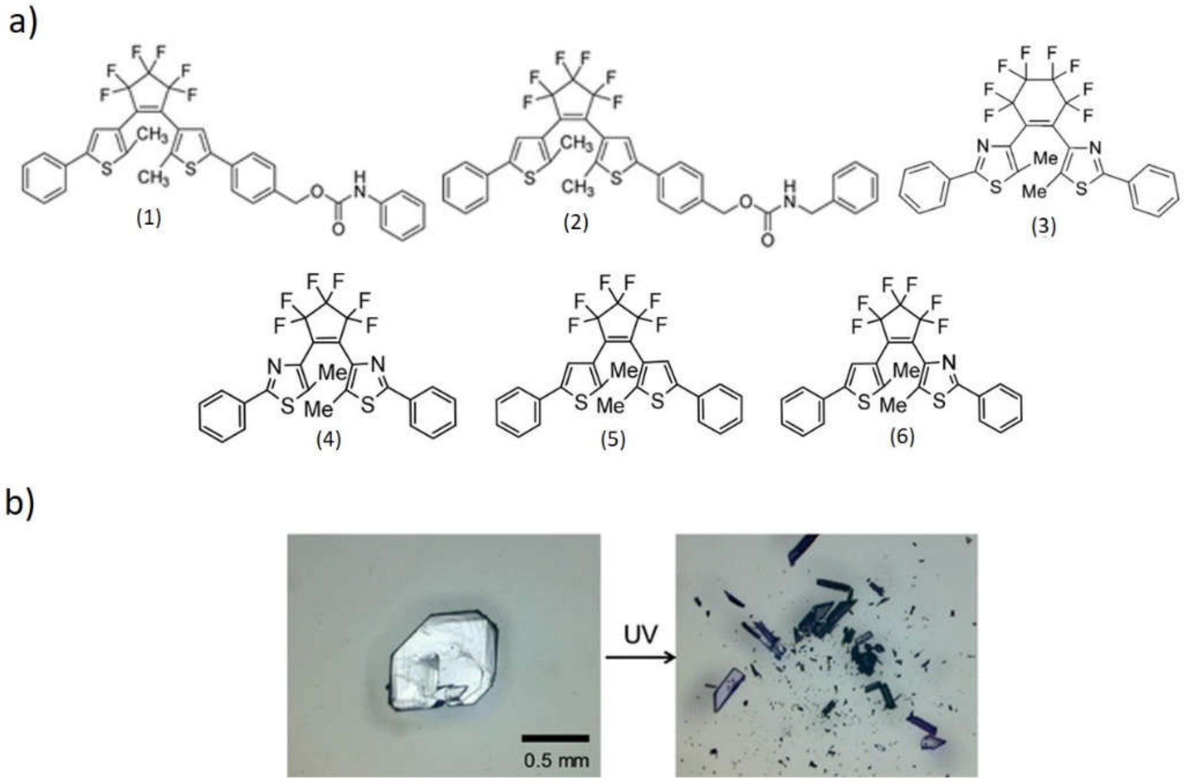

Figure I-11: Photoinduced rapid and explosive fragmentation. a) Examples of DTEs derivatives. b) Optical photographs of dithienylethene (2) crystal fragmentation before and after UV irradiation.

Recently, the photomechanical effect was found to be dependent on UV light intensity. By increasing the light intensity, photoinduced bending becomes photosalient effect. Furthermore, the dependence of photosalient phenomenon to the crystals shape is reported as being an important parameter. The change of the crystal size is more significant for asymmetrical dithienylethene than that for the symmetrical dithienylethene (Figure I-11a). As a result, the asymmetrical diarylethene crystals show much more drastic photosalient effects than those of the symmetrical diarylethene crystals upon UV irradiation.

I.3. Photoresponsive covalent bonded Polymers

I.3.1. Introduction on polymers

The properties of polymers strongly depend on the chain chemical structure and their interactions. Due to the configurational arrangements (topological arrangement of the atoms within the monomer unit) and the conformational arrangements (monomer unit arrangement within the polymer) of the macromolecular chains as well as the external conditions (kinetic cooling …), polymer materials is expected to have either totally disordered (amorphous polymer) or partially ordered (semi-crystalline polymer) behaviors.

In solid state, the amorphous polymers are macroscopically isotropic and homogeneous. Under heating, the amorphous polymer presents a transition from a glassy to a rubbery state. The associated temperature is called the glass transition temperature, T_g.

Macomolecules with a regular organization implies the formation of crystalline arrangements or crystals. The smallest macromolecular units arrange to form a three-dimensional lattice described by the unit cell. Semi-crystalline polymers combine both crystalline and amorphous states. When chains are partially disordered, some of the macromolecules arrange to form crystalline phases dispersed in an amorphous matrix (Figure I-12). The crystalline regions are connected to the amorphous regions without well-defined boundaries between the two types of regions. Upon heating, semi-crystalline polymers change from a crystal state to a melt state. The associated transition temperature is designed the melting temperature, Tm.

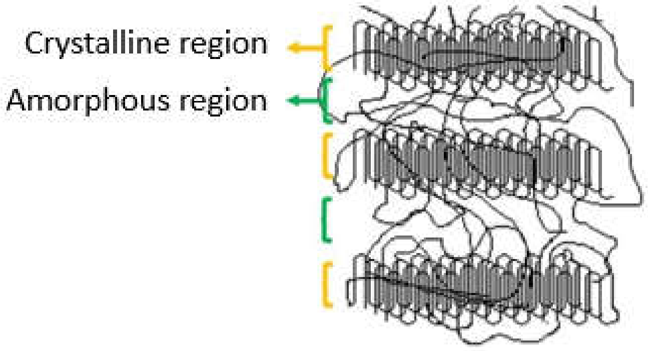

Figure I-12: Schematic illustration polymer chains arrangements, semi-crystalline behavior.

Related to the presence of amorphous and crystalline domains within macromolecular chains, polymers can be divided into three broad categories: elastomers (amorphous polymers), thermosets (amorphous polymers) and thermoplastics (amorphous or semi-crystalline polymers).

Elastomers are composed of macromolecular chains that are cross-linked with a low cross-linking density allowing their flexibility. Under external stress, their structure is reversibly deformable i.e. elastomers can be stretched easily several times from their unstretched length and can quickly return to their original dimensions. Contrarily to the elastomers case, thermosets are rigid materials with a high crosslinking density, which restricts the motions of the macromolecules. In the case of thermoplastic polymers, molecular chains are held to each other either through relatively weak intermolecular forces such as Van der Waals and hydrogen bonding or by entanglements. These polymers molded at high temperature conserve the molded shape once cooled.

However, flexibility and molding properties can be gathered in a derivative polymeric class named thermoplastic elastomer, which will be further investigated in the next section.

I.3.2. DTEs polymerization

Easy processability, cost effectiveness and tunable properties make polymers attractive materials for industrial applications. A polymer is constituted of a large number of repeating units (monomers), which covalently link to form a long chain (macromolecule) during a polymerization reaction.

The design of polymerizable photochromic molecules or the incorporation of photochromic molecules into a polymer matrix offer supplementary photocontrollable characteristics and extend the field of applications to solar cells, actuators, optical memory and switches and data storage [66-69]. Photochromic polymeric materials will be briefly reviewed for systems based on homopolymers or copolymers of DTEs derivatives and for DAEs derivatives covalently linked with polymer matrices.

DTEs homopolymers – copolymers. Homopolymer is a polymer issued from a single species of repeating units. Whereas, polymer derived from at least two types of repeating units is designed copolymer. DTEs-homopolymers and DTEs-copolymers were reported as photochromic polymers [70-72]. As example, series of three homopolymers containing different photochromic DTEs adjusted by varying the length of the linearly π-conjugated and the associated copolymer were designed [72] and then synthesized as depicted in Figure I-13a and Figure I-13b.

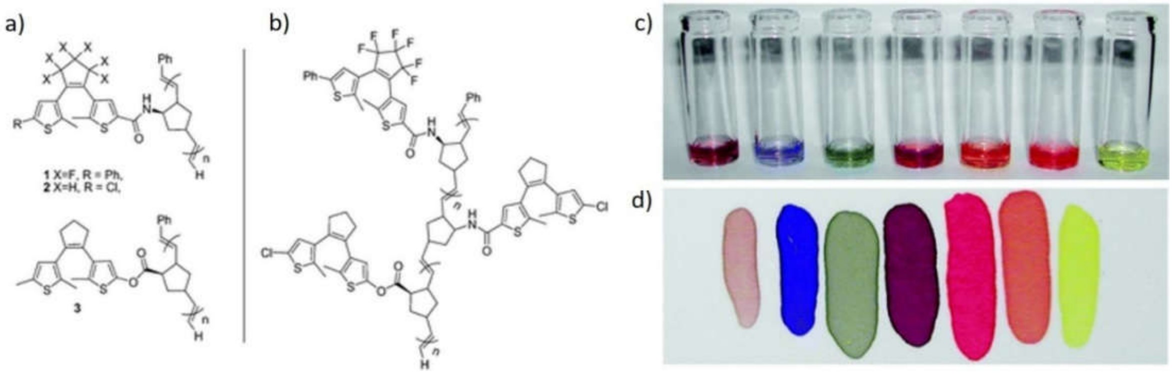

Figure I-13: Multi-colored homo- and copolymers. a) homopolymers structures; b) copolymer structure; c) Color mixing of DTEs homo- and co-polymers after UV light irradiation of solutions; d) homo- and co-polymers samples painted onto a silica plate followed by irradiation with 313-nm light. [72]

The irradiation of these homo and copolymers with appropriate light induces cycloconversion and reversion reactions. Indeed, when the CF isomer is achieved, the three DTEs derivatives homopolymers provide the primary colors: blue, red and yellow. Mixing homopolymers with copolymers at different ratios lead to a wide range of colors for the polymers in solution or when painted onto silica plate Figure I-13c and Figure I-13d.

DTEs in a polymeric matrix. There are two ways to introduce photochromic molecules in a polymer matrix: the molecules can be (i) incorporated through simple mixing or (ii) grafted to the polymer matrix. The incorporation of diarylethene derivatives into a thermoplastic polymer such as poly(methyl methacrylate) (designed PMMA) were reported by few groups [73-75]. Such polymeric materials offer a useful tool for controlling surface wettability and in radiochromic applications.

However, the covalent grafting of photochromic molecules to the polymer matrix highly improve the system properties including stability, mechanical properties. Few examples were reported in the literature with the use of polystyrene, liquid crystalline polymer or polyurethane as matrix **[76-79]**.

The DTEs polymeric materials offer new approaches of color tuning for display technology and find potential applications in high-density optical data storage.

I.4. Supramolecular assemblies based on UPy units

Molecules are connected to each other through chemical bonds: covalent bonds and/or non-covalent bonds. The covalent bonds lead generally to the formation of selective and kinetically stable molecules. These molecules can also interact through weaker and kinetically labile non-covalent interactions. Unlike conventional chemical synthesis in which covalent bonds are particularly important, non-covalent interactions play a key role in supramolecular chemistry, which can be defined as the chemistry of low energy interactions. Among the possible non-covalent interactions that can define the properties of supramolecular structures, we can find the host-guest recognition, donor-acceptor interactions, metal-ligand coordination, $\pi - \pi$ interactions and hydrogen bonding interactions.

Herein, our attention will be focused on hydrogen bonding interactions, which are known as directional interactions. More precisely, they are formed between an acidic hydrogen atom (donor site D) and an electronegative atom often oxygen or nitrogen (acceptor site A). Furthermore, they are sensitive to the external environment including the presence of competing solvent and the temperature variation. In supramolecular chemistry, hydrogen bonds are considered as the main applied interactions because they allow arrangement with excellent precision especially systems involving several hydrogen bonds that are greatly expected to increase the strength of these interactions.

I.4.1. UPy units: presentation

A new approach about hydrogen bonding was reported by Meijer and coworkers in 1997 **[80]**. They have successfully synthesized a 2-ureido-4[1H]-pyrimidinone units noted UPy. It is a hydrogen bonding motif that enables to introduce thermos-reversible linkages and molecular recognition site.

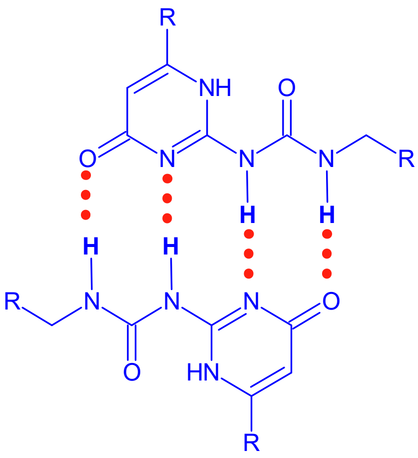

Figure I-14: UPy – UPy interactions through quadruple hydrogen bonds.

In solution, UPy unit dimerizes via four hydrogen bonds according to the DDAA sequence with a high stability [81] (Figure I-14). UPy unit possesses a dimerization constant exceeded 10^6 M^{-1} [80]. The strong dimerization of UPy is employed to obtain extended linear chains which are hold to each other via non-covalent interaction.

I.4.2. UPy telechelic supramolecular polymers

Combination of supramolecular chemistry to polymer science leads the development of supramolecular polymers where individual monometric units are self-assembled together by strong, directional, and reversible noncovalent interactions. UPy-unit is an ideal motif in designing the hydrogen bonded supramolecular polymers.

In solution, interactions between UPy-units leads to their dimerization via quadruple hydrogen bonds and the formation of linear supramolecular polymer (Figure I-15). In chloroform, the dimerization constant is about 6 10^7 M^{-1} at room temperature [82]. The quadruple hydrogen-bonded units can be attached as side groups of the polymer backbone or as telechelic units (reactive end-groups). These telechelic compounds basically lead to the formation of supramolecular polymers with more improved properties.

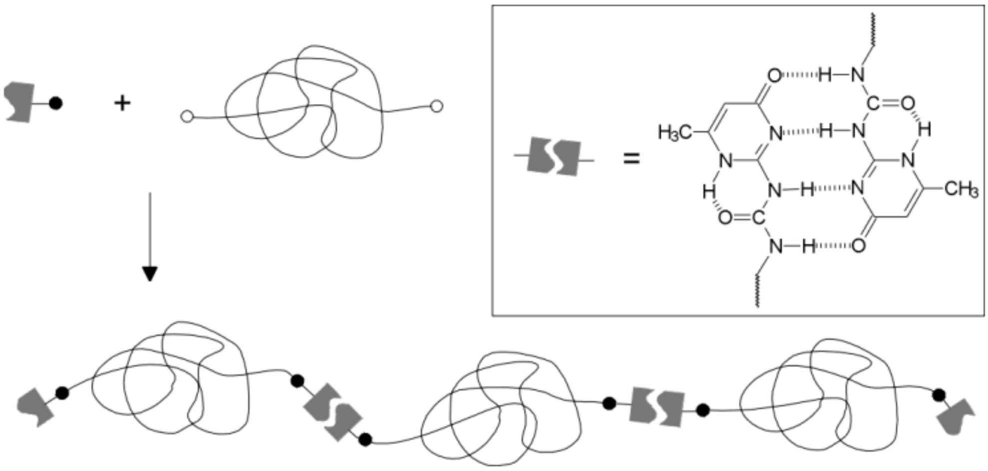

Figure I-15: Schematic drawing of functionalization of telechelic polymers with quadruple hydrogen-bonded ureidopyrimidinone units. [82]

Supramolecular polymer assemblies formed in solution are sensitive to the temperature. Indeed, a high temperature induce a weakening of the noncovalent bonds and then the depolymerization of the assembly.

The UPy units were employed in the chain extension of various telechelic polymers such as PDMS [83], polycarbonate [84], poly(ethylene-butylenes) (PEB) [85], polyether [85] and poly(ethylene-co-propylene) (PEP) [86]. The obtained telechelic polymers combine mechanical properties of conventional polymers and low melt viscosity of organic compounds.

I.4.3. UPy telechelic PEB

I.4.3.1. Physical properties

Thermoplastic elastomers (TPEs) are polymers that combine characteristics of soft elastomers and thermoplastics. Indeed, the materials exhibit rubberlike properties at room temperature (elastomer) and the reversibility of the bonding allows its processability (as a thermoplastic polymer).

In the case of copolymer with different segments or blocks, the reversible cross-links of TPE originate basically from the crystallization of at least one of its blocks. Such rigid crystallizable block is called “hard block” (for instance polyester, polyamide, or polyurethane segments) while the non-crystallizable block giving material elasticity is called “soft block”.

Poly(ethylene/butylene) copolymer noted PEB is a random copolymer belonging to the polyolefin family. The functionalization of PEB involving UPy-end groups and urethane groups were reported by Meijer et al. [85] as illustrated in Figure I-16a. The PEB-UPy chains lead to the formation of supramolecular polymers containing less than 0.2% of residual hydroxyl groups.

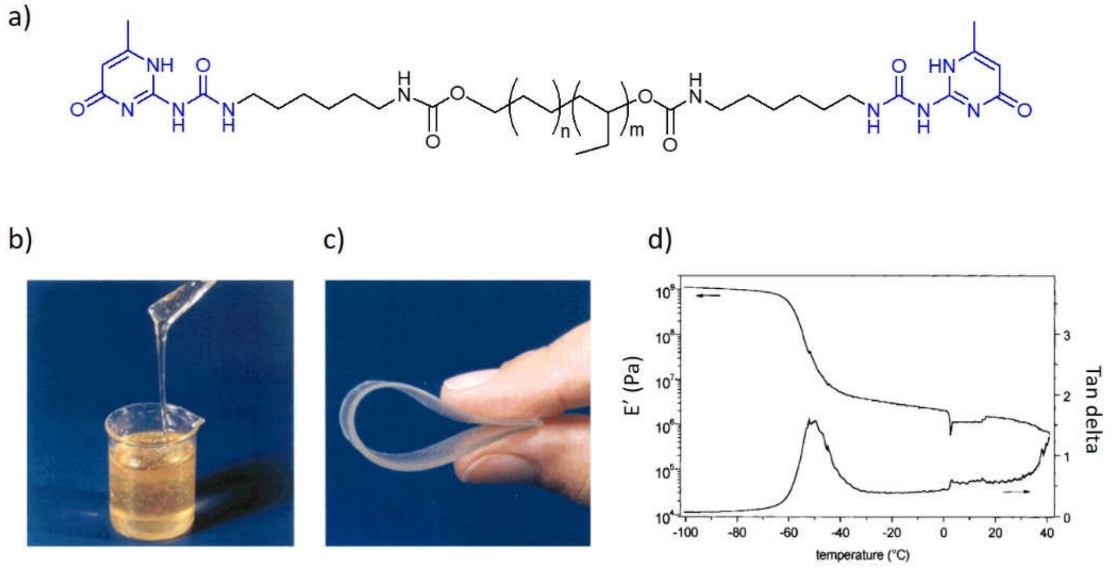

Figure I-16: Telechelic PEB-UPy supramolecular assembly. a) Chemical structure of PEB-UPy. b) PEB with OH end groups. c) PEB with UPy end groups [88]. d) DMTA curves of PEB-UPy. [84]

I.4.3.2. Thermal properties

While the hydroxy-telechelic PEB is a viscous semifluid liquid (Figure I-16b), the PEB-UPy presents a transparent appearance when casted (Figure I-16c). When the UPy-functionalization of amorphous PEB was occurred, the appearance of a single glass transition at -50°C was accompanied with a rubber plateau at 5×10^6 Pa. Such results confirm the amorphous state of the material despite its functionalization. The hydrogen-bonded units do not lead to apparition of crystalline domains. Thus, PEB-UPy was found to exhibit the characteristic of soft rubber at room temperature (Figure I-16d) [84].

Investigation of telechelic PEB-UPy films were also investigated through studying the effect of combining directional lateral aggregation through urea motifs (U) and urethane motifs (T) [87]. As illustrated in Figure I-17, three copolymers obtained from the PEB precursor (Figure 18a) are compared: PEB-UPy (Figure I-17b), PEB-T-UPy (Figure I-17c) and PEB-U-UPy (Figure I-17d).

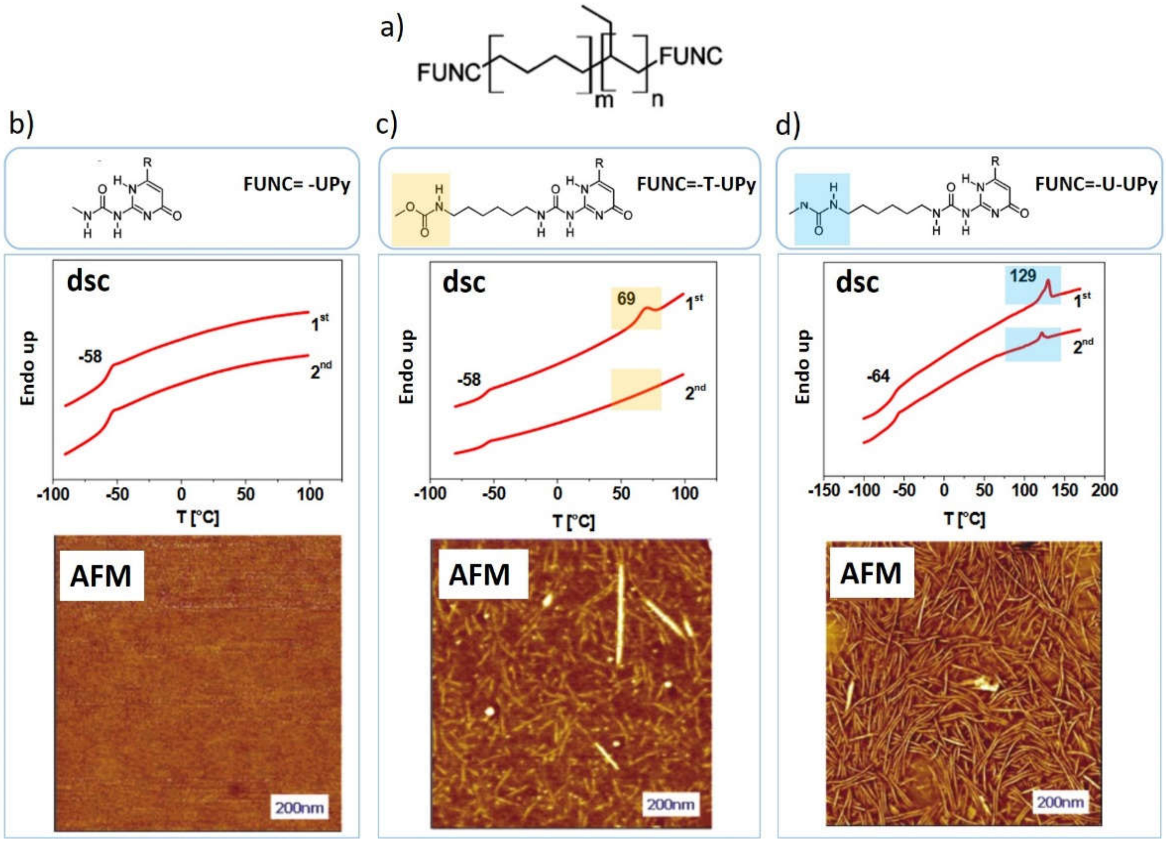

Figure I-17: DSC and tapping mode AFM images of telechelic PEB supramolecular assembly functionalized with various end groups. a) Chemical structure of telechelic PEB to functionalize. b) PEB-UPy. c) PEB-T-UPy. d) PEB-T-UPy. [87]

From DSC traces, PEB-UPy demonstrates the absence of a melting point. In contrast, PEB-T-UPy and PEB-U-UPy have melting points at respectively 69°C and 129°C. This suggests the existence of a supplementary self-assembly which is stronger for the PEB-U-UPy since the melting occurs at higher temperature.

I.4.3.3. Structure and morphology

By continuing the same investigation involved above, morphological observations by AFM in tapping mode reveal interesting features such as the presence of nano-fibrillary segregation with different sizes and densities depending on the hydrogen bonding strength within T or U motifs. Besides the strong quadruple hydrogen bonding of the UPy groups, lateral interactions can occur in one-dimensional aggregation, which play a key role in the enhancement of mechanical properties. Rowan et al. [88] reported similar conclusions by studying the key role played by the weak hydrogen bonds to obtain polymers with film-forming properties.

The UPy-urea nanofiber formation process was investigated by Appel et al. [89] as illustrated in Figure I-18a. The aggregation first step is associated to the UPy-monomers dimerization (depicted in blue), allowing the formation of UPy-dimers. The lateral hydrogen bonding interactions through urea motifs (depicted in red) gives arise to the formation of stacks. Multiple stacks are gathered by secondary nucleation to form nanofibers. The inter-stack distance within a nanofiber is dependent on the UPy-substituent size (depicted in green). When this substituent is methyl group, the stack-to-stack distance was reported to be at roughly 1 nm (Figure I-18b).

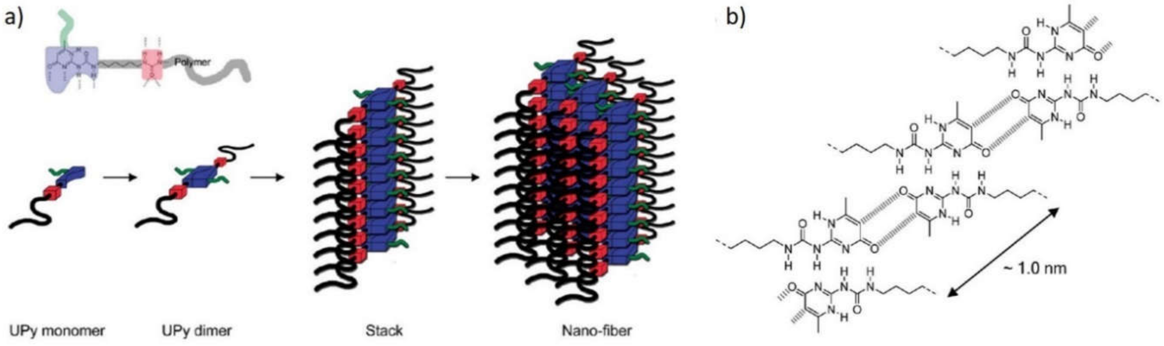

Figure I-18: Schematic representation of the theoretical aggregation. a) Process of aggregation steps of the UPy-end groups (blue), urea-motifs (red) into nanofibers. b) Proposed interstack interaction involving UPy-substituent (depicted in green). [89]

In the case of PEB-PLA combination, i.e. soft segments of PEB were alternated with poly(lactic acid) noted PLA in order to generate multiblocks supramolecular polymers functionalized via hydrogen bonding sites (Figure I-19a) [90, 91]. As the stereostructure of PLA is changeable, two series of multiblocks have been studied: non-crystallizable PLA designed PDLLA and crystallizable PLA designed PLLA. PEB, PEB-PLA with low fraction of PLA oligomers exhibit semifluid behavior. The functionalization with UPy-units leads to transparent and elastic films, which confirm again the strong effect of hydrogen bondings on the physical properties of materials. The PEB-PDLLA functionalized by UPy motifs remaind amorphous while the high strength of UPy-units significantly suppresses the crystallinity of PLLA blocks.

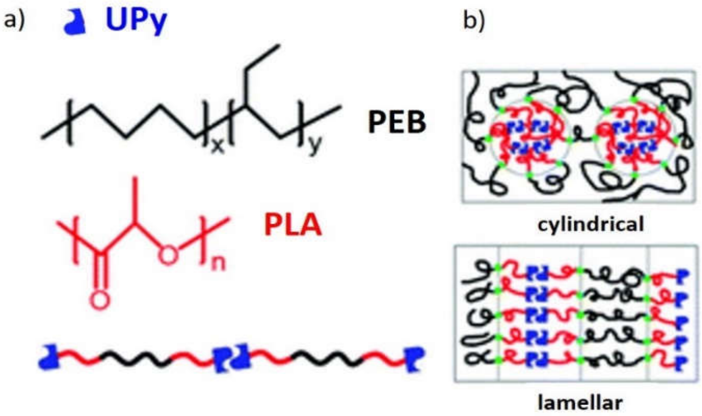

Figure I-19: UPy-bonded PLA/PEB supramolecular assembly. a) Schematic illustration of self-assembly. b) Schematic illustration of cylindrical and lamellar structure.

Additionally, the authors reported the structural organization of PEB/PLA multiblocks and their UPy-bonded supramolecular assembling by means of SAXS measurements where the morphology can lead to cylindrical or lamellar morphology depending on the PLA fraction (Figure I-19b).

I.4.4. The DTE-UPy supramolecular assembly

Introducing photochromic molecules within the polymer assembly can induce promising photoresponsive changes.

Takeshita et al. was the first to synthesize a photochromic molecule of DTEs derivative functionalized from both sides by UPy motifs noted DTE-UPy [92, 93]. In solution, neighbor UPy end groups tend to self-aggregate due to formation of four hydrogen bonding and then to form long supramolecular polymeric chains. The OF in chloroform (2 10^{-4} M) is colorless and preserves its clear color for several days. When the solution is irradiated with UV light, the blue photogenerated CF started to precipitate in few minutes. This observation not only proves the formation of the supramolecular assembly but also suggests higher aggregation of the monomers in their CF compared to their OF (Figure I-20).

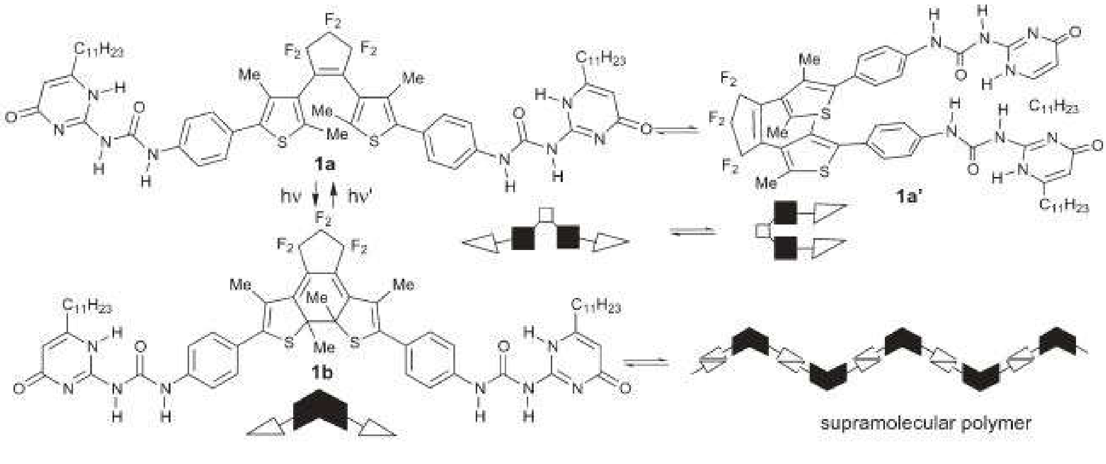

Figure I-20: Concept for photoswitchable supramolecular polymer. [92]

Indeed, the initial OF is described as flexible structure due to the mobility of both benzene rings carrying the UPy-end units. This mobility is not favorable for supramolecular assembly but allow the formation of two conformers (AP and P) in an equilibrium state. Although room temperature can induce slow conformers exchange, only the AP conformer from the OF leads to the formation of CF. Thanks to the C-C electrocyclisation, this CF regains structural rigidity allowing molecular interactions and then the formation of a supramolecular assembly. Large supramolecular assembly was characterized through DLS measurements (See chapter IV for more details) and eye-naked observation of a strong blue precipitate.

I.5. Photomechanical effect of DTE/Thermoplastic elastomer system

Although the azobenzenes are the most used photoreactive molecules in revealing macroscopic photomechanical effects, diarylethenes were successfully coupled to various polymer materials through covalent links with rarely notification about their macroscopic photomechanical changes.

The only example found in literature was about cross-linked liquid-crystalline (LC) polymers and a diarylethene derivative as depicted in Figure I-21a [94]. Mamiya et al. have designed and synthesized a photochromic diarylethene derivative covalently linked from both sides to biphenyl mesogens with LC property. The characteristic of this photoresponsive covalently bended polymer is that the system induces macroscopic deformations upon irradiation.

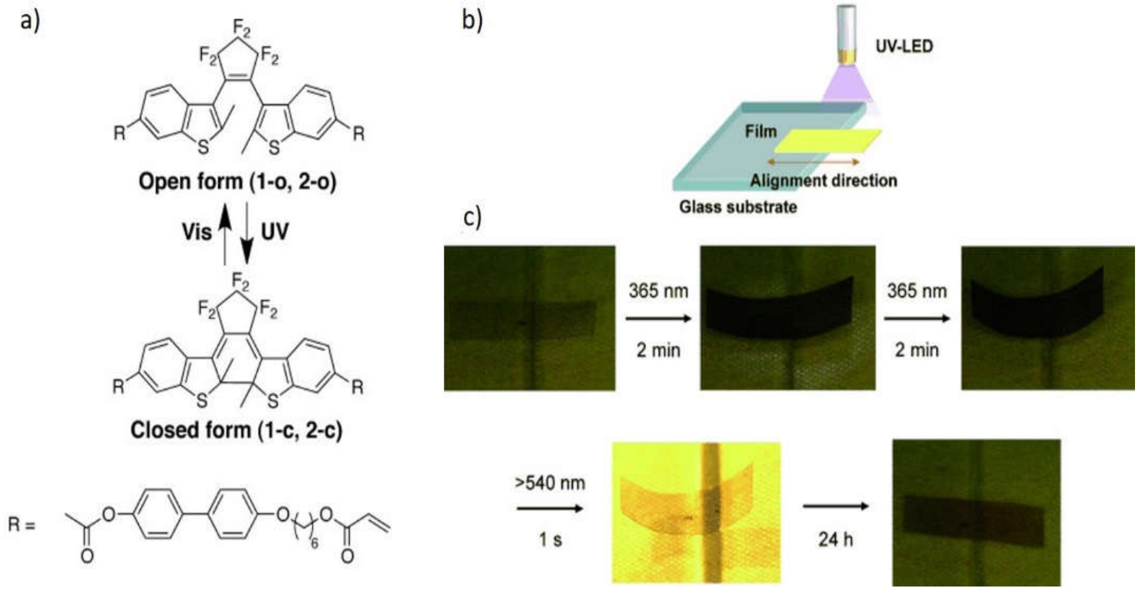

Figure I-21: Photoinduced bending behavior of diarylethene-based LC derivative thin film prepared. a) Chemical structure of the diarylethene based LC derivative and their photochromic reactions. b) Schematic illustration of the experimental setup. c) Bending photographs of the film upon irradiation with UV and visible light at 120 °C. Size of the film: 10 mm×5 mm. Thickness of the film: 20 µm. [94]

Upon irradiation with UV light, the elaborated film turned from colorless to purple color due to photocyclization reaction. Subsequent exposure to visible light reverted it reversibly to its initial color. In order to evaluate the photomechanical behavior of nematic film, this latter is deposited on glass substrate and irradiated with actinic light source as shown in Figure I-21b. The irradiation with UV light induces an instantaneous color change following by a bending of the films toward the actinic light source. Upon exposure to visible light, the film maintains its bended-shape despite the reverted original color. If the film is left in the dark at 120 °C for 24 h, it reverts to the initial flat state (Figure I-21c). The film left in the dark at 120°C after irradiation with UV light shows high thermal stability as the color and shape of the films remained unchanged even after 36h thanks to the thermally irreversible isomerization of diarylethenes. Unfortunate, apart the reported macrosocopic photomechanical changes, none of structural nor morphological study were studied since then.

From the other hand, photomechanical responses of supramolecular polymer assemblies are considered as unexplored system up to day. To our knowledge, none studies about the photomechanical responses of supramolecular assemblies resulting from self-assembled diarylethene derivatives and/or diarylethene derivatives self-assembled with polymeric matrix via complementary hydrogen bonds have ever been reported.

References

[1] Mrinalini, M. and S. Prasanthkumar, Recent Advances on Stimuli-Responsive Smart Materials and their Applications. ChemPlusChem, 2019. 84(8): p. 1103-1121.

[2] Kim, T., et al., Organic Photomechanical Materials, in ChemPhysChem. 2014: Weinheim. p. 400-414.

[3] Stuart, M.A.C., et al., *Emerging applications of stimuli-responsive polymer materials.* Nature Materials, 2010. **9**(2): p. 101-113.

[4] Inaba, S., H. Kumazaki, and K. Hane, Photothermal vibration of fiber core for vibrationtype sensor. Japanese Journal of Applied Physics, 1995. 34(4R): p. 2018-2021.

[5] Poosanaas, P., K. Tonooka, and K. Uchino, Photostrictive actuators. Mechatronics, 2000. 10(4): p. 467-487.

[6] Yerushalmi, R., et al., *Stimuli responsive materials: new avenues toward smart organic devices.* Journal of Materials Chemistry, 2005. **15**(42): p. 4480-4487.

[7] Yu, H. Dancing with Light: Advances in Photofunctional Liquid-Crystalline Materials; Jenny Stanford Publishing, 2015.

[8] Zhao, Y.; Ikeda, T. Smart Light-Responsive Materials: Azobenzene-Containing Polymers and Liquid Crystals; Wiley, 2009.

[9] Yun, J.-H., et al., Multiscale modeling and its validation of the trans-cis-trans reorientation-based photodeformation in azobenzene-doped liquid crystal polymer. International Journal of Solids and Structures, 2017. 128: p. 36-49.

[10] Bouas-Laurent, H., Durr, H. Organic photochromism. Pure and Applied Chemistry, 2001. 73(4): p. 639-665.

[11] Crano, J.C, Guglielmetti, R. J. Organic Photochromic and Thermochromic Compounds. éd. R. J Guglielmetti J.C Crano. Vol. 2, New York: Plenum, 1999.

[12] Dürr, H., Bouas-Laurent, H. Photochromism Molecules and Systems. Amsterdam: Elsevier, 1990.

[13] Barillé, R. Molécule azobenzène - Propriétés et applications photomécaniques de la commutation moléculaire. Techniques de l'Ingénieur. Janvier 2017, vol. E6440 V1 p.

[14] Bandara, H.M. and Burdette, S.C. (2012) Photoisomerization in different classes of azobenzene. Chem. Soc.Rev., 41 (5), 1809–1825.

[15] Merino, E. (2011) Synthesis of azobenzenes: the coloured pieces of molecular materials. Chem. Soc. Rev., 40 (7), 3835–3853.

[16] Natansohn, A. and P. Rochon, Photoinduced motions in azo-containing polymers. Chemical reviews, 2002. 102(11): p. 4139.

[17] Ishow, E.n., et al., Spontaneous Formation of Complex Periodic Superstructures under High Interferential Illumination of Small-Molecule-Based Photochromic Materials. Advanced Functional Materials, 2009. 19(5): p. 796-804.

[18] Irie, M., Diarylethenes for memories and switches.(Statistical Data Included). Chemical Reviews, 2000. 100(5): p. 1685.

[19] Irie, M. and M. Mohri, Thermally Irreversible Photochromic Systems. Reversible Photocyclization of Diarylethene Derivatives. Journal of Organic Chemistry, 1988. 53(4): p. 803-808.

[20] Heller, H.G. and S. Oliver, Photochromic heterocyclic fulgides. Part 1. Rearrangement reactions of (E)-α-3-furylethylidene(isopropylidene)succinic anhydride. Journal of the Chemical Society, Perkin Transactions 1, 1981(0): p. 197-201.

[21] Darcy, P.J., et al., Photochromic heterocyclic fulgides. Part 2. Electrocyclic reactions of (E) -α-2,5-dimethyl-3-furylethylidene(alkyl-substituted methylene)succinic anhydrides. J. Chem. Soc., Perkin Trans. 1, 1981(0): p. 202-205.

[22] Barrez, E., et al., Comparative photophysical investigation of doubly-emissive photochromic-fluorescent diarylethenes. Physical Chemistry Chemical Physics, 1997. 20(4): p. 2470-2479.

[23] Irie, M., et al., Photochromism of 1,2-bis(2-methyl-5-phenyl-3-thienyl)perfluorocyclopentene in a single-crystalline phase. Journal of the American Chemical Society, 2000. 122(20): p. 4871-4876.

[24] Hamdi, I., et al., Excited-State Dynamics of Dithienylethenes Functionalized for Self-Supramolecular Assembly. The journal of physical chemistry. A, 2018. 122(14): p. 3572.

[25] Hamdi, I., et al., New insights into the photoswitching mechanisms of normal dithienylethenes. Physical Chemistry Chemical Physics, 2016. 18(40): p. 28091-28100.

[26] Uchida, K., Y. Nakayama, and M. Irie, Thermally irreversible photochromic systems. Reversible photocyclization of 1,2-bis(benzo(b)thiophen-3-yl)ethene derivatives. Bulletin of the Chemical Society of Japan, 1990. 63(5): p. 1311-1315.

[27] Spangenberg, A., et al., Multiscale Approach of Photochromism: Synthesis and Photochromic Properties of a Diarylethene in Solution, in Nanoparticles, and in Bulk Crystals. Advanced Materials, 2009. 21(3): p. 309-313.

[28] Irie, M., Photochromism of diarylethene single molecules and single crystals. Photochemical & Photobiological Sciences, 2010. 9(12): p. 1535-1542.

[29] Kobatake, S., et al., Single-crystalline photochromism of diarylethenes: reactivity-structure relationship. Chemical communications (Cambridge, England), 2002(23): p. 2804.

[30] Terao, F., M. Morimoto, and M. Irie, Light-driven molecular-crystal actuators: rapid and reversible bending of rodlike mixed crystals of diarylethene derivatives. Angewandte Chemie (International ed. in English), 2012. 51(4): p. 901.

[31] Reddy, C. M.; Krishna, G. R.; Ghosh, S. Mechanical Properties of Molecular Crystals Applications to Crystal Engineering. CrystEngComm 2010, 12, 2296-2314

[32] Kim, T.; Zhu, L. Y.; Al-Kaysi, R. O.; Bardeen, C. J. Organic Photomechanical Materials. ChemPhysChem 2014, 15, 400-414.

[33] T. Fukaminato, S. Kobatake, T. Kawai and M. Irie, Three-dimensional erasable optical memory using a photochromic diarylethene single crystal as the recording medium, Proc. Jpn. Acad., Ser. B, Phys. Biol. Sci., 2001, 77, 30–35.

[34] Kobatake, S., et al., Rapid and reversible shape changes of molecular crystals on photoirradiation. Nature, 2007. 446(7137): p. 778.

[35] Kobatake, S., H. Hasegawa, and K. Miyamura, High-convertible photochromism of a diarylethene single crystal accompanying the crystal shape deformation. Crystal Growth and Design, 2011. 11(4): p. 1223-1229 ;

[36] Irie, M., et al., Reversible Surface Morphology Changes of a Photochromic Diarylethene Single Crystal by Photoirradiation. Science, 2001. 291(5509): p. 1769-1772.

[37] Irie, M., et al., Photochromism of Diarylethene Molecules and Crystals: Memories, Switches, and Actuators, in Chem. Rev. 2014. p. 12174-12277.

[38] Terao, F., M. Morimoto, and M. Irie, Light-driven molecular-crystal actuators: rapid and reversible bending of rodlike mixed crystals of diarylethene derivatives. Angewandte Chemie (International ed. in English), 2012. 51(4): p. 901.

[39] Kitagawa, D., R. Tanaka, and S. Kobatake, Photoinduced stepwise bending behavior of photochromic diarylethene crystals. CrystEngComm, 2016. 18(38): p. 7236-7240.

[40] Uchida, K., et al., Photoresponsive rolling and bending of thin crystals of chiral diarylethenes. Chemical communications (Cambridge, England), 2008(3): p. 326.

[41] Irie, M., Photochromism of diarylethene single molecules and single crystals. Photochemical & Photobiological Sciences, 2010. 9(12): p. 1535-1542.

[42] Kitagawa, D. and S. Kobatake, Photoreversible current ON/OFF switching By the photoinduced bending of gold-coated diarylethene crystals. Chem. Commun.,2015. 51(21): p. 4421-4424.

[43] Hirano, A., et al., Dependence of Photoinduced Bending Behavior of Diarylethene Crystals on Ultraviolet Irradiation Power. Crystal Growth and Design, 2017. 17(9): p. 4819-4825.

[44] Kitagawa, D., R. Tanaka, and S. Kobatake, Dependence of photoinduced bending behavior of diarylethene crystals on irradiation wavelength of ultraviolet light. Phys. Chem. Chem. Phys., 2015. 17(41): p. 27300-27305.

[45] Kitagawa, D. and S. Kobatake, Crystal thickness dependence of photoinduced crystal bending of 1,2-bis(2-methyl-5-(4-(1 naphthoyloxymethyl)phenyl)-3-thienyl) perfluorocyclopentene. Journal of Physical Chemistry C, 2010. 117(40): p. 20887 20892.

[46] Morimoto, M.; Irie, M. A diarylethene cocrystal that converts light into Mechanical work. J. Am. Chem. Soc. 2010, 132, 14172–14178

[47] Daichi, K., et al., Quantitative Evaluation of Photoinduced Bending Speed of Diarylethene Crystals. Crystals, 2015. 5(4): p. 551-561.

[48] Kuroki, L., et al., Photoinduced shape changes of diarylethene single crystals: correlation between shape changes and molecular packing. Photochemical & Photobiological Sciences, 2010. 9(2): p. 221.

[49] Uchida, K., et al., Photoresponsive rolling and bending of thin crystals of chiral diarylethenes. Chemical communications (Cambridge, England), 2008(3): p. 326.

[50] Kitagawa, D. and S. Kobatake, Crystal thickness dependence of the Photoinduced Crystal bending of 1-(5-methyl-2-(4-(p vinylbenzoyloxymethyl)phenyl)-4thiazolyl) 2-(5-methyl-2 phenyl-4-thiazolyl)perfluorocyclopentene. Photochem. Photobiol. Sci., 2014. 13(5): p. 764-769.

[51] Kim, T.; Zhu, L.; Mueller, L.J.; Bardeen, C.J. Mechanism of photoinduced bending and twisting in crystalline microneedles and microribbons composed of 9-methylanthracene. J. Am. Chem. Soc. 2014, 136, 6617–6625.

[52] Nath, N.K.; Pejov, L.; Nichols, S.M.; Hu, C.; Saleh, N.; Kahr, B.; Naumov, P. Model for photoinduced bending of slender molecular crystals. J. Am. Chem. Soc. 2014, 136, 2757–2766.

[53] Timoshenko, S. Analysis of bi-metal thermostats. J. Opt. Soc. Am. 1925, 11, 233–255.

[54] Kitagawa, D., R. Tanaka, and S. Kobatake, Dependence of photoinduced bending behavior of diarylethene crystals on irradiation wavelength of ultraviolet light. Phys. Chem. Chem. Phys., 2015. 17(41): p. 27300-27305.

[55] Baldeck, P.L., et al., Photochromic organic microcrystals jump under light irradiation. 2005. p. 59350U-59350U-4.

[56] Colombier, I., et al., Diarylethene microcrystals make directional jumps upon ultraviolet irradiation. Journal of Chemical Physics, 2007. 126(1).

[57] Colombier, I., Effets photomécanique dans les cristaux organques photochromes, Université Joseph Fourier - Grenoble 1, 2005.

[58] Trommsdorff, H., Ueber Santonin. Annalen der Pharmacie, 1834. 11(2): p. 190-207.

[59] Skoko, Z.e., et al., The thermosalient phenomenon. "Jumping crystals" and crystal chemistry of the anticholinergic agent oxitropium bromide. Journal of the American Chemical Society, 2010. 132(40): p. 14191.

[60] So, H.-S., et al., Thermosalient effect of two polymorphs of a diketopyrrolopyrrole dye with different crystal systems and molecular arrangements. CrystEngComm, 2018. 20(36): p. 5317-5320.

[61] Nath, N.K., et al., Thermally induced and photoinduced mechanical effects in molecular single crystalsa revival. CrystEngComm, 2014. 16(10): p. 1850-1858.

[62] Medishetty, R., et al., Cover Picture: Single Crystals Popping Under UV Light: A Photosalient Effect Triggered by a [2+2] Cycloaddition Reaction (Angew. Chem. Int. Ed. 23/2014). Angewandte Chemie, 2014. 53(23): p. 5713-5713.

[63] Kitagawa, D., et al., Photoinduced Rapid and Explosive Fragmentation of Diarylethene Crystals Having Urethane Bonding. Chem. Mat., 2016. 28(14): p. 4889-4892.

[64] Nakagawa, Y., et al., Photosalient Effect of Diarylethene Crystals of Thiazoyl and Thienyl Derivatives. Chemistry â€" A European Journal, 2019. 25(33): p. 7874-7880.

[65] Hatano, E., et al., Photosalient Effect of a Diarylethene with a Perfluorocyclohexene Ring. Chemistry A European Journal, 2016. 22(36): p. 12680-12683.

[66] Granstrom, M., et al., Laminated fabrication of polymeric photovoltaic diodes. Nature, 1998. 395(6699): p. 257.

[67] Smela, E., Conjugated Polymer Actuators. MRS Bulletin, 2008. 33(3): p. 197-204.

[68] Frigoli, M. and G.H. Mehl, Modulation of the Absorption, Fluorescence, and Liquid Crystal Properties of Functionalised Diarylethene Derivatives. Chemistry A European Journal, 2004. 10(20): p. 5243-5250

[69] Jeong, Y.-c., et al., Highly fluorescent photochromic diarylethene with an excellent fatigue property. Journal of Materials Chemistry, 2008. 19(1): p. 97-103.

[70] Jeong, Y.-C., et al., Polymerization of a Photochromic Diarylethene by Friedel Crafts Alkylation. Macromolecules, 2006. 39(9): p. 3106-3109.

[71] Jeong, Y.C., et al., A High Content Diarylethene Photochromic Polymer for an Efficient Fluorescence Modulation. Macromolecular Rapid Communications, 2006. 27(20): p. 1769-1773.

[72] Wigglesworth, T.J. and N.R. Branda, A Family of Multiaddressable, Multicolored Photoresponsive Copolymers Prepared by Ring-Opening Metathesis Polymerization. Chemistry of Materials, 2005. 17(22): p. 5473-5480.

[73] Asai, K., et al., Radiochromic properties of organic films based on a diarylethene molecule. Nuclear Inst. and Methods in Physics Research, A, 2019.

[74] Huang, X.-Q., et al., Synthesis and the effect of alkyl chain length on photochromic properties of diarylethene derivatives. Tetrahedron, 2019. 75(6): p. 784-790.

[75] Kitagawa, D., I. Yamashita, and S. Kobatake, Photoinduced micropatterning by polymorphic crystallization of a photochromic diarylethene in a polymer film. Chemical communications (Cambridge, England), 2010. 46(21): p. 3723.

[76] Kobatake, S. and H. Kuratani, Photochromism of Diarylethene-functionalized Polystyrene with High Conversion in a Solid-state Polymer Film. Chemistry Letters, 2006. 35(6): p. 628-629.

[77] Hayasaka, H., et al., Helically α-Stacked Conjugated Polymers Bearing Photoresponsive and Chiral Moieties in Side Chains: Reversible Photoisomerization-Enforced Switching Between Emission and Quenching of Circularly Polarized Fluorescence. Advanced Functional Materials, 2010. 20(8): p. 1243-1250.

[78] Yu, M., et al., Photoswitchable diarylethene-based polyurethane film for photorewritable patterning and stable information storage. Journal of Applied Polymer Science, 2019. 136(20): p. n/a.

[79] Mamiya, J.I., et al., Photomobile Polymer Materials: Photoresponsive Behavior of Cross-Linked Liquid-Crystalline Polymers with Mesomorphic Diarylethenes. Chemistry - A European Journal, 2015. 21(8): p. 3174-3177.

[80] Sijbesma, R. P., Reversible Polymers Formed from Self-Complementary Monomers Using Quadruple Hydrogen Bonding. Science, 1997, 278, n°5343, p. 1601-1604.

[81] Beijer, F.H.F., et al., Strong dimerization of ureidopyrimidones via quadruple hydrogen bonding. Journal of the American Chemical Society, 1998. 120(27): p. 6761-7863.

[82] Söntjens, S.H.M., et al., Stability and lifetime of quadruply hydrogen bonded 2-Ureido-4[1H]-pyrimidinone dimers. Journal of the American Chemical Society, 2000. 122(31): p.7487-7493.

[83] Hirschberg, J.K., et al., Supramolecular polymers from linear telechelic siloxanes with quadruple- hydrogen- bonded units. Macromolecules, 1999. **32**(8): p. 2696-9297.

[84] Folmer, B.J.B., et al., Supramolecular Polymer Materials: Chain Extension of Telechelic Polymers Using a Reactive Hydrogen-Bonding Synthon. Advanced Materials, 2000. **12**(12): p. 874-878.

[85] Keizer, H.M., et al., Scale-up of the synthesis of ureidopyrimidinone functionalized telechelic poly(ethylenebutylene). Polymer, 2003. **44**(19): p. 5505-5511.

[86] Elkins, C.L., K. Viswanathan, and T.E. Long, Synthesis and Characterization of Star-Shaped Poly(ethylene- c o -propylene) Polymers Bearing Terminal Self-Complementary Multiple Hydrogen-Bonding Sites. Macromolecules, 2006. **39**(9): p. 3132-3139.

[87] Kautz, H., et al., Cooperative End-to-end and Lateral Hydrogen-Bonding Motifs in Supramolecular Thermoplastic Elastomers. Macromolecules, 2006. 39(13): p.

4265-9297.

[88] Sivakova, S., et al., Utilization of a combination of weak hydrogen bonding interactions and phase segregation to yield highly thermosensitive supramolecular polymers. Journal of the American Chemical Society, 2005. 127(51): p. 18202.

[89] Appel, W.P.J.W., et al., Aggregation of ureido-pyrimidinone supramolecular thermoplastic elastomers into nanofibers : a kinetic analysis. Macromolecules, 2011. 44(17): p. 6776-9297.

[90] Chang, R., et al., Alternating poly(lactic acid)/poly(ethylene-co-butylene) supramolecular multiblock copolymers with tunable shape memory and self-healing properties. Polymer Chemistry, 2015. 6(32): p. 5899-5910.

[91] Huang, Y., et al., Polylactide- b -poly(ethylene- co -butylene)- b -polylactide thermoplastic elastomers: role of polylactide crystallization and stereocomplexation on microphase separation, mechanical and shape memory properties. RSC Advances, 2014. 4(89): p. 47965-47976.

[92] Takeshita, M., et al., Photoreversible supramolecular polymer formation. Chemical Communications, 2005(6): p. 761-763.

[93] Takeshita, M., M. Hayashi, and T. Miyazaki, A fully photoreversible supramolecular polymer having a diarylethene photoswitch. Chemistry Letters, 2010. 39(2): p. 82 83.

[94] Mamiya, J.I., et al., Photomobile Polymer Materials: Photoresponsive Behavior of Cross-Linked Liquid-Crystalline Polymers with Mesomorphic Diarylethenes. Chemistry - A European Journal, 2015. 21(8): p. 3174-3177.

Chapter II.

Basic materials, samples preparation and characterization techniques

As a reminder, the objective of this thesis is to highlight the multiscale photomechanical effects and to determine their relationships with the structure and the morphology of supramolecular assembly. More particularly, it is about bringing out the influence of self-assembling a dithienylethene with a thermoplastic elastomer within thin film elaboration. Both of them are functionalized by UPy-units. Thus, during this PhD project, these two molecules were separately studied without and with functionalization. All of these materials preparation and their synthesis will be detailed in this Chapter.

II.1. Molecules synthesis pathways

II.1.1. DTE-UPy photoswitch

The designed surpramolecular photoswitch is composed of dithienylethene (DTE) and ureidopyrimidinone group designed by UPy-units. As UPy-end groups react easily under acidic conditions, DTE-UPy is synthesis following the two-step routes published by Hamdi et al. [1]. The method consist on synthesizing the carboxylic acid DTE core and then its functionalization with UPy-units bearing different alkyl chains. The used dithienylethene is a symmetric diarylperfluorocycopentene. Typical synthetic first route from molecules (1) till (8) is illustrated in Figure II-1. While, functionalization second route concerns molecules incrementing from (8) till (11).

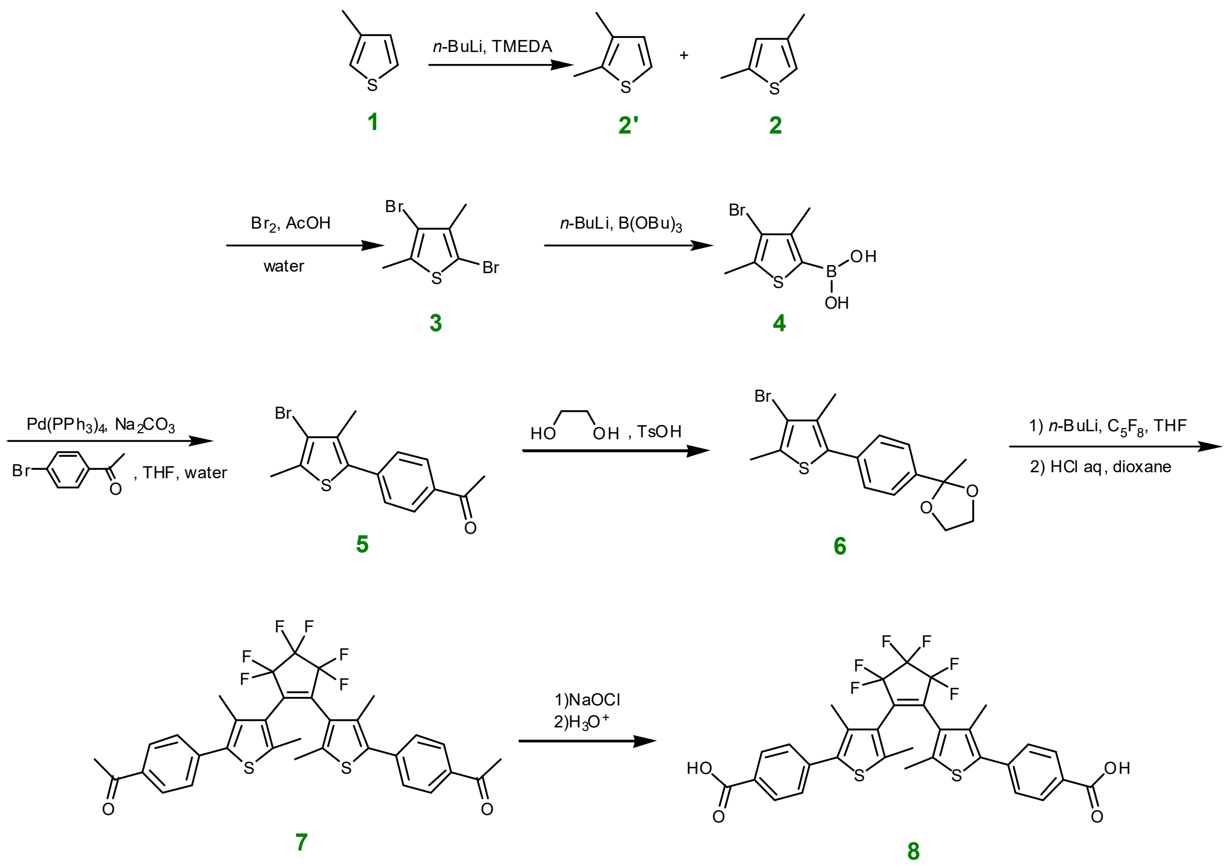

Figure II-1:Synthetic first route - telechelic carboxylic acid of DTE.

Commercially available starting compound 3-methylthiophene (1) is used to obtain the intermediate 2,4-dimethylthiophene (2) by employing n-Butyllithium chemistry. After that, Wohl-Ziegler bromination reaction condition gives rise to bi-brominated intermediate of 2,4-bibromo-3,5dimethylthiophene (3). The alcohol terminal end of 4-bromo-3,5-dimethylthiophene-2-boronic acid (4) is obtained via organometallic compound based on lithium with borate ester. The intermediate 4-(4-bromo-3,5-dimethylthiophen-2-yl) acetophenone (5) is prepared using palladium-catalyzed Suzuki coupling bromoacetophenone. Acetal protection is carried out through ethylene glycol and toluene sulfonic acid leading to intermediate (6). Coupling (6) and perfluorocyclopentane gives rise to the symmetric compound (7) designed 1,2-bis[5-(4-acetylphenyl)-2,4-dimethylthiophen-3-yl] hexafluorocyclopentene. Carboxylic acid (8) is successfully acidified through hypochlorite and dioxane solutions.

UPy-units with four associative hydrogens are synthesized separately. They were obtained through isocytosine and diisocyanate reaction bearing four different sizes of alkyl chains designed R (R=C_7H_{15}, R=$C_{11}H_{23}$, R=$C_{13}H_{27}$, R=$C_{17}H_{35}$).

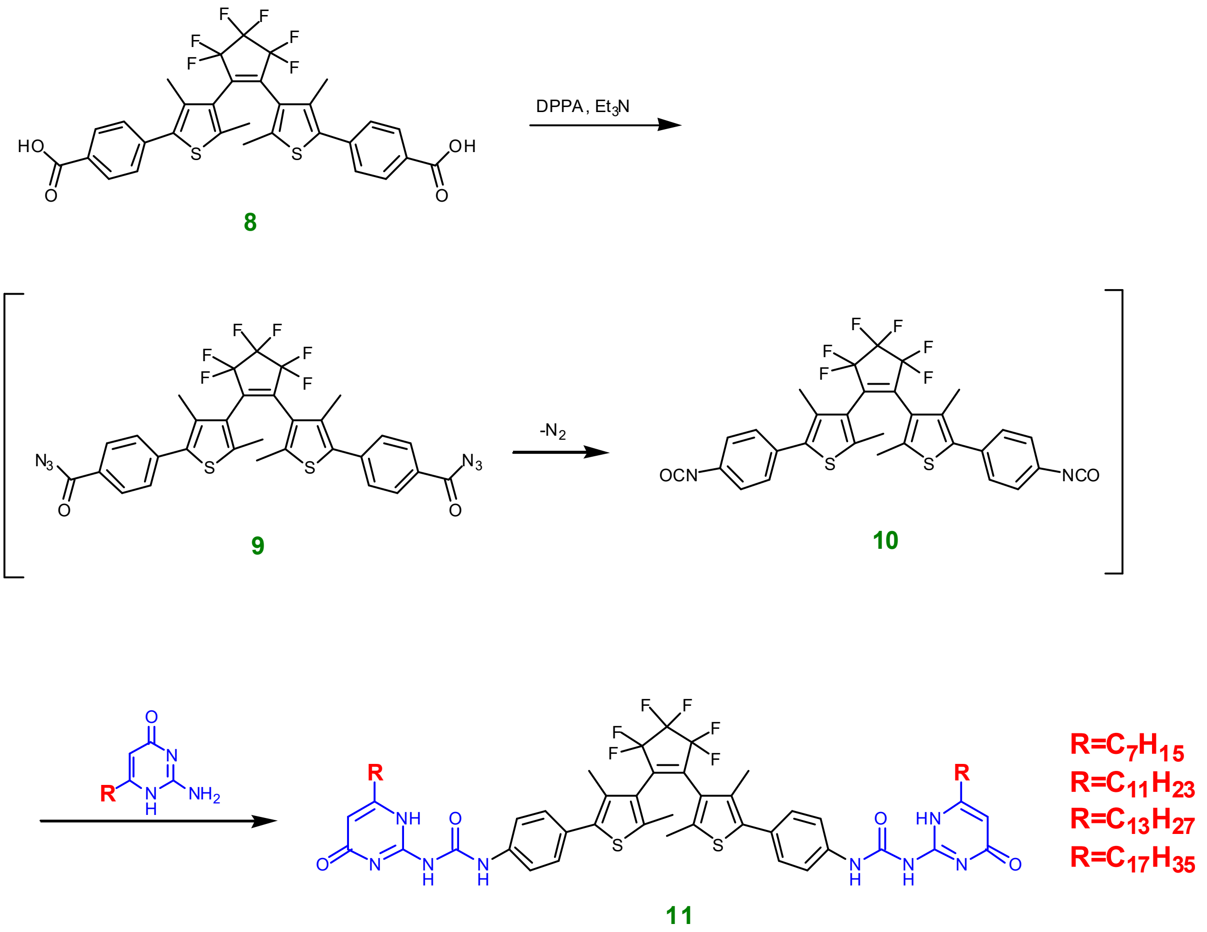

Figure II-2: Synthetic second route - functionalized DTE-UPy.

By employing the Schmidt reaction as depicted in Figure II-2, the carboxylic acid of DTE (8) reacts with azide group (DPPA) and forms the protonated azido ketone DTE (9). Through rearrangement reaction, a migration over the C-N bond with expulsion of nitrogen leads to the protonated isocyanate DTE (10). Accordingly, UPy-end units with various substituent (R) are added subsequently to intermediate (10) in order to synthesize successfully DTE-UPy(R) (11).

The main used functionalized dithienylethene is DTE-UPyC11 (also designed DTE-UPy) where UPy-substituent is R=$C_{11}H_{23}$. Contrarily to other substituents, DTE-UPyC7 (R=C_7H_{15}), DTE-UPyC13 (R=$C_{13}H_{27}$), DTE-UPyC17 (R=$C_{17}H_{35}$) are synthesized in order to elucidate complex organization throught UPy-end groups.

For comparison with the functionalized DTE-UPy, commercially available DTEcore from Tokyo Chemical Industry Co. Ltd as shown in Figure III-1 is also investigated.

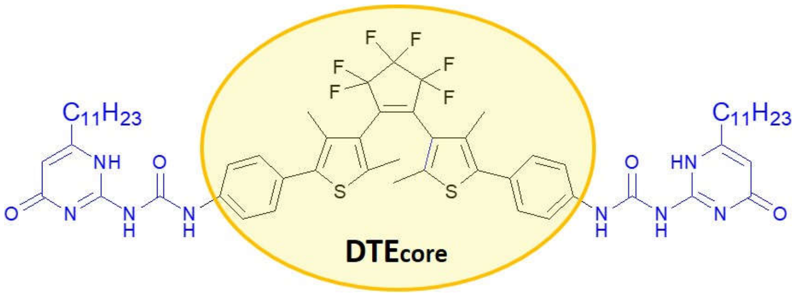

Figure II-3: Chemical structure of DTE-UPy with DTEcore in yellow and the UPy-groups in blue.

II.1.2. PEB-UPy thermoplastic elastomer

Synthesis protocol of PEB-UPy was adapted and optimized from several protocols described in the literature and more particularly from the synthesis reported by Meijer et al. [2].

In these supramolecular polymers, the main principle is that PEB monomers are bi-functional molecules. They are expected to connect two strongly dimerizing UPy-groups with an intermediate linker.

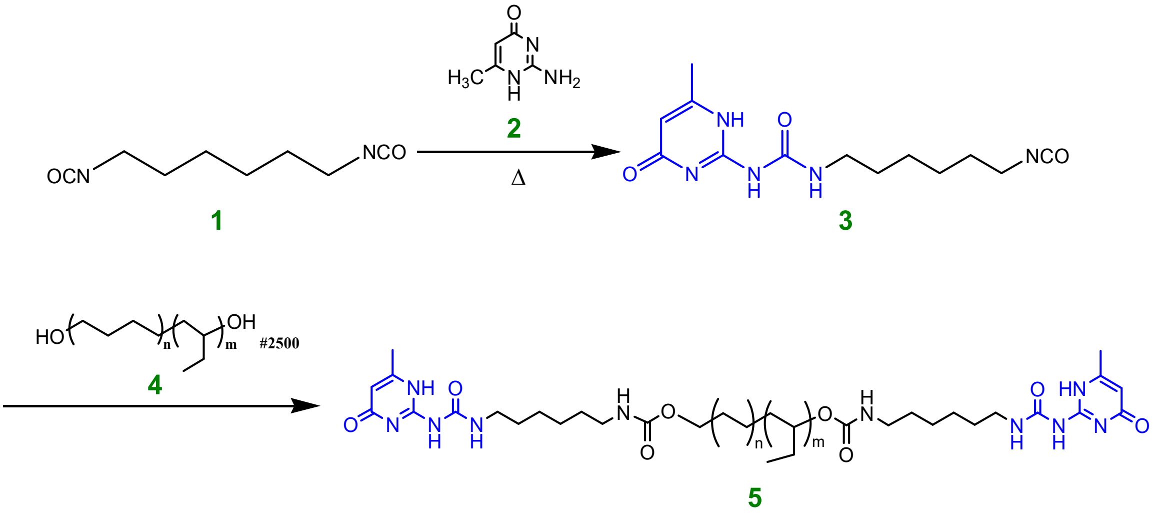

Figure II-4: Synthesis of telechelic PEB-UPy.

As mentioned in Figure II-4, the synthesis is based on two steps. The first step involves coupling of fourfold excess of the methylisocytosine **(2)** to hexamethylenediisocyanate **(1)**, which are commercially available. From the reaction of mixture, the obtained precipitate represents an ureidopyrimidinone (UPy) with an isocyanate function attached into a linker chain **(3)** that can easily react on hydroxy telechelic polymers. For this propose, a telechelic polymer PEB$(OH)_2$ commercially available with a molecular weight of 2500 g/mol is applied. PEB$(OH)_2$ is a hydrogenated random copolymer of 1,2- and 1,4-polymerized of 1,4-butadiene units. The two-hydroxyl end group of $PEB(OH)_2$ **(4)** are functionalized with the issued **(3)** involving the formation of urethane group. The UPy-end PEB **(5)** was accurately determined.

II.2. Sample preparations

II.2.1. DTE recrystallization

Recrystallization is one of the most commonly used method to re-reform crystals with well-defined sized-shape and with purer content than those of the original sample (solute). Although the choice of solvent is a critical parameter to succeed the recrystallization, this impediment can be surmounted by using in most cases a mixture of two organic solvents with different polarity characteristics toward the solute [3-5]. In order to explore the potential of DTE photoswitch commercially available as a raw white powder noted DTEpwd, recrystallization of raw powder is applied.

DTEpwd is re-dissolved in hexane/acetone solvents. Moreover, a subsequent slow evaporation is followed. Once the solution saturation is reached, the crystals start to re-develop while continuing the slowly evaporation. Such process can take time ranged between one day and few weeks. When recrystallized, block-shaped crystals are obtained. These crystals are noted DTErecrys.

II.2.2. DTE-UPy precipitation

As it has been explained in Chapter I, DTE-UPy photoswitchs self-assemble to each other through the UPy recognition patterns allow monomers to make quadruple hydrogen bondings and then form a supramolecular assembling [6]. Large supramolecular assembly is observable only for the rigid CF conformers because the conformers are too flexible to sticks themselves within large proportion (only small oligomers are expected).

The synthetized DTE-UPy (OF) is dissolved in chloroform. According to the supramolecular principle, these species are expected to only form the self-assembly of small oligomers. Such assembly obtained from raw powder is denoted DTE-UPy_{pwd} (OF).

When the solution of the DTE-UPy (OF) in chloroform is irradiated with UV light, the colorless solution turns into blue due to photocyclisation process. Concurrently, the accumulating CF starts to precipitate (noted DTE-UPy_{prp}) suggesting high aggregation of the CF-monomers compared to OF-monomers.

Note that the size distribution of the aggregation process is reported to be dependent to the solution concentration. Indeed, blue precipitate appears from initial concentrations up to 200 µM (Figure II-5).

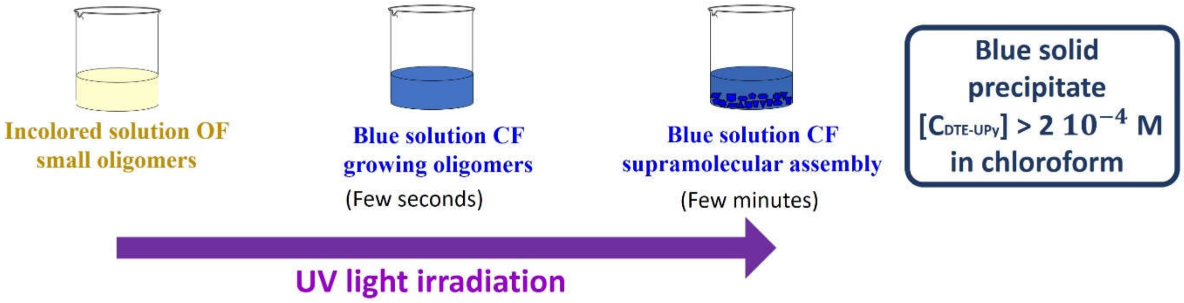

Figure II-5: Schematic illustration of precipitate formation.

For this propose, chloroform solution of DTE-UPy are prepared (5.10-3 M). The first few seconds of UV irradiation evidenced the apparition of blue precipitate floats within the solution surface. The photogenerated precipitate upon UV light was collected and then dried under vacuum.

In this study, DTE-UPy$_{pwd}$ (OF) and DTE-UPy$_{prp}$ (CF) will be investigated in Chapter IV.

II.2.3. Thin film preparation

II.2.3.1. PEB-UPy thin film

The thin film elaboration method is tuned in order to investigate the impact of the elaboration process on PEB-UPy arrangements and morphology. The synthetized PEB-UPy is dissolved in chloroform at 50°C and then stirred at room temperature as shown in Figure II-6.

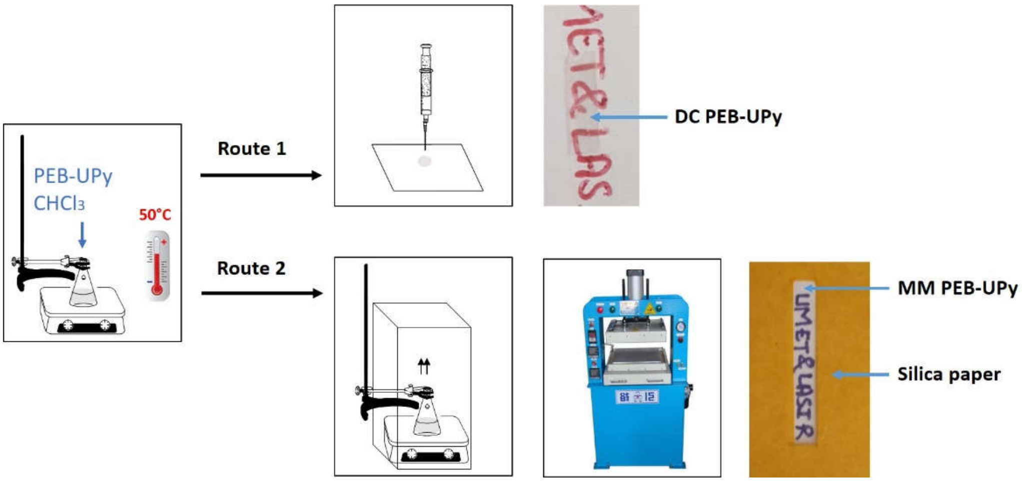

Figure II-6: Schematic illustration of PEB-UPy thin film elaboration.

Two different routes are followed. For the first route (route 1), the solution is drop cast on PTFE plates in order to obtain the drop cast thin film (designed DC PEB-UPy). For the second route (route 2), the solution is covered for slow solvent evaporation. Once chloroform evaporates, the recovered product is hot pressed at 120°C (100 bars) in order to obtain the melt molded thin film (designed MM PEB-UPy). Both DC PEB-UPy and MM PEB-UPy were dried under vacuum at room temperature.

II.2.3.2. PEB-UPy/DTE-UPy thin film

In solution, the DTE-UPy/PEB-UPy system with approximately equimolar ratio of (DTE-UPy: PEB-UPy) leads to a supramolecular assembly. Typically, we have chosen a mass ratio (DTE-UPy: PEB-UPy) being (1:3) to be sure that every DTE-UPy will make hydrogen bonds with PEB-UPy.

The thin films are elaborated using two different techniques: the drop casting (DC) and the melt molding (MM). In order to highlight the role played by possible DTE-UPy precipitation, DC solutions were proceeded in different ways. Indeed, precipitation of CF large assembly depends on concentration: the higher is the initial [CF] concentration, the larger is the supramolecular system CF≡CF≡…≡CF≡CF. The most difficult step is the solvation of such precipitate, whereas the easiest is its precipitation. To avoid precipitation before DC, a column reflux has been mounted to the reactor. By consequence, two DC procedures were employed: drop cast non-refluxed solution (noted DC-NR) and drop cast refluxed solution (noted DC-R). The detailed procedures are illustrated in the Figure II-7.

For this propose, PEB-UPy is dissolved in chloroform and stirred at 55°C in order to dissociate small oligomers if they exist (step 1, Figure II-7a and Figure II-7b). Once dissolved, DTE-UPy

(OF) is added to the solution and then heated at 55°C for 1 hour (step 2, Figure II-7a and Figure II-7b) under sonication. For the DC-R solution, after the PEB- DTE-UPy/PEB-UPy solution is refluxed for 2 hours (step 5, Figure II-7a). Whereas in DC-NR, solution is not refluxed. Concurrently, the solutions from the three described procedures are irradiated with excitation wavelength of 570 nm (step 3, Figure II-7a and Figure II-7b) and subsequently with excitation wavelength of 302 nm (step 4, Figure II-7a and Figure II-7b) while stirring during 1 hour.

The drop casting is considered as conventional film formation method with the lack of the adequate control of thin film characteristic such as an inhomogeneous thickness. Both DC-NR (step 5, Figure II-7a) and DC-R (step 6, Figure II-7a) solutions are cast on PTFE plate combined with ultrasonic substrate vibration in order to control the good distribution of sample on the substrate. Unfortunately, solution volume injected with glass syringe on the substrate surface is not controlled. After pouring the appropriate volume of solution, the substrate is left in darkness under room temperature for at least 1 day. Once the chloroform evaporated, the resulting DC-NR and DC-R thin films are cut using a scalpel.

Contrarily to the DC solutions, the MM solution are covered for slow evaporation of solvent (step 5, Figure II-7b). The obtained product is hot pressed at 120°C in order to obtain the MM-NR thin film (step 6, Figure II-7b). All films are dried under vacuum at room temperature.

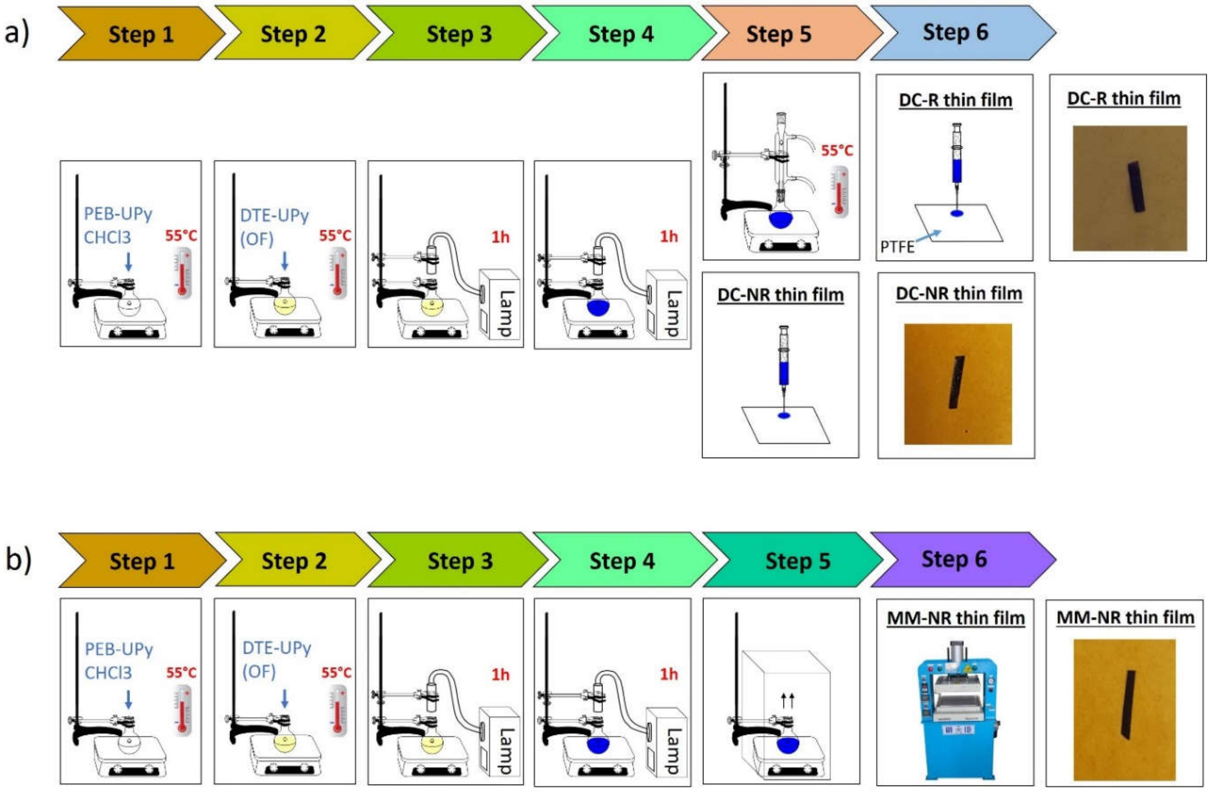

Figure II-7: Schematic illustration of DTE-UPy/PEB- UPy thin film elaboration: a) DC thin film. b) MM thin film.

II.3. Characterization methods

II.3.1. Irradiation system

Preparations of DTE, DTE-UPy in both solution and thin film in CF or OF were carried out upon exposure in situ to Visible or UV irradiation respectively. The adopted device is based on an optical fiber connected to a UV-Visible Hamamatsu LC8 lamp as shown in Figure II-8. The LC8 combines a mercury-xenon lamp (200 W). Therefore, two types of Band-pass filters are provided for selecting the irradiation light (240-400nm and 400-700nm). In optical fiber output, a lens is used to collimate the light beam on the sample. In order to select the excitation wavelength, an additional interference filter centered at 302 nm (UV-light, 3 mW/cm^2) or at 575 nm (UV-light, 5 mW/cm^2) are interposed at the optical fiber output.

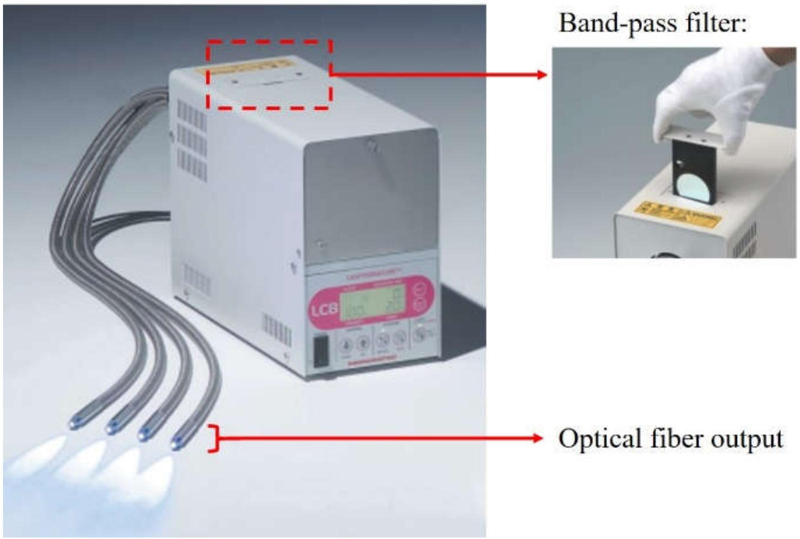

Figure II-8: UV-Visible Hamamatsu LC8 lamp used during this PhD.

II.3.2. Photochromic properties

The photochromic reaction of dithienylethene between OF and CF was evidenced through UV-visible spectroscopy. The efficiency of this reaction is highlighted via photocyclization and photoreversion yields. Herein, details about the applied stationary technique and the involved procedure are developed.

II.3.2.1. UV-Visible stationary absorption spectroscopy

The stationary UV-visible absorption spectra of the photochromic molecules in solution or thin films are recorded via a CARY100 bio-visible UV-Vis spectrometer (VARIAN). The spectral range covers the 200 and 800 nm. In the case of solution, chloroform is always taken as a reference. The stationary measurements are performed in dual front beam mode at room temperature using a fused silica cuvette of 1 cm optical path for concentrations ranging from 10^{-5} to 10^{-6} mol.L^{-1}. For thin film case, the air is used as reference. The stationary measurements were performed in single front beam mode at room temperature.

II.3.2.2. Quantum yield calculations

As mentioned in Chapter I, accessing to the quantum yield is necessary to quantify the efficiency of photochromic systems. For this propose, a method developed by Métivier et al. [7] was applied to determine the photochemical parameters. The method that does not required a reference compound is based on spectrokinetic measurement type A→B. The set-up combining homemade spectrometer and light irradiation in situ is illustrated in Figure II-9.

Experimentally, a coloration (OF→CF) or decoloration (CF→OF) kinetics, typically absorbance of CF as a function of time, is registered for low concentrated solution until PSS is reached. Then, the resulting curve is fitted numerically starting with a chosen kinetics models (set of differential equations). The constant inputs are: the excitation and observation wavelength, the exact volume in the cell, the molar fraction of starting reactant and the exact intensity of exciting light (measured independently with a multimeter). The parameters are the extinction coefficients at both excitation and observation (in principle, those value have to be kept constant). Finally, the variables are the quantum yields for both reactions and possible thermal constants (kept to zero for bistable DTE).

Moreover, this photokinetic method is accessible thanks to the development of continuous millisecond photolysis device allowing rapid monitoring of absorbance over the irradiation time. As mentioned in Figure II-9a, a low concentrated photochromic solution is prepared in cuvette and absorption measurements are carried out in situ upon UV and visible irradiations. The spectrum acquisition is carried out within 0.7s and collected within the light exposure time, for at least 3000 seconds.

As is has been developed in Chapter I, dithienylethene photoswitch has two forms, the open form (OF) and the closed form (CF). Both forms absorb in the UV and only form CF absorbs in the visible. The monitoring of the reaction in the visible is preferred because we only probe the form CF. However, the observation wavelengths are at 575 nm regardless the UV or visible irradiation as depicted. Indeed, the excitation wavelengths are respectively 313nm (UV light) and 575nm (visible light). Figure II-9b presents the molar absorption coefficient as a function of wavelength.

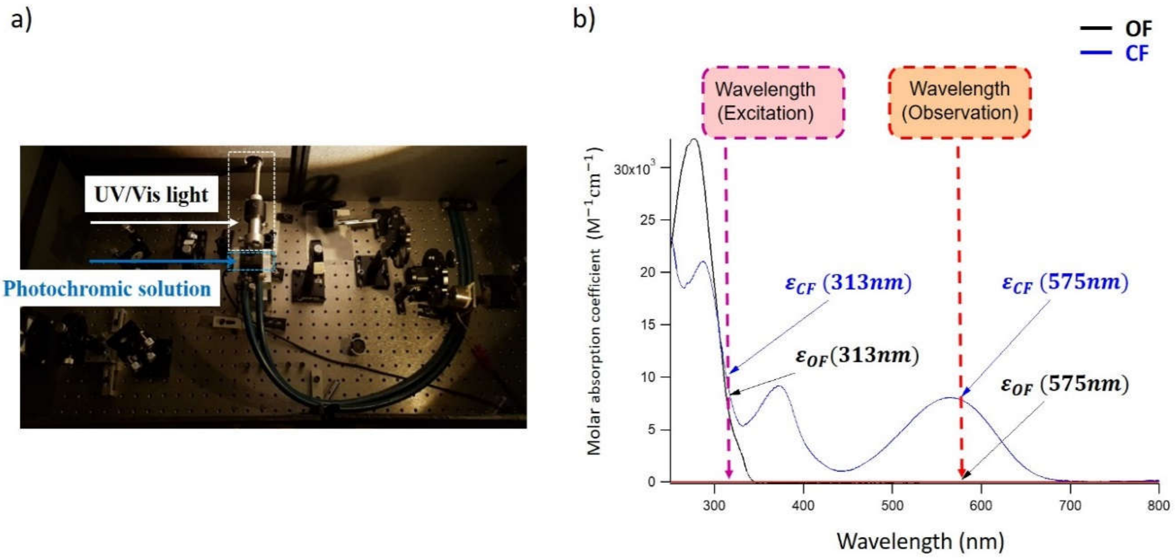

Figure II-9: a) Set-up photolysis device. b) Molar absorption coefficient as a function of wavelength.

The determination $\phi_{OF\rightarrow CF}/\phi_{CF\rightarrow OF}$ needs the access to the molar absorption coefficient and molar fraction. The applied equations are as following:

$$\varepsilon_{OF} = \frac{A_{OF}}{I\ C_0} \tag{II.1}$$

$$\varepsilon_{CF} = \frac{A_{PSS} - A_0(1 - \alpha_{CF})}{I\ C_0 \alpha_{CF}} \tag{II.2}$$

where A_{OF} and A_{PSS} are the absorbance of OF and PSS respectively. C_0 is the solution concentration α_{CF} is the mole fraction of CF.

According to Beer-Lambert law, the progress of the photocyclization reaction α is:

$$\alpha_{CF} = 1 - \frac{I_{PSS}}{I_{OF}} \tag{II.3}$$

where I_{OF} and I_{PSS} are the intensities of OF and PSS respectively. The absorption spectroscopy is combined with NMR measurements in order to determine the intensity ratio of the NMR peaks of the OF and CF. Alternatively, this value can be determined from fitting procedure outputs.

II.3.3. Photomechanical measurements

II.3.3.1. Macro-scaled measurements

With the aim to predict macroscopic photomechanical effectiveness upon irradiation with UV and visible lights, a homemade device was developed as illustrated in Figure II-10. Measurements are carried out on thin film with well-defined geometry. Thin film is hold from one extreme of the longest dimension into a metallic clamp. Thus, thin film is irradiated with 302 nm (3 mW/cm^2) light from the left side and then irradiated with visible light 570 nm (5 mW/cm^2) from the left side. Thus, light irradiation generates a force perpendicularly to the thin film surface. As response, the thin film may occur photomechanical behavior. The thin film evolution of the expected deformation as a function of exposure time is quantified by analysis the resulting images using the ImageJ software.

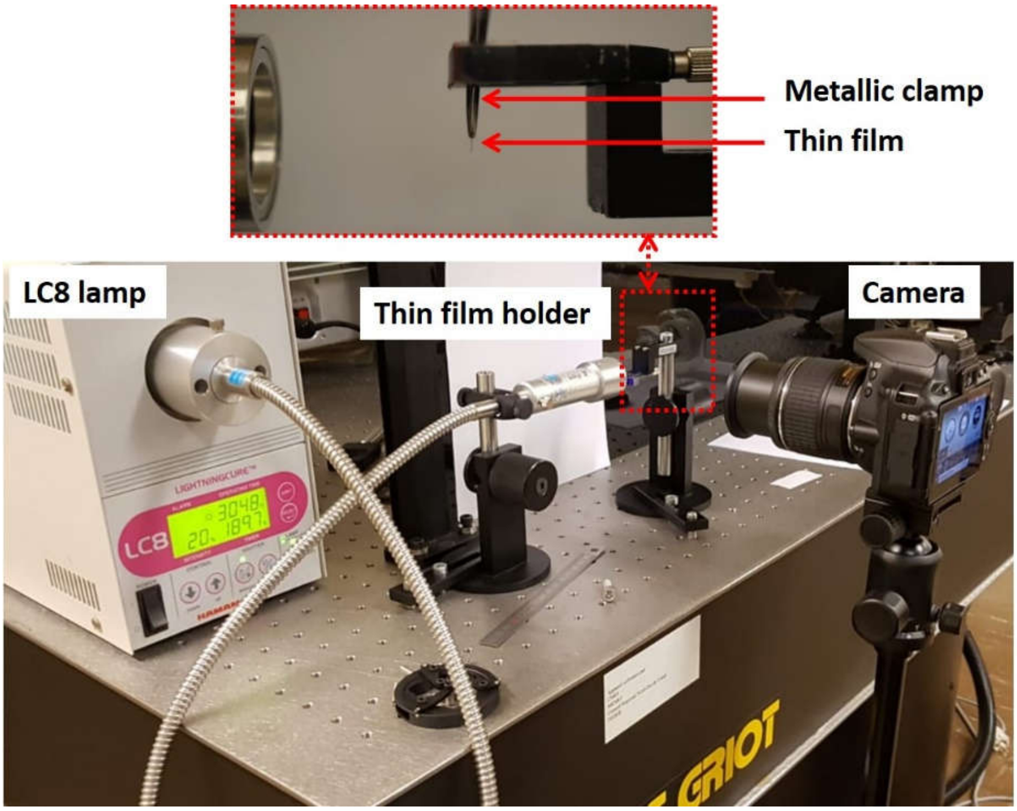

Figure II-10: Schematic illustration of the macroscopic experimental setup.

II.3.3.2. Micro-scaled measurements

Wild-field microscope with in-situ UV-visible irradiation was developed in the PSSM Laboratory (ENS Paris-Saclay) in order to investigate in details, the relationships between the photophysical properties of the materials in the solid state and their photomechanical response at the micro-scale. Accordingly, this configuration can be used to collect light on a solid sample, record optical intensity images and transmission spectra upon UV-visible light exposure.

The schematic description of this instrumental setup is illustrated in Figure II-11. Thus, the optical microscope is designed to operate in the wide-field with continuous-wave or pulsed lasers. Furthermore, it is possible to monitor a large variety of optical signals including transmission or scattering in a wide range of wavelengths (330-850nm) on (i) a conventional CCD camera applied for spectroscopy acquisitions and (ii) a high sensitive EM-CCD camera accurately used to the optical images.

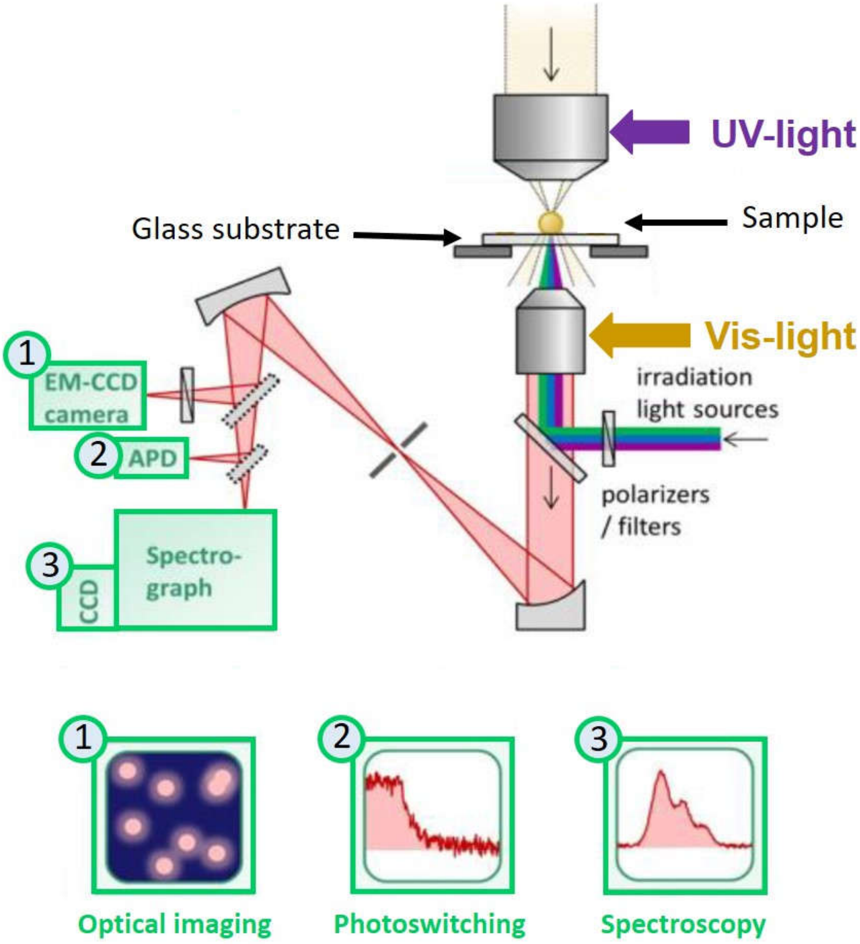

Figure II-11: Schematic description of the wild-field microscopy with in-situ irradiation available at the PSSM laboratory.

This device will enable to follow shape changes (subsequent optical images within defined range time) but also optical modifications such as coloration-discoloration of the materials under light illumination.

After deposition of sample on a glass substrate, photo-induced mechanical effect is investigated upon irradiation from upper side with UV light (313nm, 44µW/cm^2) and from lower side with visible light (550nm, 12mW/cm^2). Indeed, the level of light attenuation within the sample is followed by absorption spectroscopy and correlated to the mechanical deformation recorded by the in-situ optical microscope.

Moreover, thanks to the possibility offered by the optical images recorded under microscope in a time exposure range, photoinduced microscaled changes of materials can be highlighted by plotting their kinetic evolution measured on a well-defined area. The deformation evolution followed using ImageJ software.

II.3.4. Chemical characterization

Nuclear Magnetic Resonance NMR 1H is a technique widely used in chemistry to allow the identification and characterization of organic molecules. This technique was used to determine the fraction of Polybutylene (PB) in thermoplastic elastomer PEB.

The NMR principle is based on the observation of transitions between different energy levels. In the absence of a magnetic field ($\vec{B}$), the nuclei spins are oriented in a random manner. Thus, the total magnetic moment is therefore zero. When the system is immersed in a magnetic field, the spins align within $\vec{B}$ direction and then the sample acquires a total magnetization. The main principle of NMR spectroscopy is to unbalance this system and measure the necessary time to return to its original state. By applying a pulse with very short duration at the proton resonant frequency, the total magnetic moment achieves a reorientation. When this pulse ceases, the system returns to its equilibrium state. By relaxing, the total magnetic moment induces an alternating current in a coil generating the NMR signal of the concerned nucleus.

The spectrum is composed of several peaks providing information about the local environment of the nuclei (symmetry, number of close neighbors), the cores number of concerned by the signal, etc.

NMR experiments are performed with the Brüker Avance III 400MHz spectrometer equipped with a QNP probe for 1H, 13C and 19F mono or two-dimensional analysis. For this study, only proton NMR are used and NMR spectrum are obtained at room temperature. To perform the NMR analyzes, 10 mg of PEB material was dissolved in 1 mL of chloform-d2 at 50 °C under stirring.

II.3.5. Thermal properties

Thermal analysis involves techniques where the sample exhibits the change of properties related to a variation of temperature.

II.3.5.1. Thermogravimetric Analysis (TGA)

Thermal gravimetric Analysis (TGA) is a thermoanalytical technique that measure the amount and rate of change in weight of a polymer material over both temperature and time under controlled atmosphere. It can provide valuable information regarding thermal stability, degradation characteristics, failures in the aging/life cycle, and kinetics of chemical reactions.

A TGA analysis is performed by gradually raising the temperature of the sample in a furnace. The sample weight is measured by a sensitivity-calibrated drive coil. If a thermal event involves loss of a volatile component, a mass loss is observed through the differential mass measurement. The weight is measured on an analytical balance that remains outside of the furnace. The collected thermogravimetric data is compiled into a thermogram of sample mass or percentage of its initial mass plotted against temperature or time. The derivative curve of TG allows the determination of material mass loss rate and then the identification of the main decomposition steps.

Herein, the TGA is used to evaluate the thermal stability of a materials upon heating and determine their degradation temperature. The applied technique is carried out on a TGA-Q5000 of TA instruments calibrated according to standard procedures. For the analyses, samples (6-10 mg) are placed in open vitreous alumina crucibles, and then heated at nominal heating rate of 10°C/min. The mass loss is characterized in the range from 30 ºC up to 700°C. The experiments are conducted in flowing of oxidative atmospheres.

II.3.5.2. Differential Scanning Calorimetry (DSC)

Differential Scanning Calorimetry (DSC) is a method of thermal analysis in which the variation of enthalpy is measured under controlled range of temperature. Thus, characteristic transitions can be revealed as first-order of phase transition (melting, crystallization) and/or second-order of phase transition (glass transition).

The principle underlying this power compensated DSC is that the sample and the reference material are placed in the two different furnaces under controlled atmosphere and then, thanks to a platinum probe, the evolution of the temperature of the device is controlled and recorded (Figure II-12). The integral loop allows the programming of a rise in temperature of the sample (T_1) and the reference (T_2). The differential loop, adjusts the heating power so that at each moment T_1 is equal to T_2, by compensating for the exothermic or endothermic events of the sample. The electrical power difference between the sample and reference measures the heat flow of the sample. The plotted data presents the heat flow against temperature, called thermogram, where T_g, T_{crys}, T_m are the temperature of glass transition, the temperature of crystallization and the temperature of melting.

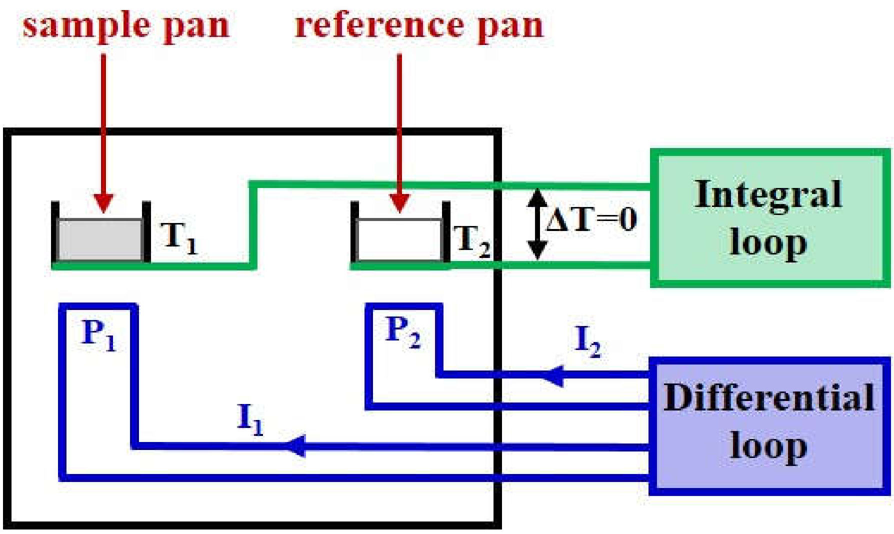

Figure II-12: DSC principle.

Thermal characterization of samples was performed with a DSC-Q20 Perkin-Elmer instrument calibrated according to standard procedures. For the analyses, samples (4-10 mg) are placed into aluminum pans and heated at a rate of 10°C/min in a nitrogen atmosphere. The temperature range is defined according to the degradation temperature of sample obtained by means of TGA.

In the case of endothermic event (melting) and exothermic event (crystallization), the integration is performed with the TA Instruments Universal Analysis software. The crystallinity of the sample is calculated from the melting and crystallization enthalpies using equation reported in Table II-1.

Table II-1: Calculation of crystallinity level.

Sample	**Crystallinity**
DTE	$\chi_c = \frac{\Delta H_m - \Delta H_c}{\Delta H_m^0}$
PEB	$\chi_c = \frac{\Delta H_m}{\Delta H_m^0}$
PEB-UPy	$\chi_c = \frac{\Delta H_m}{\Delta H_m^0}$
DTE-UPy/PEB-UPy system	$\chi_c = \frac{1}{f}\left(\frac{\Delta H_m}{\Delta H_m^0}\right)$

With:

- ΔH_m: peak area of melting.
- ΔH_c: peak area of cold crystallization.
- ΔH_m^0: standard enthalpy of melting. The ΔH_m^0 of a polyethylene when supposed to be 100% crystalline is about 288 J/g [8].
- f: the polymer fraction

In the case of DTE-UPy/PEB-UPy system, 1eq of DTE-UPy and 3eq of PEB-UPy leads to 4eq in solution. The value f of PEB-UPy is then 0.75.

II.3.6. Viscoelastic properties (DMA)

Because of their viscoelastic behavior, polymeric materials may exhibit variations of mechanical properties as a function of frequency and temperature. It is possible to characterize these viscoelastic properties by dynamic mechanical analysis (DMA) in various modes including tension, traction or torsion. During DMA experiment, a sinusoidal uniaxial strain with a small amplitude is applied in order to remain in a linear regime.

The imposed strain on the sample follows the equation:

$$\varepsilon(t) = \varepsilon_0 \sin(\omega t) \qquad (II.4)$$

where ε_0 and ω represent the imposed amplitude of strain and the frequency of strain ($\omega = 2\pi f$), respectively.

The resulting response to the imposed strain is a sinusoidal stress, which is measured over the time. However, it may have a phase angle with respect to the imposed strain that indicate the degree of viscoelasticity in the material. The resultant stress on the sample follows the equations:

$$1\,\sigma(t) = \sigma_0 \sin(\omega t + \delta) \qquad (II.5)$$

$$\sigma(t) = \sigma_0 \sin(\omega t)\cos(\delta) + \sigma_0 \cos(\omega t)\sin(\delta) \qquad (II.6)$$

where σ_0 represents the resulted amplitude of stress and δ is the phase angle between stress and strain.

When δ=0°, the phase is indicative of a purely elastic material according to Hooke's law $\sigma = E\varepsilon$. Whereas, a full phase lag (δ=90°) is indicative of purely viscous material. Two characteristic parameters can then be defined:

E', the storage modulus that measure of the elastic response of a material.

$$\mathrm{E}' = \frac{\sigma_0 \ \cos(\delta)}{\varepsilon_0} \tag{II.7}$$

E'', the loss modulus that measure of the viscous response of a material.

$$\mathrm{E}'' = \frac{\sigma_0 \ \sin(\delta)}{\varepsilon_0} \tag{II.8}$$

The associated loss factor (tan δ) is related to the storage and loss modulus as follows:

$$\tan(\delta) = \frac{E'}{\mathrm{E}''} \tag{II.9}$$

Dynamic mechanical measurements were performed on RSAIII model (TA instrument). A parallelepiped thin film sized $7 \times 2.5 \times 0.07$ mm^3, is subjected to a sinusoidal strain in tension mode. The amplitude of the sinusoidal deformation ($\varepsilon_0 = 0.01\%$) is kept constant at a frequency of 1 Hz. The measurements were carried out over a temperature range of -80°C and 100°C with a heating rate of 2 °C/min.

II.3.7. Structural properties

II.3.7.1. Wide angle X-ray scattering (WAXS)

Wide Angle X-Ray Scattering (WAXS) is a technique used to characterize the structure of a polymer material at the atomic scale. This technique relies on radiation-matter interactions. The diffraction is carried out in transmission mode. The investigated sample is exposed to a monochromatic X-ray beam. A part of the beam is diffracted by the crystalline planes in position of Bragg at 2θ angle and another part is diffused by the amorphous phase of the sample. The WAXS principle is schematically illustrated in Figure II-13.

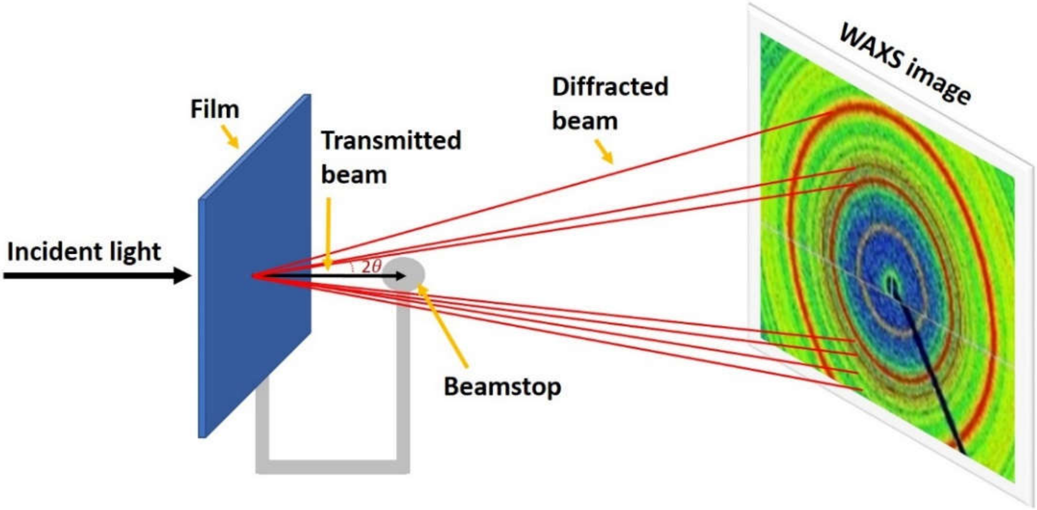

Figure II-13: Schematic illustration of WAXS principle.

According to the Bragg law, the half angle of deviation θ can be associated to the inter-reticular distance of the planes hkl (d_{hkl}).

$$n\lambda = 2\, d_{hkl} \sin(\theta) \qquad (II.10)$$

where n the diffraction order and λ the wavelength of X-ray beam.

The calculated distance d_{hkl} allows the determination of the crystalline unit cell parameters and thus to identify the crystal phases of the material.

Diffraction pattern depends on the structural organization within the sample. In the case of an isotropic amorphous material, only a broad and diffuse halo is observed as shown in Figure II-14a. Whereas an isotropic semi-crystalline polymer leads to intense rings additionally to its amorphous halo as shown in the Figure II-14b.

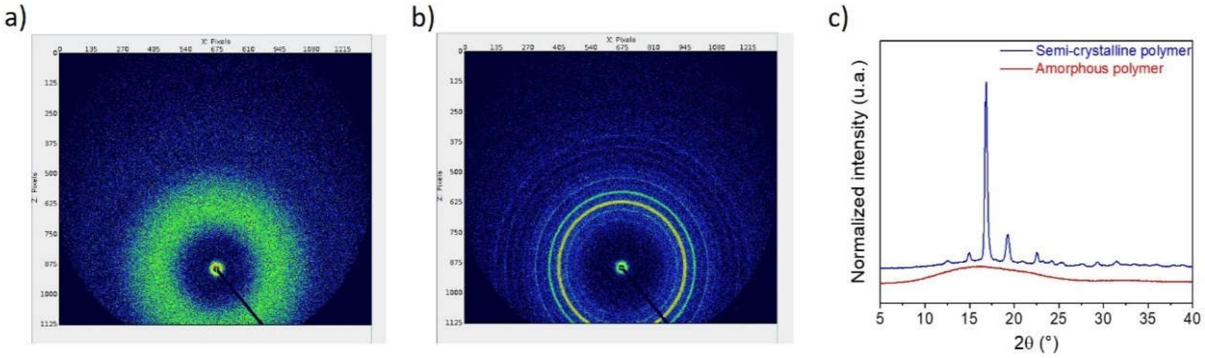

Figure II-14: Examples of WAXS patterns: a) amorphous and b) semi-crystalline polymers and c) the corresponding integrated profiles.

WAXS measurements were performed via diffractometer with a Micro-source source Genix Collimated Cu (Xenocs). The source is equipped with a copper anticathode tube. The used radiation is the copper Kα line (λ = 1.54 Å). The acceleration voltage is 50 kV and the intensity of 1 mA. The diffracted signal is collected on a CCD Photonic Science camera. The sample-camera distance is set at about 12 cm to obtain a range of 2θ between 5° and 28°. The samples are analyzed in glass capillary. The average exposure time is 5 minutes and the acquisition rate for temperature experiments is 10°C/min.

The WAXS pattern is radially integrated using Fit2D® software to obtain the intensity profile as a function of the 2θ angle (Figure II-14c). The diffractogram allows the identification of crystal phases by indexing the diffraction peaks. Peak fit® software is used for the diffractogram deconvolution.

II.3.7.2. Small angle X-ray scattering (SAXS)

Small angle X-ray scattering (SAXS) probes the structure at nanometric scale. From a technical point of view, the experimental setup is similar to that of WAXS measurements. The only difference is that the distance between the sample and the detector varies and is 1001 mm.

To overcome the air diffusion phenomena, a vacuum section is placed between the sample and the detector. The integrated SAXS image leads to a diffractogram (Iq^2) as a function of the diffusion vector q, independent to wavelength of incident light. The scattering vector q is defined as following:

$$q = \frac{4\pi \sin(\theta)}{\lambda} \qquad (II.11)$$

In semi-crystalline polymer, X-ray diffusion leads the access to the long period (L_p) because of the difference in electron density between amorphous (L_a) and crystalline (L_c) distributions. This periodicity is defined as a repetition distance occurred between L_a and L_c blocks (Figure II-15b). In some case, a distance different from L_p and defined as a correlation distance d_c (Figure II-15c) can be observed. In order to calculate L_p or d_c, Iq^2 is represented as a function of scattering vector q (Figure II-15a).

$$L_p = \frac{2\pi}{\mathrm{q}_{max}} \qquad (II.12)$$

$$d_c = \frac{2\pi}{\mathrm{q}_{max}} \qquad (II.13)$$

where q_{max} represent the q-value at the maximum of diffusion.

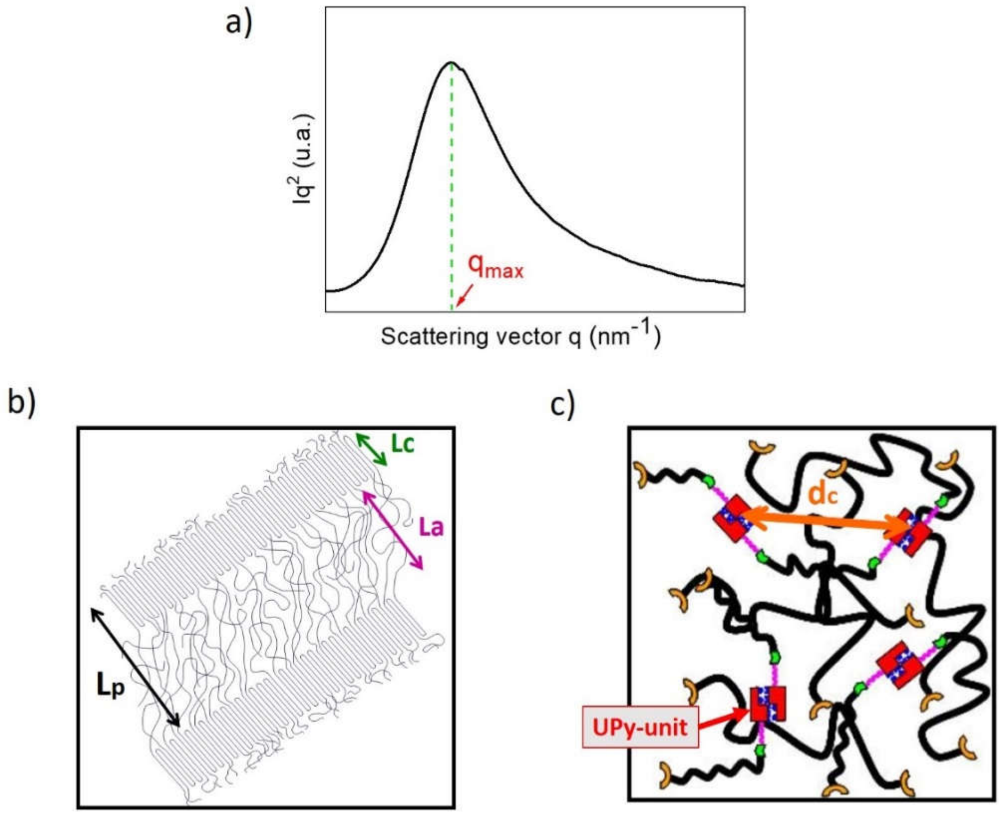

Figure II-15: a) SAXS profile of Lorentz representation Iq² =f(q). Schematic representation of b) long period Lp and c) correlation distance dc (in orange). [9]

Evolution of structural rearrangements upon heating/cooling are studied using SAXS experiment. Temperature-dependent profiles during heating/cooling cycles are recorded with a rate of 10°C/min using a remote-controlled Linkam DSC stage.

II.3.7.3. Synchrotron radiation

Synchrotron radiation induces an X-ray beam much more intense and brilliant than that generated by laboratory equipment. These X-rays are produced by a high-energy of electrons moving at a highly speedness rate. The experiments were carried out at the European Synchrotron Radiation Facility (ESRF) in Grenoble (Figure II-16).

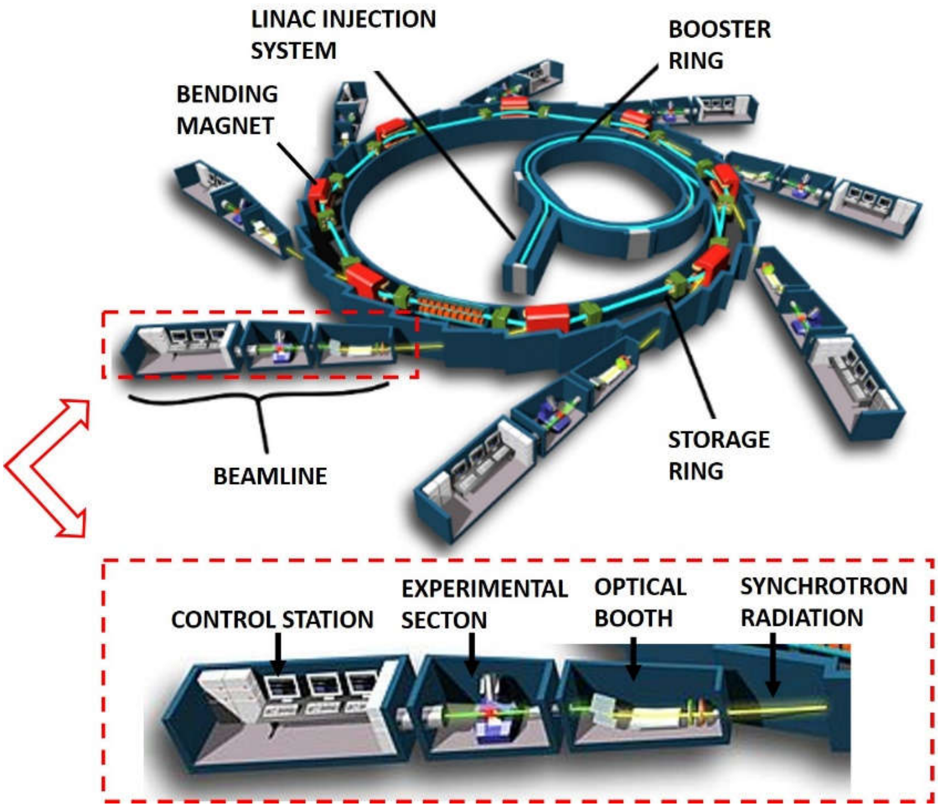

Figure II-16: Schematic illustration of synchrotron and beamline details.

Synchrotron is obtained following 4 principle divisions. At first, the electrons are generated and then accelerated linearly in the LINAC (LINear ACcelerator). They pass to the booster (circular accelerator of about 300 meters in circumference) in which, they make several thousand turns in order to reach their final energy of 6 GeV in few minutes. Once this energy level is reached, they are injected into the storage ring (about 800m in diameter at the ESRF) where they circulate for several hours at constant energy. During their circulation, the electrons pass through different types of magnets. They undergo accelerations and lose energy by emitting electromagnetic radiation designed synchrotron light. This radiation is sent to different beamlines (44 beamlines in ESRF) where the experiments take place.

Moreover, every light line is composed of three elements:

Optical booth: where optical instruments are found in order to give the beam the necessary characteristics for the experiment to be carried out.

Experimental booth: which contains the experimental device where the sample and the detector are positioned;

Control station: which groups together the various elements to control the experience and manage data acquisition.

The experiments were carried out on D2AM beamline. This beamline has the particularity of simultaneously recording SAXS and WAXS images. Such particularity allows the structural characterization of the same materials at two different scales.

For our experiments, the energy was fixed at $\lambda = 0.1378$ nm. Furthermore, the WAXS detector was positioned at a distance of 18 cm from the sample and the SAXS detector at 112 cm. These conditions make possible to scan a diffusion vector range of 0.1 to 30 nm^{-1}.

II.3.8. Morphological observations

Scanning electron microscope (SEM) is a technique used to reveal information about material surface including its external morphology i.e. texture and its chemical composition by means of an electron beam. SEM uses a focused beam of high-energy electrons to generate a variety of signals at the surface of sample. The interaction radiation-matter induces the emission of two types of electrons:

- The secondary electrons emitted by the sample surface and gave information relating to the topographic contrast.
- The backscattered electrons emitted by deeper interactions and gave information relating the local chemical composition. Since it depends on the chemical nature of the atoms encountered, the heavier elements will emit more electrons in contact with the incident beam. As result, a brighter phase contrast appears on the SEM photograph.

From SEM observations, thin films were cryo-fractured in liquid nitrogen bath. Thereby deposing thin films on carbon substrate, the SEM topographic examination was carried out directly on sample after coating with a transparent thin layer of carbon in order to make them conductive and thus avoid the effects of charging.

SEM observations in secondary electrons are performed using a SEM FEG Hitachi S4700. The acceleration voltage is about 2kV and the distance of about 10 mm. SEM quantification in backscattered electrons is carried out with SEM JCM 6000 Jeol. The acceleration voltage is about 5kV with a distance of about 10 mm.

The domain analysis in the thin film surface is measured using ImageJ software. In order to assess further the identification and then the quantification of the chemical elements distribution, an energy dispersive X-ray spectrometer (EDX) was coupled with SEM images.

References

[1] Hamdi, I., et al., Excited-State Dynamics of Dithienylethenes Functionalized for Self-Supramolecular Assembly. The journal of physical chemistry. A, 2018. 122(14): p. 3572.

[2] Keizer, H.M., et al., Scale-up of the synthesis of ureidopyrimidinone functionalized telechelic poly(ethylenebutylene). Polymer, 2003. 44(19): p. 5505-5511.

[3] Irie, M., et al., Photochromism of 1, 2-bis (2-methyl-5-phenyl-3-thienyl) perfluorocyclopentene in a single-crystalline phase. Journal of the American Chemical Society, 2000, 122, 4871-4876;

[4] Yamada, T., et al, Crystal Structure− Reactivity Correlation in Single-Crystalline Photochromism of 1, 2-Bis (2-ethyl-5-phenyl-3-thienyl) perfluorocyclopentene, Journal of Organic Chemistry, 2001, 66, 6164-6168.

[5] Kitagawa, D., et al., Control of Photomechanical Crystal Twisting by Illumination Direction. Journal of the American Chemical Society, 2018. 140(12): p. 4208.

[6] Takeshita, M., et al., Photoreversible supramolecular polymer formation. Chemical Communications, 2005(6): p. 761-763.

[7] Metivier, R., et al., Fluorescence Photoswitching in Polymer Matrix: Mutual Influence between Photochromic and Fluorescent Molecules by Energy Transfer Processes. Journal Of Physical Chemistry C, 2009. 113(27): p. 11916-11926.

[8] Sierra, C.A., et al., Thermal and mechanical properties of poly-(styrene-b-ethylene co-butylene-b-styrene) triblock copolymers. Polymer, 1997. 38(17): p. 4325-4335.

[9] Arnaud, G., Réseaux élastomères nanostructurés par combinaison de processus d'assemblages supramoléculaires et de polymérisations, Thèse, L'Institut National des Sciences Appliquées de Lyon, 2008

Chapter III.

New insights toward reversible dynamic motions of dithienylethene supramolecular assembly

In this chapter, we will investigate the photomechanical effect the DTE-UPy molecule core i.e. DTE (DTE molecular structure.). In fact, these DTE molecules were synthesized in 2001 by Pr. Irie [1] (see more details in chapter I) when the surface crystal change was reported upon light irradiation. Except this example, surprisingly, no photomechanical effect was reported for this molecule.

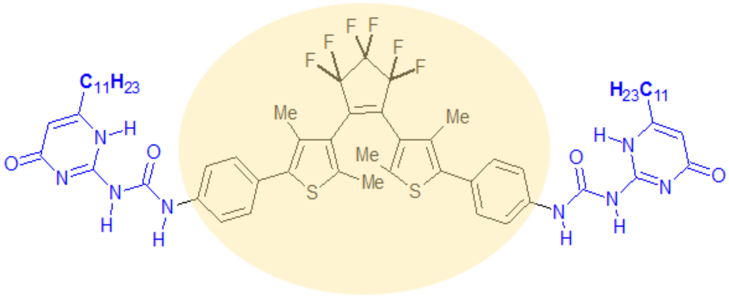

Figure III-1: DTE molecular structure.

Kitagawa and co-workers [2] have investigated photomechanical effect of similar diarylethene to our DTE. The only difference between them is the absence of methylation at the fifth (5,5’) positions of the thiophene rings. Thereby using the different techniques and solvents, recrystallization has led to large block shaped crystals and ribbon shape crystals. These large block shaped crystals were found to not exhibit any photomechanical motion due to their large bending inertia. The ribbon shape crystals photoreversible crystal twisting.

Herein, the first part within Chapter III is dedicated to the investigation of DTE structure and properties. Then, the second part is devoted to highlight the microscopic photomechanical responsiveness of DTE molecules under wield-field microscopy setup with in-situ illumination.

III.1. Photochromism of DTE

Because of the commercial availability of DTE, the photochromism of these molecules have already been characterized in either solution or solid states [3,4]. Photochromic parameters are gathered in Table III-1.

In hexane, DTE undergoes a photochromic reaction as shown in Figure III-2. The colorless OF solution turns immediately to blue color after UV light irradiation with a quantum yield of ϕ_{cycl}=0.46. It is worth to remind that the coloration process is induced by electrocyclization reaction between the two reactive carbons on thiophene rings leading two possible conformations AP and P. Only the AP conformer is photoactive. Then, subsequent irradiation of the blue solution by visible light induces the back reaction and reverts the initial color with lower efficiency ϕ_{rev}=0.015.

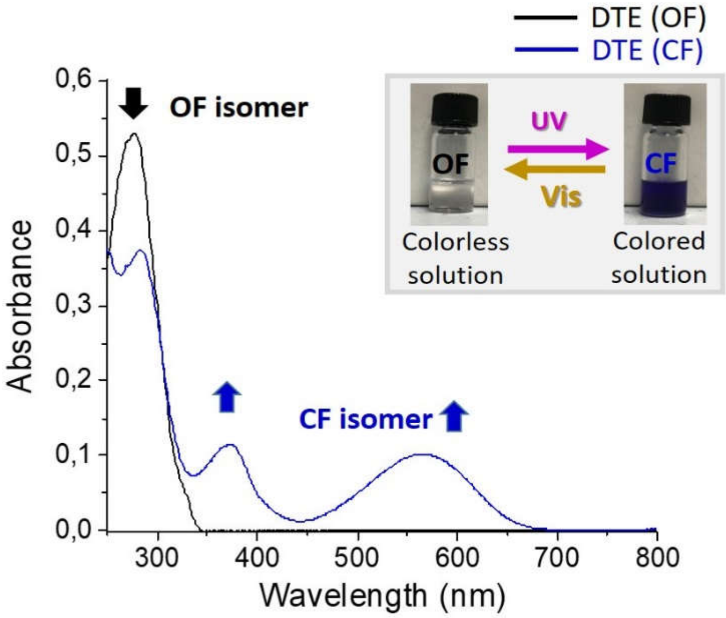

Figure III-2: Absorption spectra of OF-isomers (black solid line) and PSS (blue solid line) before and after irradiation with 313 nm wavelength at room temperature in hexane (1.6×10^{-5} M).

The absorption spectra are presented in Figure III.2. The OF has its characteristic band in the UV region at 268 nm. After a long UV irradiation, the photostationnary state is reached with a conversion efficiency of 79%. Actually, both OF and CF species absorb UV light. This latter is responsible for undesired reversion. From the other hand, CF species present a large band in the visible region, peaking at 562 nm responsible for the blue color.

Table III-1: Absorption characteristic and photochromic properties of DTE in both solid state [3] and hexane[4].

DTE		λ_{abs}^{max}(nm)		α	$\varepsilon(10^4 mol^{-1}\, L\, cm^{-1})$		Quantum yield	
		OF	CF		OF	CF	ϕ_{cycl}	ϕ_{rev}
In Hexane	**Irie et al[a]**	262	562	-	2.8	1.1	0.46	0.015
Crystalline Phase	**Exp[a]**	370	630	1	-	-	0.96	0.027

In solid state, the photocyclisation yield is close to unity [3] due to the fact that the majority of OF molecules belong to the anti-parallel conformation. The photoreversion is two times more efficient compared to solution.

III.2. Thermal analysis of DTE

Melting and crystallization behaviors are processes of prime importance especially for photothermal active materials (see Chapter I). Indeed, the matter thermal properties is required for the best detanglement of pure mechano-optical effect from mechano-thermal effect (or a combination of both).

Diarylethene derivatives are always described as thermally stable photochromic compounds in solution and solid states [5]. In order to study the structural stability of DTE molecules during temperature investigation, TGA measurements were performed on DTE-OF as shown in Figure III-3.

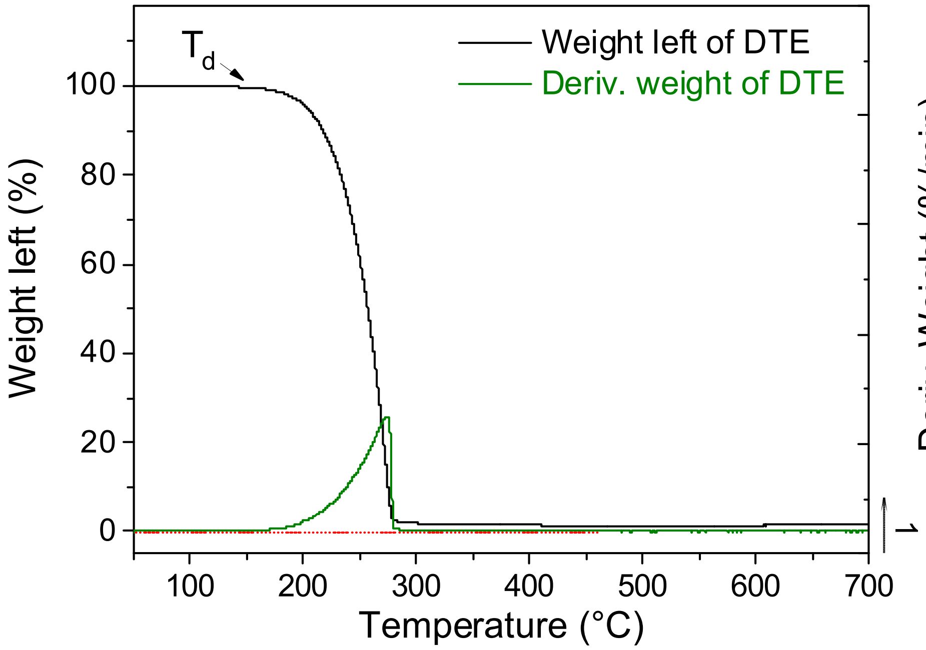

Figure III-3: TGA curve for thermal decomposition of DTE in dioxygen atmosphere.

Under oxidative atmosphere, one stage weight loss is observed. Under heating, the photochromic molecule starts to degrade from 165°C. The main chains of molecules are totally broken down at nearly 300°C. Meanwhile, the TGA curves contain some irregularities mentioning a noticeable residue left up to 700°C assigned to impurities.

As depicted in Figure III-4, DSC analysis was undertaken in order to follow the melting process of crystals and highlight its characteristic temperatures.

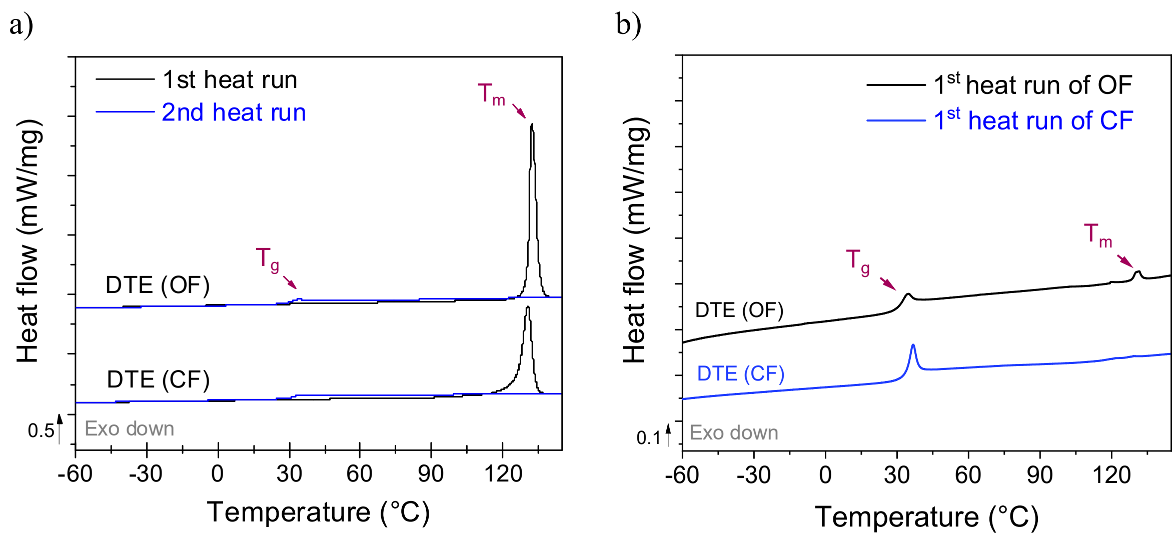

Figure III-4: Crystals heated up to melt of DTE for both OF- and CF- isomers as a function of time. a) First day. b) Four weeks later.

The 1st heating reveals endotherms at 132.2°C and 130.8°C for OF and CF respectively. These endotherms are attributed to the melting of crystals. Surprisingly, the thermograms of the 2nd heating, i.e. after sample cooling from the melt, present only an endothermic step associated to a glass transition. This means that DTE is amorphous. The associated glass transition temperature T_g is about 34°C (OF) and 36°C (CF). However, this amorphous state is stable at room temperature for few weeks as mentioned in Figure III-4.

Table III-2: Thermal properties of DTE.

	OF-DTE		**CF-DTE**	
	1st heat run	**2nd heat run**	**1st heat run**	**2nd heat run**
T_g (°C±1)	34.2	34.4	34.5	35.8
T_m (°C±1)	132.2	-	130.8	-
ΔH_m (°C±1)	63.8	-	53.7	-

Unfortunately, crystallinity level cannot be calculated as the heat fusion of 100% crystalline DTE (ΔH_m°) is missed. As pointed out in Table III-2, comparison of total melting enthalpies (ΔH_m) propose that despite DTE-OF flexibility, these molecules remain slightly more crystalline than CF isomers.

Moreove, a small endothermic peak at 131.6°C characteristic of DTE-OF crystals developpement start to appear and reformulate beginning from the fourth week. In contrast, such melting transition is not detected for DTE-CF sample.

III.3. Structural properties of DTE made by different process method

The structure of DTE will be investigated according to three different process method: i) DTE-powder as received from the commercial company; ii) DTE after a recrystallization procedure in hexane/acetone; and iii) amorphous DTE obtained after cooling from the melt.

III.3.1. DTE powder (noted DTE-pwd)

The proper description of crystalline structure needs a WAXS investigation. As illustrated in Figure III-5a and Figure III-5b, the 2D-patterns of DTE-pwd within its OF- and CF- isomers show several concentric rings related to their high crystalline structures at room temperature. The integrated intensity profiles registered at room temperature are presented in Figure III-5c.

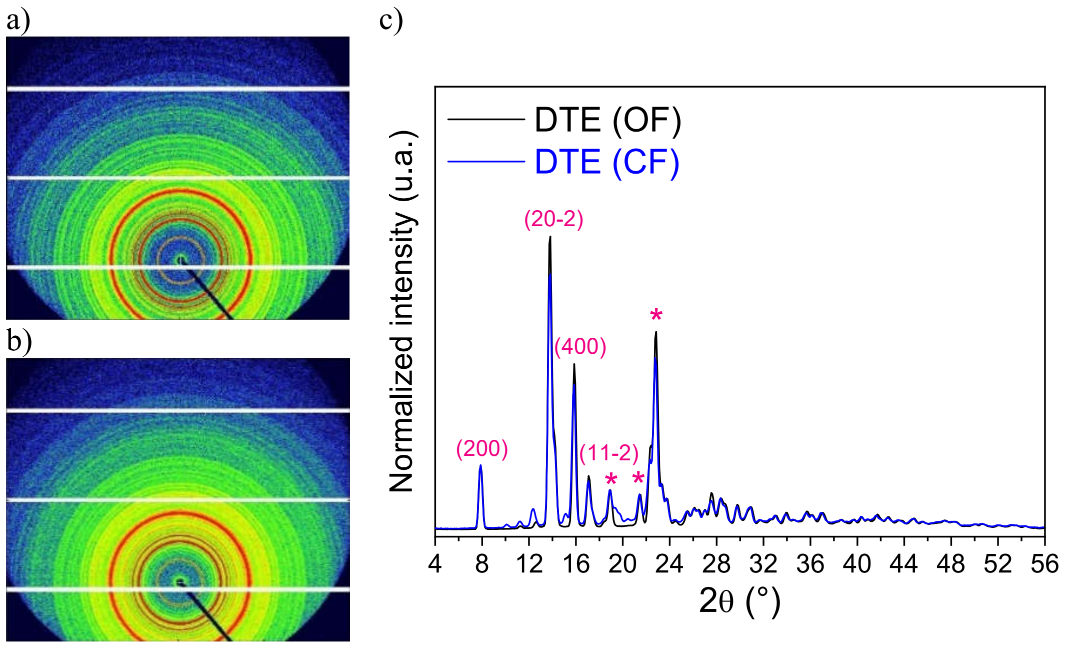

Figure III-5: 2D WAXS pattern of DTE-pwd in a) OF, b) CF and c) the integrated intensity profiles.

Both OF and CF diffractograms appear quasi-similar. In order to understand the crystal structure, the profiles are compared to the WAXS data calculated from a monoclinic arrangement as reported in the literature **[1,6]**. Actually, the dominant peaks at 2θ=13.6° and 2θ=15.6° correspond to the (20-2) and (400) Miller planes, respectively. The smaller peaks at

2θ=7.8° and 16.9° are attributed to (200) and (11-2) Miller planes, respectively. While, for some peaks (noted * in Figure III-5c) at 2θ=18.9°, 21.4° and 22.8°C, it seems difficult to assign even from literature. One tentative explanation is that DTE has different polymorphic crystal forms at room temperature.

It was expected that when the OF will be exposed into UV light to form the CF, the peaks will sharper or shift to lower 2θ-values due to the occurred electrocyclization, but it is not the case.

III.3.2. Recrystallized DTE (noted DTE-recrys)

Recrystallization principle was evoked in chapter II. In order to form DTE single crystals with well-defined size, shape and with purer content than those of the original sample, DTE-pwd (OF) were dissolved in hexane/acetone solvents. Then, a subsequent slow solvent evaporation was initiated.

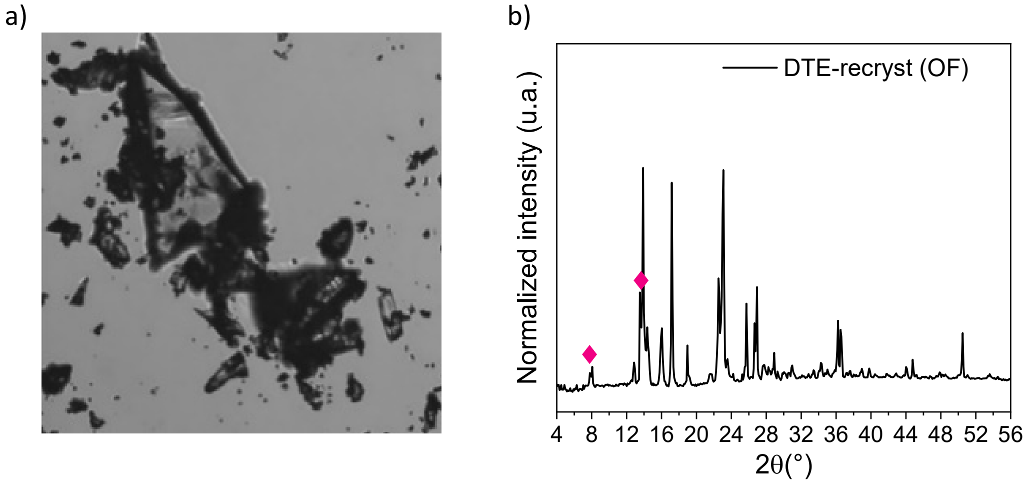

Figure III-6: a) Optical microscopy photograph and b) WAXS integrated profile of DTE formed single crystals.

The targeted DTE recrystallizes (noted DTE-recrys) successfully at room temperature. The slow evaporation implies large block-like crystals with different sizes as depicted in Figure III-6a. The WAXS experiment was performed on DTE-recrys single crystal. Figure III-6b illustrates the integrated profile at room temperature. As previously, the data are compared to the calculated data from monoclinic arrangements [1,6]. Only diffraction peaks at 2θ = 7.8° and at 2θ = 13.6° (noted ♦ in Figure III-6b) and associated to the (002) and (20-2) Miller planes were successefully attributed. This means that instead of crystallizing mainly in monoclinic form as shown previously for DTE powder, these single crystals tend to form a new crystal form for which we were not able to them identification. Moreover, the formed crystals are expected to be purer and more crystalline than those of the commercially product as they present sharper diffraction peaks.

III.3.3. Amorphous DTE (noted DTE-am)

DSC measurements were previously performed to study the thermal properties of DTE-pwd. The thermograms revealed that DTE become amorphous at room temperature after cooling from the melt. To confirm this amorphous structure, WAXS measurement was performed on cooled DTE from the melt. As shown in Figure III-7, no diffraction peaks corresponding to the Miller planes were depicted. Instead, an overlaid broad amorphous halos appears at around 2θ = 11°, 14° and 21°. Therefore, the cooling from the melt with conventional speedness does not allow the DTE re-crystallization.

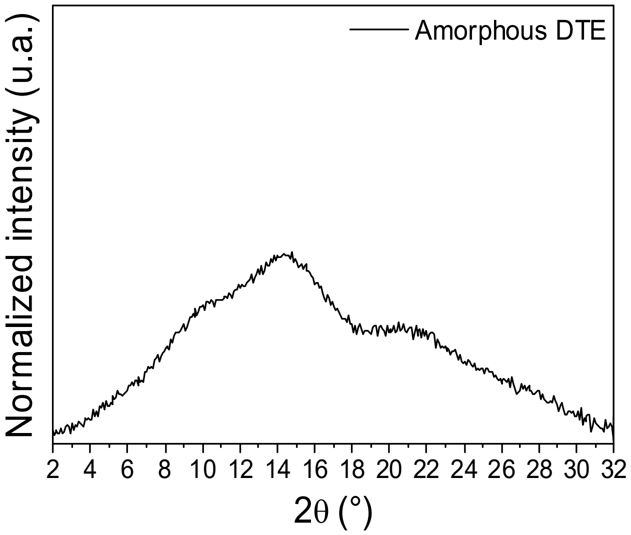

Figure III-7: WAXS integrated pattern of amorphous DTE-am at room temperature.

III.4. Photoresponsive DTE – Jumping vs bending phenomenon

Various types of diarylethene photomechanical motions such as contraction [1, 7-8], expansion [9-10], bending [11-16], twisting [2, 17-18], jumping [19] and fragmentation [20-21] were mentioned with more details in Chapter I. A key parameter to understand the photo-induced motions is the crystal shape and dimensions. Indeed, Lu and coworkers have reported the shape-dependency of photo-induced bending, curling, rolling and salient behaviors within styrylbenzoxazole derivatives molecular crystals [22]. Since it is clear that the crystal is one of the critical parameters to improve motions, the photo-induced motions of DTE obtained different methods were studied.

Thus, DTE-pwd, DTE-recrys and DTE-am were investigated under wield-field microscopy setup with in-situ illumination. The video duration acquired by the CCD camera is 10 minutes.

Every picture was taken every 1 second (600 pictures). Illumination sequence is always the same: ~10 seconds without light and then ~50 seconds under light irradiation. Sample is illuminated in situ with visible irradiation (550 nm band pass filter) from upper side and UV irradiation from below side (313 nm band pass filter). The videos presented in this part are accelerated 100 times. Their total duration are 6 seconds.

III.4.1. DTE powder

III.4.1.1. Presentation of the photomechanical effect

The DTE-pwd was deposited on glass slip. When irradiated during 600 seconds, various types of morphological deformations were induced during photochromic transformation. Figure I-8 illustrates a series of snapshots from accelerated videos upon visible light (video III-1, ▷) and UV light (video III-2, ▷).

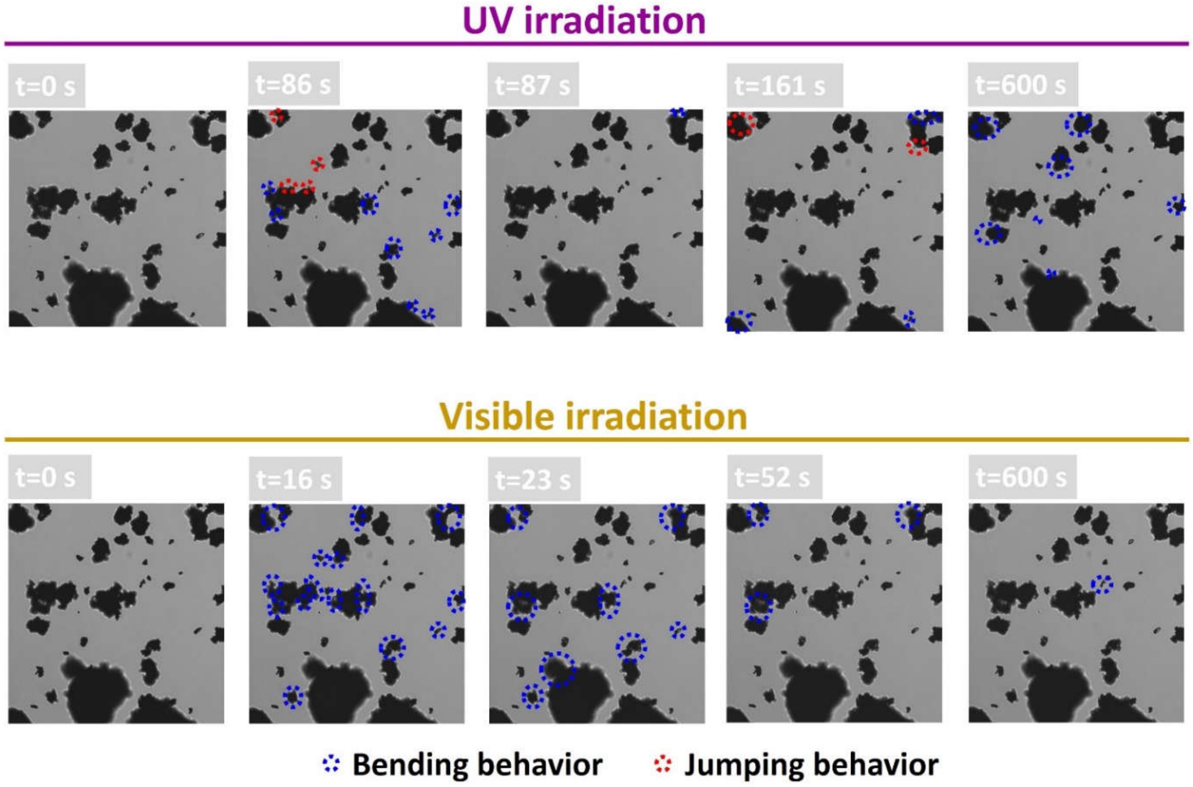

Figure III-8: Photoinduced motions of DTE-pwd (OF). a) The crystals were irradiated with UV-light and b) then irradiated with visible-light.

Upon irradiation, some nanocrystals bent instantaneously toward or away from the light source (blue dotted circle, Figure III-8). An additional photomechanical motion was observed (red dotted circle, Figure III-8) for some other crystals consisting on their sudden jumping at respectively 86 seconds and 161 seconds. This spontaneous hooping was only observed upon UV irradiation even when irradiation power was varied.

In order to get quantitative information, a pixel was chosen from the optical microscopic photograph. The main principle was to follow this chosen pixel changes plotted against the exposure time upon UV/visible irradiation.

However, two kinetic slices were chosen:

- To track the photomechanical response, typically the border of a crystal letting the light passing or not as long as it is moving.
- To follow the photocoloration/decoloration process typically in the center of a crystal. The chosen crystal must does not exhibiting photomechanical response.

III.4.1.2. Under UV irradiation

Jumping crystals. Time evolution of the intensity transmitted at the camera through the microscope (optical signal) during 313 nm light excitation was observed for three distinct pixels in order to follow step-by-step the jumping behavior of DTE-pwd crystals and photocoloration. Pixel 1 (red curve) and pixel 2 (blue curve) represent the trajectory of crystal displacement as illustrated in Figure III-9. Pixel 3 (green curve) represents the kinetic slice of photocoloration process (Figure III-9).

DTE-pwd crystals were white-colored in darkness. Upon UV light, the solid turns gradually to blue color and the optical signal intensity (pixel 3) decreases from 10 s to 600 s due to the photocoloration reaction.

For the pixel 1 at 113×178, two-time ranges were observed: during the first range from 0 s to 84 s (UV-irradiation began at 10 s), the optical signal decrement indicates that DTE-pwd crystal absorbs UV light due to the photocoloration. As response, the DTE-pwd crystal suddenly disappears by jumping. Then, for the second range i.e. from 84 s until 600 s, the registered optical signal is constant as it is associated to the light optical density (absence of crystal).

The crystal jumps from a first position (pixel 1, at 113×178) into a second position (pixel 2, at 171×135). The difference between both positions defines the length of jump (l_{jump}).

$$l_{jump} = 72.2 \text{ pixels} = 43.6\ \mu\text{m} \qquad (III.1)$$

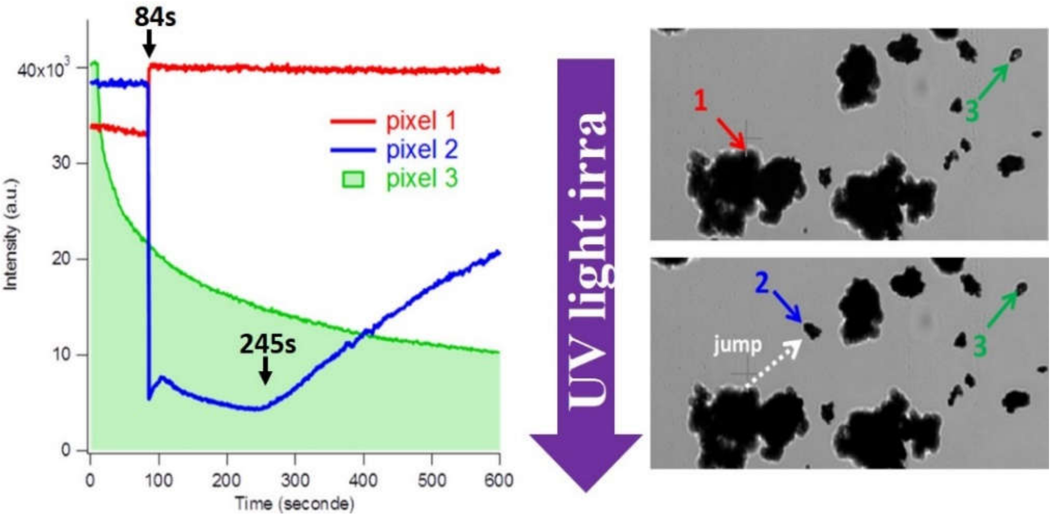

Figure III-9: Kinetic slice of DTE-pwd (OF) relative to the UV irradiation time - pixel 1 (photomechanical response), Pixel 2 (photomechanical response) and Pixel 3 (photocoloration response).

As seen on the kinetic slice (pixel 2), the jump is followed with a subsequent bending from 84 s to 245 s. It is important to compare the kinetic of the jump (pixel 1 and pixel 2) with the photocoloration kinetic (pixel 3). The jump at t = 84 s does not require a full photochromic conversion to occur. This result suggests that the forces inducing the jumping rather originate from the surface than from the bulk. This hypothesis will be discussed later.

Bending/rocking crystals. The second behavior reported for the DTE crystals was bending (or rocking) behavior. Our attention was focused on the small crystal with a shape of bark as depicted in Figure III-10a where three snapshots are represented upon irradiation. As the sample bends, four kinetic slices at the four borders of the crystal were plotted as illustrated in Figure III-10a.

By looking to the variation of optical signal intensity, we can notice that: (i) drastic change of intensity around 90-100 s; (ii) two or three oscillations probably due to some rocking behaviors. With anticipation, those results ascribed to: (i) the same surface effect reported previously for the jumping but with less amplitude (the jumping became a bending) (ii) the oscillations are due to some mechanical relaxation in order to find equilibrium position.

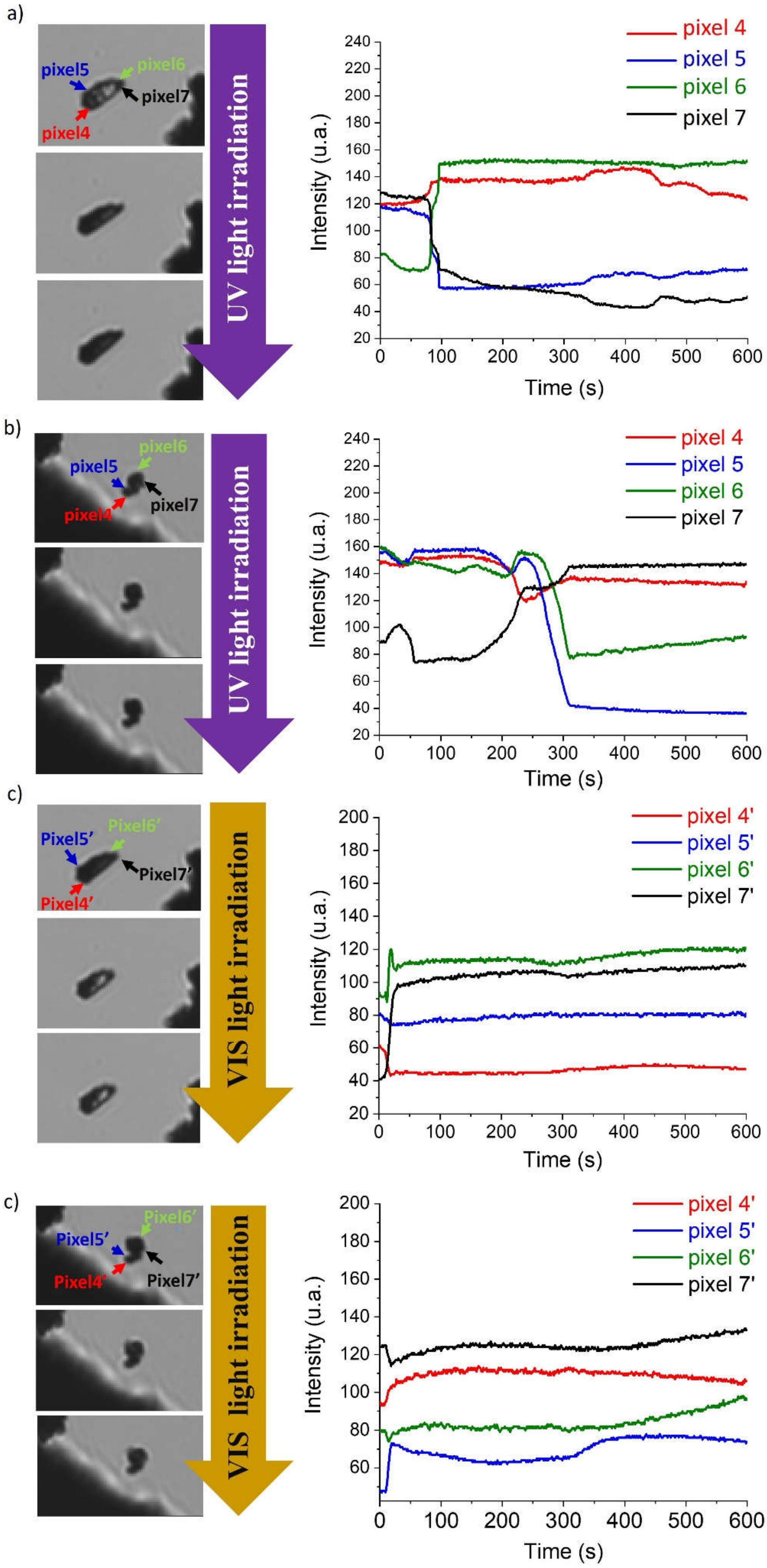

Figure III-10: Kinetic slice of DTE-pwd relative to the irradiation time. a) Photoinduced response of bark shaped crystal - UV light. b) Photoinduced response of comma shaped crystal - UV light. c) Photoinduced response of bark shaped crystal - VIS light. d) Photoinduced response of comma shaped crystal - VIS light.

For the crystal with a shape of comma, it seems to spin around a fixed point as noticed from the three snapshots represented upon irradiation in Figure III-10b. Likewise, the described first example described above, four kinetic slices at the four borders of the crystal were plotted as illustrated in Figure III-10b. However, the drastic change of intensity is still noticed but for a time located around 250 - 300 s. As an evidence, because all the crystalline planes do not exhibit an answer toward light in a similar way, the surface effect proposed above depends probably on the way the crystal is standing on the glass slip.

III.4.1.3. Visible irradiation and reversibility

After Crystal jumping. Using the same concept by following the intensity transmitted at the camera through the microscope during 550 nm light excitation of DTE-pwd crystals, the first reported crystal jumping evoked above is followed step-by-step. For this propose, two distinct pixels were investigated. Unfortunately, the designed crystal moved in a way that we could not follow exactly Pixel 2 (absence of sample). Thus, a Pixel 2' (nearly to Pixel 2) represents trajectory of crystal displacement as illustrated in Figure III-11. The pixel 3 represents kinetic slice of photodecoloration process.

DTE-pwd crystals was blue colored in darkness. Upon VIS light, the solid reverts gradually to its initial color and optical signal intensity (pixel 3) increases from 10 s to 600 s due to the photodecoloration reaction.

For the pixel 2' at 170×132, two-time ranges were observed: during the first range from 0 s to 200 s (UV-irradiation began at 10 s), the optical signal intensity increases due to the color change of crystal as response, DTE-pwd bends slowly. It is important to note that it was difficult to precise the bending direction. Upon further exposure to UV-irradiation (above 200 s), the DTE-pwd continues bending in another direction like spinning around a fixed point.

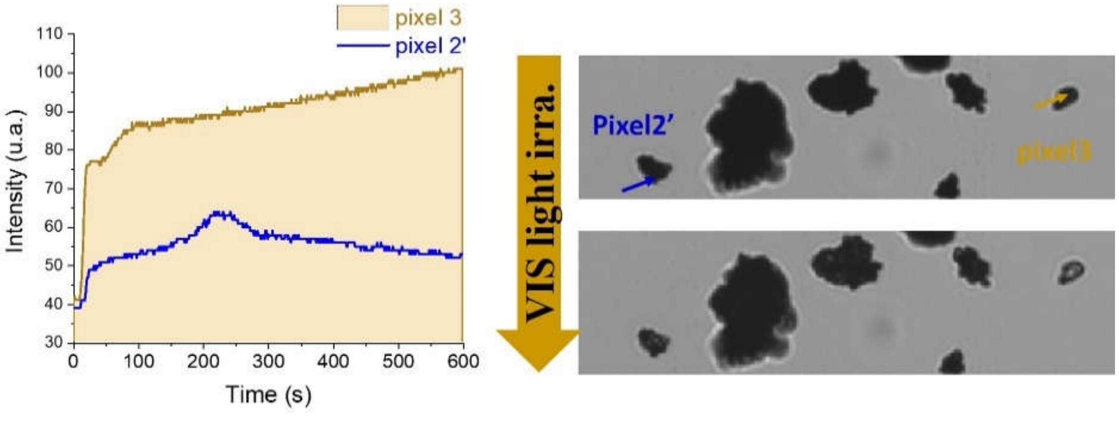

Figure III-11: Kinetic slice of DTE-pwd CF) relative to the visible irradiation time - pixel 2' (photomechanical response) and Pixel 3 (photodecoloration response).

After bending/rocking crystals. The second behavior reported for the DTE crystals (bark-shaped or comma-shaped) continues bending upon visible irradiation.

For bark-shaped crystal, three snapshots from the video are represented upon irradiation accompanied with the plotted four kinetic slices at the four-crystal border as illustrated in Figure III-10c. The photoinduced bending occurs slowly but the direction of bending was difficult to precise, as the crystal photograph became blurry. This means that the bending can occur toward or away from the irradiation source. Unfortunately, we can not follow the same pixels as the crystal moved comparing the initial position before UV/VIS irradiation. However, by looking to the variation of optical signal intensity, we can notice that: (i) weak change of intensity around 300 s; (ii) absence of oscillations compared those induced upon UV light exposure. With anticipation, those results ascribed to: (i) the same surface effect reported previously for the bending (UV light) but herein this slow bending occurs with less amplitude, (ii) absence of oscillations can be relative to the achieved equilibrium within crystal position.

Similarly, three snapshots from the comma-shaped crystal video are illustrated during irradiation accompanied with the plotted four kinetic slices at the four-crystal border as shown in Figure III-10d. It seems that the crystal continues spinning around a fixed point as noticed before. Moreover, the weak change of intensity is still noticed but around 300 s - 400 s. Those results are ascribed to a slow bending occurring with less amplitude.

From the snapshots upon UV and visible light, it is difficult to say whether the sample regains its initial shape. We need more sophisticated method allowing the following of the geometry change.

III.4.1.4. Summary about DTE-pwd

In summary, it is thus of prime importance to notice:

(i) Heterogeneities of motions applied on crystals upon alternating UV and Visible irradiations going from sudden jumping to moderate bending or rocking.

(ii) Bending effect, which is reversible switching between UV and Visible irradiation.

III.4.2. Recrystallized DTE

As mentioned in the beginning of this part, dependency toward the growth of well-shaped crystals may influence the photoinduced response. In order to re-form crystals with well-defined shape, the DTE-pwd was recrystallized. Herein, the reformed DTE-recryst are investigated whether they lead to more efficient morphological changes.

III.4.2.1. Presentation for UV/Visible irradiation

Deposing DTE-recryst on glass substrate, the photomechanical behavior was investigated from upper side (UV light) and from down side (visible light) for 600 s. Figure III-12 illustrates a series of snapshots from accelerated videos upon UV light (video III-3, ▷) and visible light (video III-4, ▷). Various types of morphological deformations were observed during photochromic transformation.

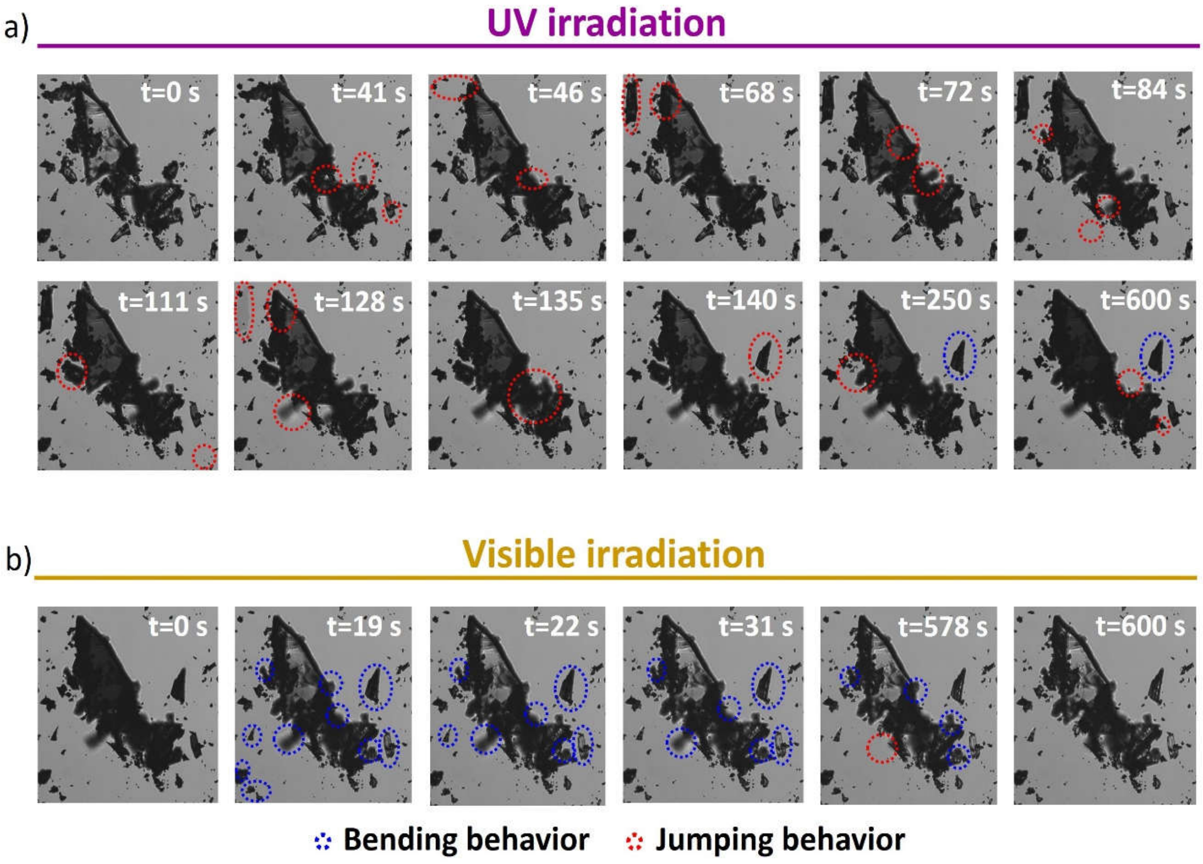

Figure III-12: Photoinduced various responses of DTE-recrys. a) UV light irradiation. b) visible light irradiation.

When irradiated with UV light (Figure III-12a), the colorless single-crystals turn blue progressively due to photo-cyclization transformation undergoing drastic photomechanical response: a sudden jumping from their original positions (red dotted circle) with random directions. The peripheral small crystals hooped vigorously at 41 s, 46 s, 68 s, 72 s, 84 s, 111 s, 128 s, 135 s, 140 s, 250 s and 600 s.

By changing the irradiation wavelength from 313 nm into 550 nm (Figure III-12b), the blue single-crystals returned into the initial colorless state upon photo-reversion transformation but the block-crystals do not jump. Apparently, they undergo different effects including mostly the bending behavior and secondarily the crystal jumping at only 578 s.

With longer exposures up to 600s, it remains important to note that the biggest middle crystal does not induce photomechanical behavior neither upon UV illumination nor visible illumination. It seems that only the smallest crystals induce faster photomechanical response.

III.4.2.2. Reversibility – UV/visible illumination cycles

Jumping crystals. In order to get quantitative information about the described jumping, a pixel was chosen from the optical microscopic photograph of DTE-recrys. Concurrently, a pixel from the biggest crystal was followed during the photocoloration and photodecoloration processes. These two chosen pixels were plotted against the exposure time as illustrated in Figure III-13a.

Upon 313 nm light excitation, the DTE-recrys undergoes a photocyclization leading to color change into blue. The kinetic slice associated to photocoloration shows a gradual decrease within the optical signal intensity from 10 s to 600 s. The biggest crystal in the middle remains stable. Whereas, a jumping of crystal occurs instantaneously within 30 s of exposure into light. This crystal hooped to unknown place, which explains the constancy of optical signal once the crystal was absent even after subsequent visible irradiation. While, the pixel photodecoloration regains its initial value of intensity and the crystal returns into colorless confirming the reversibility of occurred photochromism in DTE-recrys.

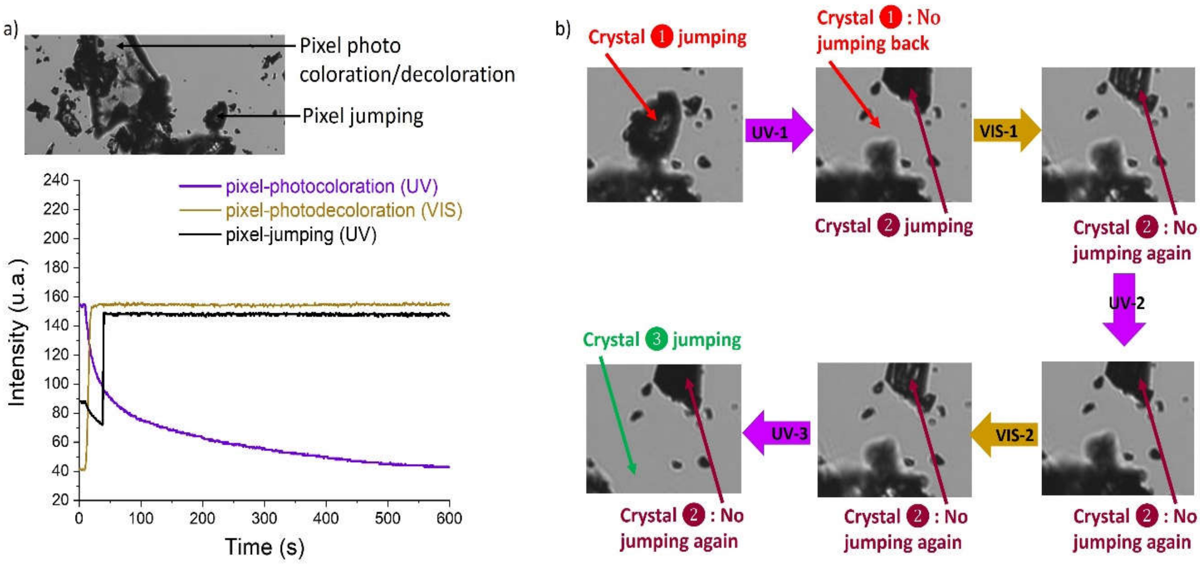

Figure III-13: a) Irreversible photoinduced jumping of DTE-recrys single upon UV and visible irradiations. b) Associated kinetic slices as a function of exposure time.

From other hand, this jumping phenomenon was investigated under two illumination cycles (UV-1, VIS-1, UV-2, VIS-2, UV-3) as illustrated in Figure III-13b. Before UV light irradiation, the crystal ❶ is stable at room temperature. When irradiated with 313 nm wavelength, the photo-transformation leads to local stress over the DTE-recryst, which induces its jumping.

Interestingly, a new crystal ❷ appears on the photograph through jumping. Subsequent visible light exposure does not induce further jumping. Moreover, the associated hopping does not re-appear neither upon visible light (VIS-2) nor upon UV light (UV-2) i.e. upon the second illumination cycle. The third UV light irradiation (UV-3) induced a sudden hooping of crystal ❸ with no noticeable re-appearance of crystal ❶ or crystal ❷. This effect can be interpreted with different hypothesis: (i) the jumping phenomenon is irreversible; (ii) after jumping, the crystal stands on a non-responsive crystallographic plane; (iii) this is due to our set-up configuration; (iv) the visible irradiation is coming from the lower side inducing some forces annihilated with the resistance of the glass strip.

Bending crystals. The second behavior reported for the DTE-recrys was the bending behavior. The crystal shaped as parallelepiped was similarly investigated under two illumination cycles (UV-1, VIS-1, UV-2, VIS-2, UV-3) as illustrated in Figure III-14a. The snapshots represented upon irradiation cycles depicts that the chosen crystal exhibits a bending behavior as response to light excitation. The UV light exposure is accompanied with a color change and a bending behavior. Concurrently, the crystal reverts its initial color and recovers its original shape when exposed to visible light. As the sample bends and this bending occurs reversibly at room temperature, five kinetic slices upon every light irradiation of the crystal tip were plotted to confirm the proposed statement as mentioned in Figure III-14b.

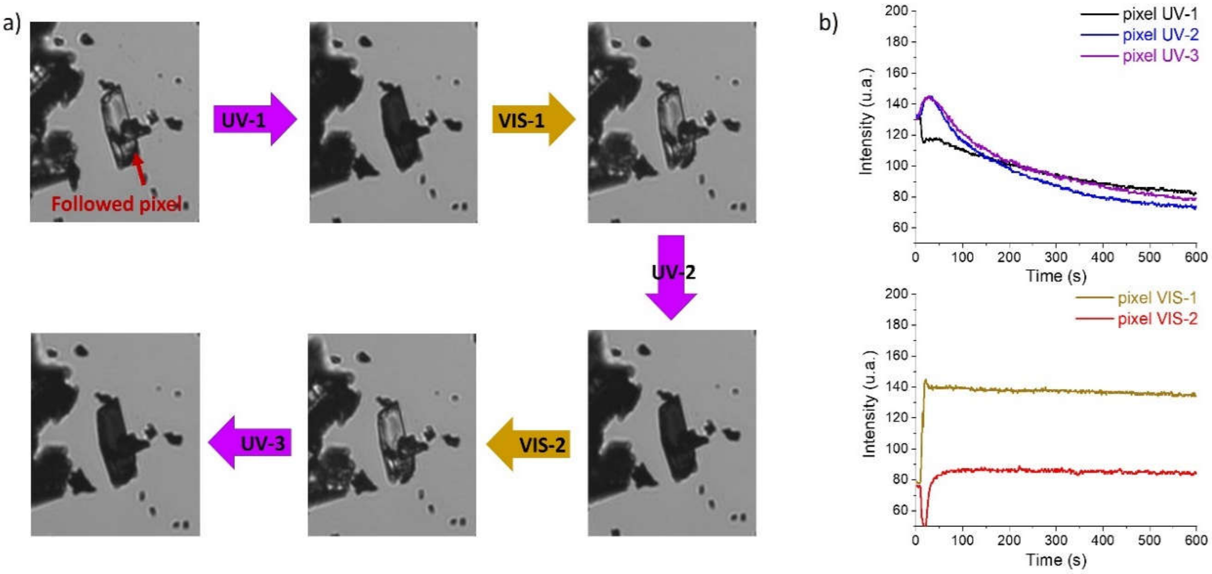

Figure III-14: a) Reversible photoinduced bending of DTE-recrys single upon UV and visible irradiations. b) associated kinetic slices as a function of exposure time.

By following the same pixel, the variation of optical signal intensity indicates:

(i) change of intensity with various amplitude around 26 s ascribed to the crystal bending within the same direction (UV-1, UV-2, UV-3);

(ii) instantaneous drastic change of intensity, similarly to the case of crystal hooping kinetic profile, coincides with absence of crystal tip within the return back direction (VIS-1, VIS-2).

Those results lead to reversible bending occurred with less amplitude compared to the jumping. Contrarily to DTE-pwd, the oscillations absence suggest that the well-reformed crystals do not exhibit mechanical relaxation to find equilibrium position.

III.4.2.3. Summary about DTE-recrys

In summary, it is there noteworthy to notice:

(i) Heterogeneities of motions exhibited by crystals upon irradiation.

(ii) Photomechanical effect is jumping phenomenon, mostly occurred upon UV light exposure.

(iii) Photomechanical effect is bending behavior, mostly occurred upon visible light exposure.

III.4.3. Amorphous DTE

The photomechanical behavior is usually ascribed to a reversible photochromic reaction of crystalline molecules. Therefore, the amorphous state of DTE-am presented previously, appears as a challenge to investigate the photoinduced motions upon exposure into UV and visible lights up to 600 s. After cooling the raw s dithienylethene from the melt, DTE-am was deposited on glass substrate. Figure III-15 illustrates a series of snapshots from accelerated videos upon UV light (video III-5, 🎞) and visible light (video III-6, 🎞).

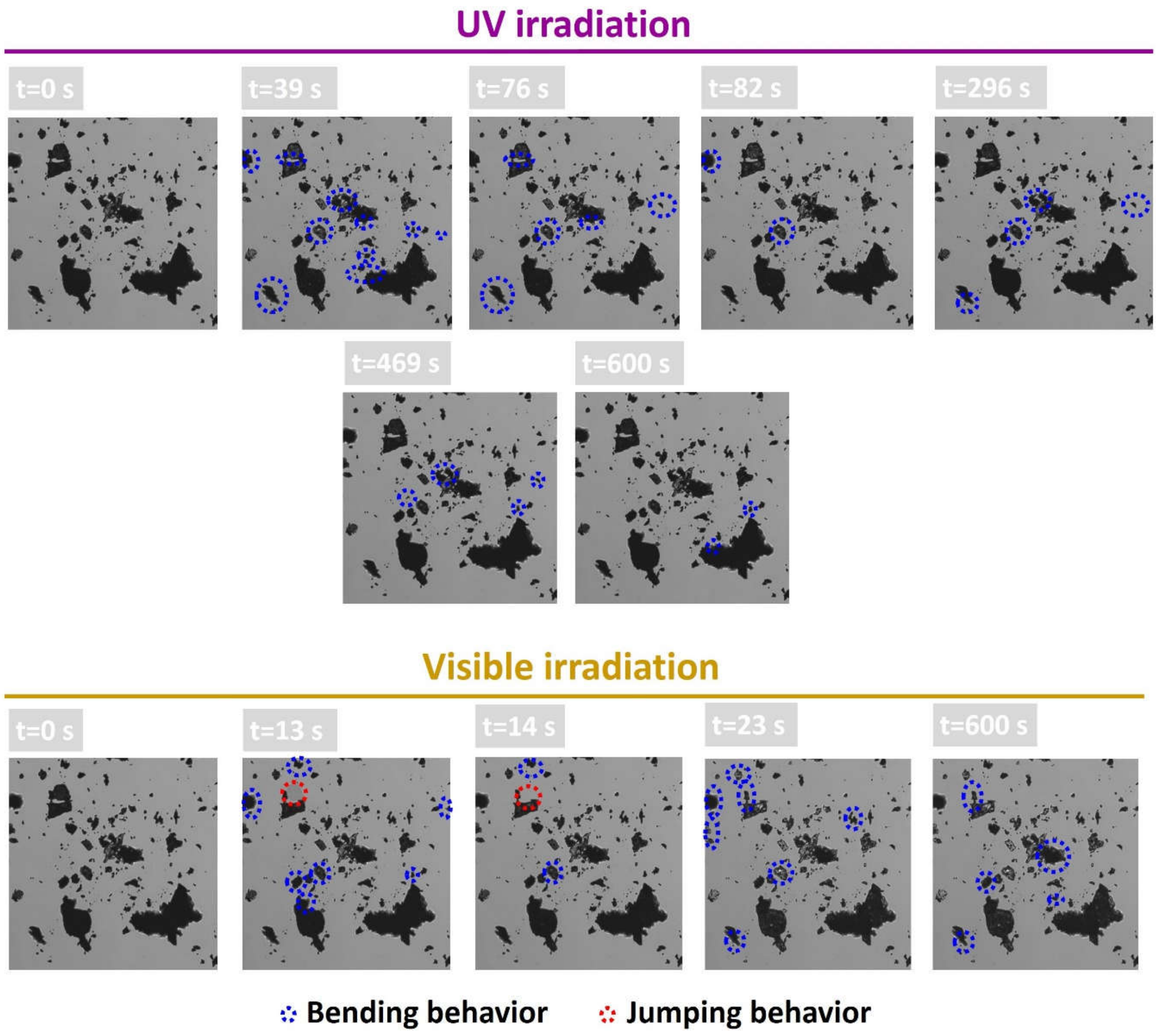

Figure III-15: Photoinduced motions within amorphous DTE. a) UV irradiation was carried out from upper side. b) Visible irradiation was carried out from down side

III.4.3.1. Under UV/visible irradiation

When irradiated with UV light, the white amorphous powder turns into blue color progressively. Moreover, this photo-transformation is concurrently followed by photo-active deformations at respectively 39 s, 76 s, 82 s, 296 s, 469 s and 600 s. Seemingly, DTE-am does not jump when exposed into UV-light compared to DTE-recrys or DTE-pwd. Instead, DTE-am rather undergoes bending behavior.

Upon exposure to visible light, the DTE-am powder reverts to the initial white state while bending or expanding since 13 s. Surprisingly, some of DTE-am jump instantaneously into unknown position with random direction. The impressive leaping can be probed due to the created high strain inside the non-organized lattice. Thereby longer exposures up to 600 s, the smallest powder continues bending at 14 s, 23 s and 600 s.

III.4.3.2. Bending behavior

As bending and jumping behaviors were described above with other DTE examples, the amorphous DTE seems exhibiting the same photomechanical behaviors as illustrated in Figure III-16. Our attention was focused on the small crystal displacement as illustrated in Figure III-16-a where six snapshots were represented upon irradiation. Evolution of photoinduced motion was followed by applying kinetic slice.

DTE-am was white colored in darkness. DTE-am is photochromic (Figure III-16-c). Upon UV light, the solid turns gradually to blue and optical signal intensity (pixel photocoloration) decreases from 10 s to 600 s due to the photocoloration reaction. Subsequent visible light exposure reverts the sample its initial color and concurrently the intensity within the optical signal increases.

Apparently, the bending behavior seems to occur upon instantaneous UV irradiation by spinning around fixed points. The crystal snapshots show through the red arrows the direction of bending. By increasing the exposure time, the sample continues bending perpendicularly into the direction of incident light. When visible light was applied, the sample progressively returns to its initial shape.

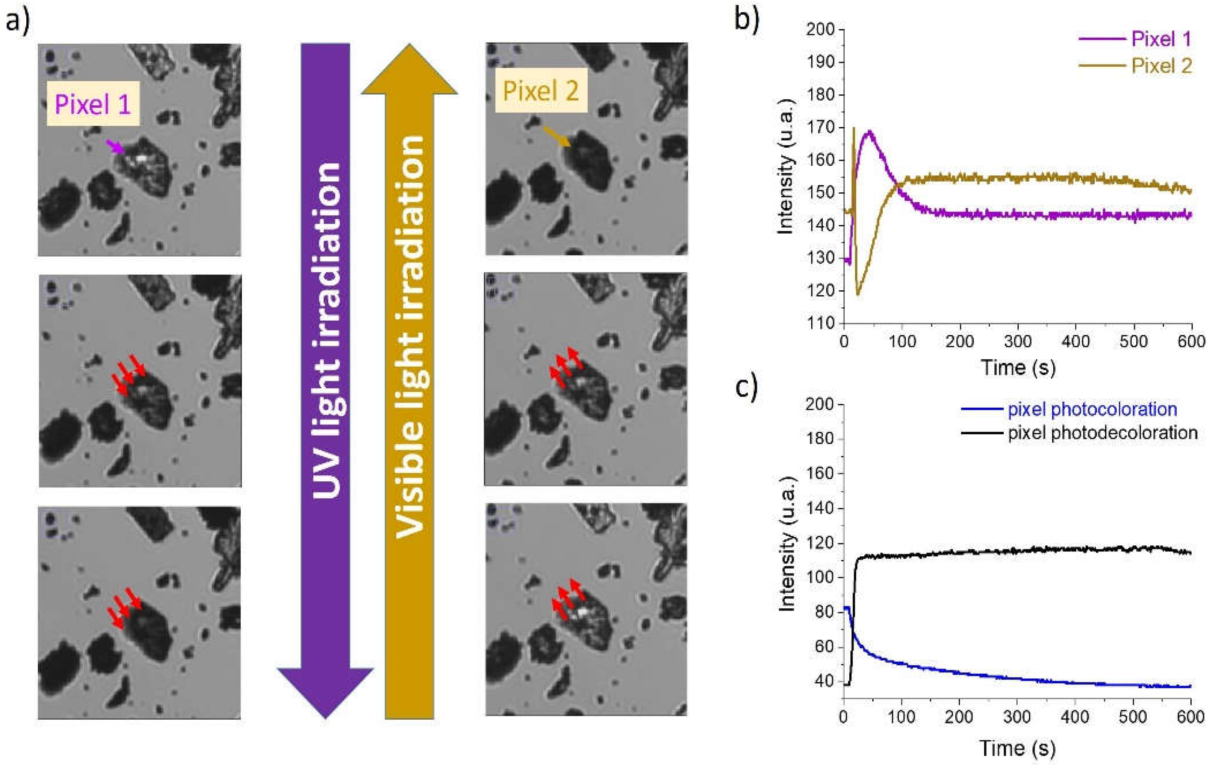

Figure III-16: Photomechanical behavior of single crystals of DTE-am. a) Reversible photoinduced bending. b) Associated kinetic slices as function of exposure time.

In order to gain further quantitative information about these reversible drastic changes, the evolution of the same recorded pixel was followed: pixel 1 (UV light) and pixel 2 (visible light) as shown in Figure III-16b. It seems that the reported behavior occurs within 100 s. For UV light exposure, the optical intensity initial value is about 130. This value occurs an increase beginning from 10 s until 40 s and then decreases gradually to become stable. From the other hand, the optical intensity increases and then remains constant around 140-150 due to visible light. Surprisingly, the optical intensity does not regain exactly its initial value maybe because the crystal needs more exposure into visible light.

III.4.3.3. Summary about DTE-am

Regardless the amorphous or crystalline state of DTE, various photomechanical effects were reported:

- Jumping effect, which is observed only for visible irradiation but not for UV irradiation in DTEam.
- Bending effect, which is reversible switching between UV and Visible radiation.
- Unexpectedly, important and reversible photomechanical effect have been reported for the amorphous DTE.

III.4.4. Physical Interpretation of the Photo-Mechanical effect

III.4.4.1. Jumping of crystals

The reported DTEs crystals jumping occur mostly upon UV irradiation. Irie et al. [19] demonstrated that microcrystals of a diarylethene undergo similarly jumping behavior upon UV irradiation. The origin of these jumps was purely due to the photomechanical transformations designed by photo-salient effect (salient is derived from the Latin salire and means leaping). Whereas, it was reported by Ding et al. [23] that when crystals are heated above or cooled below the temperature of phase transition, they can occur thermos-salient effect. Contrary to these thermosalient crystals, the origin of our reported jumps cannot be thermal but photochemical because DSC measurements of DTE does not present any phase transition between the room temperature and the melting point. Later Baldec et al. [24, 25] have interestingly suggested a hypothesis that the observed jumps and cracks (that appears on crystal surface when prevented from jumping) are related a Grinfeld instability achieved due to a periodic deformation.

To explain more their approach, they proposed a schematic illustration about photomechanical effects under UV irradiation (Figure III-17a). However, the crystal is subjected to a uniaxial stress perpendicular to the direction of maximum absorption. The stress relaxes in the form of a Grinfeld instability i.e. the crystal surface, which was initially plane before irradiation, has a periodic modulation perpendicular to the applied stress. This deformation then relaxes as jumps or by the formation of cracks within the surface when the crystal is attached to the plane.

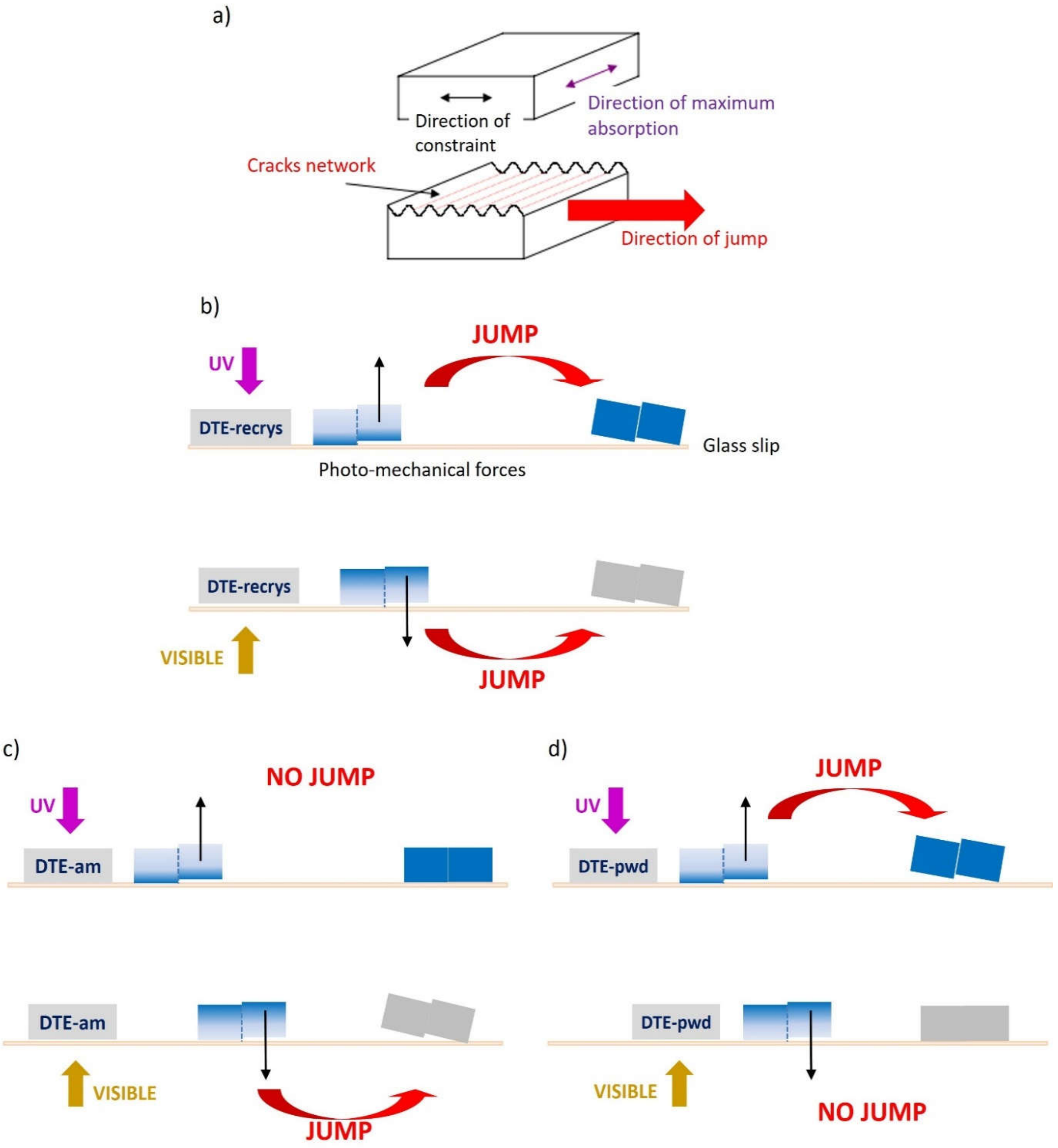

Figure III-17: Schematic illustration of photoinduced jumping. a) Proposed explanation [25]. b) DTE-recrys sample. c) DTE-am sample. d) DTE-pwd sample.

Herein, the jumps occur upon UV/visible light in the case of recrystallized commercial powder of DTE. The most efficient and homogenous jumping behavior was obtained through

DTE-recrys (Figure III-17b). This can underline the importance of plane surface in increasing the chances of hooping compared to DTE-am (Figure III-17c) and DTE-pwd (Figure III-17d). In the case of amorphous DTE, jumps occur only upon visible light. This arises the question about the key role played by molecules and specially their structural organization impact in inducing different photomechanical effect toward light.

III.4.4.2. Bending of DTE crystals

Among various photomechanical motions, the bending behavior is the most common motion for photomechanical actuators. To discuss the photoinduced bending behavior, a simplified bimetal model introduced by the Timoshenko's equation. The principle is based on a correlation between the initial speedness of photoinduced curvature and crystal thickness. The crystal bending **[13-17]** is assessed by:

(i) a contraction or an expansion of the photoreacted layer (crystal surface denoted h_2) within the crystal according to the photoinduced ring-closing/opening reaction;

(ii) then, along the crystal thickness, the photochromic reaction continues spreading in the depth upon further irradiation.

Moreover, it was reported that photoinduced bending effectiveness depends directly to h_2 crystal surface from the crystal thickness, which plays a crucial role in achieving a speedy bending **[13-15]**. When the crystal is thin, the motion proceeds rapidly and largely. Thicker crystals lead to slower bending behavior. Different parameters were judged to influence the photoresponsiveness of crystal including illumination parameters (light power, used wavelength, light direction) **[2, 27-28]**.

Here, we tried to use the same experimental conditions (same light power, same wavelength, UV light from upper side and visible light from lower side) in order to allow the comparison between DTEpwd and DTErecrys. The sample thickness was not possible to maintain constant. By deposing the samples on glass substrate, we have reported successfully for the first time the bending of DTE. Generally, the bimetal model is adopted to examine the relationships between the speed of the bending and the thickness of the crystal. In our case, unfortunately, it was difficult to follow the curvature changes and bending direction as the sample could not be fixed to an attachment point (except the recrystallized DTE). Further investigation will be offered to reinvestigate these crystals by trying to rationalize their motions by the Timoshenko bimetallic model.

III.4.4.3. Bending of amorphous DTE

Generally, photomechanical responses are induced by changes in molecular geometry and/or intermolecular interaction in crystalline phase. In our case, DTE-am represents visually microscopic photo-induced changes despite its amorphous state. Since the most of studied diarylethene molecules are known to exhibit photomechanical response in crystalline state, it appears quite challenged to report a photomechanical effect of amorphous diarylethene. Such photo-induced responses cannot be explained by Timoshenko's bimetal model as the DTE-am molecules are not organized in definite lattice pattern. Thus, neither the change in the cell parameters nor crystal thickness can explain the photomechanical behaviors. Instead, the photochemical transformation plays an important role in inducing synergic response.

III.4.5. CONCLUSION

In this chapter, we have reported the photomechanical effect of a series of DTE samples in either crystalline or amorphous state. These molecules present unexplored aspect in literature and a new possibility for molecular crystals as functional materials.

Two types of photomechanical motions upon exposure to UV and visible lights are successfully reported: bending and jumping behaviors.

Irreversible jumping = explained by surface effect induced by Greinfield instability; non reversible that does not follow the photocoloration kinetic. As soon as the accumulated energy is up to a threshold to induced the Greinfield instability, then the crystal jumps.

Reversible Bending = caused by initial heterogeneous photoconversion that continues occurring within the crystal depth according to the gradient of photo-transformed molecules inside the bulk paralleling the photocoloration (reversion) kinetic.

Since DTE exhibits significantly different motions, they depend mostly on the way of elaboration. However, every handling or small change in the procedure of elaboration may induce changes at the molecular arrangement. By comparing photo-induced motions of DTE respectively in crystalline and amorphous states, it seems that DTE-recrys occurs vigorously faster. Therefore, it is there noteworthy to note the outstanding ability of DTE amorphous state moving despite its non-organization in a well-definite lattice pattern. This result will be paramounted later when DTE-UPy photomechanical effect is going to be investigated within Chapter IV.

References

[1] Irie, M., et al., Reversible Surface Morphology Changes of a Photochromic Diarylethene Single Crystal by Photoirradiation, 2001. 291(5509): p. 1769-1772.

[2] Kitagawa, D., et al., Control of Photomechanical Crystal Twisting by Illumination Direction. Journal of the American Chemical Society, 2018. 140(12): p. 4208.

[3] Irie, M., et al., Photochromism of dithienylethenes with electron-donating substituents. Journal of Organic Chemistry, 1995. 60(25): p. 8305-8309.

[4] Shibata, K., et al., Photocyclization/Cycloreversion Quantum Yields of Diarylethenes in Single Crystals. The Journal of Physical Chemistry A, 2002. 106(1): p. 209-214.

[5] Irie, M., et al., Photochromism of 1,2-bis(2-methyl-5-phenyl-3-thienyl)perfluorocyclopentene in a single-crystalline phase. Journal of the American Chemical Society, 2000. 122(20): p. 4871-4876.

[6] Tong, F., et al., Photomechanical motion of diarylethene molecular crystal nanowires, Nanoscale, 2018. 10(7): p. 3393-3398.

[7] Kobatake, S., et al., Rapid and reversible shape changes of molecular crystals on photoirradiation. Nature, 2007. 446(7137): p. 778.

[8] Kobatake, S., H. Hasegawa, and K. Miyamura, High-convertible photochromism of a diarylethene single crystal accompanying the crystal shape deformation. Crystal Growth and Design, 2011. 11(4): p. 1223-1229.

[9] Morimoto, M. and M. Irie, A diarylethene cocrystal that converts light into mechanical work. Journal of the American Chemical Society, 2010. 132(40): p. 14172.

[10] Al-Kaysi, R.O., A.M. Mueller, and C.J. Bardeen, Photochemically driven shape changes of crystalline organic nanorods. Journal of the American Chemical Society, 2006. 128(50): p. 15938.

[11] Irie, M., et al., Photochromism of Diarylethene Molecules and Crystals: Memories, Switches, and Actuators, in Chem. Rev. 2014. p. 12174-12277.

[12] Koshima, H., N. Ojima, and H. Uchimoto, Mechanical motion of azobenzene crystals upon photoirradiation. Journal of the American Chemical Society, 2009. 131(20): p. 6890.

[13] Kitagawa, D. and S. Kobatake, Crystal thickness dependence of photoinduced crystal bending of 1,2-bis(2-methyl-5-(4-(1-naphthoyloxymethyl)phenyl)-3-thienyl) perfluorocyclopentene. Journal of Physical Chemistry C, 2010. 117(40): p. 20887-20892.

[14] Kitagawa, D. and S. Kobatake, Crystal thickness dependence of the photoinduced crystal bending of 1-(5-methyl-2-(4-(p-vinylbenzoyloxymethyl)phenyl)-4-thiazolyl)-2-(5-methyl-2-phenyl-4-thiazolyl)perfluorocyclopentene. Photochem. Photobiol. Sci., 2014. 13(5): p. 764-769.

[15] Kitagawa, D., et al., Quantitative Evaluation of Photoinduced Bending Speed of Diarylethene Crystals. Crystals, 2015. 5(4): p. 551-561.

[16] Kitagawa, D., R. Tanaka, and S. Kobatake, Photoinduced stepwise bending behavior of photochromic diarylethene crystals. CrystEngComm, 2016. 18(38): p. 7236-7240.

[17] Kitagawa, D., H. Nishi, and S. Kobatake, Photoinduced Twisting of a Photochromic Diarylethene Crystal. Angewandte Chemie International Edition, 2013. 52(35): p. 9320-9322.

[18] Zhu, L., R.O. Al-Kaysi, and C.J. Bardeen, Reversible photoinduced twisting of molecular crystal microribbons. Journal of the American Chemical Society, 2011. 133(32): p. 12569.

[19] Colombier, I., et al., Diarylethene microcrystals make directional jumps upon ultraviolet irradiation. Journal of Chemical Physics, 2007. 126(1).

[20] Kitagawa, D., et al., Photoinduced Rapid and Explosive Fragmentation of Diarylethene Crystals Having Urethane Bonding. Chem. Mat., 2016. 28(14): p. 4889-4892.

[21] Naumov, P.e., et al., Dynamic Single Crystals: Kinematic Analysis of Photoinduced Crystal Jumping (The Photosalient Effect. Angewandte Chemie International Edition, 2013. 52(38): p. 9990-9995.

[22] Wang, H., et al., Bending, Curling, Rolling, and Salient Behavior of Molecular Crystals Driven by [2+2] Cycloaddition of a Styrylbenzoxazole Derivative. Angewandte Chemie International Edition, 2017. 56(32): p. 9463-9467.

[23] Ding, J., et al., A crystal that hops in phase transition, the structure of trans, trans, anti, trans, trans-perhydropyrene. Acta Crystallographica Section B, 1991. 47(5): p. 739-742.

[24] Baldeck, P.L., et al., Photochromic organic microcrystals jump under light irradiation. 2005. p. 59350U-59350U-4.

[25] Colombier, I., Effets photomécanique dans les cristaux organques photochromes, Université Joseph Fourier - Grenoble 1, 2005.

[26] Kitagawa, D., R. Tanaka, and S. Kobatake, Dependence of photoinduced bending behavior of diarylethene crystals on irradiation wavelength of ultraviolet light. Phys. Chem. Chem. Phys., 2015. 17(41): p. 27300-27305.

[27] Hirano, A., et al., Dependence of Photoinduced Bending Behavior of Diarylethene Crystals on Ultraviolet Irradiation Power. Crystal Growth and Design, 2017. 17(9): p. 4819-4825.

[28] Kitagawa, D., R. Tanaka, and S. Kobatake, Dependence of photoinduced bending behavior of diarylethene crystals on irradiation wavelength of ultraviolet light. Phys. Chem. Chem. Phys., 2015. 17(41): p. 27300-27305.

Chapter IV.

Photomechanical effect of the DTE-UPy supramolecular self-assembly

As have been reported in chapter I, the supramolecular self-assembly of telechelic DTE featuring ureidopyrimidinone motifs noted DTE-UPy was characterized by Takeshita et al. [1] using Dynamic Light Scattering (DLS) measurements (Figure IV-1b). The supramolecular principle of such molecule is subtle.

The open form (OF) of DTE-UPy molecules being flexible (thermal equilibrium between anti-parallel (AP) and parallel (P) conformers) as depicted in Figure IV-1a, they are not suitable for intermolecular linking through the UPy recognition patterns. Indeed, for these OF species in chloroform, any object with a size lower than 10 nm (DLS signal sensitivity) is not detectable giving evidence about the lack of large supramolecular system.

After UV light irradiation, the solution initially colorless becomes blue due to photocyclisation process leading to a rigid closed form (CF). Thanks to this rigidity, the interaction of UPy groups allows the formation of quadruple hydrogen bonding and then the assembly of DTE-UPy molecules create a supramolecular assembly of 600 nm (100 μM in chloroform). The overall kinetics (OF → CF) take more than several hours at ambient temperature.

Note that aggregation process is so efficient where a strong blue precipitate is observed for initial concentrations up to 200 μM. The total recovery of the starting material (CF → OF) is possible providing illumination with visible light, additional heating is eventually necessary.

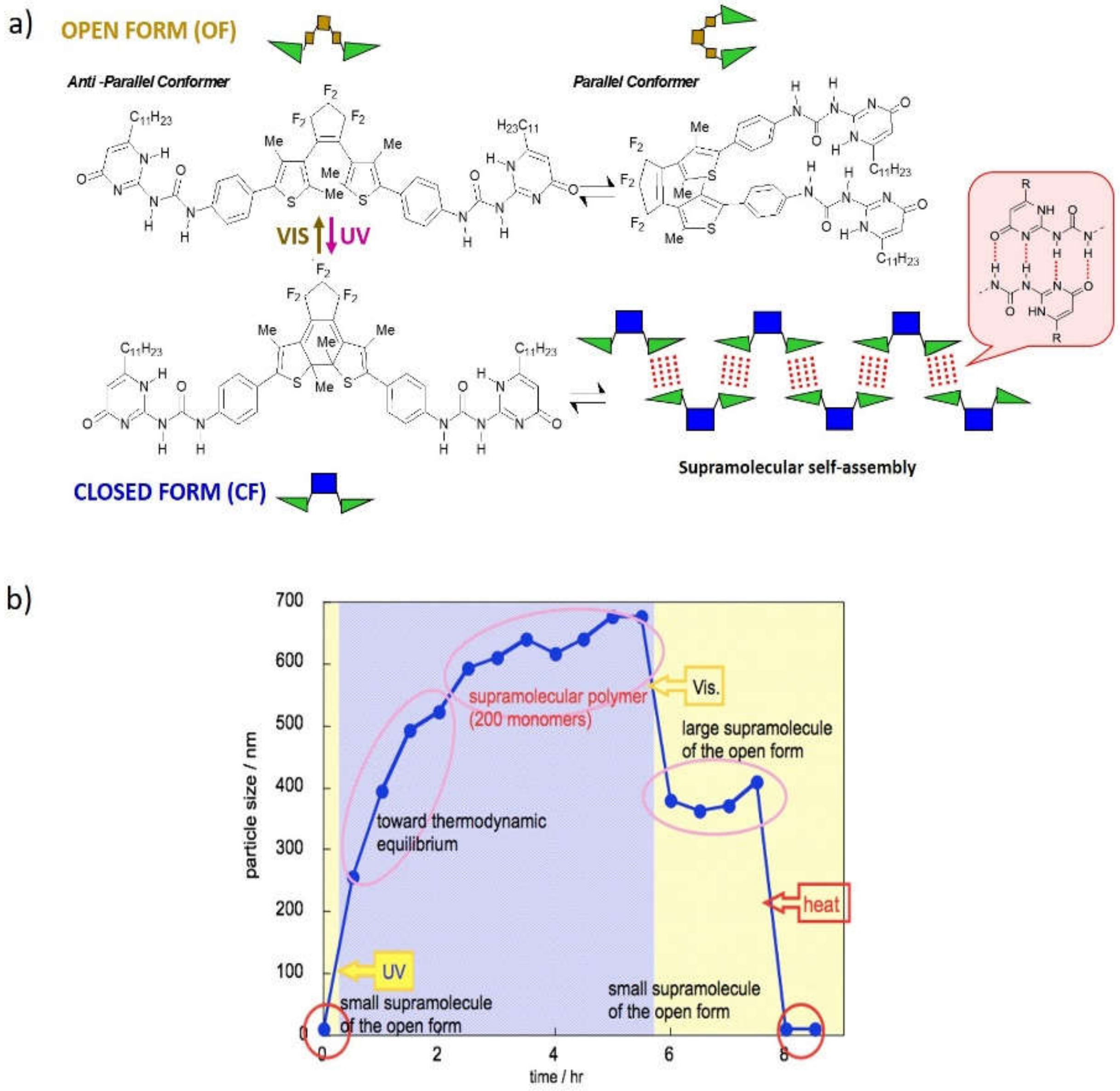

Figure IV-1: a) DTE-UPy in OF with antiparallel (AP) and parallel (P) conformers and in CF with the supramolecular self-assembly. b) DLS Particle size change of the photoswitch aggregation upon irradiation with UV and visible light [1].

Furthermore, by analogy with oligomers with UPy end groups, the association constant between two molecules is expected to be very high ($K > 10^6$). Indeed, UPy units are known to dimerize with a dimerization constant of around $6\ 10^7\ M^{-1}$ in chloroform (at 300 K). Their association promotes to the formation of the supramolecular assembly [2,3]. In brief, the question of the exact structure of dimer, trimer or other small oligomer with UPy moieties engaged within hydrogen bonding, is still an open question.

IV.1. Photochromic properties of DTE-UPy in solution

IV.1.1. Absorption spectra

Photochromic properties of DTE-UPy was measured in chloroform (5.10^{-5} M). Figure IV-2a shows the UV-visible absorption spectra at room temperature. The OF isomer initially present in solution exhibits a sharp absorption peak at 295 nm (black absorption spectrum). Upon irradiation with UV light, the colorless solution turned to blue color as observed in Figure IV-2. The photo-generated form (blue absorption spectrum) demonstrates the disappearance of the OF characteristic band and the emergence of two new bands at around 330 nm and 575-580 nm associated to the formation of CF isomer. Furthermore, an isosbestic point is observed at 320 nm in the photostationary state. Absorption features are closed to those of the DTE molecules described in Chapter III.

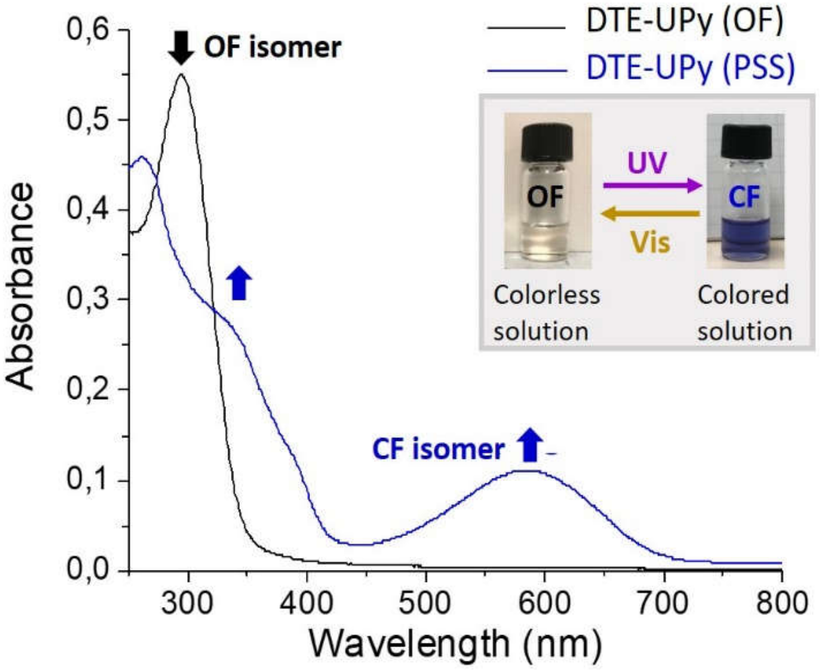

Figure IV-2: DTE-UPy photochromism (5.10^{-5} M) in chloroform upon UV/visible illumination - absorption spectra and solution color changes.

IV.1.2. Photochromic parameters

IV.1.2.1. Extinction coefficients

According to the procedure described in Chapter II (combination of absorption spectroscopy with NMR), the molar extinction coefficients of the DTE-OF and DTE-CF were determined by exploring the absorbance before and after UV irradiation as shown in Figure IV-3a. The calculated conversion α is about: $\alpha = 1 - (I_{PSS}/I_0) = 1 - 0.11 = 89\%$.

However, by means of this mole fraction α, the extinction coefficients of wavelength maxima have been calculated according to the equations depicted in chapter II (Figure IV-3b). However, $\varepsilon(OF)$ and $\varepsilon(CF)$ values are respectively 31800 M^{-1} cm^{-1} (λ_{abs}^{max}= 295 nm) and 7200 M^{-1} cm^{-1} (λ_{abs}^{max}= 575 nm).

In order to apply the procedure described in photokinetic method described in chapter II, it was important to calculate the extinction coefficients at the excitation and observation wavelengths (Figure IV-3b).Therefore, $\varepsilon(OF)$ and $\varepsilon(CF)$ values are respectively 23900 M^{-1} cm^{-1} and 16500 M^{-1} cm^{-1} within the excitation wavelength (λ = 313 nm). Whereas, the $\varepsilon(OF)$and $\varepsilon(CF)$ values within the observation wavelength (λ = 575 nm) are 200 M^{-1} cm^{-1} and 7200 M^{-1} cm^{-1}, respectively.

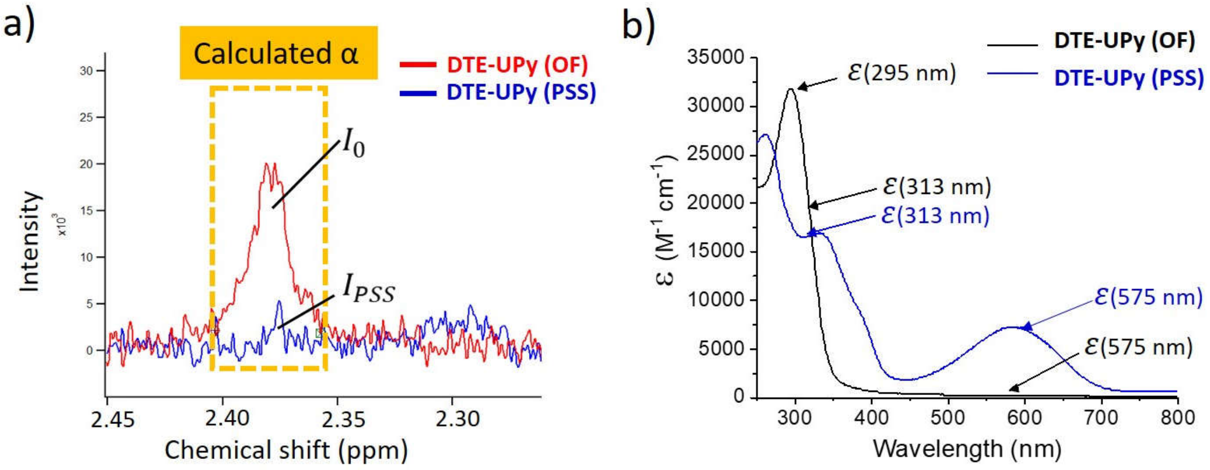

Figure IV-3: Molar absorption coefficients determinations through combination of stationary UV-Visible spectroscopy with NMR spectra before and after UV irradiation. a) NMR spectra obtained in hexane (5×10^{-5} M). Spectra of molar extinction coefficients for OF and CF isomers of b) wavelengths maxima and c) wavelengths observation and excitation.

IV.1.2.2. Quantum yields

To determine the photocyclization and photoreversion yields, the photocoloration and photodecoloration kinetics were registered and fitted with a classical spectrokinetic model (neglecting thermal relaxation). From the OF, the CF absorption maximum at 575 nm is plotted versus the UV irradiation time as depicted in Figure IV-4a.

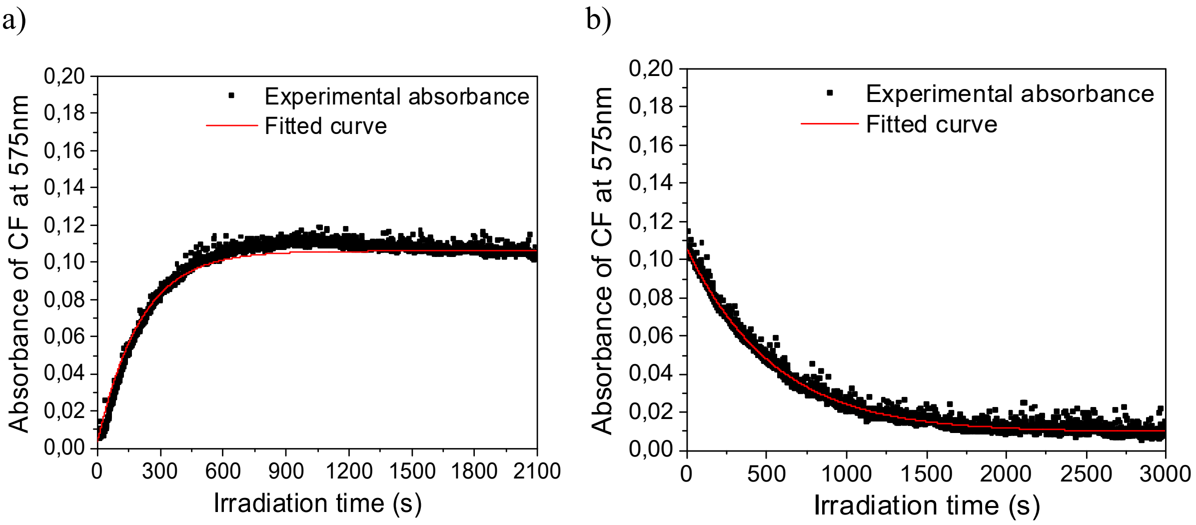

Figure IV-4: Time profile of CF absorbance at 575 nm upon a) UV and b) visible irradiations.

The CF absorbance reaches a plateau beginning from 600 s upon UV light irradiation. It is interesting to note that the photocyclization kinetic (OF → CF) is not perfectly fitted due to the superposition of the supramolecular assembly kinetic. The CF disappearance under visible irradiation is the signature of the cycloreversion reaction (CF → OF) as illustrated in Figure IV-4b. This reaction takes longer time since the plateau is reached only after 2500 s of visible irradiation.

In a previous investigation of the DTE-UPy assemblies [4], it was found that quantum yields were sensitive to the presence of oxygen. Therefore, DTE-UPy chloroform solution was degassed with inert gas as argon. Then, this solution was investigated by a photolysis approach. The photocyclization and photoreversion yields were determined according to the procedure described in Chapter II and were summarized in Table IV-1.

Table IV-1: Optical properties of DTE-UPy in hexane upon irradiation at 313 nm. The obtained values compared to those of literature (*). [5]

	λ_{abs}^{max} (nm)		α	ε ($10^4 mol^{-1}\ L\ cm^{-1}$)		Quantum yield	
	OF	**CF**		**OF**	**CF**	ϕ_{cycl}	ϕ_{rev}
DTE*	273	575	-	2.38	0.71	0.46	0.015
DTE-UPy (Ar)	295	575	0.89	3.18	0.72	0.36	0.008

From one hand, photoreversion yields of respectively DTE and DTE-UPy appear with a similar magnitude order regardless the proceeded determination method. Thus, this suggests that the opening ring reaction of DTE core is weakly influenced by the presence of UPy-end groups. From the other hand i.e. the photoconversion yields case, functionalization of DTE core with UPy-motifs induce a decrease of the quantum yield. From 0.46 (DTE), the photoconversion yield goes down to 0.36 for (DTE-UPy). Hamdi and coworkers [4] attributed this decreases to the fact that the UPy-motifs modify the photochemical process of DTE and thus alter the photoconversion reaction.

IV.2. Evidence for DTE-UPy supramolecular assembly in the solid state

The synthesized DTE-UPy powder is expected to present species majoritarily within their OF oligomers. Their colorless solution with a concentration up to 2.10^{-4} M in chloroform becomes dark blue when illuminated with a UV light. After several minutes of UV illumination, a precipitate appears floating within the solution surface as illustrated in Figure IV-5 (video IV-1, ▷). Such observed phenomenon is the consequence of the formation of the supramolecular assembly formation which takes place only for the CF species as explained in the beginning of this Chapter (Figure IV-1). Indeed, after enough time of UV illumination (Photo Stationary State: PSS), the supramolecular assembly occurs (see DLS curve in Figure IV-1b) until the solvation threshold is reached. Beyond this limit, the supramolecular assembly is no longer solvated and the precipitate appears. As evidence, to gain more insight about the UPy-UPy organization, it is of prime importance to collect the solid blue precipitate and then dried under vacuum at room temperature.

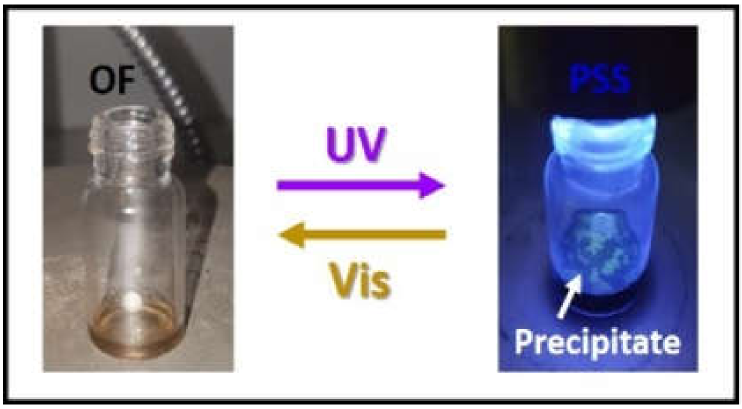

Figure IV-5: Formation of the precipitate.

In the following, the CF precipitate will be denoted DTE-UPy$_{prp}$ (CF) and will be systematically compared to the less organized powder (synthesis products) denoted DTE-UPy$_{pwd}$ (OF) in order to assess the photochemical, thermal, structural and photomechanical properties. As previously discussed, the DTE-UPy$_{pwd}$ (OF) in solution cannot form a supramolecular assembly, only small oligomers are present. The macromolecular assembly of OF can only be obtained by visible light illumination of DTE-UPy$_{prp}$ (CF) and is noted DTE-UPy$_{prp}$ (OF).

IV.3. DTE-UPy supramolecular system: thermal analysis

IV.3.1. Degradation kinetics

In order to check the structural stability of the DTE-UPy molecules during temperature investigation, the degradation kinetic was followed by TGA analysis (Figure IV-6) under dioxygen atmosphere.

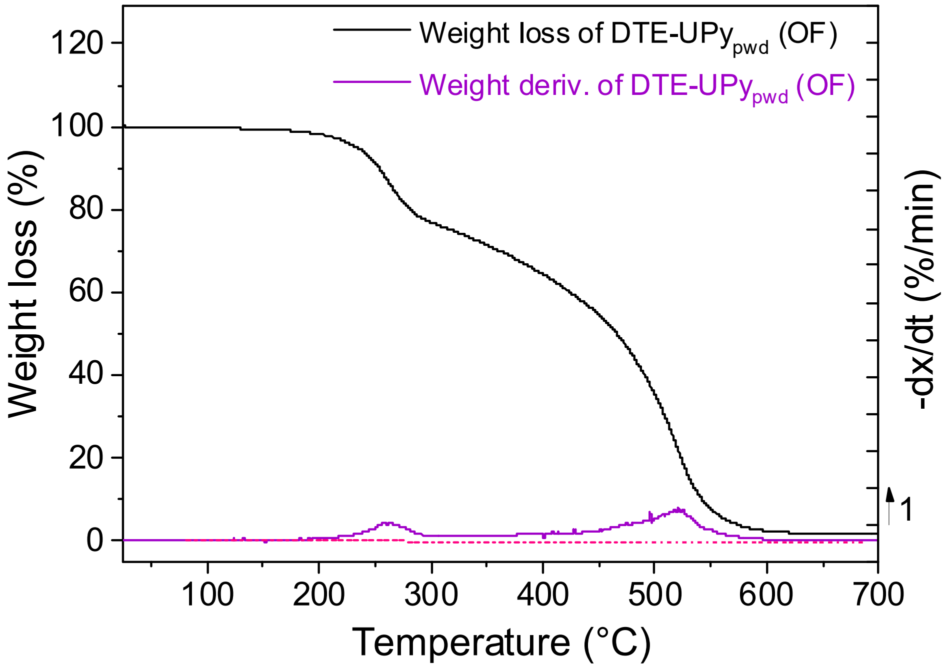

Figure IV-6: TGA curve of thermal decomposition of DTE-UPy.

Two weight losses are observed. The first one started at around 189°C and is ending about 300°C. The second one occurs in the temperature region of 376-610°C. Generally, such observation can be explained by the fact that a thermo-oxidative degradation may occur under O_2 atmosphere. This degradation begins via an initiation step induced by physical (temperature, UV light...) and chemical (traces of peroxides...) factors. The propagation steps may occur and give birth to different steps of mass loss. Compared to DTE, the thermal stability of DTE-UPy was improved and shifted to higher temperatures: T_{deg} (DTE-UPy) = 189°C > T_{deg} (DTE) = 165°C. This observation suggests that UPy-end groups improve the thermal stability of DTE under realistic atmospheric conditions.

IV.3.2. Thermal transitions

The thermal properties of DTE-UPy$_{pwd}$ (OF) and DTE-UPy$_{prp}$ (CF) were assessed by DSC. Thermograms are reported in Figure IV-7.

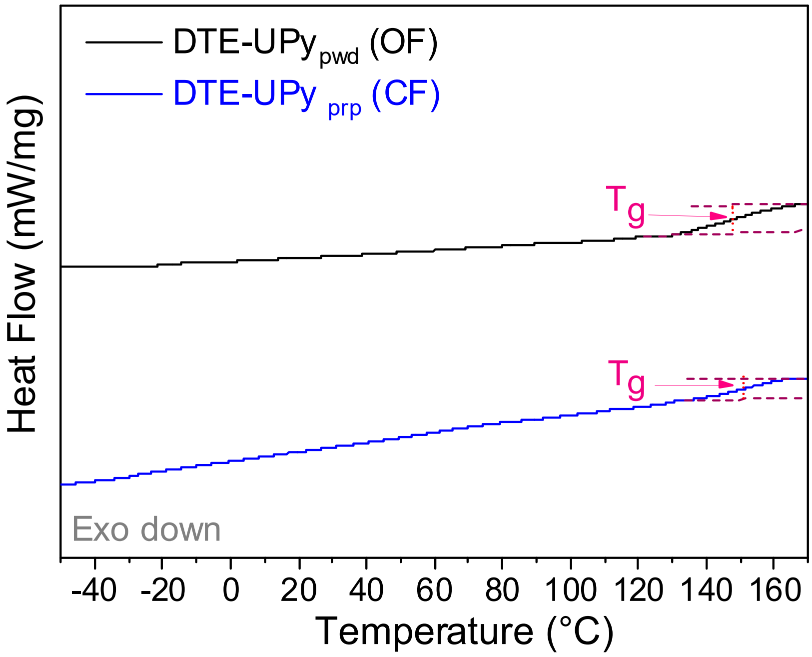

Figure IV-7: DSC curves of DTE-UPy isomers. First heat run with heating rate of 10°C/min.

Each thermogram present an endothermic step characteristic of the glass transition (transition of the glassy state to the liquid state) with a temperature (T_g) of around 148°C for DTE-UPy$_{pwd}$ (OF) and 151°C for DTE-UPy$_{prp}$ (CF). Unlike DTE with T_g values at roughly 34°C for DTE (OF) and 36°C for DTE (CF), no endothermic peak characteristic of crystals melting is detected. The absence of endothermic peaks and also the large differences between DTE and DTE-UPy glass transitions are related to:

i) a large and strong UPy-UPy interactions;

ii) a less "flexible" photochromic core due to bulky UPy moieties.

Indeed, since the core is more "flexible", DTE can crystallize in different polymorphic forms [6-8]. The incorporation of rigid UPy-moieties and the formation of strong quadruple hydrogen bonding disrupts the DTE freedom and consequently inhibits the crystals growing. As consequence, no crystallization can occur. Therefore, the presence of UPy moieties induce the transformation from semi-crystalline DTE into amorphous DTE-UPy.

IV.4. DTE-UPy supramolecular system: structural analysis

IV.4.1. Evidence for quadruple hydrogen bonds by WAXS

DSC experiments have provided insight into the structural features of DTE-UPy. Such observations are consistent with WAXS experiments (Figure IV-8) performed on DTE-UPyprp (CF) and DTE-UPypwd (OF). At room temperature, both samples present broaden amorphous halo peaking near 2θ = 20° and no signature of diffraction rings ascribable to a crystalline structure.

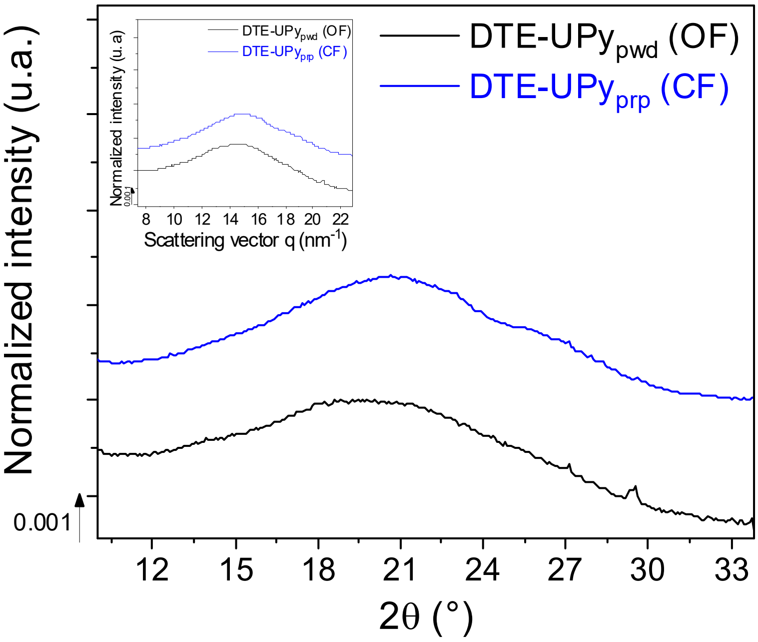

Figure IV-8: WAXS intensity profiles of DTE-UPy.

IV.4.2. Long range distances

- **First insight about arrangement**

Further characterization of the amorphous DTE-UPy was monitored through the SAXS investigation of DTE-UPypwd (OF) and DTE-UPyprp (CF). At room temperature, no discernable scattering peak was observed in the small q-range of [0.2 - 1.4 nm^{-1}] (Figure IV-9a). While two scattering peaks (noted peak-1 and peak-2) are visible at higher q (Figure IV-9b). The beginning of a scattering peak belonging to peak-1 was verified in the medium q range i.e. [1.4 - 2 nm^{-1}] but not presented herein (see appendix IV).

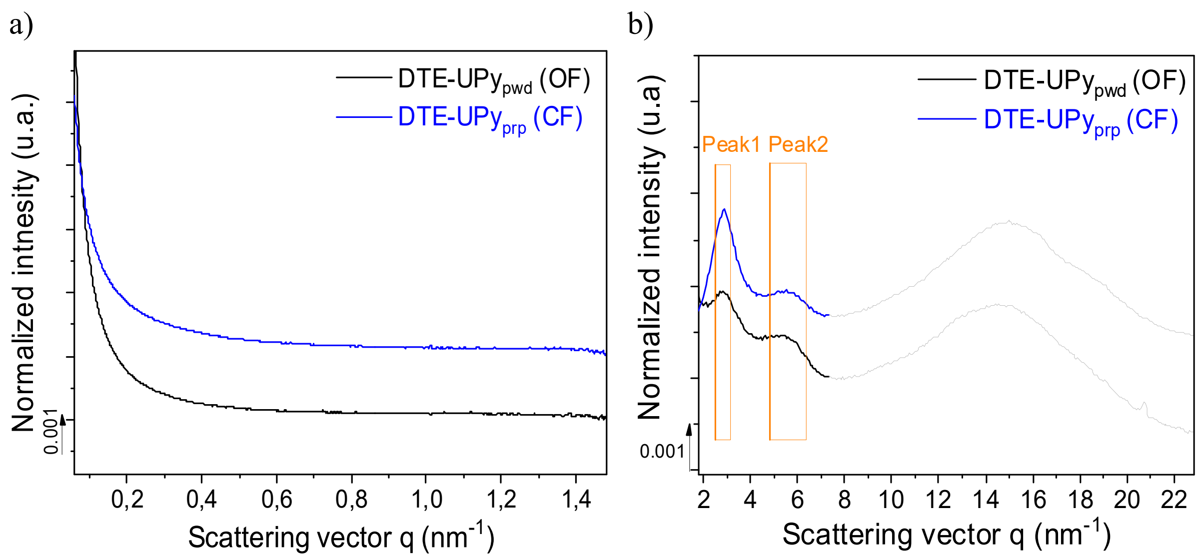

Figure IV-9: OF- and CF-assemblies within DTE-UPy. a) SAXS pattern at room temperature. b) WAXS pattern at room temperature.

According to the Bragg's law ($d = 2\pi/q_{max}$ with q_{max} the position of the peak maximum), the d spacing was estimated and the values are reported in Table III.2. For both samples, the characteristic distance d_1 were identical. The only difference concerns the peak intensity, which is higher for DTE-UPy$_{prp}$ (CF) suggesting a more organized assembly. The distance d_2 slighly shifted value to higher distance from 1.08 nm to 1.15 nm for DTE-UPy$_{prp}$ (CF) and DTE-UPy$_{pwd}$ (OF), respectively.

Table IV-2: d-spacing estimation.

	peak-1		**peak-2**	
	q_{max-1} (nm^{-1})	**d_1 (nm)**	**q_{max-2} (nm^{-1})**	**d_2 (nm)**
DTE-UPy$_{pwd}$ (OF)	2.88	2.18	5.44	1.15
DTE-UPy$_{prp}$ (CF)	2.89	2.17	5.81	1.08

- **Assignment of the peaks**

In order to assign both peaks, new dithienylethenes functionalized from both sides with UPy-end groups presenting various lengths of lateral alkyl chains (R = C_7H_{15}, $C_{13}H_{27}$, $C_{17}H_{35}$) have been synthesized (see Chapter II for more details). The different DTE-UPy (noted DTE-UPyC7, DTE-UPyC13, DTE-UPyC17) in OF conformation were compared to our studied DTE-UPyC11 (i.e. DTE-UPy with an alkyl chain length of R = $C_{11}H_{23}$) also noted DTE-UPypwd (OF). The intensity profiles are depicted in Figure IV-10.

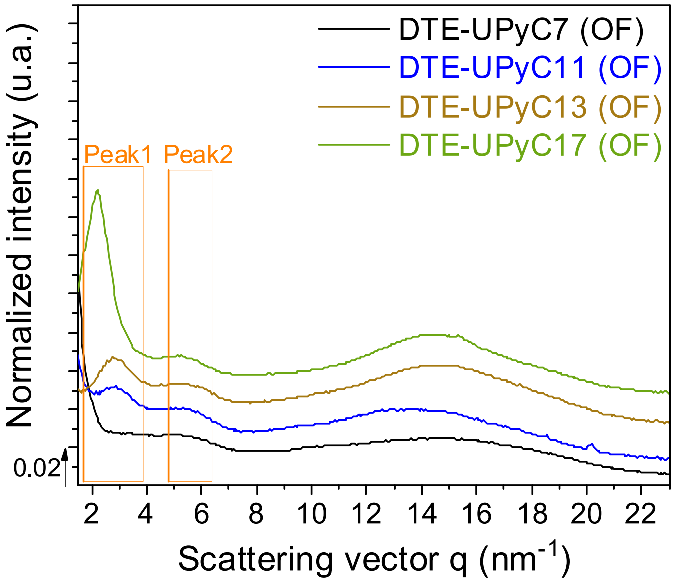

Figure IV-10: Intensity profiles of DTE-UPy (OF) with various substitutions.

As the length of DTE alkyl chains increase, peak-1 shifts to smaller q values and the peak intensity increases. Meanwhile, the position and the intensity of peak-2 are fixed with an average value of around d_2 = 1.18 nm.

Table IV-3: Peaks positions and characteristic d-spacing distances.

	peak-1		**peak-2**	
	q_{max-1} (nm^{-1})	**d_1 (nm)**	**q_{max-2} (nm^{-1})**	**d_2 (nm)**
DTE-UPyC7	3.12	2.02	5.47	1.14
DTE-UPyC11	2.88	2.18	5.44	1.15
DTE-UPyC13	2.73	2.30	5.35	1.17
DTE-UPyC17	2.20	2.86	5.23	1.20

Peak-1. A d-spaced ordering associated to the peak-1 varies drastically with the length of alkyl chains suggesting that peak-1 can be related to the intermolecular distances between neighboring molecules.

Peak-2. An identical value of the distance d_1 = 1 nm has already been reported by Meijer et al. [9] and is associated to the distance between two successive stacked molecules, also called the stack-to-stack distance. The author demonstrated that this distance is quasi-identical whatever the nature of UPy lateral alkyl groups. Herein, we expect a similar assembly of the DTE-UPy molecules.

- Difference between DTE-UPy$_{prp}$ (CF) and DTE-UPy$_{pwd}$ (OF) (DTE-UPyC11)

For peak-1 at q = 2.9 nm^{-1}, diffractograms present the same characteristic distance d_1 = 2.17 nm underlining the fact that the intermolecular assembly is identical for both samples. The observed difference of intensity is associated to a higher contribution of DTE-UPy$_{prp}$ (CF) molecules. Concurrently, the intensity of peak-2 for both samples is identical. The only difference concerns the shift of d_2 from 1.08 nm to slightly higher distance of 1.15 nm for DTE-UPy$_{prp}$ (CF) and DTE-UPy$_{pwd}$ (OF), respectively. This result is in agreement with the higher organization within DTE-UPy$_{prp}$ (CF) assembly.

- Temperature effect

To confirm the assignment of the two peaks, a temperature rise up was performed. DTE-UPyC11 was heated in the temperature range of 30-170°C as illustrated in Figure IV-11.

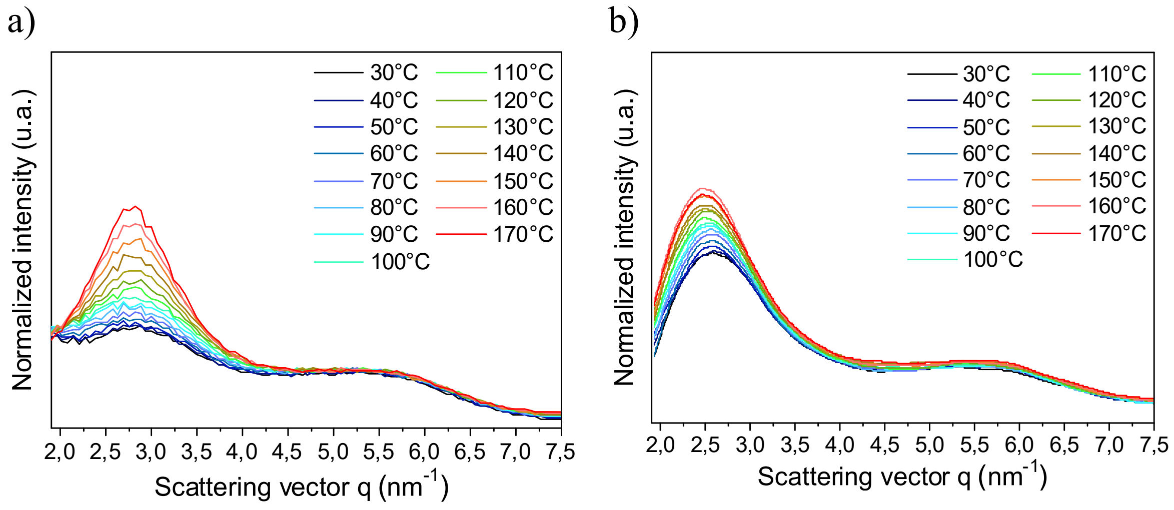

Figure IV-11: DTE-UPy structural evolution upon heating. a) OF-powder and b) CF-precipitate.

During heating, it appears that peak-1 of both samples shift slightly to lower q-values. The corresponding distances from diffractograms are gathered in Table IV-4. The distance d_1 increases with temperature due to the intermolecular network dilatation. After reaching the set temperature, the intensity of peak-1 increases for both DTE-UPy$_{pwd}$ (OF) and DTE-UPy$_{prp}$ (CF) suggesting that the temperature promotes the interaction contribution. Concurrently, the peak-2 presents the same intensity and position regardless the nature of sample (OF or CF). The stack-to-stack distance is not influenced by temperature.

Table IV-4: Temperature dependency of peaks positions and characteristic d-spacing distances.

	peak-1		peak-2	
	qmax-1 (nm^{-1})	d1 (nm)	qmax-2 (nm^{-1})	d2 (nm)
DTE-UPy$_{pwd}$ (OF) / T30	2.88	2.18	5.44	1.15
DTE-UPy$_{prp}$ / T30	2.89	2.17	5.81	1.08
DTE-UPy$_{pwd}$ (OF) / T170	2.77	2.27	5.44	1.15
DTE-UPy$_{prp}$ / T170	2.79	2.25	5.81	1.08

Noting that the glass transition at T_g = 150°C does not influence the temperature evolution. The stability is expected to be maintained until the degradation temperature i.e. T_{deg} = 189°C.

IV.4.3. Light effect on structure

The light effect on the structure of DTE-UPy$_{pwd}$ (OF) small oligomers as well as large supramolecular assembly of DTE-UPy$_{prp}$ (CF) were investigated.

- **Small oligomers**

The evolution of the DTE-UPy$_{pwd}$ (OF) assembly was investigated under illumination. WAXS intensity profiles measured in situ under UV-illumination are illustrated in Figure IV-12.

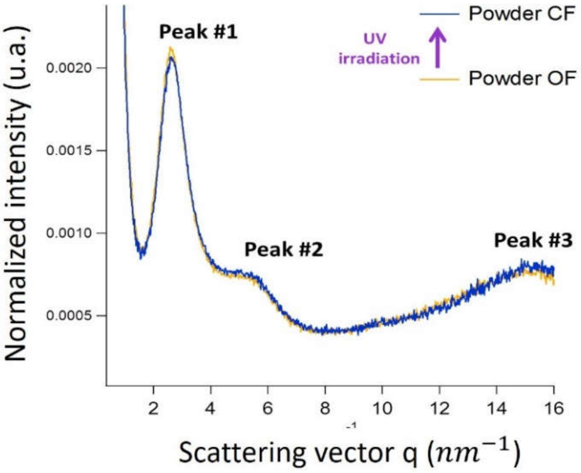

Figure IV-12: DTE-UPy structural evolution in situ under UV-illumination from OF-powder to CF-powder.

Both diffractograms exhibit the two characteristic peaks at respectively q = 2.8 nm^{-1} (peak-1) and q = 5.4 nm^{-1} (peak-2) as have been described above. The peak-3 belonging to the amorphous halo is present at around q = 15.1 nm^{-1}. Surprisingly, the positions of peaks are found to be non-affected by UV-irradiation. Concerning the peaks intensity, it is difficult to explore. Accordingly, no structural change induced by UV light illumination can be reported.

- **Large supramolecular assembly**

Similarly, to the previous experiment, a sample of DTE-UPyprp (CF) was analyzed in situ under visible light illumination. This illumination was carried out for 1 hour to ensure a maximum of conversion from OF → CF. The diffractograms before and after irradiation are illustrated in Figure IV-13.

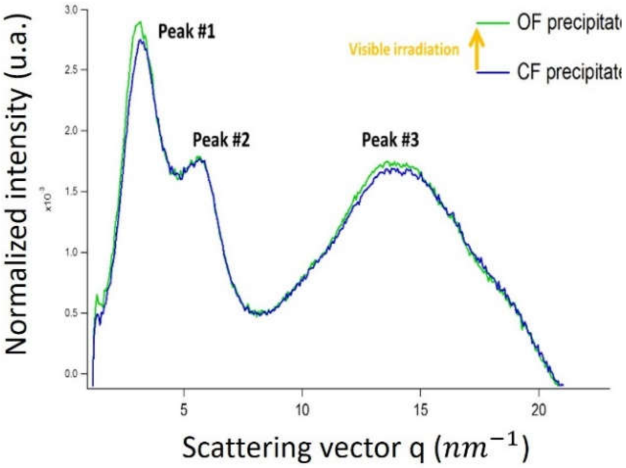

Figure IV-13: DTE-UPy structural evolution in situ under visible-illumination from CF-precipitate to OF-precipitate.

Despite the applied visible light, peak-1, peak-2 and the amorphous halo appear at the same positions as reported above. This leads to emphasize that no structural change induced by UV light illumination can be reported. It is noticeable that peak-1 and peak-3 gained a slight intensity. While, peak-2 remains intact. The exact reason for this phenomenon is still unclear and may need further experiments to confirm this observation.

IV.4.4. Schematic representation of the structure

In order to summarize this part about the structural analysis of DTE-UPy, a schematic representation of the molecular organization was drawn and then illustrated in Table IV-5. The designed oval representation is related to the unknown number of self-assembled DTE-UPy regardless OF or CF isomers. Results about the influence of the: (i) alkyl chain length (R) of the UPy substituents within their OF, (ii) the differences between OF-powder and CF-precipitate, (iii) temperature arise impact and (iv) illumination impact on assemblies are gathered and reported.

Table IV-5: DTE-UPy structural organization.

Schematic representation	Amorphous DTE-UPy molecules or macromolecules in OF or CF 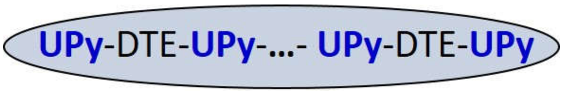	
R ↑	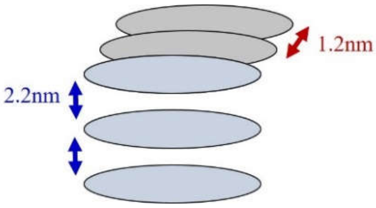 DTE-UPyC11(OF)	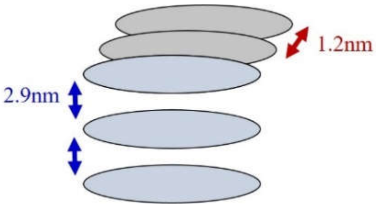 DTE-UPyC17 (OF)
OF-pwd / CF-prp	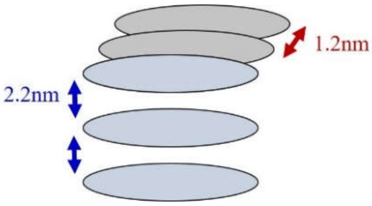 DTE-UPy$_{\text{pwd}}$ (OF)	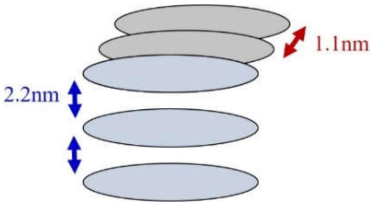 DTE-UPy$_{\text{prp}}$ (CF)
T ↑	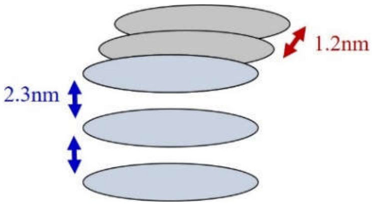 DTE-UPy$_{\text{pwd}}$ (OF) (T170)	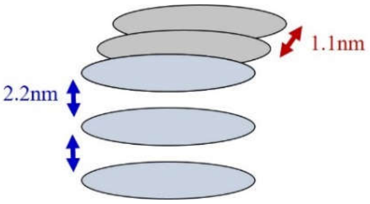 DTE-UPy$_{\text{prp}}$ (CF) (T170)
in situ UV-illumination	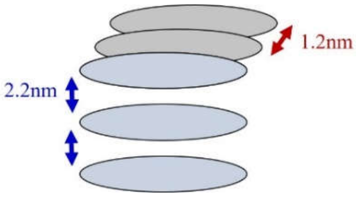 DTE-UPy$_{\text{pwd}}$ (OF)	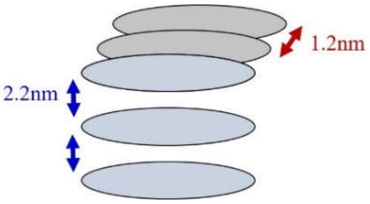 DTE-UPy$_{\text{pwd}}$ (CF)
in situ visible-illumination	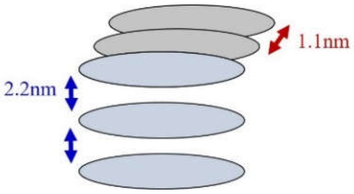 DTE-UPy$_{\text{prp}}$ (CF)	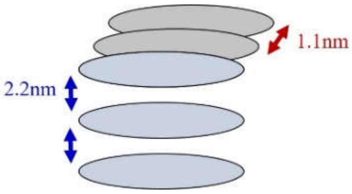 DTE-UPy$_{\text{prp}}$ (OF)

It is important to note that at nanometric scale, both samples of large supramolecular assembly of DTE-UPy$_{prp}$ (CF) and small oligomers of DTE-UPy$_{pwd}$ (OF) exhibit approximatively the same structural signature.

IV.5. Photomechanical effect of DTE-UPy supramolecular systems: presentation

This section is devoted to highlight the microscopic photo-responsiveness of DTE-UPy self-assemblies under wield-field microscopy setup with in-situ illumination. The video duration acquired by the CCD camera is 10 min with one picture every 1 s (600 pictures). The illumination sequence is always the same: ~10 seconds without light and then ~50 seconds under light irradiation. The sample is illuminated in-situ with visible irradiation (550 nm band pass filter) and UV irradiation (313 nm band pass filter). Moreover, it is there noteworthy to precise that the light spot covers the entire observed matter. The video of 360 frames are accelerated 100 times with a total duration of 6 s.

IV.5.1. Small oligomers for DTE-UPypwd (OF)

It is worth to remain that for DTE-UPy the average change of particle size upon UV and visible lights was estimated by means of DLS experiments **[1]**. These measurements have revealed that DTE-UPy$_{pwd}$ (OF) has no signature because the size of the molecular assembly is lower than the apparatus detection limit (10 nm). Only small oligomers are expected.

The photomechanical behavior of DTE-UPy$_{pwd}$ (OF) was investigated upon irradiation. By analogy to DTE, a granular powder was deposited on glass slip and then exposed from above to UV light irradiation (313 nm). Figure IV.14 illustrates a series of snapshots (10 min gap) of the accelerated video (6 s duration, video IV-2, ▷).

Mechano-optical microscopy revealed that the sample first bends perpendicularly to the incident light (to the right in Figure IV.15a) after 200 s of irradiation and then bends perpendicularly to the light source in the opposite direction (to the left) after 400 s. Therefore, the ring-closed reaction (OF → CF) seems leading a morphological change of assembly.

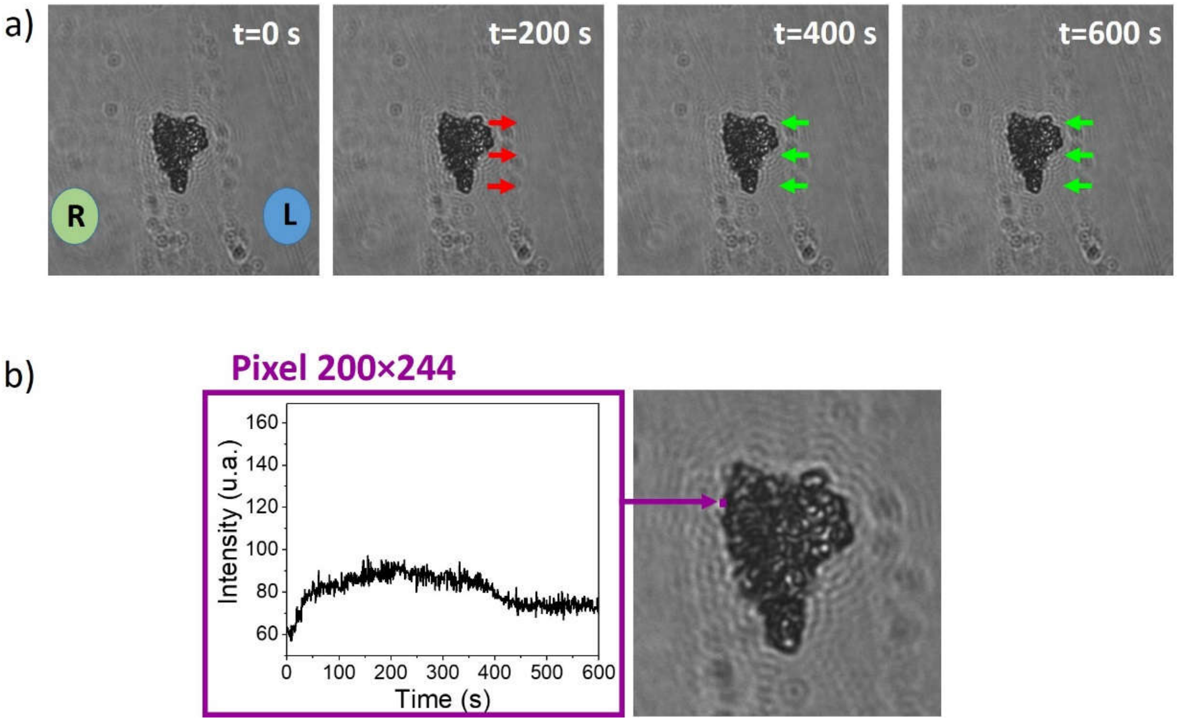

Figure IV-14: Photoinduced morphological changes of self-assembled OF upon UV-irradiation. a) Photographs from top side view and b) kinetic evolution of photomechanical bending with exposure time. Red arrows associated to bending direction. Green arrows associated to bending return-back direction. R (right side) and L (left side) assigned to the bending sense according to the viewing plane.

Moreover, kinetic slice at the center of the granular is expected to indicate a complete conversion from OF- into CF-isomers. Thus, it leads to follow the kinetic photochemical conversion. Unfortunately, the entire sample was moving upon UV irradiation, which implies that no indication about whether the photomechanical effect follow/do not follow the photochromism process.

The response of photoinduced bending is presented in Figure IV-14b through the evolution versus the exposure time of one representative pixel (pixel 200×244). A slowly displacement was observed since the first irradiation seconds as the optical signal increase upon irradiation. Once a bearing is reached nearby 360 s, optical signal decrement is seemingly associated into the edge return-back of sample. The return-back bending suggests: (i) possible thermal induced relaxation which has to be confirmed whether the sample maintain its shape when light is turned off; (ii) mechanical relaxation in the sense that the photoinduced force stop when the conversion is totally induced along the sample as illustrated in Figure IV-15.

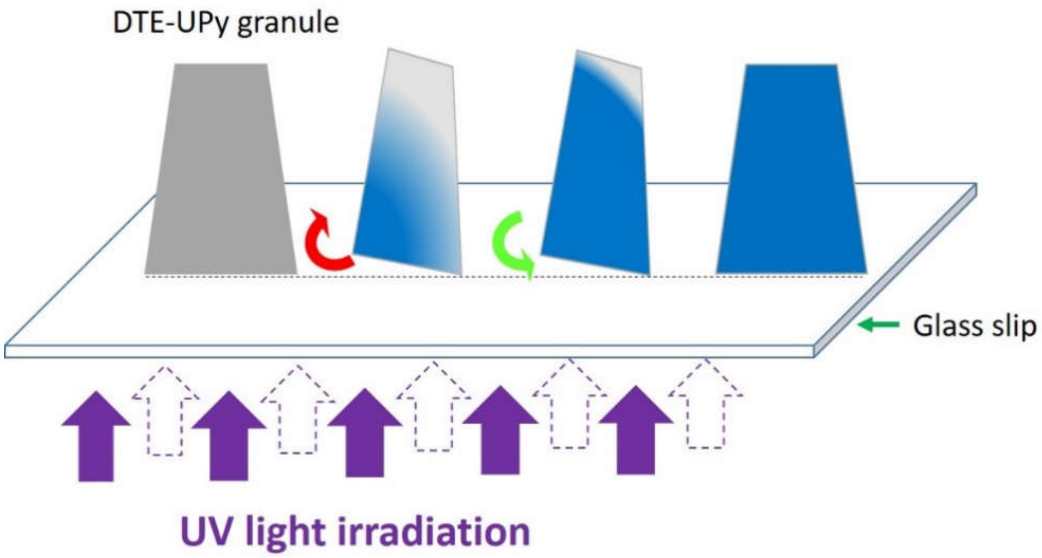

Figure IV-15: illustration of DTE-UPy$_{pwd}$ photo-induced mechanical approach. Red arrow associated to the mechanical bending. Green arrow associated to the mechanical relaxation.

IV.5.2. Large supramolecular assembly for DTE-UPy$_{prp}$ (CF)

IV.5.2.1. Aggregation Induced Emission upon visible light

After deposition on glass slip, the amorphous blue precipitate DTE-UPy$_{prp}$ (CF) was exposed into visible light from bottom side. Figure IV-16a illustrates a series of snapshots (10 min gap) from the accelerated video (6s duration – video IV-3, ▷).

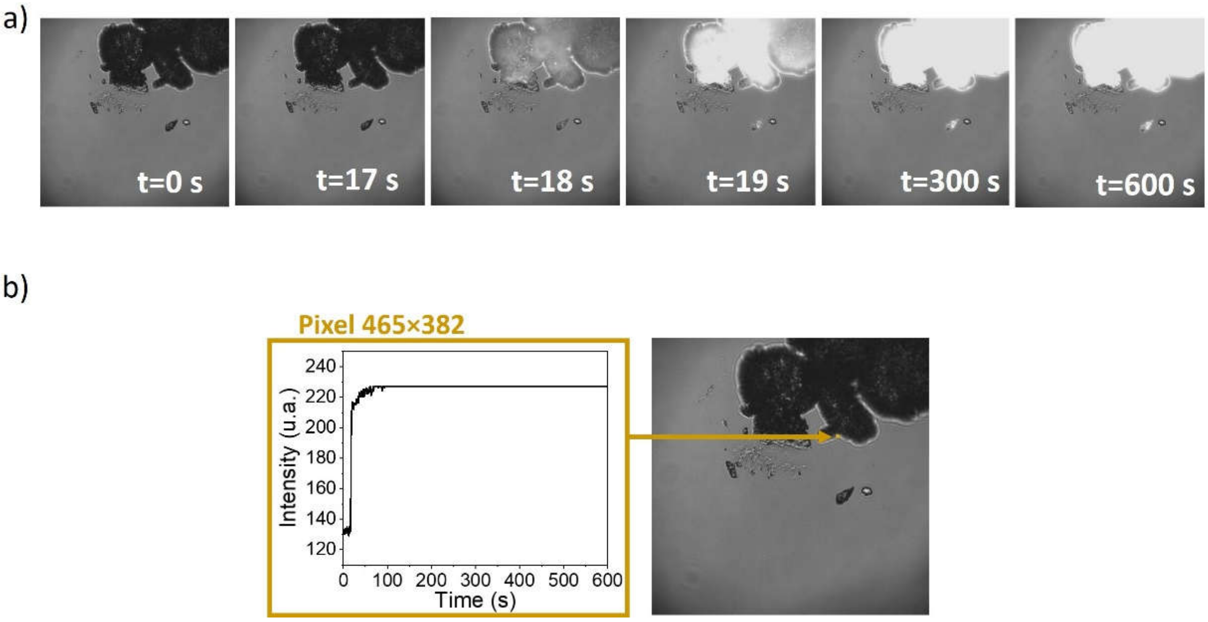

Figure IV-16: Visible-induced re-emission of DTE-UPy precipitate. a) Stepwise through visible-induced fluorescence in DTE-UPy (The irradiation beginning was 17 seconds). b) Evidence of visible-induced re-emission by following the kinetic evolution of the pixel 465×382 against exposure time.

Surprisingly, DTE-UPy$_{prp}$ (CF) appears to gain bright white light instantaneously at the first seconds of exposure time. The emitted radiation stops almost immediately when the incident irradiation stops. What is the origin of such unexpected light? Indeed, this emission is reported only for visible excitation but not for UV excitation. Because PEB films do not display similar process (see next chapter), DTE-UPy molecules have to be responsible for such light. Despite the fact that DTEs are well known to be non-fluorescent, we have undertaken photochemical measurement in chloroform solutions (in situ thin film will be undertaken in the future). As seen in Figure IV-17, fluorescence of both OF (λ_{max} = 477nm; ϕ_{fluo} =0.0008) and CF (λ_{max} = 588nm; ϕ_{fluo} =0.0003) were detected regardless their very low quantum yields.

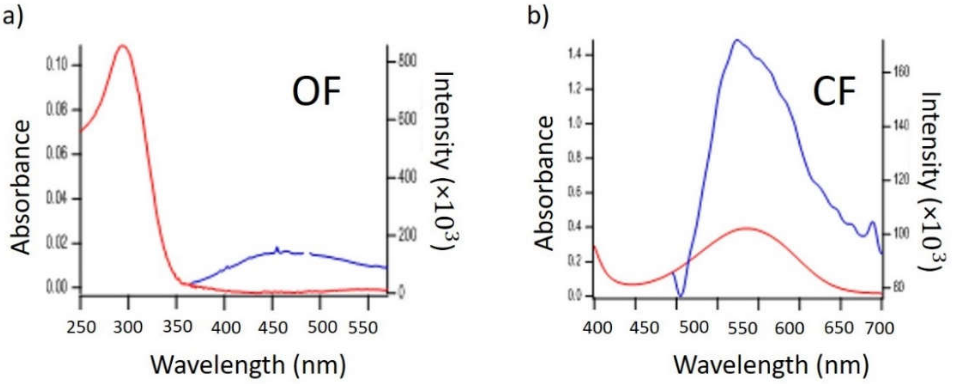

Figure IV-17: Visible-induced fluorescence identified by fluorescence microscopy (bleu spectra) correlated to absorption measurements (red spectra) for OF and CF isomers, respectively.

By comparison with DTE (Table IV-6), the stock shift (energy gap between absorption state and emission state) is constant for OF isomer. The stock shift of CF isomer is reduced a factor of 50 probably due to UPy-UPy interactions. This result is probably a first insight of a possible aggregation induced emission (AIE) [10]. Based on that result for the solution, this unexpected emission reported can be related with AIE effect of DTE-UPy (CF) large assembly. Even if it is attempting to invoke the AIE of OF isomer, the lake of emission within UV excitation has to be achieve in the future.

Table IV-6: Spectroscopic parameters.

	OF				**CF**			
	λ_{max}(Abs) (nm)	**λ_{max}(Fluo) (nm)**	**Δσ (cm^{-1})**	**ϕfluo**	**λ_{max}(Abs) (nm)**	**λ_{max}(Fluo) (nm)**	**Δσ (cm^{-1})**	**ϕfluo**
DTE	270	417	13056	0.003	566	678	2919	0.001
DTE-UPy	294	477	13049	0.0008	586	588	58	0.0003

IV.5.2.2. Photomechanical effect upon visible light

Because of this mentioned impressive white light re-emission, it was difficult to observe the photo-generated motions. By following the evolution of a representative pixel (465×382) from the edge of the precipitate, a saturation of the optical signal occurs after 18 seconds (Figure IV-16b).

In order to underline whether DTE-UPy$_{prp}$ (CF) displays dynamic motions by photo-irradiation despite its light emission, the sample is fixed by one side to an attachment point as a way that the precipitate does not touch the glass slip. Figure IV-18 illustrates a series of snapshots (10 min gap) from the accelerated video (6 s duration – video IV-4, 🎞).

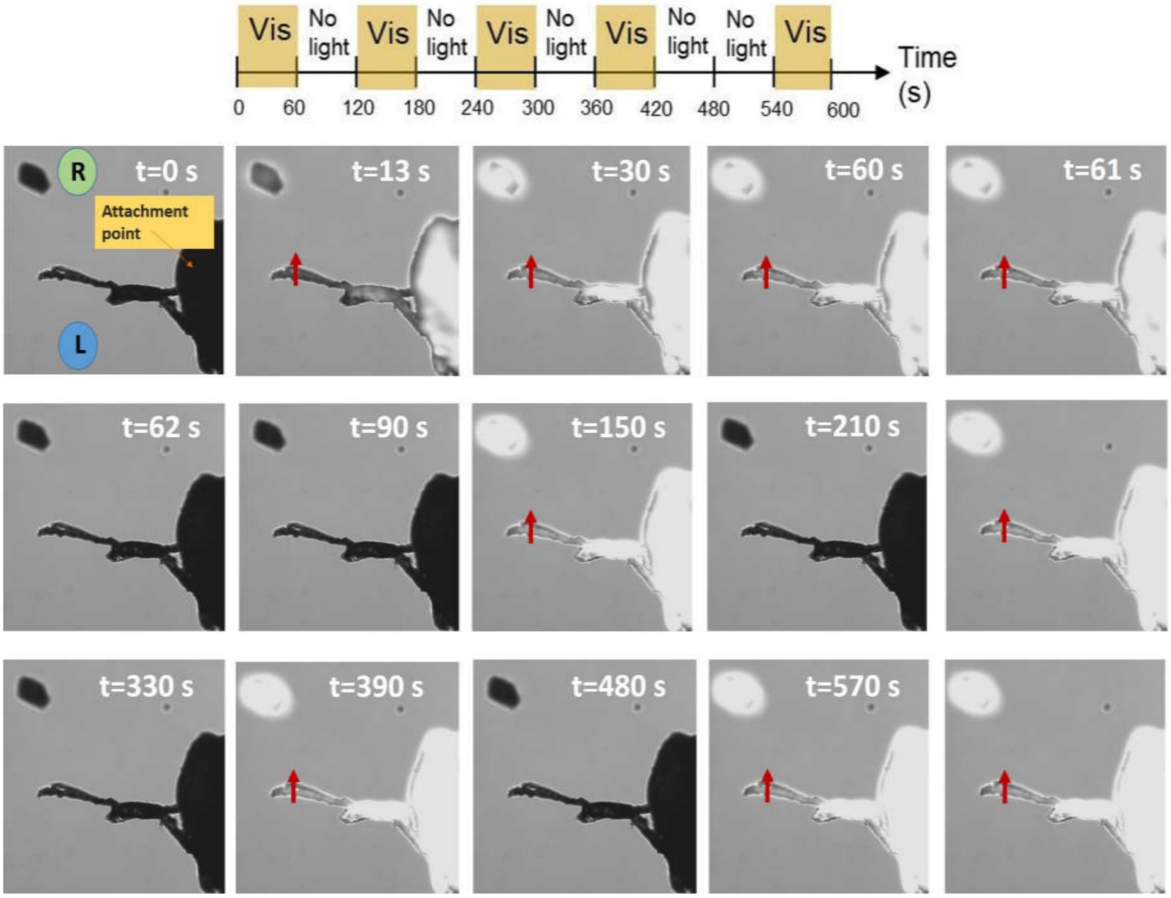

Figure IV-18: Photoinduced bending behavior of DTE-UPy$_{prp}$ (CF). Sample is irradiated with visible light (570 nm) from bottom side (the irradiation beginning was 17 seconds). Red arrow designs the direction of bending. R (right side) and L (left side) assigned to the bending sense according to the attachment point.

By exposure into visible light from below side, the photo-reversion transformation occurs. Concurrently, the sample bends quasi-instantaneously perpendicularly to the incident light direction within the viewing plan (right side designed R-side to the attachment point). After 60 s, the visible illumination is stopped. The sample returns back to its initial position. Different sequences of visible light irradiation (duration ~ 60 s) and no irradiation (duration ~ 60 s) are presented in Figure IV-18. After reaching the 600 s of irradiation, we observed that the sample continues bending perpendicularly to the light source direction (R-side to the attachment point) only under irradiation. It always reverts to the initial position in the dark. This can be explained by a thermal and/or mechanical relaxation as previously described.

This bending behavior is followed versus exposure time. Figure IV-19 illustrates the response of two representative pixels in order to illustrate the difference between photomechanical and photochromic signals. The first was chosen from the edge of the precipitate (red square on sample photograph) and the second in the center of another sample existing in the same photograph, which does not exhibit motions upon UV/visible light irradiations.

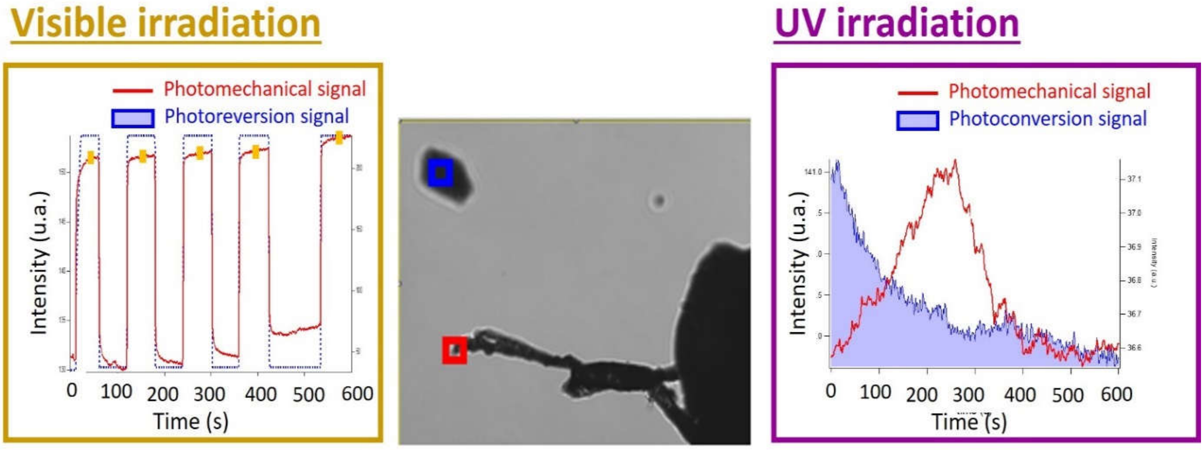

Figure IV-19: Kinetics of photo-induced bending behavior of CF-precipitate versus the irradiation time upon UV and visible light.

Upon visible light, the blue signal shows saturate signal. By stopping light, the signal returns back to its initial value. This proves that the chosen sample does not move. Whereas, in the case of red signal, we can see clearly from the beginning of visible irradiation that there is a difference. The increase of optical signal from the initial level is ascribed to the photo-induced displacement of sample. When the irradiation is stopped, the optical signal decrement seems to be associated to the sample partial return-back (not exactly to the initial position). Upon on/off visible irradiation cycles, same motions are observed.

IV.5.2.3. Photomechanical effect upon UV light

By changing the irradiation wavelength from 550 nm (visible) into 313 nm (UV) from below to above side, the morphological change of previous sample i.e. the precipitate (OF resulting from visible illumination of CF). Figure IV-20 illustrates a series of snapshots (10 min gap) from the accelerated video (6 s duration – video IV-5, ▷).

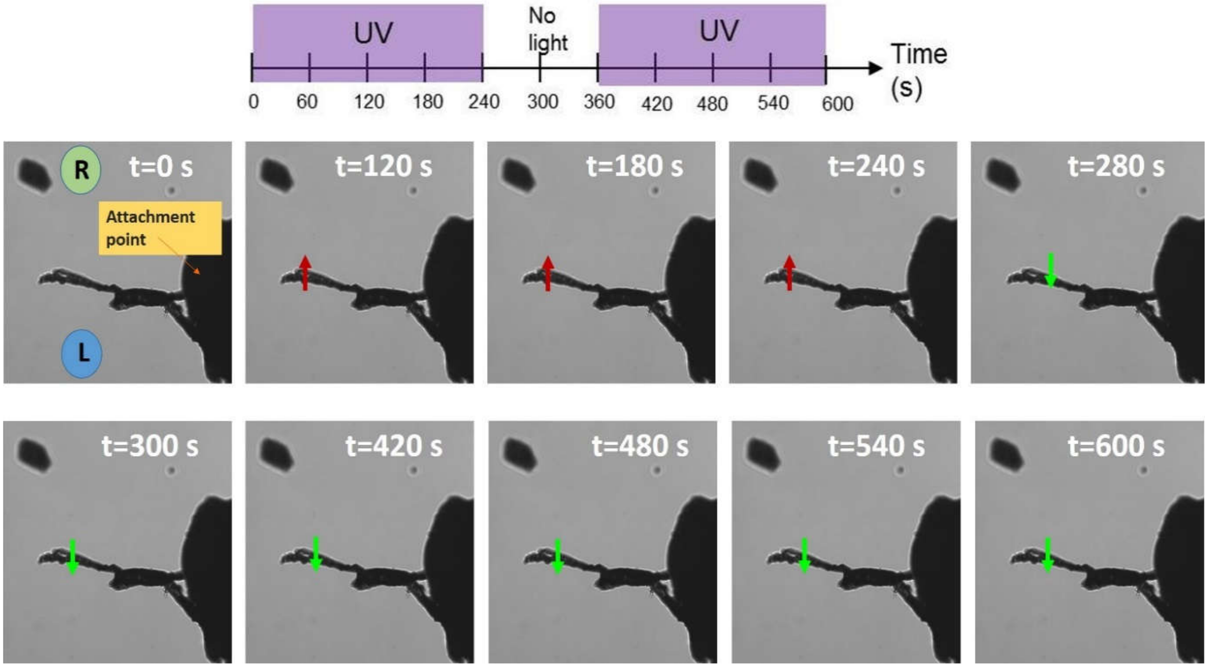

Figure IV-20: Photoiduced bending behavior of DTE-UPy$_{prp}$ (OF). Sample is exposed to 313 nm UV-light from upper side (the irradiation beginning was 17 seconds). Red arrow designs the direction of bending. Red arrow designs the direction of bending. R (right side) and L (left side) assigned to the bending sense according to the attachment point.

Under illumination, the DTE-UPy$_{prp}$ (OF) bends slowly perpendicularly to the incident light direction within the viewing plan (right side designed R-side to the attachment point). The evolution under illumination of the representative pixel of photoconversion signal exhibits instantaneous decrement confirming that photocyclization reaction occurs successfully up to 600 s (Figure IV-20).

Concurrently, photoconversion signal (red signal) can be divided into 3 steps. Firstly, the optical signal increases upon UV light. When the irradiation is stopped (t = 240 s), the optical signal is constant and it was difficult to see if the sample is bending to the left or right side. After 280 s, the optical signal begun to decease the indicating that mechanical relaxation may exist. The recovery of the UV-illumination shows that the optical signal continues decreasing. This decrement was difficult to explain and arose the question about the complete mechanical relaxation of the sample and/or could be attributed to the fact that the sample was bending to the left side (L-side) and then returning-back to its initial position.

IV.6. Photomechanical effect of DTE-UPy supramolecular systems: rationalization

In order to describe the photo-mechancial effect, we supposed that CF-precipitate is composed of successive layers. When the sample irradiated with visible light, the opening-form reaction occurs randomly (CF-precipitate → OF-precipitate). The irradiation induces a molecular volume change of DTE core and consequently implies the expansion of the first photoactive layer. The spreading of this layer in pattern volume emphasizes the bending phenomenon away from the source light. Note that a thermal and/or mechanical relaxation are observed after the visible illumination stopping.

The UV light irradiation of the OF-precipitate induces the closing-form reaction (OF-precipitate → CF-precipitate) randomly of the photoactive layer. The photoinduced electrocyclization exhibits a reduction of the molecular volume explaining the bending phenomenon. When the light is turned-off, the sample maintains its shape meaning the photo-induced motion is not due to thermal effect.

Kitagawa and coworkers have reported the photoinduced bending behavior when describing rod-like crystal motions of diarylethene derivative fixed to a glass capillary **[11]**. The crystal illumination was investigated under UV light from the left side and visible light from the right side to the glass capillary. The crystal bends toward the UV light source direction (365 nm) and then away from the visible light source direction (<500 nm) i.e. the crystal continue bending within the same trajectory direction. A change in unit cell parameters in crystal unit cell accompanied with the photochromic reaction ought to justify photoinduced behavior through Timoshenko's bimetal model described within Chapter I.

Herein, amorphous DTE-UPy induces motions in the same direction regardless the side of illumination. However, upon alternating irradiation with UV and visible light, a change in molecular volume occurs within DTE core between them OF and CF isomers during the photochromic reaction. Contrarily to crystalline state, amorphous DTE-UPy i.e. DTE core owing quadruple hydrogen bonds should react cooperatively and induce a cumulative morphological change in the case of amorphous supramolecular assemblies leading to a bending phenomenon upon irradiation within the same direction (except the mechanical relaxation phenomenon). Therefore, it is there noteworthy to underline that the motions amplitude within crystalline state were more pronounced than those of amorphous state, which was expected.

IV.7. Conclusion

This chapter concerns structural and photomechanical studies of DTE-UPy for either small aggregates DTE-UPy$_{\mathrm{pwd}}$ (OF) and large aggregates DTE-UPy$_{\mathrm{prp}}$ (CF).

One of our first objectives was to figure out the specific signature between UPy recognition sites. Thanks to SAXS experiments, we successfully picked out two characteristic peaks within distances of 1 nm and 2 nm, respectively. The distance 1 nm is intact regardless the temperature change and light excitation. This result indicates that light activation of photochromic core does not change their neighboring structure. Confirmation of peak-1 and peak-2 assignation and invariant structure upon excitation have to be confirmed in the future with advanced molecular dynamic calculations.

Unexpectedly, DTE-UPy was found to be totally amorphous (Tg~150°C) compared to crystalline DTE. This is related to both arguments: presence of quadruple hydrogen bonds between molecules and introduction of lateral alkyl chain.

Concerning photomechanical effect and in continuity with the surprising results from the previous chapter i.e. amorphous DTE being photomechanical, DTE-UPy being amorphous as well (regardless small (OF) or large (CF) assemblies) presents reversible light induced changes. This result will be investigated in chapter VII dealing DTE-UPy/PEB-UPy concerning whether the presence of photochromic molecules agglomeration can play a key role in inducing photmechanical effect.

References

[1] Takeshita, M., et al., Photoreversible supramolecular polymer formation. Chemical Communications, 2005(6): p. 761-763.

[2] Söntjens, S.H.M., et al., Stability and lifetime of quadruply hydrogen bonded 2-Ureido-4[1H]-pyrimidinone dimers. Journal of the American Chemical Society, 2000. 122(31): p.7487-7493.

[3] Folmer, B.J.B., et al., Supramolecular polymer materials: Chain extension of telechelic polymers using a reactive hydrogen-bonding synthon. Advanced Materials, 2000. 12(12): p. 874-878.

[4] Hamdi, I., et al., Excited-State Dynamics of Dithienylethenes Functionalized for Self-Supramolecular Assembly. The journal of physical chemistry. A, 2018. 122(14): p. 3572.

[5] Irie, M., et al., Photochromism of dithienylethenes with electron-donating substituents. Journal of Organic Chemistry, 1995. 60(25): p. 8305-8309.

[6] Fujinaga, N., et al., Photoinduced topographical changes on microcrystalline surfaces of diarylethenes. CrystEngComm, 2016. 18(38): p. 7229-7235.

[7] Irie, M., et al., Reversible Surface Morphology Changes of a Photochromic Diarylethene Single Crystal by Photoirradiation, 2001. 291(5509): p. 1769-1772.

[8] Tong, F., et al., Photomechanical motion of diarylethene molecular crystal nanowires, Nanoscale, 2018. 10(7): p. 3393-3398.

[9] Appel, W.P.J.W., et al., Aggregation of ureido-pyrimidinone supramolecular thermoplastic elastomers into nanofibers: a kinetic analysis. Macromolecules, 2011. 44(17): p. 6776-9297.

[10] Hong, Y., J.W.Y. Lam, and B.Z. Tang, Aggregation-induced emission. Chemical Society Reviews, 2011. 40(11): p. 5361-5388.

[11] Kitagawa, D., R. Tanaka, and S. Kobatake, Dependence of photoinduced bending behavior of diarylethene crystals on irradiation wavelength of ultraviolet light. Phys. Chem. Chem. Phys., 2015. 17(41): p. 27300-27305.

Chapter V.

Telechelic ureidopyrimidonone functionalized thermoplastic elastomer supramolecular properties

The thermoplastic elastomer PEB-UPy is used as a “matrix” to amplify the photomechanical response of the photochromic molecules DTE-UPy. The Chapter V is dedicated to investigate the structure and properties of the thermoplastic elastomer. The first part of this Chapter deals with the PEB “core” properties. Within its second part, the PEB-UPy is studied and compared to PEB in order to identify the influence of UPy motifs on supramolecular assembly.

V.1. Structure and morphology of PEB

V.1.1. Chemical content analysis

Poly(ethylene-co-butylene) denoted PEB ($\mathrm{M_n = 2.5\ kg\ mol^{-1}}$) is a random copolymer of ethylene and butylene segments (chemical structure in Figure V-1). The physical properties of PEB are very dependent on the copolymer crystallinity which can be impacted by the fraction of ethylene and butylene segments and their distribution along the polymer backbone [1,2]. The access to the crystallinity through the assessment of polyethylene (PE) and polybutylene (PB) fractions in the copolymer is possible by means of proton NMR spectroscopy (400 Hz). NMR spectrum of PEB is reported in Figure V-1.

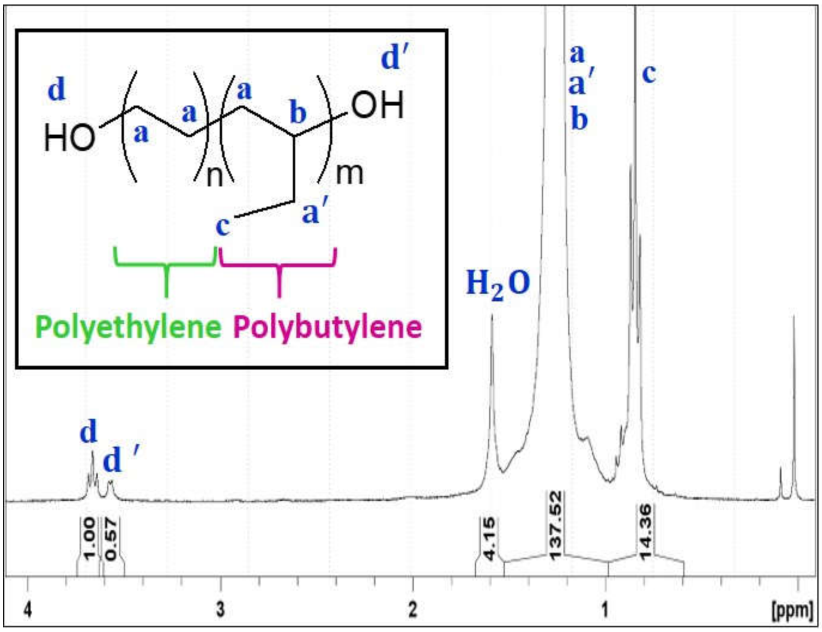

Figure V-1: Proton NMR spectra and assignment of PEB peaks.

The peaks of ethylene and butylene in the region of 0.9 – 1.4 ppm were attributed using literature [3]. The spectrum shows two groups of signals. The assignments of these groups from the proton NMR spectrum are based on the fact that:

i. CH_3 groups attached to saturated carbon from butylene (indexed c) appears at a value of 0.9 ppm.

ii. those of the CH_1 bonded to two double bonded carbon from butylene and hydroxyl group (indexed b) or saturated carbon CH_2 of both ethylene and butylene (indexed a and a' respectively) at 1.3 ppm.

The followed methodology to determine signal intensities from proton NMR and estimate hydrogen content allow the access to the molar fraction of polyethylene (PE) and polybutylene (PB) using the following equations:

$$\%\mathrm{mol(PE)} = \frac{I_{H\,(PE)}}{I_{H\,(PE)} + I_{H\,(PB)}} = 85\% \qquad (V.1)$$

$$\%\mathrm{mol(PB)} = 100 - \%\mathrm{mol(PE)} = 15\% \qquad (V.2)$$

These proportions suggest that the PEB chains crystallize due the high content of PE. Indeed, Sierra et al. [4] observe a decrease of the degree of crystallinity because high butylene chains fraction lead to the interruption of the ethylene sequences rearrangements. High content of PB (upper 50%), the crystallinity is suppressed and PEB is amorphous. In our case, the PB content is low (below 50%). The crystallinity is then expected as non-negligible.

V.1.2. Thermal behavior

V.1.2.1. Degradation of PEB

The thermal degradation of PEB was studied by means of Thermo-Gravimetric Analysis (TGA). More precisely, the kinetic analysis could allow to elucidate degradation mechanisms as well as in predicting the thermal stability of the polymer. Then, PEB was heated from room temperature until 700°C at a heating rate of 10°C/min. Figure V-2 shows the TGA scan under dioxygen air atmosphere.

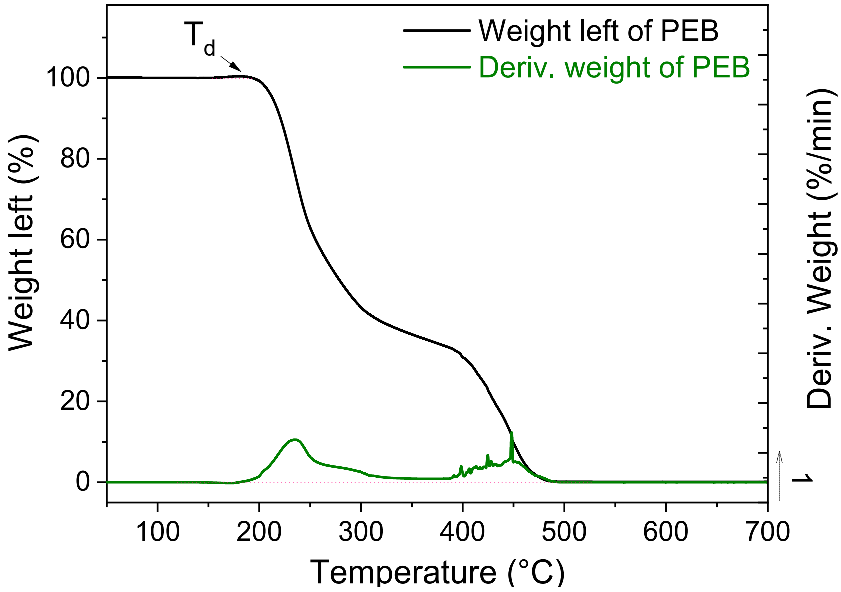

Figure V-2: TGA curves for the thermal decomposition of PEB in air. Heating rates of 10°C/min. Inset plot is derivative graph of loss for degradation in oxidative atmosphere.

At lower temperature, no significant weight change is evidenced. From 186°C, a loss weight of approximately 60% related to the beginning of the degradation is observed. The derivative plot of mass loss indicates that PEB oligomers degrades in three main steps. The well-defined first step begins at 186°C. The second step is figured out through the small shoulder at 260°C. The irregular third step increases from 380°C up to 490°C. Under oxidative degradation, PEB sample has degraded completely without leaving any noticeable residue. Therefore, the temperature range is limited to a temperature lower to 170°C.

V.1.2.2. Thermal transitions

Differential scanning calorimetry analysis (DSC) is carried out to assess the thermal behavior of the PEB under three successive heatings (denoted 1st to 3rd runs)**.** PEB thermogram of the 1st run shown in Figure V-3 presents three main transitions. The first transition is an endothermic step assigned to the glass transition. The associated temperature (T_g) is around -31 ± 3 °C. The second and the third transitions appear as double endothermic peaks at respectively 62°C and 73°C, characteristic of the melt of crystals. The transition temperatures, the enthalpy values and the resulting crystallinity values are reported in Table V-1**.**

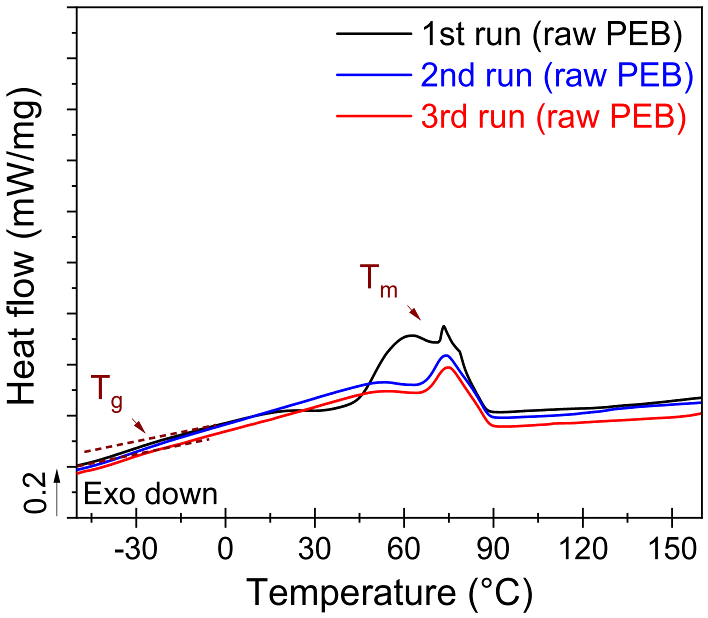

Figure V-3: Thermograms of PEB upon consecutVe heating (heating rate of 10°C/min).

For the 2nd and 3rd runs thermograms, the second transition shifts to lower temperature whereas the third transition loom up in the same position (see associated Table V-1). This may indicate that at higher temperature range, a fraction of the crystallites is stable over the raise of temperature while at lower temperature range, crystallites are less stable probably due to the sample process.

Table V-1: Thermal characteristic of PEB.

	T_g (°C)	T_m (°C)	T_m (°C)	ΔH_m (J/g)	χ(%)
Run 1	-27.5	62.4	73.3	69.5	24.1
Run 2	-	53.3	74	59	20.5
Run 3	-	54.8	74.6	56.8	19.7

The double melting transition arises another question about the degree of crystallinity of the PEB after different process (initially in powder form and crystallized from the melt after the 1st heating). Based on the integrated area of the melted endotherms, the crystallinity is calculated from the enthalpy of 100% crystalline polyethylene, ΔH_m^0 = 288 J/g [4]. The crystallinity degree of the sample before and after crystallization from the melt is about 24% and 20% respectively.

Different hypothesis can explain the double melting phenomenon. The first hypothesis is associated to a melting-recrystallization process involved in several melting transition reports of semi-crystalline polymers such as syndiotactic 1,2-polybutadiene (sPB) [5], poly (ether ether ketone) (PEEK) [6], syndiotactic polypropylene (sPP) [7], poly(ethylene-hexene) (PEH) [8]. The less stable crystallites (defective crystals or smallest crystals) melt at lower temperature. Then, it can recrystallize after the first heating and form thicker and more perfect crystals with a higher melting temperature. The second hypothesis is related to the polymorphic character of the semi-crystalline polymers. In this case, each peak could be associated to the melt of different PEB crystal phases.

V.1.3. Mechanical relaxation of PEB

Highlighting mechanical relaxations in PEB is possible by means of Dynamic Mechanical Analysis (DMA). Drop cast thin films of PEB are very brittle at room temperature. The melt molded thin films are then considered as the alternative for the DMA experiments upon temperature raise. The tensile storage modulus E′, the loss modulus E″ and the phase angle tan δ are plotted as function of temperature in Figure V-4 at a frequency f = 1 Hz.

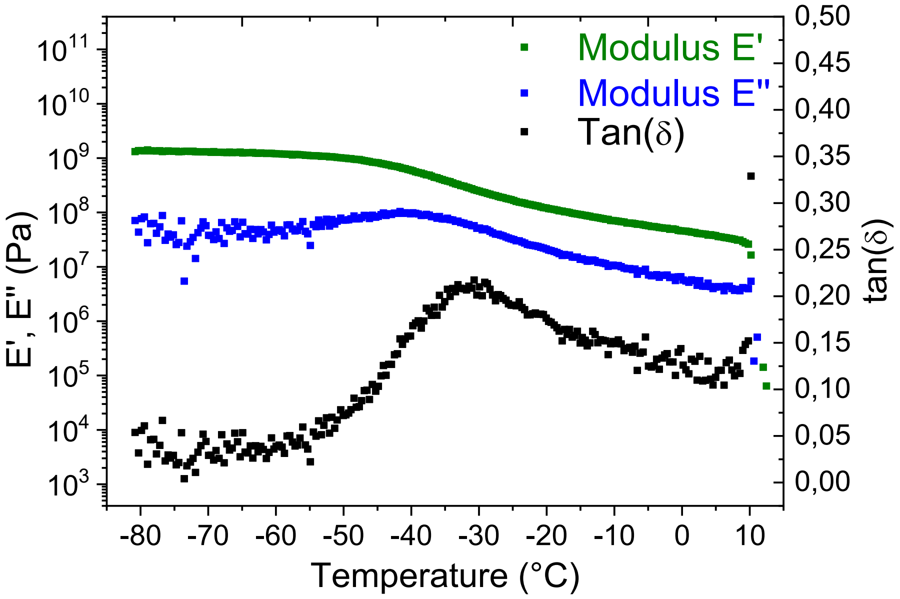

Figure V-4: Viscoelastic behavior of a melt molded PEB thin film (7×2.5×0.07 mm^3).

Below -55°C, the sample is as glassy solid with storage modulus E′ values around 1 GPa. Upon heating, the loss of E′ is observed. The peak of E″ and the maxima of tan δ are designated as the α-mechanical relaxation [4,9] characteristic of the mechanical signature of the glass transition. The peak maxima (Tα) at around -31°C is very close to the value of T_g previously measured by DSC (Table V-1). By continuing heating, E′ decreases progressively and approaches an average value of 3×10^7 Pa at around 10°C. Unfortunately, at higher temperature the sample does not maintain the modulus level as the film began to flow (beginning of the crystal melting). Therefore, at room temperature, the melt-molded film of PEB has a mechanical modulus of around 30 MPa.

V.1.4. Crystal phase analysis of PEB

In order to observe the crystalline signature of copolymer, the structural characterization is carried out by wide-angle X-ray scattering (WAXS) (Figure V-5).

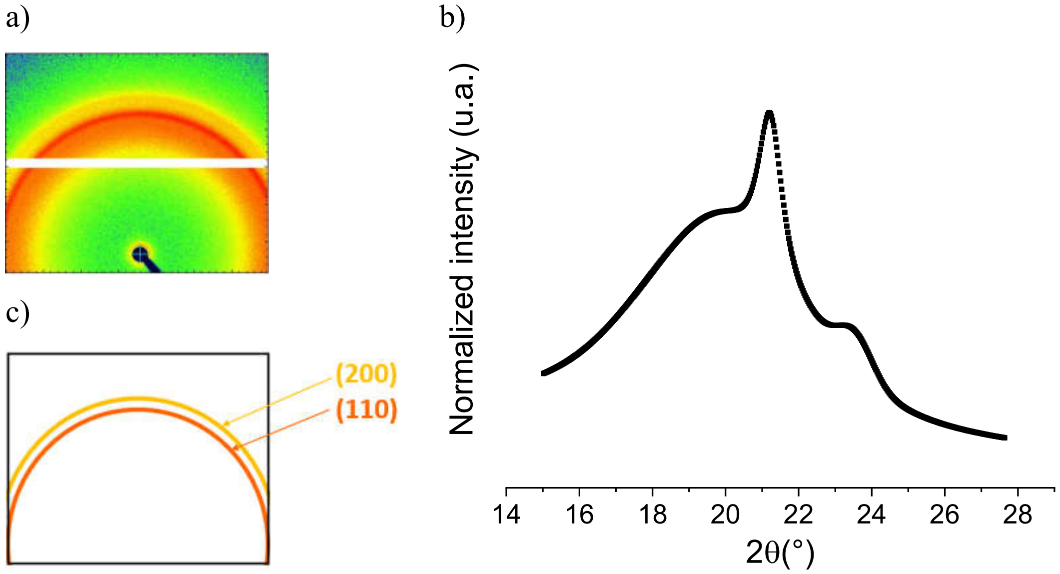

Figure V-5: a) 2D WAXS image and b) intensity profile of PEB. c) Schematic representation of 2D WAXS image.

In Figure V-5a, the diffraction image shows the presence of two rings, indicative of an isotropic distribution of the crystal lamellae. The associated integrated profiles (Figure V-5b) exhibit two main peaks at 2θ = 21.2° and 2θ =23.5°, trapped by a large halo characteristic of the amorphous fraction. Using Bragg law, d-spacing are calculated (d = 0.37 nm and d = 0.33 nm respectively) and correspond to the (110) and (200) reflections of the orthorhombic unit cell of polyethylene (a = 7.40 Å, b = 4.93 Å, c = 2.54 Å) as mentioned in Figure V-5c [10].

In order to identify the presence of different crystal phases, the structure of PEB was deeply analyzed at ambient temperature by the deconvolution of WAXS spectra. The intensity profile of PEB obtained before and after crystallization from the melt are reported in Figure V-6.

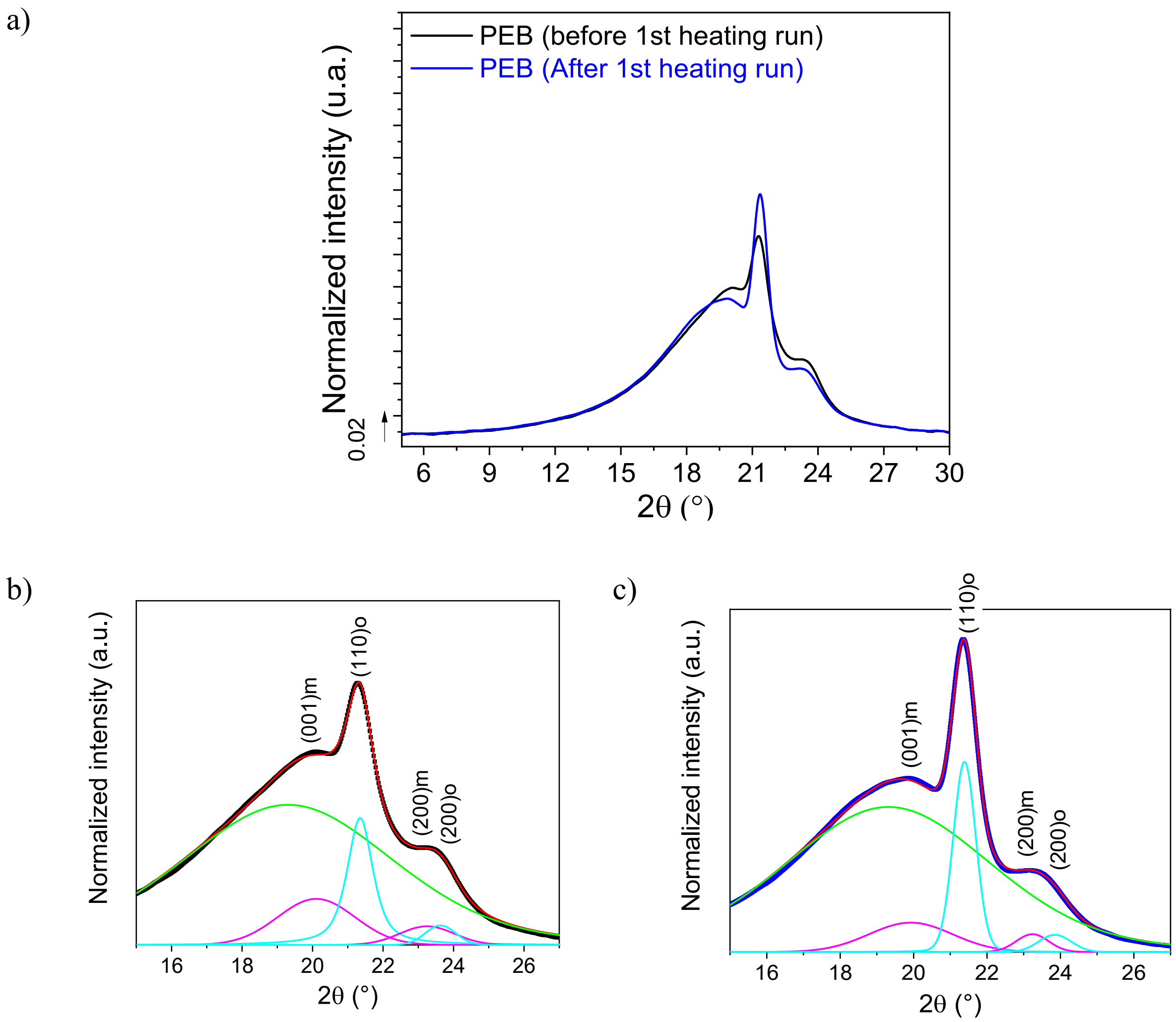

Figure V-6: a) WAXS profiles and deconvolution of sample diffractograms b) before and c) after recrystallization from the melt.

The deconvolution of PEB intensity profile was performed by using Peak Fit software according to the procedure described in Chapter II. Note the direct identification of the phase is not possible because the (200) Bragg reflection position of both orthorhombic and monoclinic forms are very close **[11, 12]**. The deconvolution shows the presence of two peaks previously described and characteristic of the orthorhombic form of polyethylene. In addition, two supplementary peaks at 2θ = 19.5° and 23.2° (d = 0.456 nm and d = 0.384 nm respectively) corresponds to (001) and (200) reflections of PE monoclinic form (a = 8.08 Å, b = 2.54 Å, c = 4.81 Å). Therefore, PEB presents two crystal forms: the orthorhombic and the monoclinic forms of polyethylene. The crystallinity degree and the fraction of the two phases are calculated from the peak areas. The data are reported in Table V-2.

Table V-2: Fraction of crystal phases in PEB.

	χ (%)	**F ortho** (%)	**F mono** (%)
PEB before crystallization from the melt	23.1	11.9	11.2
PEB after crystallization from the melt	20.5	12.8	7.7

The crystallinity values correspond to the values previously calculated by DSC. The PEB copolymer presents different crystal phase fraction influenced by the process. PEB initially in its solid state has a lower fraction of orthorhombic phase compared to PEB recrystallized from the melt. These results are in accordance with literature where cooling from the melt without physical stress mainly induces an orthorhombic phase. Therefore, the WAXS data confirm the simultaneous presence of the two-crystal phase of polyethylene.

V.1.5. Morphology of PEB

Morphological characterization is investigated by small-angle X-ray scattering analysis employing synchrotron radiation. Lorentz-corrected SAXS profile plotted as scattered intensity Iq^2 versus q is presented in Figure V-7. The long period (L_p) is calculated from Bragg equation ($L_p=2\pi/q_{max}$) where q_{max} is the q-value corresponding to the maximum of the peak of the Lorenz-corrected SAXS profile.

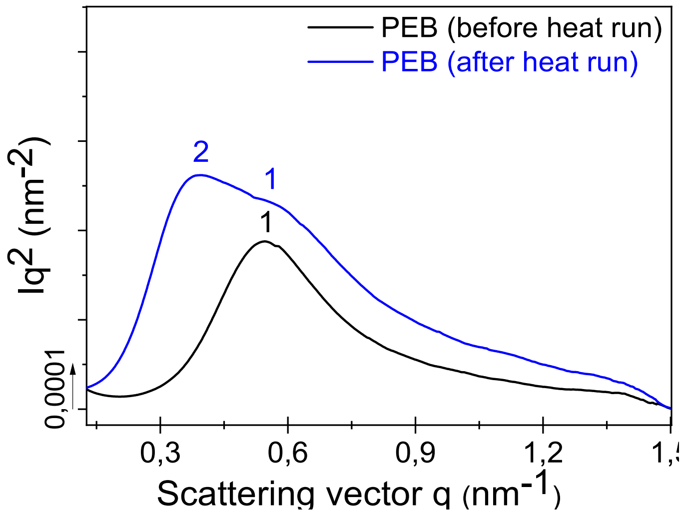

Figure V-7: SAXS pattern of PEB before and after crystallization from the melt.

As shown in Figure V-7, PEB sample shows a main scattering at q(1) = 0.54 nm^{-1} corresponding to the regular repartition of stacking between amorphous and crystalline fractions. This main scattering is associated to a long period (L_p) of 11.6 ± 0.2 nm.

Surprisingly, after heating the PEB, the SAXS profile illustrates the presence of a supplementary scattering maximum q(2). The sample exhibits two long periods associated to two different families of crystalline lamellas. One tentative explanation is that during cooling, the formation of imperfect lamellas associated to a long period of 16.1 ± 0.4 nm may occur.

For a best characterization of the seen arrangements, the structural signature will be followed upon heating. The PEB is twice heated from 30°C to 100°C with a heating rate of 10°C/min. For each temperature, the changes of periodicity were estimated. Comparisons were made between the first (Figure V-8a) and the second heat runs (Figure V-8b), i.e. between the PEB initially in brittle solid state and the PEB crystallized from the melt.

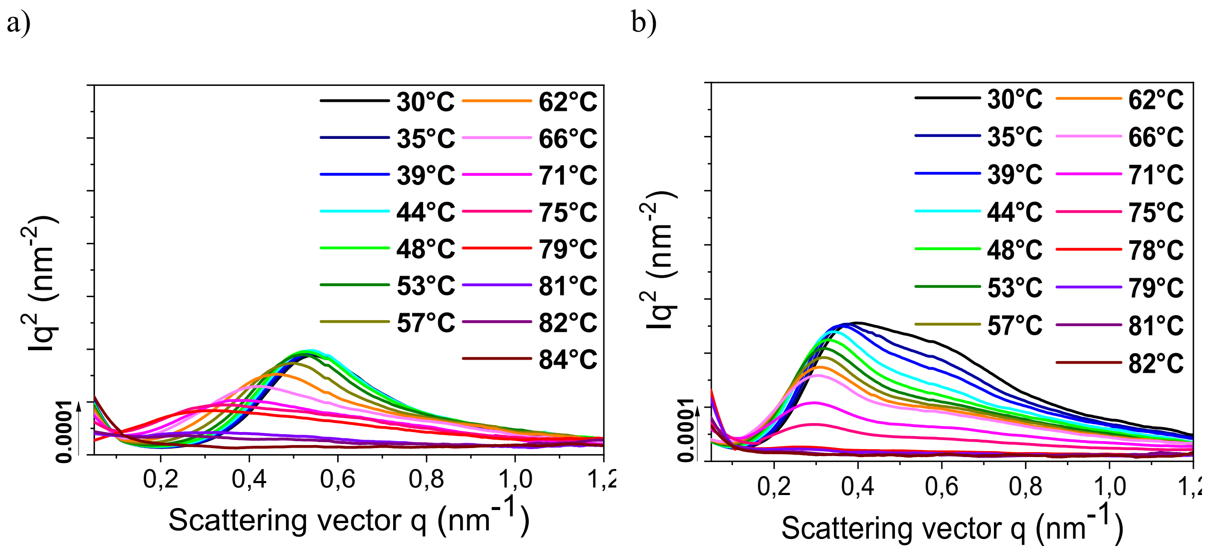

Figure V-8: SAXS evolution in situ under temperature during a) the first heat run and b) the second heat run.

The signature of L_p associated to the PEB 1st heating as function of temperature is reported in Figure V-9 (black squares).

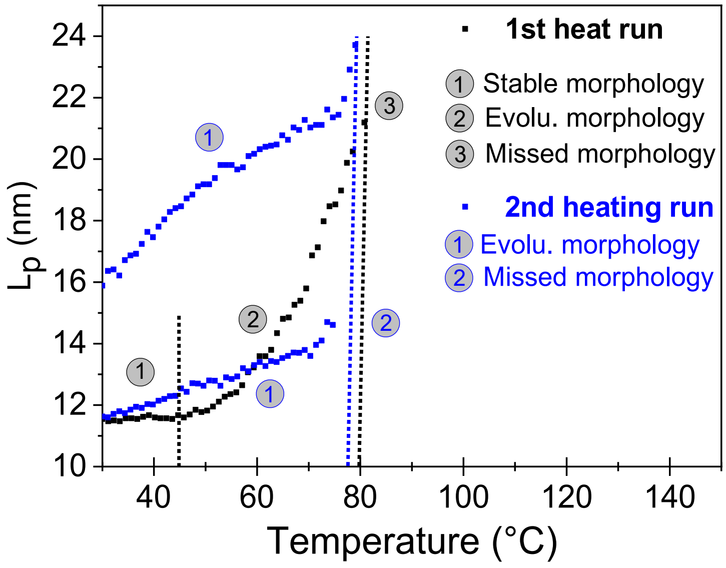

Figure V-9: Superposition of PEB long period evolution upon heating: first run in black and second heat run in blue.

Three distinct zones are observed:

- From 30°C up to 48°C, the peak position is fixed. L_p is constant. The morphology is stable.
- From 50°C to 80°C, the peak shifts and broadens progressively due to the melt of a part of the crystallites. L_p increases. The morphology changes.
- At higher temperature ($T > 84$°C), i.e. the temperature increases above the melting point, the peak disappears indicating the fully melting of PEB crystals. L_p does not exist. The morphology is missed.

Upon the second heat run, the SAXS pattern reveals an additional peak, which shift toward lower scattering vectors q indicating an increasing in the long period. The evolution of L_p in Figure V-9 (blue squares) displays two distinct zones:

- Within the temperature range ($30°C \leq T \leq 79°C$), both peaks shift at lower q and broadens progressively. L_p increases.
- At higher temperature ($T > 79$°C) over the melting temperature, both peaks disappear. L_p does not exist.

V.1.6. Summary on PEB

To summarize Poly(ethylene-butylene) characteristics:

↦ The copolymer with 85 mol% of ethylene and 15 mol% of butylene is semi-crystalline.

This crystallinity is associated to the presence of both orthorhombic and monoclinic forms of polyethylene.

- ⟼ The glass transition is around -28°C, the melt temperature from 62°C to 73°C and the crystallinity degree around 24%.
- ⟼ Isotropic repartition of stacking between amorphous and crystalline fractions defines the PEB long period $L_p = 11.6 \pm 0.2$ nm at room temperature. Upon heating, a noticeable increase of L_p is associated to the "softening" of the copolymer up to the full crystal melting.

V.2. Structure and morphology of PEB-UPy

Supramolecular polymers obtained from bi-functional PEB backbone were described in Chapter II. The dimerization of multiple hydrogen bonds through 2-ureido-pyrimidinone groups (UPy) associated into a linker containing urethane group noted UPy leads to reversible self-assembly. Thereby combining a strong quadruple hydrogen bonds through UPy units into directional lateral. PEB-UPy is deeply investigated taking into account the influence of the process on the thin film elaboration. For this purpose, two kind of thin films are elaborated: (i) drop cast thin film from chloroform solution designed DC and (ii) melt molded thin film designed MM (described in Chapter II).

V.2.1. Thermal behavior of PEB-UPy

V.2.1.1. Degradation kinetics

TGA analysis was performed in order to get information about the UPy-end substitution influence on the degradation temperature of PEB copolymer. Figure V-10 shows the thermal stability of PEB-UPy DC and PEB-UPy MM thin films heated with a rate of 10°C/min under dioxygen atmosphere.

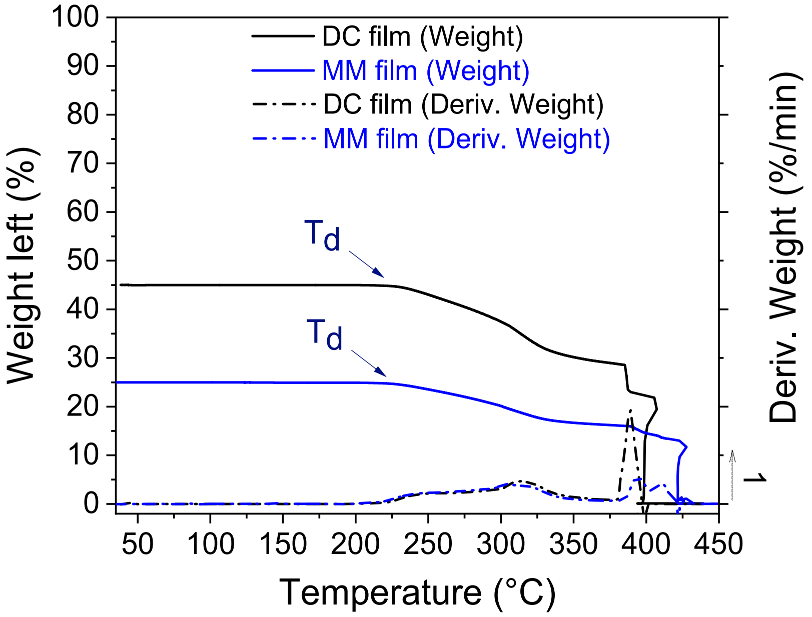

Figure V-10: TGA curves of DC and MM PEB-UPy thin films.

The derivative plots of mass loss reveal numerous degradation steps. The first step is well defined and begun at roughly 197°C for MM specimen and 218°C for DC specimen. Concurrently, the second shoulder appears around 293°C and 301°C for MM and DC samples, respectively. Despite the observed irregularities beginning from 372°C for DC PEB-UPy and 385°C for MM PEB-UPy, both samples were degraded completely without leaving any noticeable residue above 420°C. Small difference in degradation temperature is found between thin films differently processed.

The observed degradation processes are compared to those of PEB. As expected, the incorporation of UPy-moieties allows a higher stability, i.e. a stability of the copolymer PEB-UPy at higher temperature: T_d(PEB-UPy) > T_d(PEB) = 186°C.

V.2.1.2. Thermal transitions

DSC analysis of DC and MM samples are depicted in Figure V-11. Each sample is heated successively (1st heating run, 2nd heating run, 3rd heating run) with a heating rate of 10°C/min. The comparison between the thermal behaviors shows that the difference is assigned only to the first heat run while, as expected, identical signatures are obtained for the second and third runs.

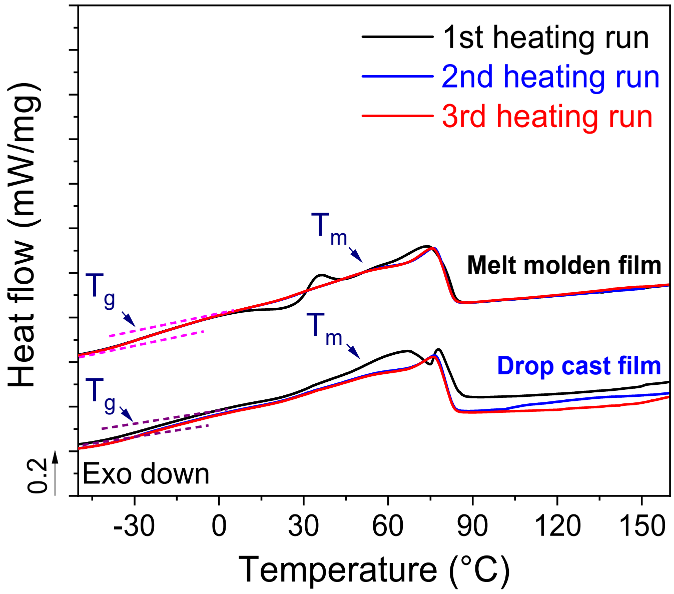

Figure V-11: DSC thermograms of PEB-UPy recorded upon subsequent heating. Heating rates of 10°C/min.

By focusing only on the first heat, both samples exhibit a glass transitions around -26°C followed by a large endotherm characteristic of two melting transition, very similar to those obtained for PEB. Interestingly, the MM sample shows an additional endothermic peak at 36°C which indicates that a new family of crystallites can be present in the molded film. The formation of highly defective crystallites is expected.

V.2.1.3. Crystallinity

The crystallinity of polymers is one of the key ingredients, which induces morphological changes and define structural and mechanical properties. The thermal transition and the crystallinity degree are reported in Table V-3 for both DC PEB-UPy and MM PEB-UPy thin films.

Table V-3: Thermal parameters of PEB-UPy thin films. For comparison, data of PEB are also reported.

	Heat run	T_g (°C)	T_{m*} (°C)	T_{m1} (°C)	T_{m2} (°C)	ΔH_m (J/g)	χ_c(%)
DC PEB-UPY	1	-25	-	66.7	77.8	60.4	23.0
	2	-26	-	58.7	76.5	57.7	20.0
	3	-25	-	59	76	58.6	20.3
MM PEB-UPY	1	-24	36	58.6	73.6	61.8	21.5
	2	-24	-	58.9	76.1	58.3	20.2
	3	-23	-	58.8	75.6	57.9	20.1
PEB	1	-27.5		62.4	73.3	69.5	24.1
	2	-27.5		53.3	74	59	20.5

Compared with PEB sample (the first heat run), the χ_c value is similar to the value of DC thin films. The presence of UPy groups has no impact on the crystallinity. Additionally, this crystallinity seems to be slightly decrease for MM thin films. This may be explained by the fact that the crystallinity is not affected by the composition (urethane groups, UPy groups) but depends on the crystallization conditions (temperature, pressure), which decrease the freedom of polyethylene segments and partially inhibit the crystals growth in PEB-UPy.

By comparing the calculated crystallinity of PEB-UPy under similar conditions of crystallization (after cooling from the melt), the χ_c values are quasi constant upon the second and the third heat runs. The PEB-UPy crystallinity is found to be around 20.2 %, similar to the value obtained for PEB.

The crystallinity is not affected by the presence of UPy-groups contrary to the results of Folmer et al. [13] on similar material. Indeed, the DSC thermogram of PEB revealed a glass transition at -59 °C and a small endotherm at -13 °C attributed to crystalline regions in random polymers. The UPy-functionalization of PEB from both sides prevented the crystallization of the copolymer due to the decrease of the macromolecular diffusional freedom. As result, DSC thermograms presented the glass transition at -57°C with the absence of endotherm [13]. In our case, whatever the process, the PEB-UPy thin films are semi-crystalline due to the high fraction of PE within the copolymer.

V.2.2. Mechanical relaxation of PEB-UPy

Variation of mechanical modulus may occur due to the incorporation of UPy units. In order to estimate this feature, the viscoelastic analysis is carried out on DC PEB-UPy thin film with DMTA.

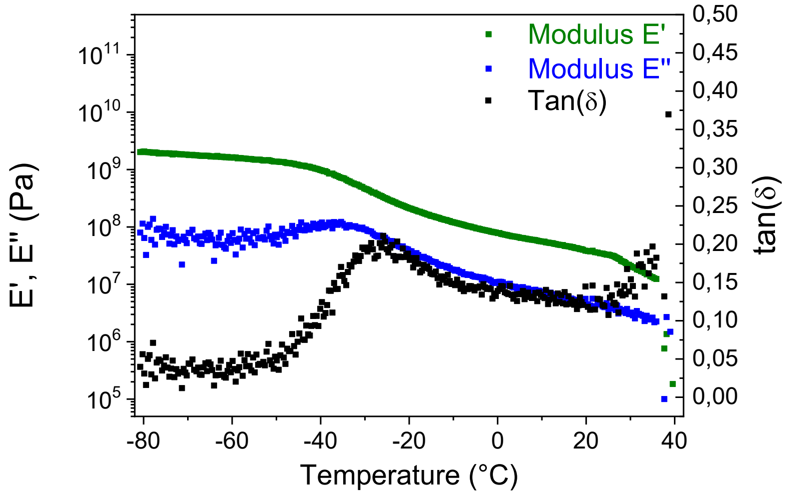

Figure V-12: Temperature dependence of the modulus and loss tangent of DC film.

Figure V-12 shows that below -60°C, the sample has a storage modulus E′ of around 2×10^9 Pa. Under heating, E′ presents a loss of modulus with a decrease up to 8×10^7 Pa. The α-relaxation associated to the loss of E′, the peaks of E″ and tan(δ) is observed at around -26°C. At higher temperature, the sample began to flow beyond 35°C (beginning of the melt observed by DSC). The mechanical parameters are reported in Table V-4.

Table V-4: Values of mechanical modulus and temperature of the α-relation.

	E' (T=-60°C) (MPa)	Tα (°C)	E' (T=25°C) (MPa)	Tflow (°C)
DC PEB-UPy	2×10^9	-26	8×107	35°C
PEB	1×10^9	-31	3×107	10°C

These results allow making comparisons between the non-functionalized and UPy-functionalized PEB copolymers. The values of E′ and the α-relaxation are almost similar. The main difference is the stability of the copolymer until 35°C.

In similar study of an amorphous functionalized PEB, a glass transition is observed at -50°C. This glass transition was followed by a rubbery plateau at 5×10^6 Pa. The material exhibits the characteristics of a soft rubber at room temperature [13]. Recall that our materials are semi-crystalline, which explain the higher level of modulus E′ after the primary α-relaxation.

V.2.3. Polymorphic crystalline structure of PEB-UPy

Molecular packing and crystalline behavior of polyethylene molecules and its copolymers were widely studied over the years. UPy-end group functionalization may influence the polyethylene chain structure and their rearrangements. For this propose, PEB-UPy was investigated by means of WAXS. Diffractogram deconvolution of DC and MM thin film, shown in Figure V-13, were performed according to the method outlined briefly in Chapter II.

At room temperature, both DC and MM thin films exhibit two main peaks at 2θ = 21.5° and 23.8° corresponding to d = 0.413 nm and d = 0.372 nm respectively and associated to (110) and (200) reflections of orthorhombic pattern (a = 7.40 Å, b = 4.93 Å, c = 2.54 Å). Concurrently, the MM thin film presents two supplementary peaks at 2θ = 19.5° and 23.2°, i.e. spacing d = 0.456 nm and d = 0.384 nm related to (001) and (200) reflections of monoclinic pattern (a = 8.08 Å, b = 2.54 Å, c = 4.81 Å) [15]. These reflections are negligible for DC thin films.

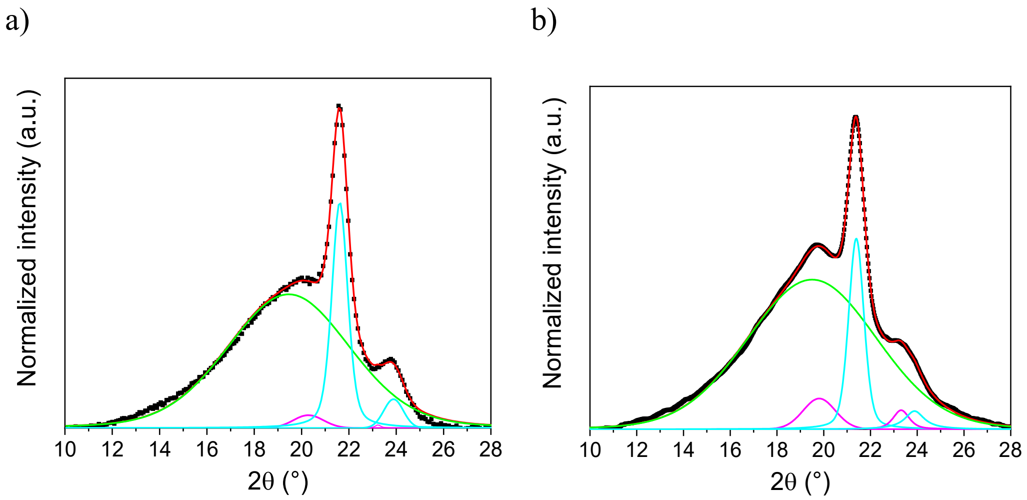

Figure V-13: Approximate deconvolution of WAXS profiles using peak-fit. a) DC thin film case. b) MM thin film case.

The crystallinity and the fraction of different crystal phases calculated from the peak areas are gathered in Table V-5.

Table V-5: Diffraction pattern details of thermoplastic elastomer rearrangements.

	χ (%)	F ortho (%)	F mono (%)
DC PEB-UPy	23.1	21.3	1.8
MM PEB-UPy	20.8	15.3	5.5
PEB	23.1	11.9	11.2

The values of crystallinity are similar to the values previously observed by DSC. In the DC thin film, polyethylene mainly crystallizes in the orthorhombic lattice (crystallinity degree about 23%). Whereas in the case of MM thin film, a part of the crystals presents a monoclinic structure. Many investigations [15-17] revealed that depending on the process, polyethylene displays structural modifications. Indeed, it was observed that monoclinic form can appear under stress (such as compression) but also during sample aging [18].

V.2.4. Morphology of PEB-UPy - correlation distances

V.2.4.1. Process impact

Investigation of the crystalline organization of PEB-UPy for DC and MM thin films is carried out via SAXS measurements. Lorentz-corrected SAXS profiles were derived from SAXS images as depicted in Figure V-14. Correlation distances d_c were estimated from Bragg equation ($d_c=2\pi/q_{max}$), in which q_{max} correspond to the maximum of Lorentz-corrected peak. The calculated characteristic parameters are summarized in Table V-6.

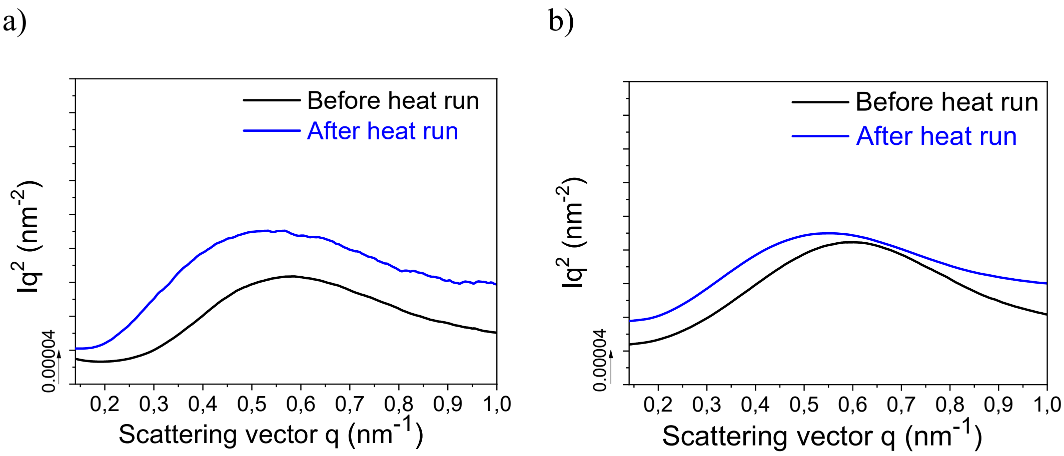

Figure V-14: Lorenz-corrected SAXS profiles of PEB-UPy: a) DC and b) MM samples.

Interestingly, a main broad scattering peak is underlined by the SAXS profiles before the heat run for both DC and MM samples at room temperature. The DC sample diffractogram reveals a correlation distance of 10.8 nm while in the MM case, the SAXS correlation peak shifted to larger q values correlated to shorter distance (10.1 nm).

Table V-6: Lattice parameters of PEB-UPy.

	DC film		**MM film**	
	Before heat run	**After heat run**	**Before heat run**	**After heat run**
q_{max} (nm^{-1})	0.58	0.56	0.62	0.55
d_c (nm)	10.8	11.2	10.1	11.4

After recrystallization from the melt, larger scattering peaks were observed for both samples indicating a higher distribution of structure. The scattered intensity exhibits a domain spacing of around 11.3 nm for both thin films comparable to the value reported for the PEB long period (l_p = 11.6 nm).

V.2.4.2. Temperature evolution

In order to assess the PEB-UPy self-organization for the DC and MM thin films, SAXS experiments were performed in-situ while varying temperature. SAXS profiles of DC thin film are reported in the temperature range from 30°C to 168°C (Figure V-15).

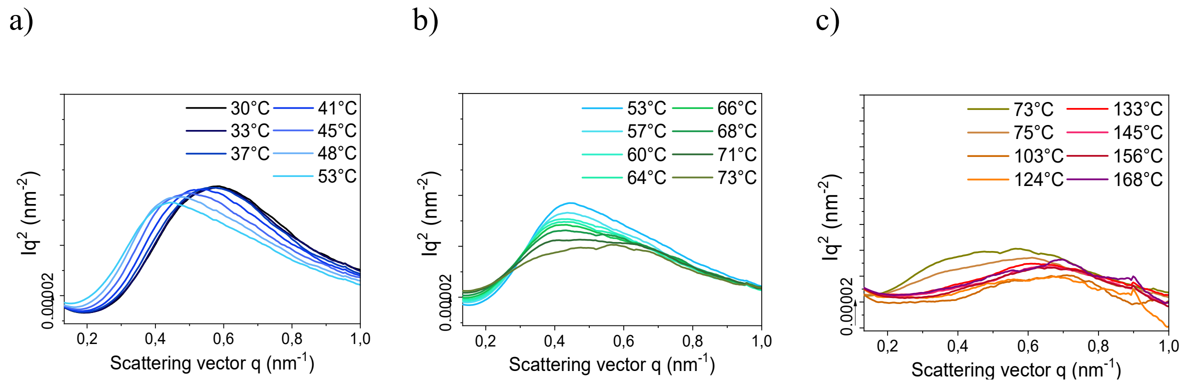

Figure V-15: SAXS profiles of DC PEB- UPy as a function of temperature (heat rate 10°C/min) for three temperature ranges: a) First range from 30°C to 53°C, b) second range from 53°C to 73°C and c) third range from 73°C to 168°C.

During the heating, the maximum of the scattering peak shifts to lower q values (1st range). Then, the peak broadens until 75°C (2nd range). At higher temperature, a hidden broad scattering peak appears at higher q-value and is observed until the end of the heating (3rd range). After a subsequent cooling, the PEB-UPy recrystallizes and the signature of SAXS profiles upon the second heat run is very similar to the first one.

The temperature evolution from 30°C to 168°C of MM sample followed during the first heat run is depicted in Figure V-16.

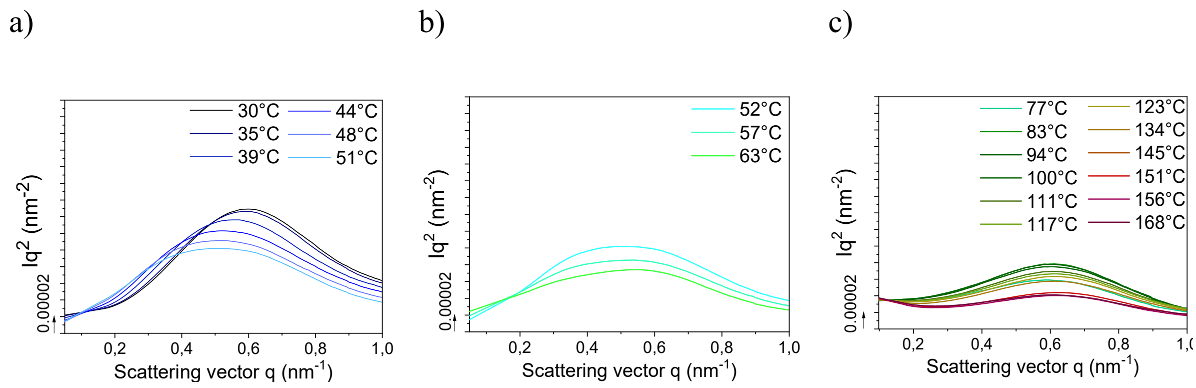

Figure V-16: MM PEB-UPy SAXS profiles as a function of temperature (heat rate 10°C/min) for three temperature ranges: a) First range from 30°C to 51°C, b) second range from 52°C to 73°C and c) third range from 73°C to 168°C.

Over the whole measured spectral range, the behavior of MM films is similar to the behavior previously described for DC thin films with three identified ranges.

The spacing domains calculations estimated from the Bragg equation ($d_c = 2\pi/q_{max}$) are presented as function of temperature for DC and MM thin films respectively in Figure V-17.

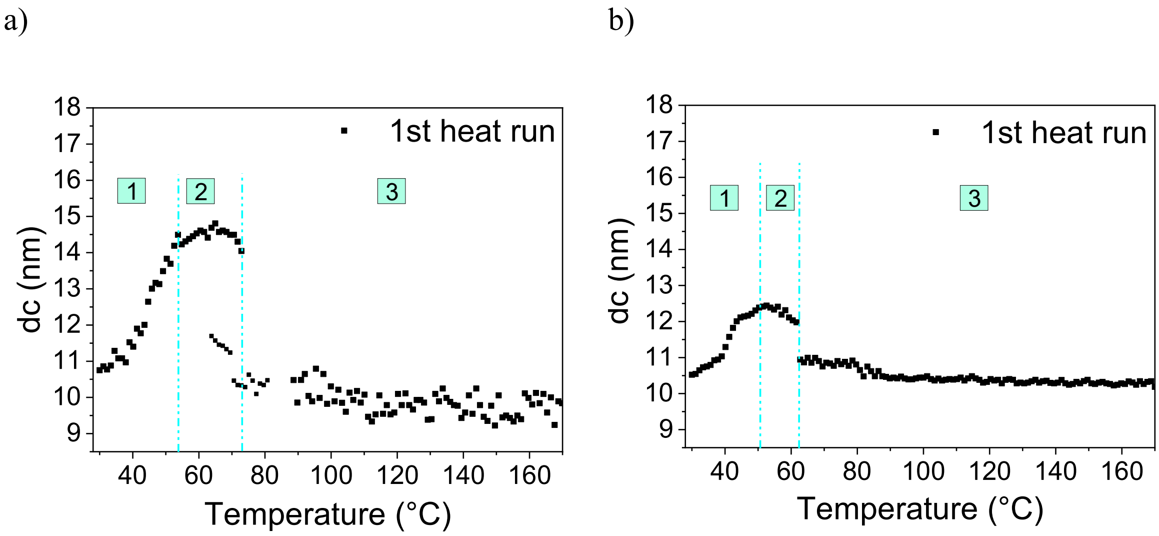

Figure V-17: Correlation distance evolution as function of temperature for a) DC and b) MM samples.

For the 1st stage, dc corresponds to the PEB long period. Upon heating, d_c increases until the beginning of the crystal melt. The maximum value of dc is lower compared to the value obtained for DC thin film maybe due to the macromolecular chain confinement induced by the melt molding under pressure. Then the long period is constant and disappears when the melt of the crystals is achieved (2nd stage). At higher temperature, i.e. over the melting point, a correlation distance persists. That can be tentatively attributed to the presence of hydrogen bondings (3rd stage). Note that this correlation distance exists over all high temperature ranges (until T = 168°C). The existence of stable morphology is emphasized at high temperature through the existence of a correlation distance $d_c \approx 10.2$ nm for both films. Since the melting of PEB segments is achieved, strong dimerization of UPy units through quadruple hydrogen bonds in the samples at the molten state is expected. Indeed, a detailed study about the UPy-dimerization revealed a strong association owing to multiple hydrogen network ($K = 6\ 10^7\ M^{-1}$) in chloroform [19,20]. Moreover, comparable SAXS results about the presence of hydrogen bondings have already been reported when α, ω-amino-polyoxypropylene (Jeffamine) functionalized UPy was investigated upon heating in solution [20].

V.2.5. Summary on PEB-UPy

The self-assembly of PEB-UPy with strong quadruple hydrogen bonding is investigated:

- ⟼ The glass transition is around -25°C. The melt temperature is ranged from 36°C to 78 °C (DC) and from 59°C to 74°C (MM).
- ⟼ Crystallization at room temperature is induced through PEB segments. The crystallinity degree is around 23% (DC) and 21% (MM), respectively.

- ⟼ Higher mechanical strength and higher viscoelastic modulus of 3.6×10^7 Pa at room temperature compared to PEB.
- ⟼ Depending on thin film elaboration procedure, variable fractions of orthorhombic and monoclinic phases of polyethylene are underlined.
- ⟼ The isotropic repartition of stacking between amorphous and crystalline fractions defines the PEB long period L_p = 10.1 nm or 10.8 nm depending of the process.
- ⟼ Above PEB melting, stable morphology associated to UPy signature is present, d_c is about 10.2 nm.

V.3. Conclusion

Chapter V was dedicated to investigate the features of un-functionalized and functionalized PEB. Although it is called thermoplastic elastomer, PEB is semi-crystalline due to the high fraction of polyethylene.

The functionalization with UPy motifs does not significantly influence the structural (crystallinity, polymer crystal phases) and the thermal properties (transition temperatures) of the copolymer. PEB-UPy has a crystallinity degree around 23% similar to the value obtained with its precursor. Moreover, PEB-UPy shows the contribution of both orthorhombic and monoclinic polyethylene crystal phases. The crystallinity and the crystal phases fractions can vary depending on the followed to elaborate thin films (drop casting or melt molding). The stability and the mechanical properties are slightly improved by the presence of UPy units.

For the copolymer morphological analysis, the SAXS appears as a powerful tool to probe the PEB long period and the UPy interactions. At ambient temperature, the long-period L_p of copolymer is observed, which correspond to the stacking of amorphous and crystalline lamellas. L_p increases with temperature until the beginning of crystal melts (around 50°C) and disappears at around 70°C. For PEB-UPy copolymer, the correlation distance exists and is attributed to the distance between UPy domains/aggregates. Table V-7 illustrates a schematic representation of the morphology evolutions while heating.

Table V-7: Schematic representation of PEB and PEB-UPy morphologies evolution with temperature.

	T < 50°C	**50°C < T < 70°C**	**T > 70°C**
PEB	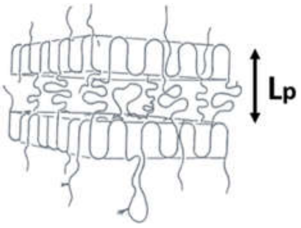	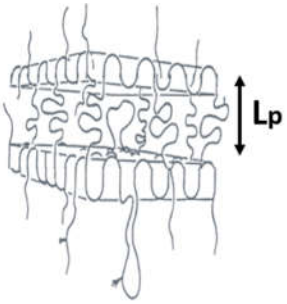	
PEB-UPy	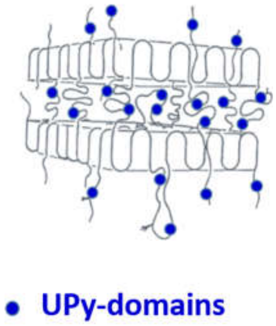	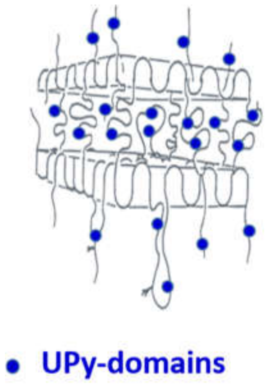	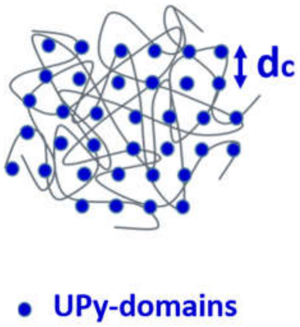

The influence of the photochromic molecules DTE-UPy incorporation on the PEB-UPy structure and morphology will be described in Chapter VII.

References

[1] Burfield, D.R. and N. Kashiwa, DSC studies of linear low-density polyethylene. Insights into the disrupting effect of different comonomers and the minimum fold chain length of the polyethylene lamallae. Makromolekulare Chemie, 1985.186(12): p. 2657-2662.

[2] Lou, X., et al., Synthesis of pyrene-containing polymers and noncovalent sidewall functionalization of multiwalled carbon nanotubes. Chemistry of Materials, 2004. 16(21): p. 4005-4011.

[3] Chang, R., et al., Alternating poly(lactic acid)/poly(ethylene-co-butylene) supramolecular multiblock copolymers with tunable shape memory and self-healing properties. Polymer Chemistry, 2015. 6(32): p. 5899-5910.

[4] Sierra, C.A., et al., Thermal and mechanical properties of poly-(styrene-b-ethylene-co-butylene-b-styrene) triblock copolymers. Polymer, 1997. 38(17): p. 4325-4335.

[5] Sasaki, T., H. Sunago, and T. Hoshikawa, Multiple Melting Behavior of Syndiotactic 1,2-Polybutadiene. Polymer Engineering and Science, 2003. 43(3): p. 629-638.

[6] Bas, C., P. Battesti, and N.D. Alberola, Crystallization and melting behaviors of poly(aryletheretherketone) (PEEK) on origin of double melting peaks. Journal of Applied Polymer Science, 1994. 53(13): p. 1745-1757.

[7] Supaphol, P., Crystallization and melting behavior in syndiotactic polypropylene: Origin of multiple melting phenomenon. Journal of Applied Polymer Science, 2001. 82(5): p. 1083-1097.

[8] Qiu, J., et al., New insights into the multiple melting behaviors of the semicrystalline ethylene/hexene copolymer: Origins of quintuple melting peaks. Journal of Polymer Science Part B: Polymer Physics, 2008. 46(19): p. 2100-2115

[9] Murayama, T., Dynamic Mechanical Analysis of Polymeric Material, Elsevier, New York, 1978.

[10] Butler, M.F., et al., A Real-Time Simultaneous Small- and Wide-Angle X-ray Scattering Study of In-Situ Deformation of Isotropic Polyethylene. Macromolecules, 1995. 28(19): p.6383-6393.

[11] Takahashi, Y., T. Ishida, and M. Furusaka, Monoclinic-to-orthorhombic transformation in polyethylene. Journal of Polymer Science Part B: Polymer Physics, 1988. 26(11): p. 2267 2277.

[12] Russell, K.E., B.K. Hunter, and R.D. Heyding, Monoclinic polyethylene revisited. Polymer, 1997. 38(6): p. 1409-1414.

[13] Folmer, B.J.B., et al., Supramolecular Polymer Materials: Chain Extension of Telechelic Polymers Using a ReactVe Hydrogen-Bonding Synthon. Advanced Materials, 2000. 12(12): p. 874-878.

[14] Kautz, H., et al., CooperatVe End-to-end and Lateral Hydrogen-Bonding Motifs in Supramolecular Thermoplastic Elastomers. Macromolecules, 2006. 39(13): p. 4265-9297.

[15] Russell, K.E., B.K. Hunter, and R.D. Heyding, Monoclinic polyethylene revisited. Polymer, 1997. 38(6): p. 1409-1414

[16] Seto, T., T. Hara, and K. Tanaka, Phase Transformation and Deformation Processes in Oriented Polyethylene. Japanese Journal of Applied Physics, 1968.7(1): p. 31-42.

[17] Wittmann, J.C. and B. Lotz, Epitaxial crystallization of monoclinic and orthorhombic polyethylene phases. Polymer, 1989. 30(1): p. 27-34.

[18] Bernazzani, P., et al., FTIR analysis of the phase content in low density polyethylene.Canadian Journal of Chemistry, 1998. 76(11): p. 1674-1687.

[19] Kautz, H., et al., CooperatVe End-to-end and Lateral Hydrogen-Bonding Motifs in Supramolecular Thermoplastic Elastomers. Macromolecules, 2006. 39(13): p. 4265-9297.

[20] Arnaud Gallon, Réseaux élastomères nanostructurés par combinaison de processus d’assemblages supramoléculaires et de polymérisations, Thèse INSA Lyon, 2008.

Chapter VI.

Photomechanical effect: various supramolecular systems (DTE-UPy, PEB-UPy) – first evidences

The main purpose of this thesis research is the elaboration of photoactive supramolecular thin films combining the photochromic dithienylethene DTE-UPy as photoswitch and the thermoplastic elastomer PEB-UPy bringing the needed flexibility. For sake of clarity, this chapter will focus exclusively on the different type of photomechanical responses under illumination (UV and Visible) at two different scales: i) microscopic scale (wild-field microscopy set up) and ii) macroscopic scale (lamp + camera set up).

The investigated thin films were elaborated in two main steps as presented in Chapter II: (1) preparation of supramolecular assembly in solution and (2) elaboration of thin film. First, one require is letting the supramolecular assembly operating between the two components. Starting with an uncolored solution of DTE-UPy (OF) (at 55°C under magnetic stirring), the solution turns to a deep blue as long as DTE-UPy (CF) is formed when UV light is sent. Then, PEB-UPy is introduced and the self-assembly proceeds gently during two hours. The starting concentration is chosen to avoid the precipitation of DTE-UPy (see Chapter IV) and alternatively, a reflux is added to avoid solvent evaporation (increasing concentration would result in the precipitate formation). After two hours, the solution is either drop casted on PTFE plate or the solvent is evaporated all the night to form a blue powder.

Then, at this stage, three different thin films are obtained with different elaboration methods including a thermal treatment (or not):

(i) Thin film obtained from drop casting of the solution with refluxed denoted **DC-R**
(ii) Thin film obtained from drop casting of the solution without refluxed denoted **DC-NR**
(iii) Thin film obtained from the melt molding (hydraulic press at 120°C; 100 bars) of the dried blue powder described above but for a solution without reflux denoted **MM-NR**.

We have brought evidences in Chapter IV and Chapter V that the UPy-UPy quadruple bonds are resistant to a temperature up to 160 °C which allows to use the melt molding technique to get more flexibility in sample preparation including shape, thickness, etc. Furthermore, this technique can be interesting in the future for industrial application.

As comparison, the reference of PEB-UPy thin film which does not contain photochromic DTE-UPy has already been studied under illumination (Appendix VI).

So, in this Chapter, we will investigate the three thin films at two different scales. First, their macroscopic photomechanical behavior with dimensions of around (20 mm x 3 mm) will be acquired with a camera at right angle from the illumination lamp. Additional information will be collected from the DMA experimental setup. Then, the microscopic analog will be acquired with the wield-field microscopy setup with in-situ illumination. As shown in Figure VI-1, a small piece of the previous film will be cut with a scalpel and clamped between two glass plates. As a matter of fact, a comparison between microscopic and macroscopic effects will be instructed.

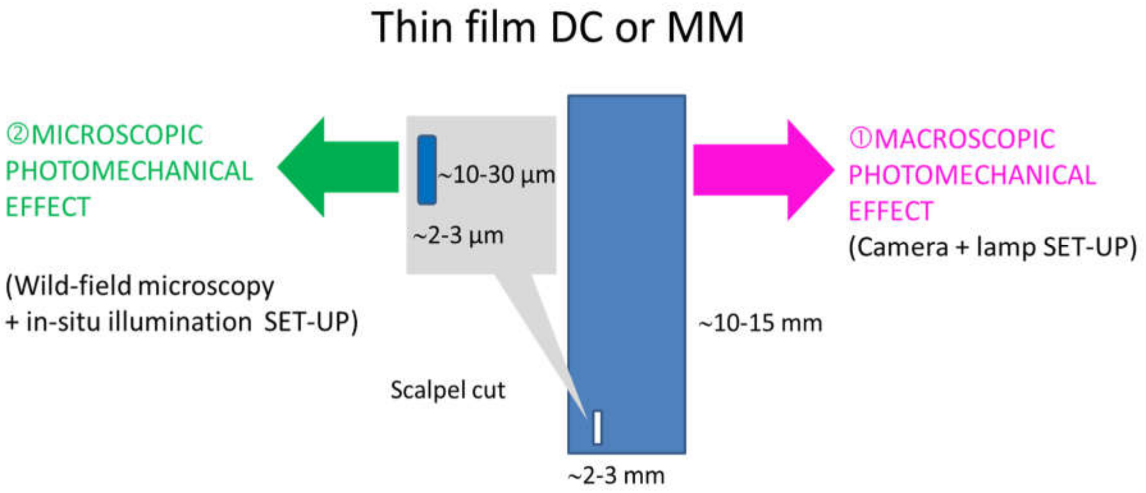

Figure VI-1: Schematic illustration of the strategy used to investigate the thin films at both microscopic and macroscopic scales.

VI.1. Photomechanical effect at Macroscopic scale

VI.1.1. Photoinduced morphological changes

Apart the change of color, the photomechanical responses upon light irradiations are investigated with the aim to highlight the influence of thin film elaboration method on the photo-induced changes if they exist. For this propose, the involved three thin films are studied. For each case, the thin film was attached from one of its longest dimension extremities into a clamp and then irradiated with visible and UV lights from the left side.

The video duration acquired by the camera is 60 min with one picture every 10 s (360 pictures). The illumination sequence is always the same: 10 minutes without light and then 50 min under light. Because the starting thin film is blue, we always start from visible irradiation (570 nm band pass filter) and then UV irradiation (302 nm band pass filter). Furthermore, it is important to note that the light spot covers the entire thin film (out of the clamps). The videos of 360 frames presented in this part are accelerated 60 times so their total duration is 6 s.

To confirm the eye-naked analysis, kinetic slices were registered on the border of the film to assess the kinetic of the thin film occurred motion. In parallel, a kinetic slice on the no-moving part of the film (on the top, just between the two clamps) was registered as well, in order to assess the kinetic on the photocoloration process of the surface only (indeed, this is not a transmitted but a reflected signal).

Finally, it is worth to precise that after illumination experiments, illuminated films were dissolved in chloroform and absorption spectra have shown that any photo-degradations have affected the three samples DC-R, DC-NR and MM-NR.

VI.1.1.1. DC-thin films

VI.1.1.1.1. DC-NR thin film

By fixing the sample, it is difficult to maintain its straight appearance when clamped. The thin film is somehow bended and makes difficult to get a perfect normal irradiation. The thin film dimensions are 1.5 mm×2 mm×62 µm.

The DC-NR thin film (CF) is first exposed to visible light and then to UV light as depicted in Figure VI-2a and Figure VI-2b with a series of snapshots (10 min gap) from the accelerated videos upon first visible irradiation (video VI-1, ▷), first UV irradiation (video VI-2, ▷), second visible irradiation (video VI-3, see ▷), second UV irradiation (video VI-4, ▷). It is worth to precise that two irradiations cycles were performed on this sample (VIS-UV-VIS-UV) allowing us to discuss about reversibility. Moreover, kinetic slices associated to photomechanical effect and photocoloration/photodecoloration of the surface are depicted in Figure VI-2c.

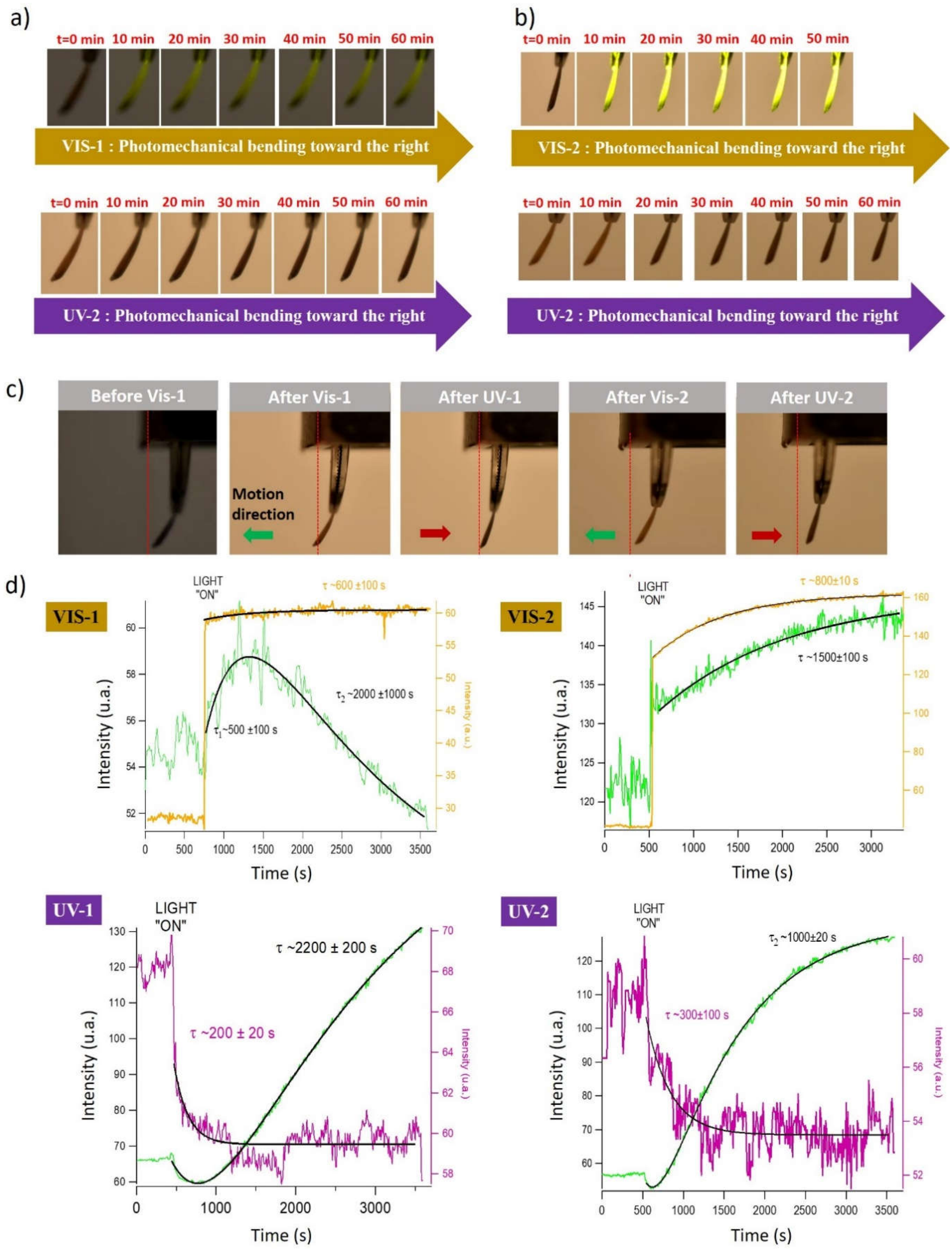

Figure VI-2: Macroscopic photomechanical behavior of DC-R thin film. a) 1st cycle upon irradiation with visible (VIS-1) and UV (UV-1) lights at room temperature. b) 2nd cycle of irradiation with visible (VIS-2) and UV (UV-2) lights at room temperature. c) Photoinduced reversibility. d) Kinetic follow as function of exposure time of photomechanical effect (green signal), photocoloration (purple signal) and photodecoloration (orange signal) respectively upon VIS-1, UV-1, VIS-2, UV-2.

VISIBLE irradiation – 1st Cycle. As seen in Figure VI-2b, the irradiation with visible light at 570 nm is accompanied with change in thin film color from dark blue into dark yellow color (before and after VIS-1). During this visible irradiation, the absence of motions is noticed upon the first few minutes. Further visible irradiation, a weak bending toward the incident light direction is underlined. Such motion continues spreading upon further visible irradiation. The inspection of the kinetic slices gives a characteristic time of ~33 min while the photocoloration of the surface takes ~10 min. This comparison is interesting and evidence that the photomechanical effect presented here is a phenomenon related to the photochromic conversion inside the bulk and not only at the surface like jumping crystals presented in Chapter III.

UV irradiation – 1st Cycle. Video and its corresponding snapshots for the UV irradiation (at 302 nm) are presented in Figure VI-2a. During the first 5 minutes after light irradiations, we clearly distinguished the yellow-brown thin film reverting into a blue color due to the occurred photochromic electrocyclization as shown in Figure VI-2c (after UV-1.) Despite this color change, the thin film shape does not achieve any remarkable changes. However, with further irradiation, a drastic bending away from light direction (right side) is observed. It is important to note that the observed photoinduced motions within the two types of bending directions need a lag time to generate a photoresponse against exposure time, which will be verified and discussed later. With the support of the kinetic slice (VIS-1, UV-1, Figure VI-2d), the bending to the right side takes more or less the same time compared to the bending to the left side (previous case), ~36 min. This is accompagnied with coloration kinetic of the surface occurring within ~3 min. Note that photocyclisation of the DTE-UPy (ϕ_{cycl}= 0.36) is expected to be much more efficient than the photoreversion (ϕ_{rev}= 0.008).

At this point, it is worth to insist on two important results about photoinduced motions:

- One can go backward using UV light and forward using visible light.
- Surprisingly, the characteristic time is more or less the same for both light induced bending.

When light is OFF, the thin film seems to be thermally stable but the videos were not recorded. Future experiments are scheduled in order to elucidate whether the color and the shape are maintained unchangeable at room temperature as a function of time. As an evidence, the second cycle will be decisive to test the reversibility of the process.

VISIBLE/UV irradiation – 2nd Cycle. Videos and its corresponding snapshots for the Visible and UV irradiations are illustrated in Figure VI-2b while kinetic slides are presented as well.

First of all, the thin film is still photochromic starting from blue to brown yellow (2nd cycle, VIS-2) and then blue again (2nd Cycle, UV-2). Despite this last blue color change, the thin film does not recover exactly its initial dark blue color but eye-naked statements have to be taken with caution. In the future, it is desired to combine in-situ miniaturize transmission spectrometer with the camera.

Together with the photochromic reaction, the reported photomechanical for the first cycle are exactlyreproduced for the second cycle i.e. bending to the left for visible irradiation followed by a bending to the right for the UV irradiation. Surprisingly, both bending rates in the second cycle occurs faster than the first step. Indeed, the inspection of the kinetic slices indicates that the photomechanical bending occurs within 25 min for the visible irradiation (against 33 min for the first cycle) and 15 min for the UV irradiation (against 36 min for the first cycle).

This result is fundamental in the sense that the strategy of our group is validated: Apart azobenzene system mentioned the in introduction, we are able to elaborated macroscopic flexible photochromic thin film displaying some reversibility (at least two cycles) switching between visible and UV light. As evidence, further tests are required in the future including the testing of at least tens cycles in order to assess the fatigue resistance.

VI.1.1.1.2. DC-R thin film

By fixing the sample into a clamp, the photomechanical experiments were performed on the thin film (Sized: 2 mm×2.5 mm×62 µm) prepared from the refluxed solution. Figure VI-3a and Figure VI-3b illustrate a series of snapshots (60 min gap) from the accelerated videos upon visible light irradiation (video VI-5, ▷) and UV light irradiation (video VI-6, ▷). Furthermore, kinetic slices representing photomechanical effect and photocoloration/photodecoloration of the surface are illustrated as well within Figure VI-3c.

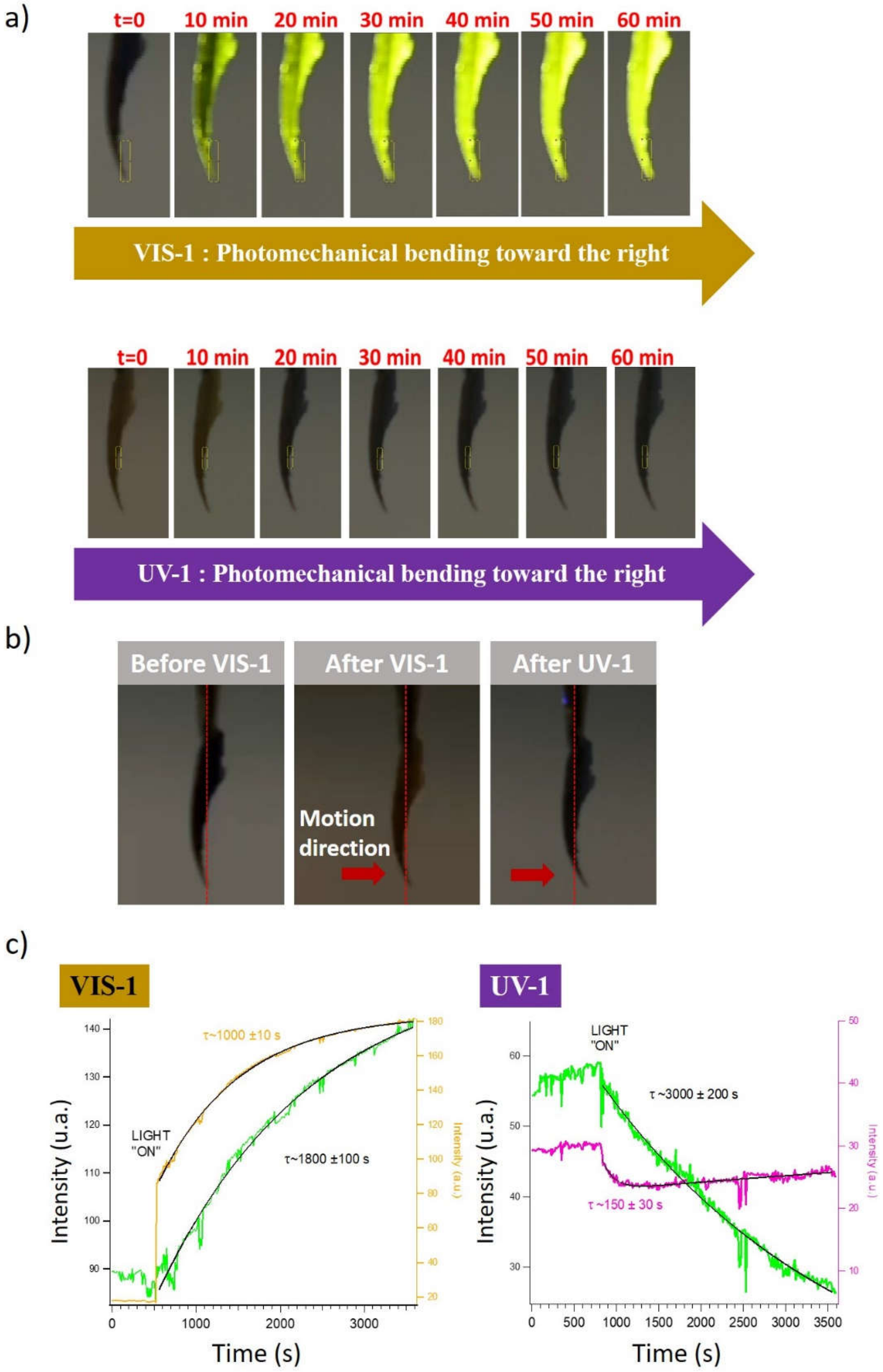

Figure VI-3: Macroscopic photomechanical behavior of DC-R thin film. a) 1st cycle upon irradiation with visible (VIS-1) and UV (UV-1) lights at room temperature. b) Photoinduced reversibility. c) Kinetic follow as function of exposure time of photomechanical effect (green signal), photocoloration (purple signal) and photdecoloration (orange signal) respectively upon VIS-1, UV-1.

The main differences with the previous experiment (DC-NR) are: i) the elaboration process is somehow different (reflux column during the supramolecular mixing) to avoid precipitate grain of DTE-UPy into the thin film (we expected better distribution between PEB-UPy and DTE-UPy); ii) the curvature appearance of the film is opposite compare to previous case; iii) only one irradiation cycle was tested.

VISIBLE irradiation. First, the exposure of DC-R thin film (CF) to visible light reveals a color change from dark blue color into dark yellow color (before and after VIS-1, Figure VI-3b). The photocoloration of the surface occurs within 16 min after switching on the lamp. Apart the photochromic behavior, a clear bending away from the incident light (right side) beginning after 10 min of irradiation (Figure VI-3a) is noticed. As clearly seen on the kinetic slice (Figure VI-3c), the bending to the right side continues occurring slowly within the same direction upon further irradiation. The characteristic time for such motion is 27 min, which is comparable to the 33 min reported for the DC-R film. However, fundamental questions arise from the comparison with DC-R: why the bending induced with visible light belongs to the opposite direction compare with DC-NR films? Is this surprising result related to the general shape of the thin film? It is attempting to corroborate the curvature of the thin film with the direction of the bending.

UV irradiation. Upon subsequent irradiation with UV light, the sample reverts its blue color before 10 min of irradiations (after VIS-1 and after UV-1, Figure VI-3b). This is corroborated by the kinetic slice with a characteristic time of ~3 min (Figure VII-3c). During one-hour of sample irradiation, the thin film bends away from the light source direction, continues occurring toward the right side. Such observation highlights a common point with DC-NR (right bending as well) although the amplitude of the bending seems to be weaker. Concurrently, the thin film seems to revert to its blue color. As have been involved in the case of DC-NR thin film (CF), DC-R thin film (CF) also does not require its initial dark color.

Unfortunately, the process reversibility within this part was not studied. Future experiments are scheduled in order to verify whether the thin film color and shape continue changing upon alternative UV and visible irradiations at room temperature.

VI.1.1.2. MM thin film

The response under irradiation of the MM-NR thin film (CF) was investigated when attached to the clamp. The sample (Sized 3 mm×2 mm×65 µm) was fixed on with straightly appearance and maintained stable at room temperature. Both Figure VI-4a and Figure VI-4b illustrate series of snapshots (10 min gap) from the accelerated videos upon first visible irradiation (video VI-

7 ▷), first UV irradiation (video VI-8, ▷), second visible irradiation (video VI-9, ▷), second UV irradiation (video VI-10, ▷). Moreover, the two irradiations cycles were carried out on this sample (VIS-UV-VIS-UV) in order to allow discussion about reversibility (Figure VI-4c).

VISIBLE/UV irradiation – 1st Cycle. On irradiating the sample with visible light (before and after VIS-1, Figure VI-4c) apart the expected change of color, any noticeable bending was clearly detected (Figure VI-4a). In the same way, with UV light, the starting blue color is recovered but any shape changes were observed (Figure VII-4a).

VISIBLE/UV irradiation – 2nd Cycle. The thin film is still photochromic starting from blue color into brown yellow color (2nd cycle, VIS-2) and then blue color again (2nd Cycle, UV-2) as seen in Figure VI-4c. Despite this blue color change, the thin film does not recover exactly its initial dark blue color but eye-naked statements have to be taken with caution. The snapshots Figure VI-4b shows any noticeable bending for the visible light irradiation. Upon UV light irradiation, a clearly bending away from the source light direction was detected.

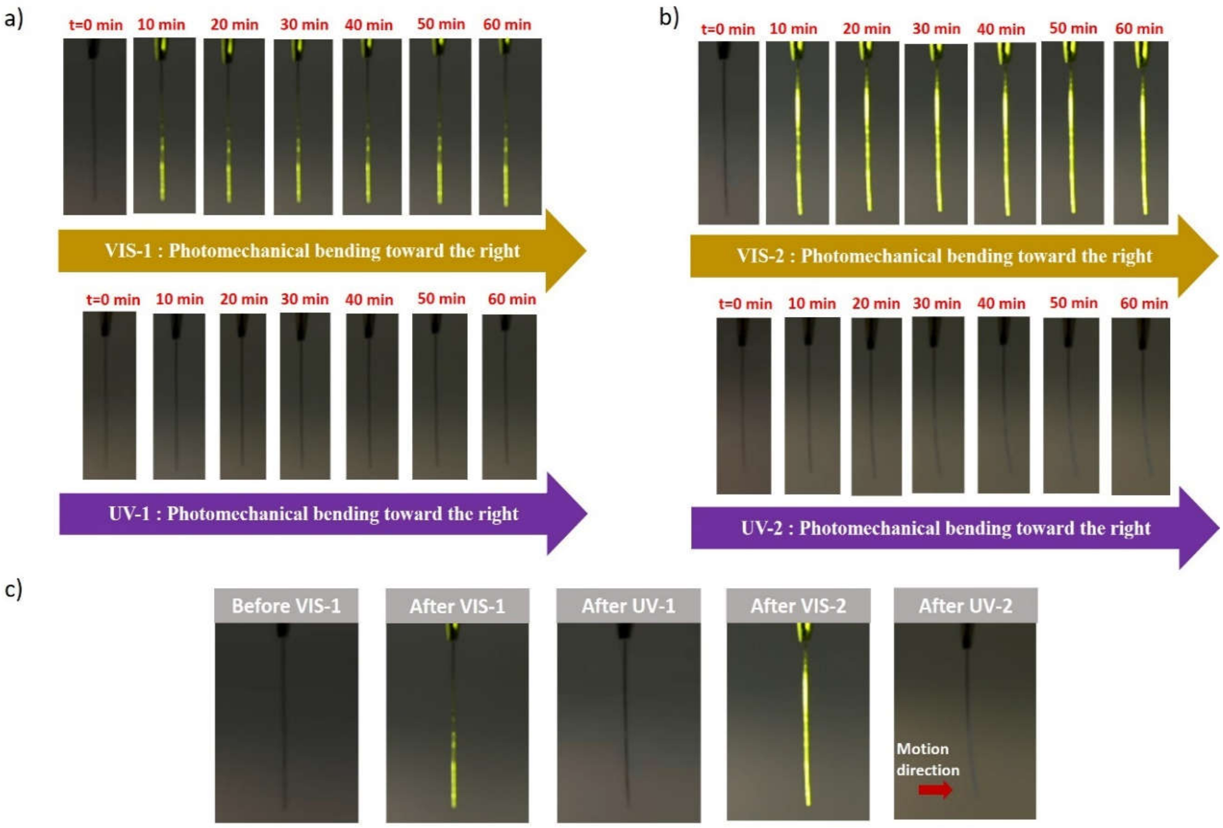

Figure VI-4: Macroscopic photomechanical behavior of MM-NR thin film. a) 1st cycle upon irradiation with visible (VIS-1) and UV (UV-1) lights at room temperature. b) 2nd cycle upon irradiation with visible (VIS-2) and UV (UV-2) lights at room temperature. c) Photoinduced reversibility.

VISIBLE/UV irradiation – Toward photomechanical quantification. With the aim to predict photomechanical effectiveness within the 1st cycle, a set-up monitored by means of dynamical mechanical analysis DMA was applied. However, thin film was clamped from both extremes of the longest dimension into the instrument holders as described in chapter II. Then, light irradiation is expected to generate a force perpendicularly to the thin film surface. As response, the actual thin film length increases or decreases owing to the mentioned bending behavior above.

When the experiment was taken place within the MM PEB-UPy at room temperature, the mechanical modulus was measured as a function of time (Figure VI-5a). Beginning from 125 s, the mechanical modulus stability allows following its variation upon UV and visible irradiations and even in dark in order to verify whether thermal relaxations may exist. As expected, the non-photoreactive thin film shows clearly a constant photomechanical modulus. This leads to confirm that no shape changes have been occurred.

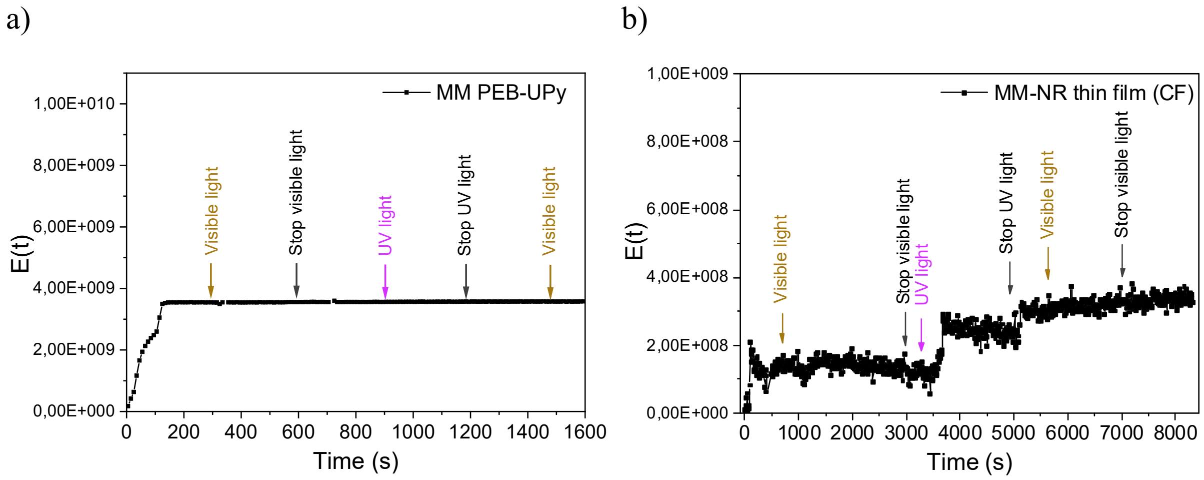

Figure VI-5: Kinetic evolution of storage modulus upon UV and visible illuminations and in darkness. a) MM thin film of PEB-UPy. The thin film sized 12.34×2.02×0.06 mm^3. b) MM-NR thin film (CF). The thin film sized 10.50×1.59×0.06 mm^3.

When photoreactive DTE-UPy units are incorporated, the photomechanical modulus measurements of the MM-NR thin film (CF) is performed by analogy as function of time under irradiation and in darkness as illustrated in Figure VI-5b.

Visible light irradiation seems inducing a slight decrease within the mechanical modulus according to a first slow exponential growth up to 1000 seconds. Upon further visible exposure, it appears that E(t) regains its initial value and then decreases again according to a second slow exponential growth up to 3000 seconds. By stopping the visible irradiation, this modulus continues seemingly decreasing. Whilst, a strong variation is occurred within few seconds when the incident UV light wavelength was changed. The stopping of this irradiation has induced a second less pronounced variation of the followed modulus. Concurrently, E(t) continues increasing progressively regardless the visible light irradiation is applied or not.

On the bases of this experiment, very weak variations (can be considered negligible) within the mechanical modulus are consistent with the photomechanical macroscopic effect evaluated in Figure VI-4a. The induced strong variation of E(t) upon UV light is not consistent with the photomechanical macroscopic effect where no noticeable bending behavior was underlined (Figure VI-4a). Thus, this arises the previous mentioned question about the effectiveness of photomechanical effect within the 1st cycle.

Compared to either DC-R or DC-NR, this lack of photomechanical effect within the first cycle can be interpreted according to two hypotheses: i) the internal structure/morphology of the films does not allow a large macroscopic effect; ii) the sample size or shape plays a key role in inducing macroscopic effect. In particular, both DC films presented an initial curvature compared to the very flat MM film.

VI.1.1.3. Discussion about the macroscopic bending behavior

One of the objectives of this study is to figure out the parameters responsible of photomechanical behavior. From the compared photographs, it seems that the elaboration method influences the thin film response under illumination.

When the CF-thin film is illuminated with visible light, photoisomerization from CF into OF isomers will be occurred expecting to lead an expansion of the photoreacted layer along the long axis of thin film. The expansion toward the incident light direction such the case of DC-NR thin film or away from the incident light direction for both DC-R case seems depending on the elaboration process as all illuminations are proceeded under the same conditions. In other word, DTE-UPy distribution within the photoreacted layer and reaction depth seems affecting the photoinduced deformation response.

Irradiating the films with UV light is expected indicating that diarylethene electrocyclization from OF into CF have to lead a contraction of the photoreacted layer along the long axis of thin film. Practically, the examined thin films are found to exhibit bending away from the incident light direction regardless the elaboration process. The correlation between the expected and the found response direction need further investigation in the future as the exact reason of the observed phenomena are still unclear.

Typical bending behavior observed for diarylethene derivative crystals are usually achieved from the initial OF-isomer. Among these diarylethene derivatives, Hirano A. and coworkers have reported an interesting bending behavior of two diarylethenes. The crystals issued from diraylethene functionalized from one side with ester group bend toward the incident UV light. Whereas, the crystals obtained from diarylethene functionalized from both side with ester group bends away from the incident UV light [1]. However, a detailed study about the correlation between the molecular packing and the bending direction was required. Therefore, this reported investigation lends further support to the explanation proffered above about amorphous nature of DTE-UPy and its distribution within the thin film.

From the other hand, Mamiya, J.I. and coworkers have reported the first tentative about photo-responsiveness of photomobile polymer materials based on cross-linked liquid crystalline polymers with mesomorphic diarylethenes [2]. The performed study revealed that the issued thin film changes its color immediately followed by bending toward an actinic light source along the alignment direction of the mesogens at 120°C within 4 minutes. Subsequent exposure into visible light reverts the thin film to its initial color. Whereas, this thin film regains it flatten shape only when left in dark for 24 hours. By analogy to the observed motions, the occurred deformations were reported not only weaker but also leading slower response time.

VI.1.2. Summary on macroscopic photo-induced changes

This is the first example of supramolecular polymer containing photoreactive diarylethene where macroscopic photoinduced deformations have been successfully elucidated.

Therefore, two types of bending direction were reported: bending away from the UV light source and bending away or toward the visible source light. Such characteristics were summarized in Figure VI-6.

The curved DC-NR thin film exhibits deformations in two different direction confirming the reversibility of process. Whilst for curved DC-R thin film, its deformation continues occurring in the same direction regardless the applied light. This arises the question about the key role played by precipitate in inducing photomechanical changes which will be discussed later. The flat MM-NR does not exhibit photomechanical effect in the first irradiation cycle. The MM thin film dending was seen only upon UV light (2nd cycle). For this purpose, first quantitative study with DMA has proven the MM thin film photoactivity and the key role of photoreactive DTE-UPy in inducing changes within the mechanical modulus upon irradiation. Accordingly, these experiments have confirmed in somehow the existence of motions against the irradiation time.

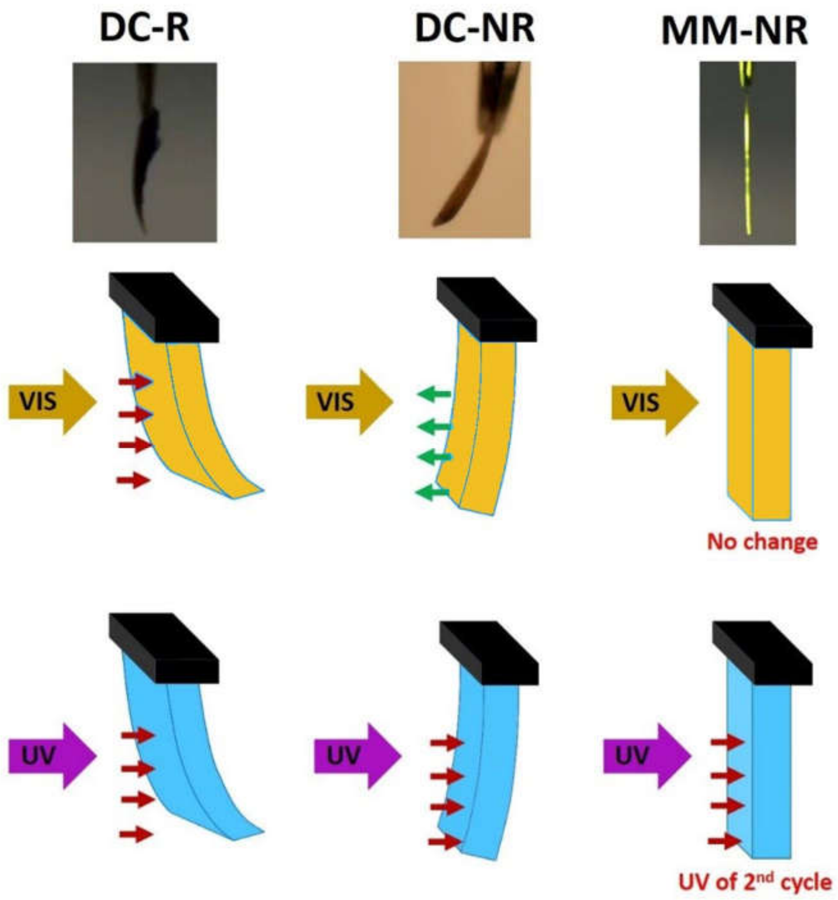

Figure VI-6: Macroscopic photo-induced changes within various thin films. Red arrow assigned the bending motion in left direction and green arrow assigned to bending motion in right direction.

However, the revealed slow photomechanical effects propose the possible existence of local strain induced by light that cumulatively induces macroscopic changes. Further study to identify whether local changes may exist with more pronounced deformations is investigated.

VI.2. Photomechanical effect at Microscopic scale

To verify the statement about the photoinduced local strains, this section is devoted to highlight the microscopic photo-responsiveness of self-assemblies between DTE-UPy and PEB-UPy. For this purpose, the photomechanical behavior is investigated under wield-field microscopy setup with in-situ illumination (Chapter II). Experiment procedure consists on cutting a thin film from the main one by means of scalpel (microscopic size typically 200-300 µm) and then fixing it from one of its extremities of the longest dimension between two glass slips (Sandwich configuration). However, a part of thin film was hidden between the two glass slips and the other part was maintained stable outside between the two glass slips maintained in the air. The fixed thin film is expected to be illuminated with UV light from upper side and with visible light from lower side due to experimental setup configuration.

The elaborated thin film is investigated within the same involved processes above, i.e. MM or DC (same batches). In this part, we will be devoted to quantify the photomechanical motions of these thin films by acquiring kinetic slices at the border of the sample. These kinetic slices will be compared with kinetic slices registered in the center of the sample as an assessment for the photocoloration/photodecoloration kinetics.

The typical illumination sequences are always the same: 10 min (600 s) of irradiation with one picture every 1 s. The light switches ON after ~10 seconds. The sample is illuminated in-situ with visible irradiation (550 nm band pass filter) and UV irradiation (313 nm band pass filter). The corresponding videos are accelerated ~100 times with a total duration of ~6 seconds.

VI.2.1. DC-thin films

It is noteworthy substantial to examine further the photoinduced changes within the DC thin films in order to compare their microscopic responses to those exhibited by the MM films. However, as have been involved in macroscopic changes, DC-NR and DC-R thin films will be respectively investigated.

VI.2.1.1. DC-NR thin film

- **Sample presentation**

The thin film was attached between two glass substrates from the extremities of the longest dimension as depicted in Figure VI-7 (glass slips border). The sample was too long, that is why the photograph was recomposed after four screenshots by CCD camera throughout the length of the sample. Therefore, the illumination spot cover only a one chosen screenshot. Herein, the photomechanical effect was studied within the sample tip sized 280 µm×158 µm×62 µm (white dotted square).

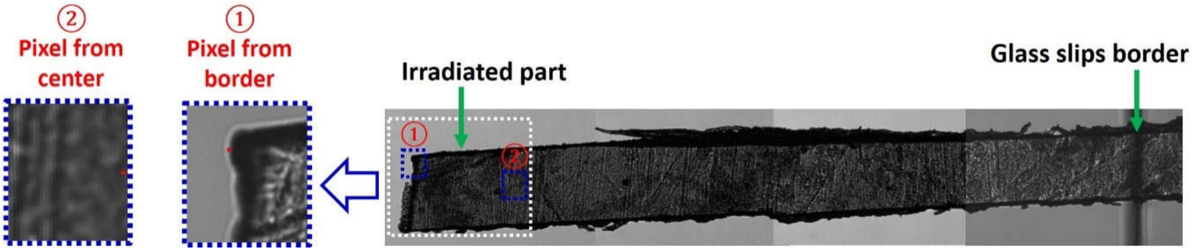

Figure VI-7: DC-NR thin film attached from one side within sandwich approach.
Size of the film: 1120 µm×158 µm. Thickness of the film: 62 µm.

The DC-NR thin film is illuminated in situ upon UV and visible irradiations. A series of snapshots of the accelerated videos upon visible irradiation (Figure VI-8a, video VI-11, 🎞) and UV irradiation (Figure VI-8b, video VI-12, 🎞). Moreover, two subsequent irradiation cycles were carried out on the same sample (VIS-1, UV-1 and VIS-2, UV-2) allowing the reversibility as depicted in Figure VI-10.

The need to describe the photoinduced deformation is carried out by following the trajectory of the tip displacement against the exposure time and comparing this movement with the rate of sample photocoloration. Two kinetic slices will be plotted all along this part. The kinetic slice assessing the photomechanical effect was chosen at a pixel from the sample border (Area-1, Figure VI-7) upon UV and visible lights (Figure VI-8c, green fitted curve). Concerning the photocoloration/photoreversion, a second pixel from the thin film center (Area-2, Figure VI-7) is plotted against the visible irradiation time (Figure VI-8c, orange fitted curve) and the UV irradiation time (Figure VI-8c, purple fitted curve).

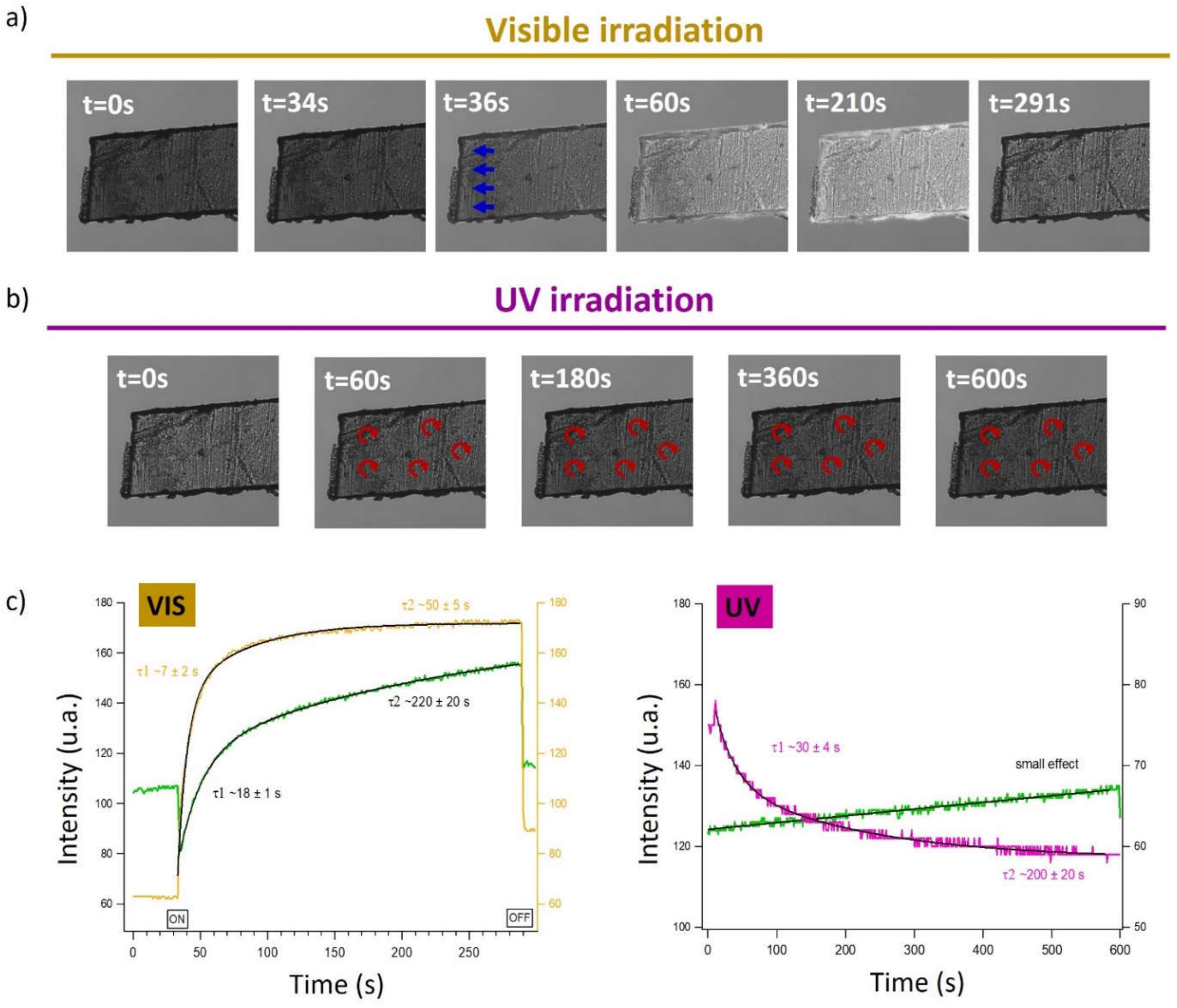

Figure VI-8: Microscopic photomechanical behavior of DC-NR thin film prepared. a) Snapshots upon irradiation with visible. b) Snapshots upon irradiation with visible. c) Kinetic follow as function of exposure time of photomechanical effect (green signal), photocoloration (purple signal) and photodecoloration (orange signal).

- Photochromism and re-emission of the sample

By applying the kinetic slice from the sample center, it was straightforward to assess the photochromic properties of the film. The irradiation with visible light (10 min) leads to change in DC-NR thin film (CF) color from dark blue into dark yellow color. Furthermore, this color change is accompanied with light re-emission (film clearer letting more transmitted intensity passing through the microscope objective). From one hand, the optical signal increment is assigned to photodecoloration reaction with a characteristic time of ~50 s. Moreover, the re-emitted light occurs with characteristic time of ~7 s. From the other hand, the optical signal decrement beginning from 10 s is attributed to photocoloration reaction with a characteristic time of ~200 s. At first glance, the DC-NR film preparation and its thermal treatment have kept the photochromic properties more or less unaffected.

- Evidences for one-step photomechanical effect with Visible irradiation

Continuous visible light. Within the first few seconds of visible exposure, the first microscopic response reveals a surprising stretching up of the thin film as mentioned in Figure VII.8a (red vertical arrow). Furthermore, this ultrafast stretching behavior occurs perpendicularly to the incident light direction without noticeable color change. Such photomechanical response maybe assigned to instantaneous expansion photo-reverted layer within the thin film. Upon further exposure with visible light, no noticeable bending of the sample has been detected.

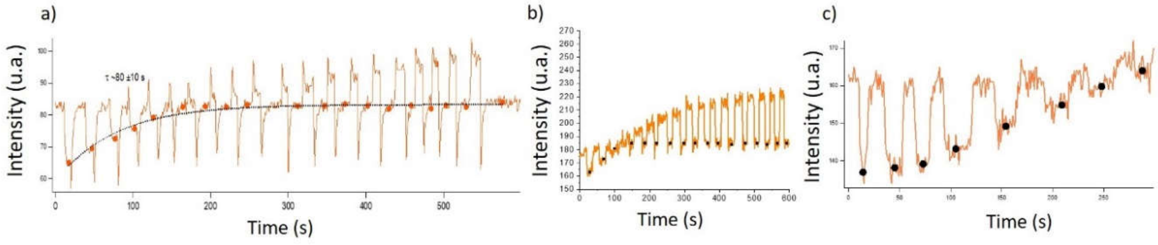

Figure VI-9: Stretching phenomenon upon visible light. a) DC-NR thin film. b) DC-R thin film. c) MM-NR thin film

ON/OFF visible light. This instantaneous stretching within the same DC-NR thin film was further examined when visible light was applied and turned off within multiple sequences. Therefore, the tip displacement of sample was plotted against visible exposure time where pixel from the border was followed (Figure VII-9a).

Before visible irradiation, the optical signal remains stable. When irradiated with visible light, the thin film occurs an instantaneous expansion motion accompanied with light re-emission. By stopping the irradiation, a relaxation with mechanical origin is followed by the return-back of the optical signal to its initial value. The irradiation ON/OFF processes induce the same photomechanical response until 600 s accompanied with light re-emission.

The thin film undergoes a strong photomechanical behavior of stretching up once the visible light is applied. This observed ultrafast stretching suggests a photomechanical mechanism justified by the thin film surface photoreaction rather than its bulk. Moreover, this unique stretching-response occurs perpendicularly to the incident light direction without noticeable color change. Due to further exposure into visible light, the sample tends to re-emit light. Such re-emission disappears by stopping the light excitation. The origin of this light was already commented in the chapter IV (pages: 118-119).

- Evidences for one-step photomechanical effect with UV irradiation

On the video, no remarkable bending behavior was underlined within the first seconds of irradiation. Further exposure into UV light does not induced a remarkable bending behavior. By zooming on the border, weak shrinkages can be noticed up to 60 s, 120 s, 240 s and even 300 s (Figure VII-7b). This effect is found with a characteristic time of 420 s.

- Reversibility - UV/ visible cycles

The repeatability of photoinduced changes were investigated in Figure VII-10a. More details about absorption spectral changes upon thin film photoirradiation were illustrated in Figure VII-10b where judgements about whether irradiation period from the bottom or the top are enough to fully convert the thin film. However, the appearance and disappearance of the CF absorption band are investigated by means of UV-Vis absorption spectroscopy.

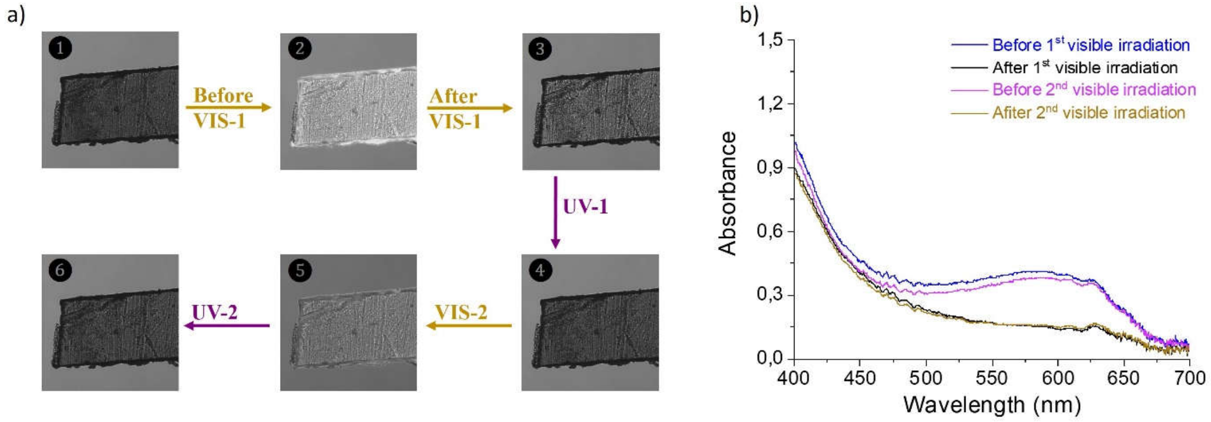

Figure VI-10: Microscopic reversible photoinduced changes of DC-NR thin film under illumination. a) Alternating the exposure upon UV and visible light. b) Absorption spectra upon irradiation.

Before the first visible irradiation, the presence of CF-band was verified through the blue absorption spectrum (before VIS-1 ❶, Figure VI-10b). Except the observed expansion within few seconds (before VIS-1 ❷), any bending motion was reported upon visible light (After VIS-1 ❸, Figure VI-10b). Therefore, the disappearance of CF-band was achieved as shown through the black spectrum (Figure VI-10b). Upon UV-irradiation (UV-1 ❹, Figure VI-10b), very weak shrinkage occurred. Concurrently, the CF-band regains its initial intensity as mentioned with the violet spectrum. Subsequent visible irradiation revealed that the regained CF-band re-disappears for the second time as mentioned in the mustard spectrum without a noticeable photoinduced changes (VIS-2 ❺, Figure VI-10b). The second irradiation with UV-2 light induced color change accompanied with CF-band re-appearance. Concurrently, very weak shrinkage presists.

In brief, very weak photomechanical effect (shrinkage behavior) upon UV light and strong expansion upon Visible light are reported for this sample. According to macroscopic experiment findings, this is an unexpected result in the sense that photomechanical response under UV irradiation was the largest one comparing the other thin films. Note that photomechanical responses at macroscopic and microscopic scales originate from the same batch. In other words, these photomechanical effects at macroscopic scale are expected to imply systematically a photoresponse at microscopic one (the reverse being not true).

VI.2.1.2. DC-R thin film

- **Sample presentation.**

The DC-R thin film was fixed between two glass substrates as depicted in Figure VI-11 (glass slips border). The illumination spot cannot cover the film length, which was reconstituted from the captured five screenshots. Thus, the photomechanical effect was studied within the sample tip sized 220 µm×150 µm×65 µm (white dotted square, Figure VI-11).

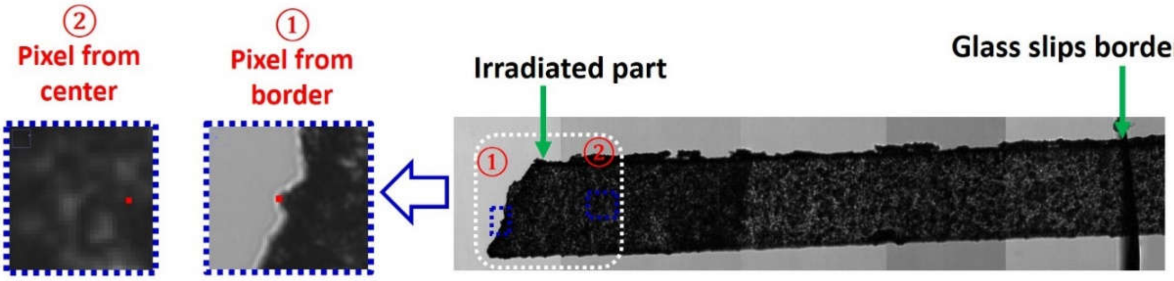

Figure VI-11: DC-R thin film attached from one side within sandwich approach.
Size of the film: 1150 µm×150 µm. Thickness of the film: 65 µm.

A series of DC-R thin film snapshots of the accelerated videos upon visible irradiation (Figure VI-12a, video VII-13, ▷) and UV irradiation (Figure VI-12b, video VII-14, ▷). In order to describe the photoinduced deformation is carried out by following the trajectory of the tip displacement from the border (Figure VI-12c, green fitted curve) as a function of exposure time and comparing the generated movements with the sample photocoloration (Figure VI-12c, purple fitted curve) photodecoloration (Figure VI-12c, orange fitted curve) rates.

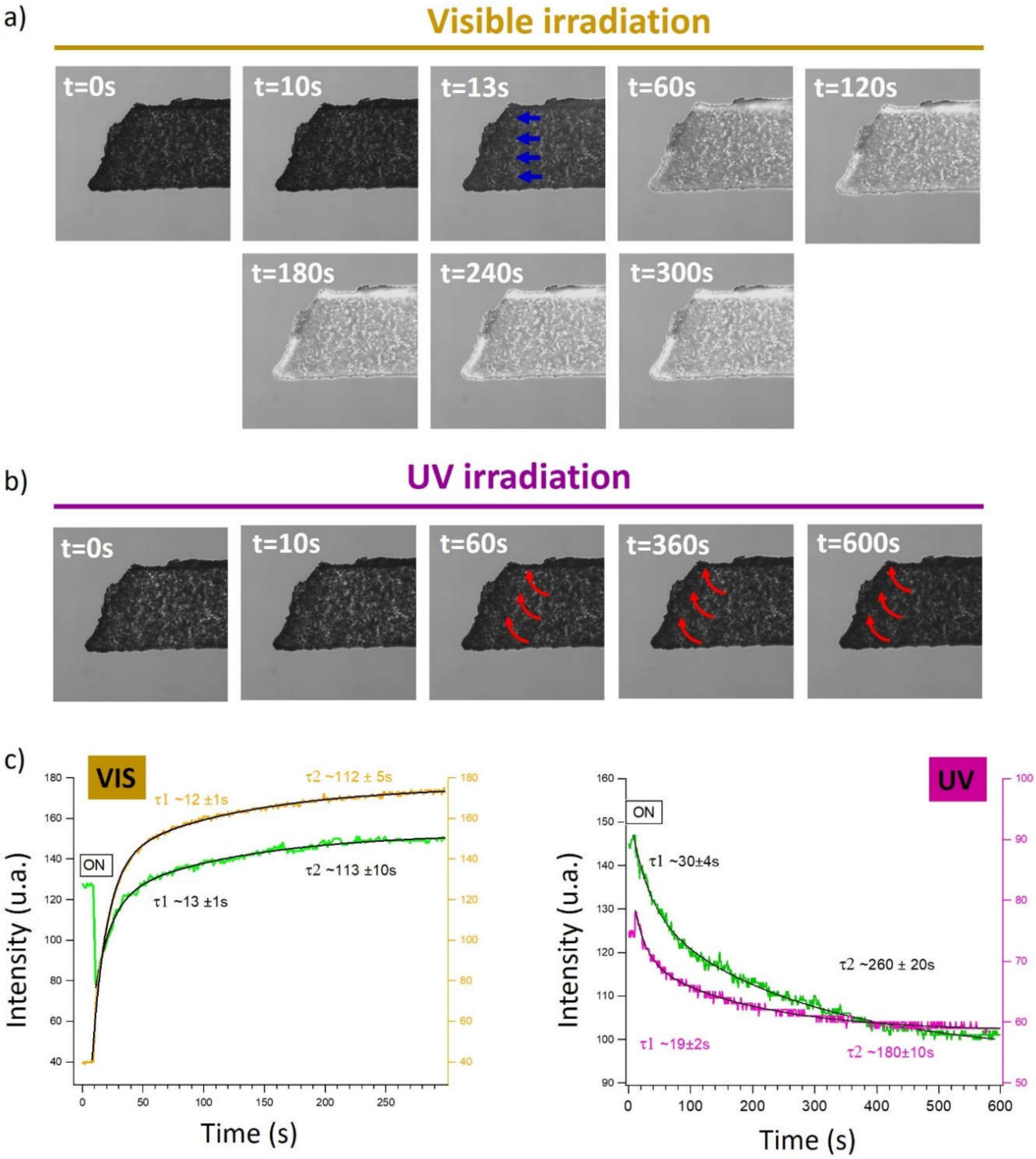

Figure VI-12: Microscopic photomechanical behavior of DC-R thin film prepared. a) Snapshots upon irradiation with visible. b) Snapshots upon irradiation with visible. c) Kinetic follow as function of exposure time of photomechanical effect (green signal), photocoloration (purple signal) and photodecoloration (orange signal).

- Photochromism and re-emission of the sample

The DC refluxed thin film is dark blue colored. The photochromic properties of the film were followed by means of the kinetic slice in the film center. Upon visible light irradiation, the film turns gradually to dark yellow color and the optical signal increases from 30 to 100 with a characteristic time of ~90 s. Concurrently, during the exposure to visible light, the thin film re-emits a white light. This re-emission occurs with characteristic time of ~12 s. Subsequent 10 min of UV light irradiation, the film returns-back to its blue color and the optical signal decreases and regains its starting value. The photocoloration reaction occurs within a characteristic time of ~20 s.

- Evidences for one-step photomechanical effect with Visible irradiation

Continuous visible light. The irradiation of refluxed sample with visible light from upper side (Figure VI-12a) revealed the same described expansion phenomenon: a stretching perpendicularly to the incident light direction without noticeable color change. This expansion behavior occurs within the first seconds of exposure (red vertical arrow). Further exposure to visible light does show any remarkable consecutive photomechanical effect such as bending behavior. The sample tends to re-emit white light. Thus, it was difficult to say whether the sample was bending at 60 s, 210 s and even until 300 s.

ON/OFF visible light. The reported expansion phenomenon of the thin film within the first few seconds was evaluated upon several intervals of exposure to visible light. As shown in Figure VI-9b, the fitted slice from the border was followed against exposure time. Before irradiation, the optical signal appears constant. The first seconds of visible light have induced the sudden decrease of optical signal. Such decrement occurs when the expansion of the photoreacted thin film was achieved. The reverted optical signal value in dark occurs a decrease less pronounced than the first one accompanied with a second expansion phenomenon. The third illumination leads to expansion accompanied with light re-emission. Above 150 seconds, the expansion continues occurring but this time, the re-emitted white light intensity seems very important. However, we can see that the expansion phenomenon can be reversibly occurred once visible light is applied.

- Evidences for one-step photomechanical effect with UV irradiation

Subsequent UV light irradiation from lower side leads to a very weak bending phenomenon as noticed in Figure VI-12b (red inclined arrow). This bending direction was difficult to precise as the phenomenon was out of focus. With longer UV light exposures, it remains that the photoinduced-bending phenomenon is persisting while reverting to its initial blue color. The border of sample seems to be flower up to 120 s, 240 s, 300 s and 600 s.

The microscopic photomechanical effect induced by the non-refluxed sample is not the same. Despite the weak bending of DC-R thin film, the absence of bending within DC-NR arises the question about the key role played by DTE-UPy precipitate in inducing photomechanical behavior.

- Reversibility - UV/ visible cycles

To understand further the reported bending behavior, the thin film reversibility upon two illumination cycles are studied as shown in Figure VI-13.

For the first cycle, VIS-1 and UV-1 were applied. The initial CF state of DC-R thin film (❶, Figure VI-13a) was verified through spectroscopy absorption. At room temperature, the characteristic photo-generated CF leads to the appearance of the characteristic absorption band (blue spectrum, Figure VI-13b). The irradiation with visible light gives arise to, except the expansion and light re-emission, uncertain bending behavior (❷, ❸, Figure VI-13a). Concurrently, the disappearance of the CF characteristic band was occurred after visible irradiation (black spectrum, Figure VI-13b). When subsequent UV light irradiation was carried out, the sample exhibits a photocyclization reaction accompanied with a slowly bending (❹, Figure VI-13b).

For the second cycle, VIS-2 and UV-2 were performed. The CF-band reappearance regains its initial absorbance value as mentioned in Figure VI-13b (violet spectrum). Upon irradiation with visible light, the thin film occurs, except the expansion and light re-emission, uncertain bending behavior ❺, Figure VI-13a) as have already observed within the first irradiation process. Concurrently, the CF-band disappears compared the initial value as depicted in Figure VI-13a (mustard spectrum) accompanied with a weak bending phenomenon.

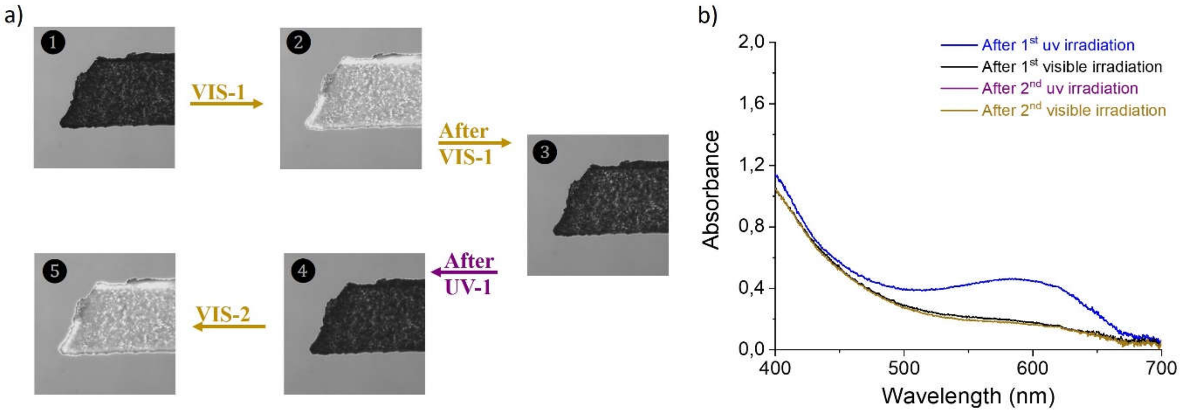

Figure VI-13: Microscopic reversible photoinduced changes of DC-R thin film under illumination. a) Alternating the exposure upon UV and visible light. b) Absorption spectra upon irradiation.

Both weak bending behavior upon UV light irradiation and instantaneous expansion accompanied with strong light re-emission upon visible light irradiation can be described as reversible phenomena for DC-R thin film.

It is important to note that microscopic and macroscopic motions are issued from the same batch. However, contrarily to the occurred macroscopic photomechanical behavior upon both UV and visible lights, the microscopic observations were expected to lead into the same motions. At this stage, we can suggest that weak photoinduced local strains within the DC thin film surface will propagate according to a gradient within the thickness and induce more pronounced behaviors within the macroscopic scale.

VI.2.2. MM thin films

Unlike DC films of the previous section, MM-NR films were found to be not photo-responsive at the macroscopic scale. Here, we want to undertake their response at microscopic scale.

- Sample presentation

Following the same procedure as DC sample, MM thin film was clamped within a sandwich approach. The film photograph is constituted from seven screenshots by CCD camera. The mechano-active behavior effectiveness was elucidated within the sample tip sized 290 µm×159 µm×65 µm (white dotted square, Figure VI-14).

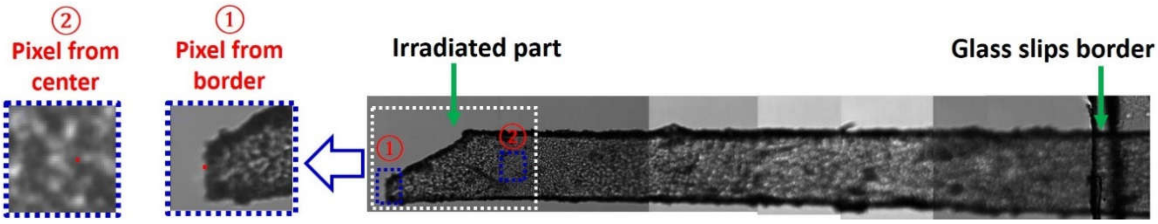

Figure VI-14: MM-NR thin film attached from one side within sandwich approach. Size of the film: 1800 µm×159 µm. Thickness of the film: 65 µm.

Figure VI-15 illustrates a series of snapshots from accelerated videos upon a first irradiation cycle: visible light (video VI-15, ▷) and UV light (video VI-16, ▷). Subsequent second irradiation cycle was carried out on the same sample. Both irradiations cycles (VIS-UV-VIS-UV) are illustrated in Figure VI-15 with the aim to evaluate the reversibility of existent photoinduced motions. From the other hand, the need to describe the photocoloration/photodecoloration and photoinduced deformation following the same strategy as above i.e. kinetic slices were plotted against the exposure time. Concerning the photocoloration reaction (Figure VI-15c, purple fitted curve) and photodecoloration reaction

(Figure VI-15c, orange fitted curve), pixels from the thin film center are plotted against the exposure time. For the photomechanical effect (Figure VI-15c, green fitted curve), a pixel from the thin film border is plotted against the exposure time.

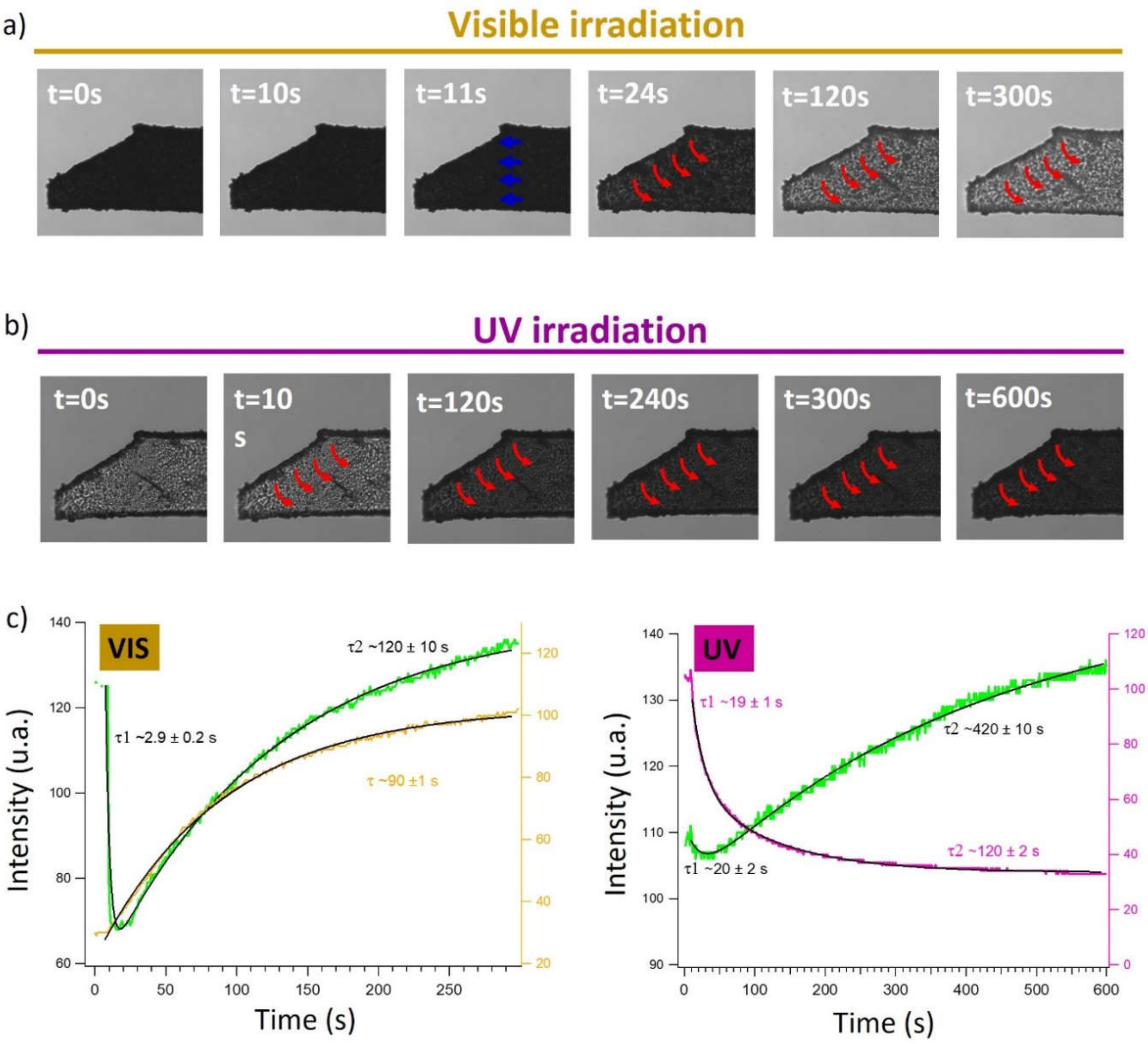

Figure VI-15: Microscopic photomechanical behavior of MM-NR thin film prepared. a) Snapshots upon irradiation with visible. b) Snapshots upon irradiation with visible. c) Kinetic follow as function of exposure time of photomechanical effect (green signal), photocoloration (purple signal) and photodecoloration (orange signal).

- Photochromism of the sample

The MM-NR thin film color starts with a dark blue. With the aid of the kinetic slice in the center of the film, the photochromic properties of the film were assessed. Upon visible light irradiation, the film turns gradually to dark yellow and intensity increases from 30 to 100 with a characteristic time of ~90 s. Surprisingly, the re-emission phenomenon was remarkably absent compared to the DC samples. By switching to UV light (after 10 min), the film reverts its blue color and its optical signal value. The characteristic time of photocoloration reaction was ~20 s.

- Evidences for the two-step photomechanical effect with Visible irradiation

Continuous visible light. On irradiating the sample with 550 nm from upper side, the sample exhibits unusual photomechanical behavior compared with that of the reported typical DTEs at macroscopic scale. As seen on the video and snapshots of presented on Figure VI-15, MM thin film is not only stretched as the DC thin film microscopic response but also two different steps are clearly observed.

Within the few seconds of visible exposure, the first microscopic response reveals an ultrafast stretching behavior occurring perpendicularly to the incident light direction without noticeable color change (Figure VI-15a, blue vertical arrow). Such first photomechanical response should be assigned to instantaneous expansion of the first photo-reverted layer within the sample. Upon further exposure with visible light, the sample tends to bend gradually up to 300 s, accompanied with clearness within the thin film color.

Note that despite the expected difference between MM and DC films, this unique ultrafast stretching occurs in the same way. Due to further exposure into visible light, the sample concurrently tends to emit white light, which disappears by stopping the irradiation.

This instantaneous stretching within the same DC-NR thin film was further examined when visible light was applied and turned off within multiple sequences. Therefore, the tip displacement of sample was plotted against visible exposure time where pixel from the border.

ON/OFF visible light. The remarkable expansion of thin film within few seconds was underlined upon several intervals of exposure to visible light as shown in Figure VI-9c where a border pixel displacement was followed against exposure time. In darkness, the optical density remains stable. Due to the first seconds of visible light, a sudden fall within the optical density was observed assigned to thin film stretching (see 15s, Figure VI-9c). By stopping the irradiation, the pixel returns to its first position and the optical signal regains its first level (see 25s, Figure VI-9c). When the visible irradiation was carried out with longer exposure time, the thin film stretches for the second time and optical signal acquires a second successive expansion behavior. It is important to note that despite the longer time exposure, the thin film jumps just one time within the mentioned irradiation range. Moreover, the observed motion occurs within 1 to 2 seconds. Thus, the extra-irradiation with visible light does not induce more jumps in this time range. Such statement was verified upon further visible irradiation with longer exposure ranges. Therefore, by taking into account the color change, a trend is seemingly increasing progressively until 300s due to photoreversion transformation (black square, Figure VI-9c).

Regardless the used thin film (DC or MM), the ultrafast stretching was observed once the visible light was applied. Thus, this leads to say that the occurred phenomenon is independent of elaboration process including organization of assembly within the films.

- Evidences for one-step photomechanical effect with UV irradiation

By changing the irradiation wavelength from 550 nm into 313 nm: if the photochromism is of course operative, the photomechanical effect is not the same. Indeed, the initial stretching phenomenon has disappeared and remarkable bending behavior has rather occurred since the first seconds of irradiation (10 s) as depicted in Figure VI-15b (red inclined arrow). Upon further exposure into UV light, it remains that the photoinduced bending behavior continues occurring progressively up to 120 s, 240 s, 300 s and even 600 s.

Note that despite the expected difference between MM and DC films, this bending within MM sample occurs more effectively and maybe assigned propagation of gradient (OF→CF) within the thin film thickness, which will be further discussed later.

- Reversibility - UV/ visible cycles

The bending is a commonly observed photomechanical response of diarylethene crystals. It is rather the first time to report such photomechanical performance within photoreactive thin film, which lay the question particularly on their effectiveness upon alternating irradiation with UV and visible light according to two illumination cycles without damaging the film as shown in Figure VI-16a. Moreover, Figure VI-16b shows typical absorption spectral changes upon photoirradiation of thin film. The photo-generated CF bears an absorption band at roughly 570-580 nm. Thus, the appearance and disappearance of this characteristic band is followed upon light exposure.

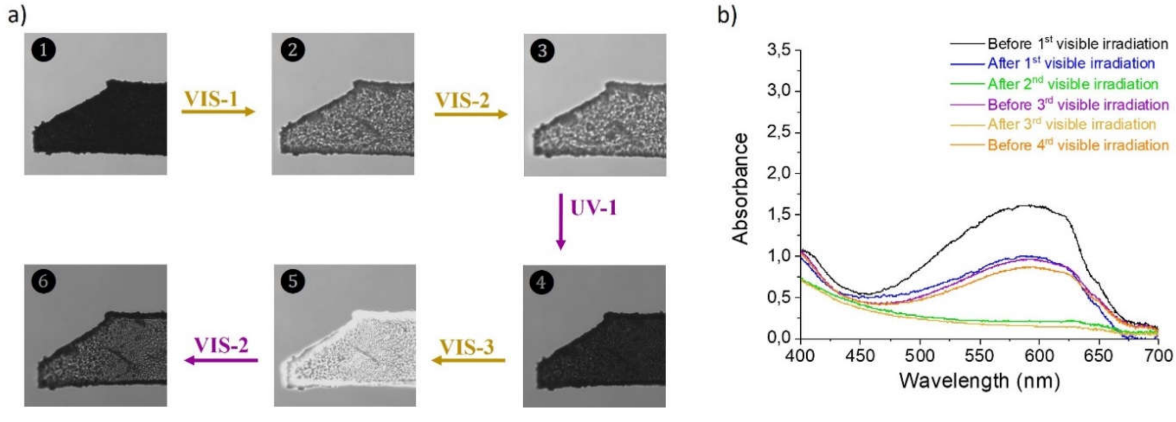

Figure VI-16: Microscopic reversible photoinduced changes of MM-NR thin film under illumination. a) Alternating the exposure upon UV and visible light. b) Absorption spectra upon irradiation.

Preceding the 1st illumination cycle, the thin film displays a dark appearance justified by CF-isomers abundancy (❶, Figure VI-16a) as confirmed within the black absorption spectrum (Before 1st visible irradiation, Figure VI-16b). When visible irradiation was carried out from upper side, apart the described transition at first, the thin film tends to bend slowly. The 580 nm band was reduced twice compared to the initial absorbance value. The disappearance of this band was occurred after a further visible irradiation (❷, blue absorption spectrum). It is important to note that this subsequent visible irradiation was accompanied by the unique described expansion. The bending continues occurring slowly, accompanied with full disappearance of CF-band (❸, green absorption spectrum). When the UV light was carried out from lower side, the sample tends to bend progressively. In other word, this bending trajectory is seemingly occurred in one direction attended with a CF-band re-appearance (❹, violet absorption spectrum). Despite various tries to get the initial absorbance value, the CF-band remains reduced twice compared the initial value.

To know whether such photomechanical performance keeps available, the thin film was exposed again to UV and visible lights (2nd cycle). However, except the expansion phenomenon due to visible light, it has been noticed an impressive white light re-emission, which ceases immediately when the incident irradiation was stopped. Unfortunately, the re-emitted light has apparently camouflaged the bending phenomenon. Consequently, it was difficult to follow step-by-step the photoinduced motion. Concurrently, full disappearance within CF-band was rather emphasized (❺, mustard absorption spectrum). By changing the wavelength from 550 nm into 313 nm, the UV exposure of thin film from lower side seems indicating that the sample tends to bend. The re-appearance of CF-band was successfully reached (❻, orange absorption spectrum). Unfortunately, it appears difficult to verify whether the thin film returns to its initial straight shape. Thus, it is interesting to think about a new experiment set-up leading the sample re-viewing within the depth profile upon alternating UV and visible irradiation.

For UV/visible irradiations, both bending behavior and instantaneous stretching accompanied with strong light re-emission are briefly reported as reversible phenomena for the MM-NR sample. By comparing these observations to quasi-absent macroscopic photomechanical behavior (1st illumination cycle), this is unexpected result in the sense that mechano-active response under visible and UV irradiations, except the stretching, induces the most pronounced microscopic bending behavior compared the DC thin films. In other words, photomechanical effects at macroscopic scale implies systematically a photoresponse at microscopic one. It is important to note that also in this case, macroscopic and microscopic experiments applied sample issued from the same batch. Moreover, we report the evidence about full conversion where we cannot rely on the supposition that irradiation time was not enough. Thus, this arise the question again about the organization and distribution between DTE/UPy and PEB-UPy within each thin film and the key role played by them in inducing photomechanical responsiveness.

VI.2.3. Comprehensive mechanism to explain the microscopic bending behavior

The CF self-assembly of DTE-UPy with PEB-UPy is found to lead to a common expansion response under visible illumination regardless the elaboration method. In order to explain such photomechanical effect, it seems that light has generated interfacial strain between the photoreacted and non-photoreacted layers of the thin film. However, the individual photoreacted DTE-UPy within the surface inducing instantaneous thin film expansion.

Compared to diarylethene derivatives within crystal phase, expansion behavior has already been reported in order to explain the bending behavior through the Timoshenko's bimetal model [3]. The proposed model involves the photoisomerization from OF- into CF-isomers that occurs at first randomly. When the crystal was irradiated with UV light. The occurred photoconversion between the OF- and CF-isomers induces contraction of the photoreacted layer. The required heterogonous photoisomerization continues occurring within the crystal depth leading to the bending of the crystal. Herein, the observed expansion of thin film presents the antagonist demonstration of the proposed mechanism as the sample are initially in their CF isomers.

From the other hand, Kitagawa and coworkers have reported also photoinduced-bending behavior of diarylethene crystals from two different sides [4]. When irradiated with 360 nm from the left side, the rod-like crystal bent toward the incident light. By changing the visible light from the right side, it returns straight through the same bending trajectory. When irradiated with 380 nm from the left side, the crystal bent away from the light source and then toward the incident light upon further irradiation. By changing the visible light from the right side, the crystal bent away from the light source and then became straight. From this viewpoint, by comparing the exhibited motions within the thin film with different elaboration processes, it seems that consecutive irradiations from two different sides maybe one of the key factors in producing unexpected photomechanical effect. As shown in Figure VI-17, the blue thin film can be converted totally with UV light. Moreover, it can also not be converted totally which may exhibit overlapping within the induced photomechanical responses leading to these observed antagonist ascertainments.

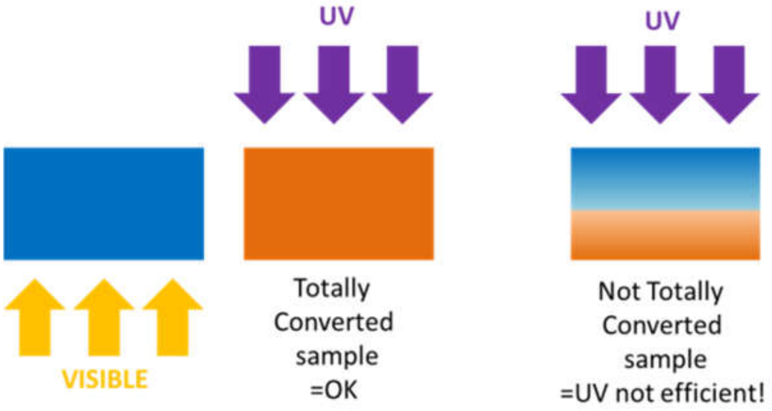

Figure VI-17: Drawback of two different sides of illumination.

However, these antagonist ascertainments can be supported by hydrogen bonding network, the second key factor in producing unexpected photomechanical effect. Contrarily to the crystalline phase of reported diaylethene, the thin film elaboration based on self-assembly through hydrogen bonding concept seems to play synergistic role in helping them spreading within the thin film thickness. Such proposition will be further investigated in the next chapter through morphological and structural organizations.

VI.2.4. Summary on microscopic photo-induced changes

Photoinduced changes of photochromic supramolecular polymer within the microscopic scale were elucidated. It was difficult to irradiate the thin film from one side within the thickness profile as have been already explained in chapter II. However, the exposure to irradiation has induced different changes. The described characteristic upon UV and visible lights are schematically presented in Figure VI-18. Mainly, the MM-NR thin film exhibits the most pronounced photomechanical effect within the microscopic scale.

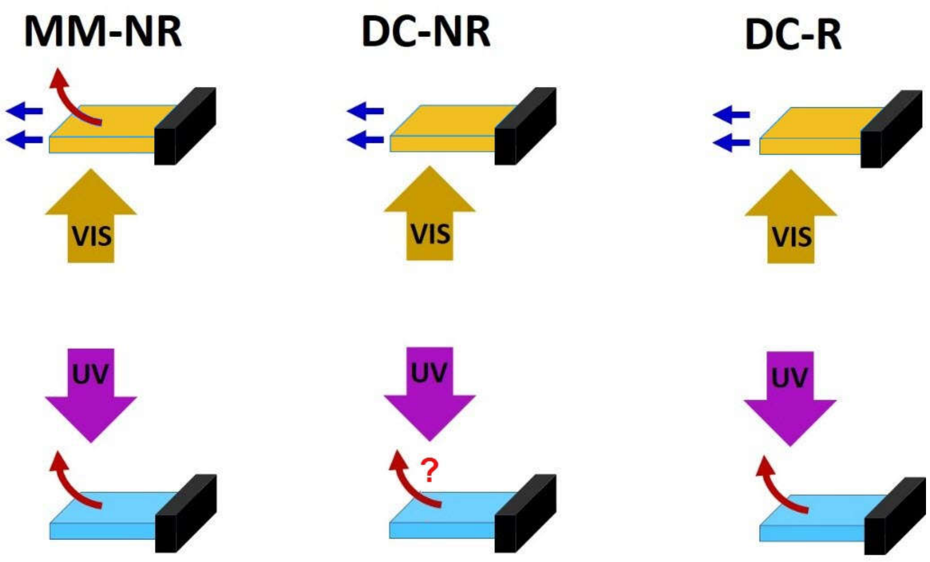

Figure VI-18: Microscopic photo-induced changes within various thin films. Red arrow assigned the bending motion and blue arrow assigned expansion motion.

Upon visible irradiation, the instantaneous expansion along perpendicularly axis of the photoreacted thin film layer occurs regardless the thin film elaboration process. Whereas, the reported bending contrary seems occurring with different rates (related to achieved characteristic time) which presumably depends on the elaboration process.

VI.3. Conclusion

In chapter VI, photomechanical effect of thin film issued from supramolecular assembly of photochromic DTE-UPy and thermoplastic elastomer PEB-UPy upon alternating UV and visible light irradiations has been successfully elucidated in microscopic and macroscopic scales. Different motions described within chapter VI are schematically represented in Figure VI-19.

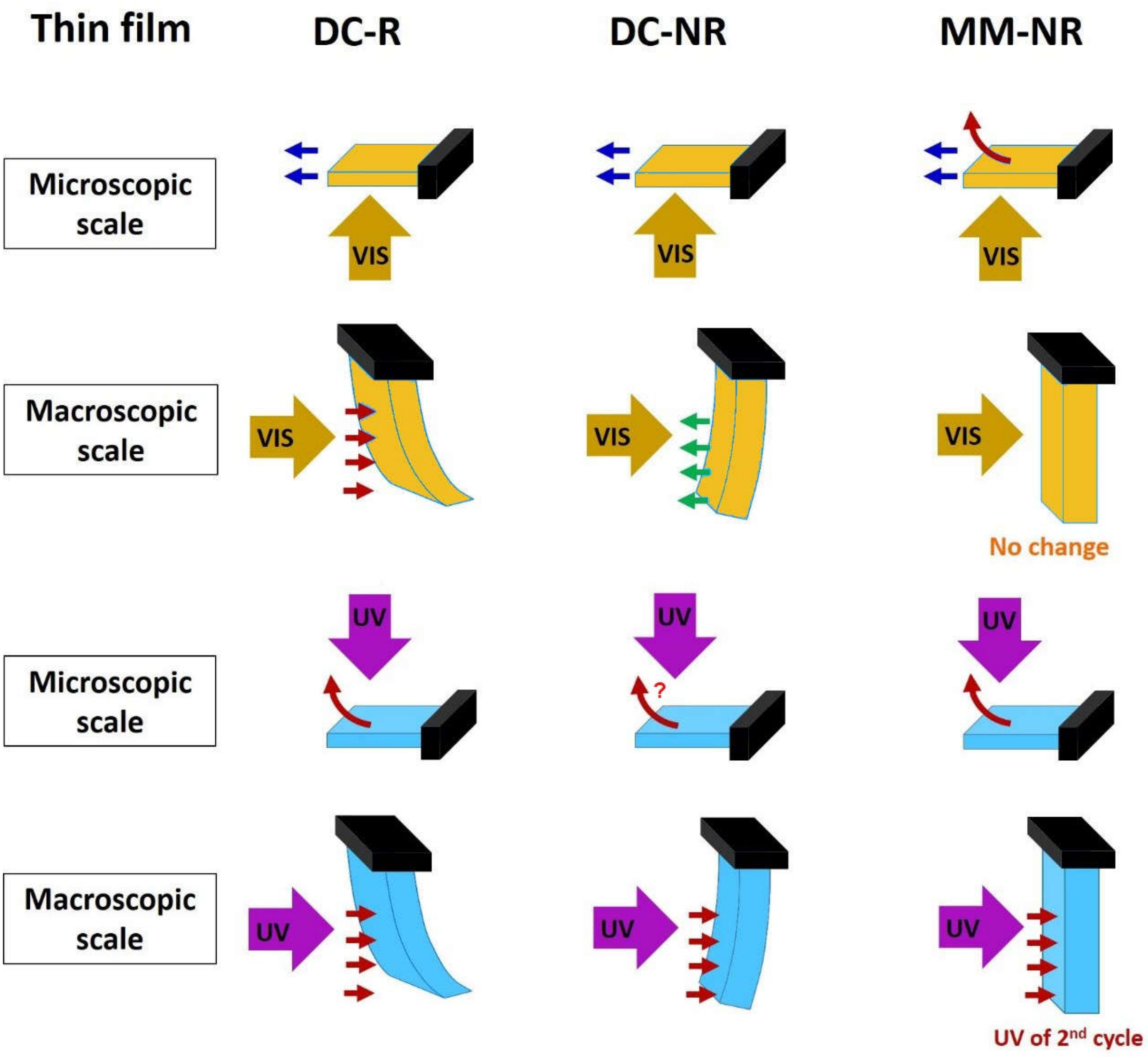

Figure VI-19: Microscopic and macroscopic photo-induced changes within various thin films upon UV/visible irradiations. Red and green arrow assigned the bending motion and blue arrow assigned expansion motion.

The microscopic scale investigation revealed that thin film can exhibit not only one ordinary motion as macroscopic scale investigation but also two different consecutive motions:

1) Fast expansion perpendicularly to incident light that can particularly occur only upon visible light within few seconds (characteristic time).
2) Bending motions toward or away to the incident light for both UV and visible lights within hundreds of seconds. Note that we reported reversible motions for MM-NR sample.

The structural, chemical and geometrical origins of the two motions have to be found.

The second motion i.e. bending behavior relies on well-known photomechanical effect reported for DTEs crystals (see chapter I) and probably related with OF/CF gradient in the sample.

Concerning the first motion i.e. expansion behavior, no hinds in the literature have been reported. Such effects are not reported to the best of our knowledge. Probably, surface effect has to be invoked through AFM experiments, which will be undertaken in the future. In the same vain, making analogies with surface effect of jumping crystals (discussed in chapter III) will bring further insight to explore this new photomechanical effect.

The macroscopic scale investigation has brought important results:

- Observation of photoinduced bending related with photochromic gradient. The fast expansion motion was not observed. (see below).
- Direction of the bending depends on the initial shape of thin film and/or the internal structure of sample.
- Reversibility of the DC-NR thin film photoinduced motions (bending, bending back) were achieved for at least to cycle of alternate UV/visible lights.

These results pave the way toward industrial application. In the future, improving the elaboration protocol, we need to amplify the magnitude and test at least ten cycles to assess the system fatigue.

Concerning the multiscale approach, the macroscopic results are not so straightforward to rely with microscopic ones because only the photoinduced bending was reported for our DC and MM thin films. However, in the case of video presented in the introduction of this thesis, the two mechanical effects were observed and the macro-/micro- analogy matches: (i) instantaneous fattening related with the fast observed expansion, (ii) bending back motion related with microscopic bending (Table VI-1). This last statement arises the question about the intimate structure of thin film and photomechanical effect efficiency. In other word, why we do not observe the two photomechanical effects at macroscopic scale whereas Pr. Takeshita does?

More than ever, the question about differences in self-assembling processes between DTE-UPy and PEB-UPy through structure and morphology has to be elucidated through the understanding of variant behaviors. This is why such statement will be further investigated within the next chapter.

Moreover, as have been reported for CF precipitate (in chapter IV), DC and MM photomechanical films display similar fluorescence (probably AIE effect). As a matter of fact, this light emission does not disturb the photomechanical behavior. In the future, we will try to find a response about the following question: is this emissive process occur in competition with photomechanical effect?

Table VI-2: photoinduced microscopic (MM thin film) and macroscopic (spin coating thin film) upon visible light motions.

	Microscopic scale	**Macroscopic scale**
1st motion	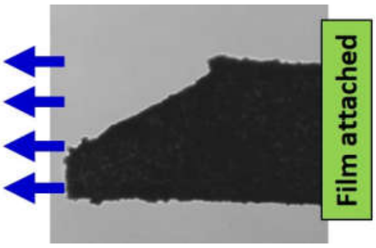 Instantaneous flattening	 Instantaneous flattening
2nd motion	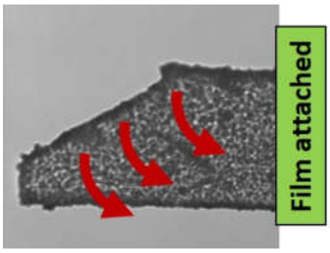 Slow bending back	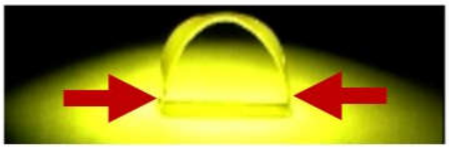 Slow bending back

For this propose quantitative measurements of photomechanical effect and quantum yield in thin films have to be simultaneously measured varying external conditions (excitation wavelength, concentration DTE-UPy, thin film thickness).

References

[1] Hirano, A., et al., Dependence of Photoinduced Bending Behavior of Diarylethene Crystals on Ultraviolet Irradiation Power. Crystal Growth and Design, 2017. 17(9): p. 4819-4825.

[2] Mamiya, J.I., et al., Photomobile Polymer Materials: Photoresponsive Behavior of Cross-Linked Liquid-Crystalline Polymers with Mesomorphic Diarylethenes. Chemistry A European Journal, 2015. 21(8): p. 3174-3177.

[3] Kitagawa, D., et al., Quantitative Evaluation of Photoinduced Bending Speed of Diarylethene Crystals. Crystals, 2015. 5(4): p. 551-561

[4] Kitagawa, D., R. Tanaka, and S. Kobatake, Dependence of photoinduced bending behavior of diarylethene crystals on irradiation wavelength of ultraviolet light. Phys. Chem. Chem. Phys., 2015. 17(41): p. 27300-27305.

.

Chapter VII.

Photomechanical effect: structural and morphological relevant parameters

The thin films characterized in Chapter VI are investigated in order to elucidate the key parameters responsible for the photomechanical behaviors. The mean results were the following:

- **At microscopic scale**, two photomechanical effects were distinguished. First, upon visible light a fast expansion movement is reported to occur perpendicularly to the incident light. Then, the second slower motion is reported for MM thin films: a bending motion toward or away to the incident light for both UV and visible lights.
- **At macroscopic scale,** only one photomechanical effect of bending type was observed with some reversibility (2 UV-VIS cycles at least). The expected reversibility upon Visible and UV successive irradiations were reported for DC-NR displaying bending/bending back motion. In contrast, DC-R thin films display two bending motions in the same direction. To rationalize such differences, the questions about geometrical shape (curvature of sample) and/or structure-morphology was raised. In consequence, the comparisons of DC-NR vs DC-R material science study will be investigated.
- **Elaboration methods of the thin films** (MM vs DC) seem to affect the Photomechanical effects reported. In particular, MM thin film obtained with thermal treatment displays more pronounced photomechanical response at microscopic scale compared to macroscopic scale. While for DC thin film (conventional method), the situation is reversed.

Therefore, this Chapter VII will be organized as following. First, we will undertake classical structural study (DSC, WAXS, SAXS) of DTE-UPy/PEB-UPy DC and MM thin films. Then, surface topography will be investigated through SEM experiments. Finally, relevant parameters for photomechanical effects will be identified by means of (i) WAXS under illumination and (ii) comparison of macro/micro videos of the previous chapter with morphological results.

VII.1. Structure of DTE-UPy/PEB-UPy thin films

The structure of DTE-UPy and PEB-UPy was detailed separetly in Chapter IV and chapter V. In the present section, DTE-UPy/PEB-UPy assembly via UPy-bonds is investigated. The thin films elaborated by drop casting (DC) and melt molding (MM) are studied in order to observe the influence of process on DTE-UPy/PEB-UPy structure.

Besides the three blue films (DTE-UPy in CF) already studied in the previous chapter (DC-NR, DC-R and MM-NR), an additional new film was obtained through drop casting the colorless solution of PEB-UPy/DTE-UPy(OF), noted DC-NR (OF). The purpose of this new film is to get more insight about DTE-UPy/PEB-UPy interactions. Indeed, due to flexibility of the OF and to them self-stabilizing within dimers (for the parallel conformer) or tetramer (antiparallel conformer). It is expected that less DTE-UPy/PEB-UPy hydrogen bonds for DC-NR (OF) compared to DC-NR (CF).

VII.1.1. Thermal behavior

The thermal properties of DTE-UPy/PEB-UPy assembly are investigated through DSC measurements of DC and MM thin films as depicted in Figure VII-1. The thermograms of OF- and CF-assemblies show several endothermic behaviors.

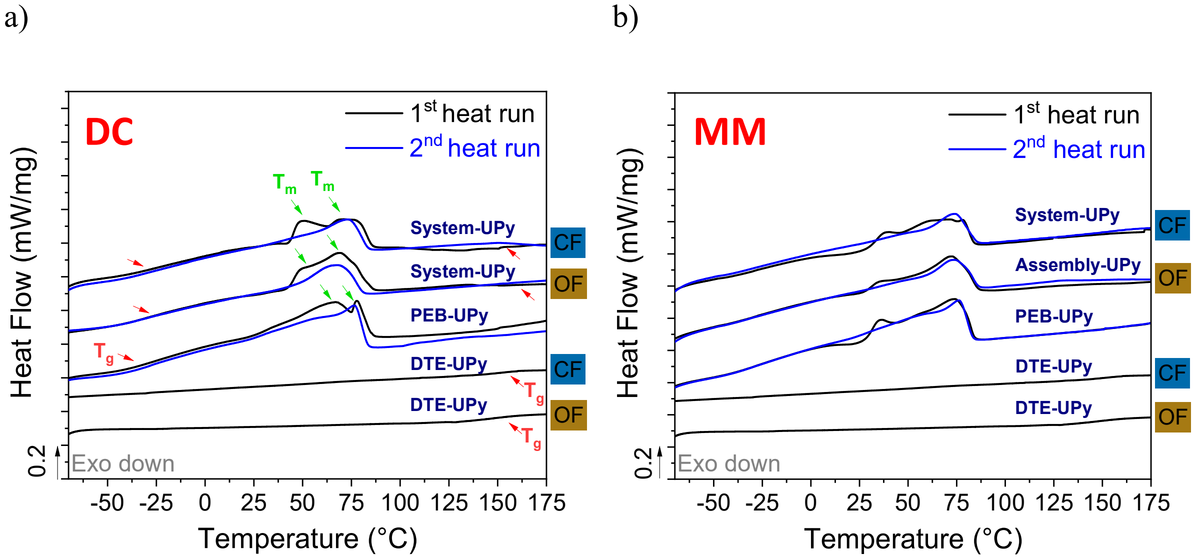

Figure VII-1: Thermograms of DTE-UPy/PEB-UPy systems (noted system-UPy in OF- and CF- assemblies). Thin films are elaborated by a) DC and b) MM. For comparison, thermograms of PEB-UPy and DTE-UPy in OF-pwd and CF-prp are also reported.

The DC thin films undergo a melting according to the endothermic behavior observed with one discernable peak for the OF-assembly and two prominent peaks for the CF-assembly (Figure VII-1a). Note the samples are heated up to 175 °C, i.e. above the glass transition temperature of DTE-UPy. Upon the second heat run, only one endothermic peak was observed for both OF- and CF-assemblies. Values of melt temperatures are reported in Table VII-1. For MM thin films, a larger multi-melting endotherm is observed. Indeed, the OF- and CF-assemblies lead to three overlaid endothermic peaks (Figure VII-1b). Meanwhile, the second heating run of samples cooled from the melt reveals the reappearance of only one large endothermic peak.

Table VII-1: Thermal properties of DC-NR samples and MM-NR samples thermal properties. The heating rate monitored of 10°C/min.

	Sample		T_m (1) (°C±1)	T_m (2) (°C±1)	T_m (3) (°C±1)	ΔH_m (J/g)	χ(%)
DC-NR thin film	OF	Heat 1	49.8	68.7	-	52.2	24.6
		Heat 2	-	66.4	-	37.9	17.5
	CF	Heat 1	50.6	-	74.5	50.2	23.2
		Heat 2	-	-	73.3	43.4	20.1
MM-NR thin film	OF	Heat 1	37.2	60.7	72.3	52.7	24.4
		Heat 2	-	-	73.6	42.9	19.8
	CF	Heat 1	39.4	63.5	77.9	47.5	21.9
		Heat 2	-	-	73.8	41.6	18.9
DC PEB-UPy		Heat 1	-	66.7	77.8	60.4	23.0
		Heat 2	-	-	76.5	57.7	20.0
MM PEB-UPy		Heat 1	36	58.6	73.6	61.8	21.5
		Heat 2	-	-	76.1	58.3	20.2

The thermal behavior of the systems is widely dominated by the behavior of PEB-UPy. However, thermograms are different due to the proceeded thermal treatment. As it has already been explained in Chapter V, DC PEB-UPy and MM PEB-UPy exhibit different melting points. The main difference between the systems concerns the values of the melt temperature. In the case of MM thin film, the values are very closed to those of MM PEB-UPy while in the case of DC thin film the values are lower for the DTE-UPy/PEB-UPy system in comparison to DC PEB-UPy. Such statement may suggest a difference of miscibility between DTE-UPy and PEB-UPy.

Concerning the direct impact of DTE-UPy addition, crystallinity level was calculated according to the described procedure in Chapter II and summarized in Table VII-1. It is interesting to note the presence of DTE-UPy does not disturb the PEB crystallinity. Seemingly, OF samples exhibit slightly higher crystallinity level compared to CF samples within the first heat run. Upon the second heat run, a similar crystallinity level is exhibited by the systems. The decrease of crystallinity between both heating run is associated to the formation of a more defective crystalline phases during the cooling.

The deep investigation of PEB-UPy by DSC analysis shows that besides UPy groups, the urethane groups have the possibility to induce lateral hydrogen bonding interactions. Therefore, urethane groups present a melting point at 69°C, which could be noticeable for the first heat and absent for the second heat (Figure I-17, Chapter I). The adding of amorphous DTE-UPy does not prevent the crystallization of PEB-UPy through urea groups. Such result suggests the absence of nano-fibrillary segregation for the DC-NR thin film.

VII.1.2. Crystal phase analysis

As described in Chapter V, the polyethylene of PEB-UPy can crystallize through two polymorphs, the typical orthorhombic form under usual/conventional conditions and the monoclinic form under stress.

In order to investigate whether the DTE-UPy introduction may influence the crystal form, the crystalline structure of the DTE-UPy/PEB-UPy is examined via WAXS experiment. Diffractogram deconvolution is depicted in Figure VII-2.

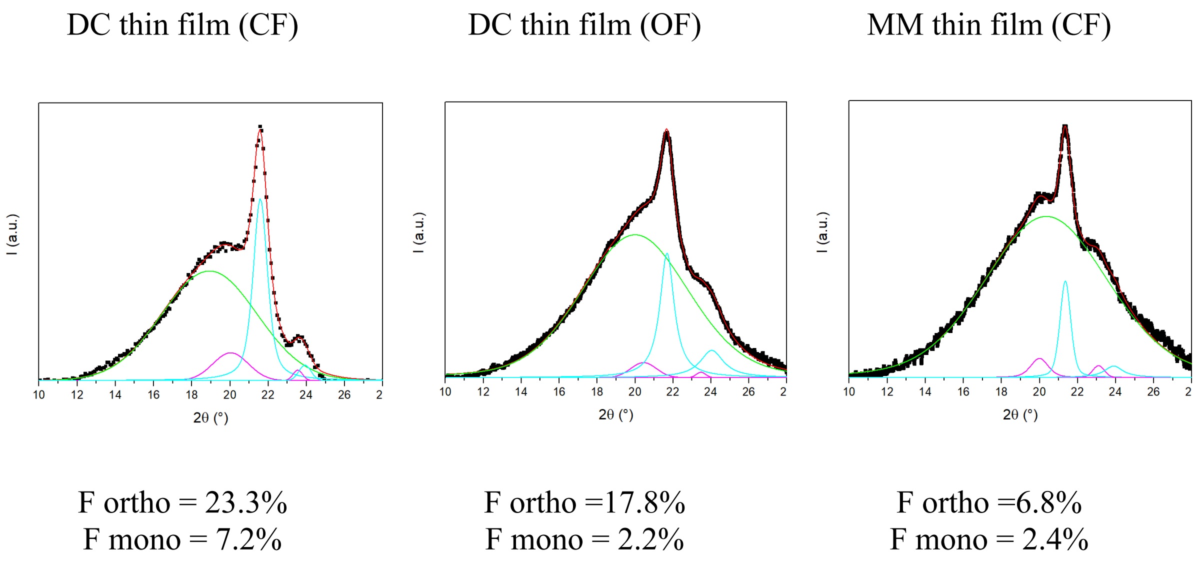

DC thin film (CF)
F ortho = 23.3%
F mono = 7.2%

DC thin film (OF)
F ortho =17.8%
F mono = 2.2%

MM thin film (CF)
F ortho =6.8%
F mono = 2.4%

Figure VII-2: WAXS profiles of the assemblies.

At room temperature, the DC thin films exhibit two main peaks at 2θ= 21.5° and 23.8° corresponding to distances d= 0.413 nm and d=0.372 nm. The WAXS profile of CF-assembly exhibited noticeably the same Bragg angles as DC PEB-UPy. The CF-assembly is mainly orthorhombic while OF-assembly presents a contribution of monoclinic form. The examined MM thin film shows also two main peaks at 2θ= 21.5° and 23.2° corresponding to distances d= 0.413 nm and d=0.384 nm. The monoclinic form is dominant within the hot-pressed sample. Moreover, the adding of amorphous DTE-UPy does not influence the present crystal phases within the PEB-UPy.

As observed for PEB-UPy, the thin film process mainly influences the fraction of orthorhombic and monoclinic forms in the samples.

The crystallinities estimation from WAXS patterns, as a function of the proceeded elaboration method, do not match with the already estimated crystallinity with DSC measurements. More particularly, the MM thin film case leads to low crystallinity level, which is expected to be reinvestigated. These results deserve more investigations.

VII.1.3. Arrangements of DTE-UPy/PEB-UPy self-assemblies

VII.1.3.1.Signature of DTE-UPy

Following our earlier investigation about DTE-UPy aggregations (Chapter IV), the molecular packing of photoresponsive supramolecular assembly between DTE-UPy and PEB-UPy was anticipated (Figure VII-3).

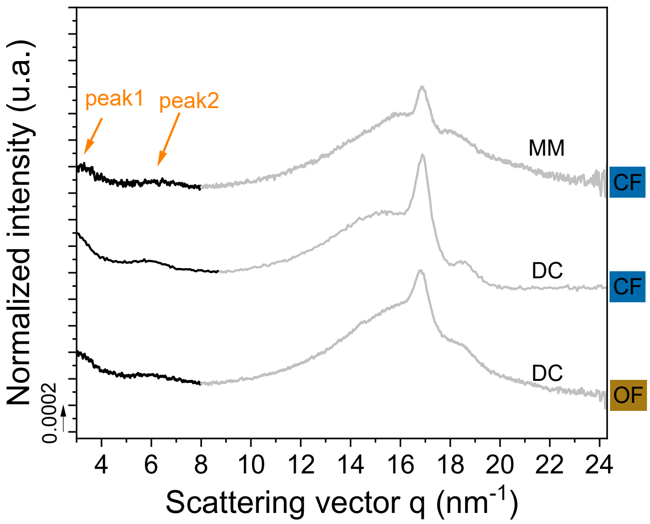

Figure VII-3: Molecular packing of DTE-UPy within the assemblies upon photoinduced OF and CF reactions. Peak-1 and peak-2 found in Chapter IV.

According to the Bragg law ($d = 2\pi/q_{max}$) where q_{max} is the position of the principal feature, two scattering broaden peaks were visualized on the WAXS intensity profile. The first peak (peak-1) was difficult to discern since the maximum is lower than 3 nm^{-1}. The second peak (peak-2) presents a maximum q_{max}. The corresponding average d-spacing are reported in Table VII-2 for the three samples.

Table VII-2: Calculated values of d-spacing from q_{max} and comparison with the values of DTE-UPy.

	q_{max} (nm^{-1})	**d (nm)**
DC (OF)	5.51	1.14
DC (CF)	5.98	1.05
MM (CF)	6.54	0.96
OF-pwd	5.28	1.19
CF-prp	5.56	1.13

The presence of peaks underline the long-range organization in the DTE-UPy/PEB-UPy systems. As previously reported in Chapter IV for DTE-UPy, the distance d = 1 nm (noted d_2 in Chapter IV) is associated to the stack-to-stack distance. The lower values of the distance for the assemblies can be caused by PEB crystals, which induces a strain on UPy-network.

VII.1.3.2.Molecular arrangements of assemblies at room temperature

Further investigation on nanoscale structure was assessed by SAXS analysis at ambient conditions before and after first heat run. The Lorenz-corrected SAXS profiles (Iq^2 vs q) show remarkably broad peaks as illustrated in Figure VII-4. The appropriate scattering q_{max} peaks indicate the presence of characteristic organization for DC and MM thin films. The calculated Bragg spacing $d = 2\pi/q_{max}$ defines the inter-domains distances for thin films which are summarized in Table VII-3 and compared to PEB-UPy d-spacing.

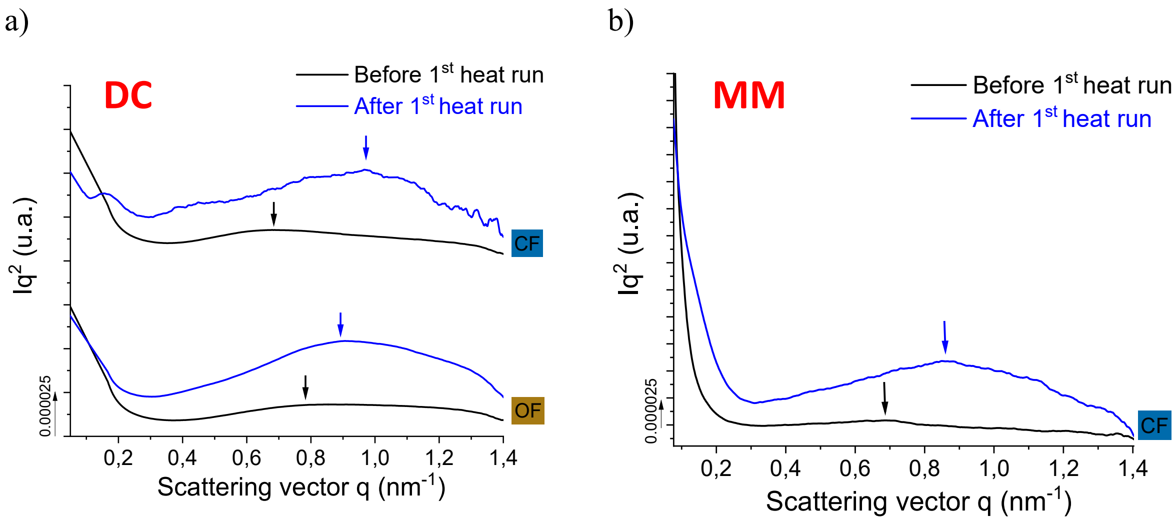

Figure VII-4: SAXS patterns of assemblies in OF and CF for a) DC and b) MM thin films.

At room temperature, the calculated distance seems associated to the long period (L_p) of PEB presented in Chapter V. For both DC and MM thin films, the L_p is lower compared to the values obtained in PEB-UPy.

By comparing these DTE-UPy/PEB-UPy systems to PEB-UPy, the average d-spacing within the thermoplastic elastomer exhibits higher periodicity. Interestingly, the crystallinity decreases through the amorphous nature of DTE-UPy and their heterogeneous self-assemblies with PEB-UPy may likely point out the explanation of differences.

Table VII-3: Interdomains properties of UPy-bonded assemblies and UPy-bonded PEB.

	Appropriate assembly	Isomer	Heat run	q_{max} (nm^{-1})	d (nm)
DC thin film	NR-Assembly	CF	Before heat	0.66	9.52
	NR-Assembly	CF	After heat	0.96	6.54
	NR-Assembly	OF	Before heat	0.78	8.05
	NR-Assembly	OF	After heat	0.92	6.82
	PEB-UPy	-	Before heat	0.58	10.83
	PEB-UPy	-	After heat	0.56	11.22
MM thin film	NR-Assembly	CF	Before heat	0.68	9.24
	NR-Assembly	CF	After heat	0.88	7.14
	PEB-UPy	-	Before heat	0.62	10.13
	PEB-UPy	-	After heat	0.55	11.42

Similar trends were observed after the first heat run. Concurrently, the principal scattering q_{max} shifts to higher values, which means that the occurred d-spacings are lower between interdomains.

VII.1.3.3.Molecular arrangements of UPy-Assemblies upon heating

UPy-end groups have generated interesting features within the photo-induced hydrogen bonded self-assemblies. In order to devote the key role of the UPy hydrogen-bonding group on structural organization between diarylethene and thermoplastic elastomer, the temperature induced changes are investigated to probe unclear phenomena revealed at room temperature. During heating/cooling cycles, the temperature-dependent SAXS patterns were recorded in a temperature range from 30°C to 170°C. The heating rate was about 10°C/min.

VII.1.3.4.1. DC-NR thin films (OF)

As previously reported, the Lorenz-corrected SAXS profile (Iq^2 vs q) shows remarkably broaden peaks at 30°C as illustrated in Figure VII-5a. This broadness suggests multiple contributions within the OF-assembly that are needed to be revealed upon heating.

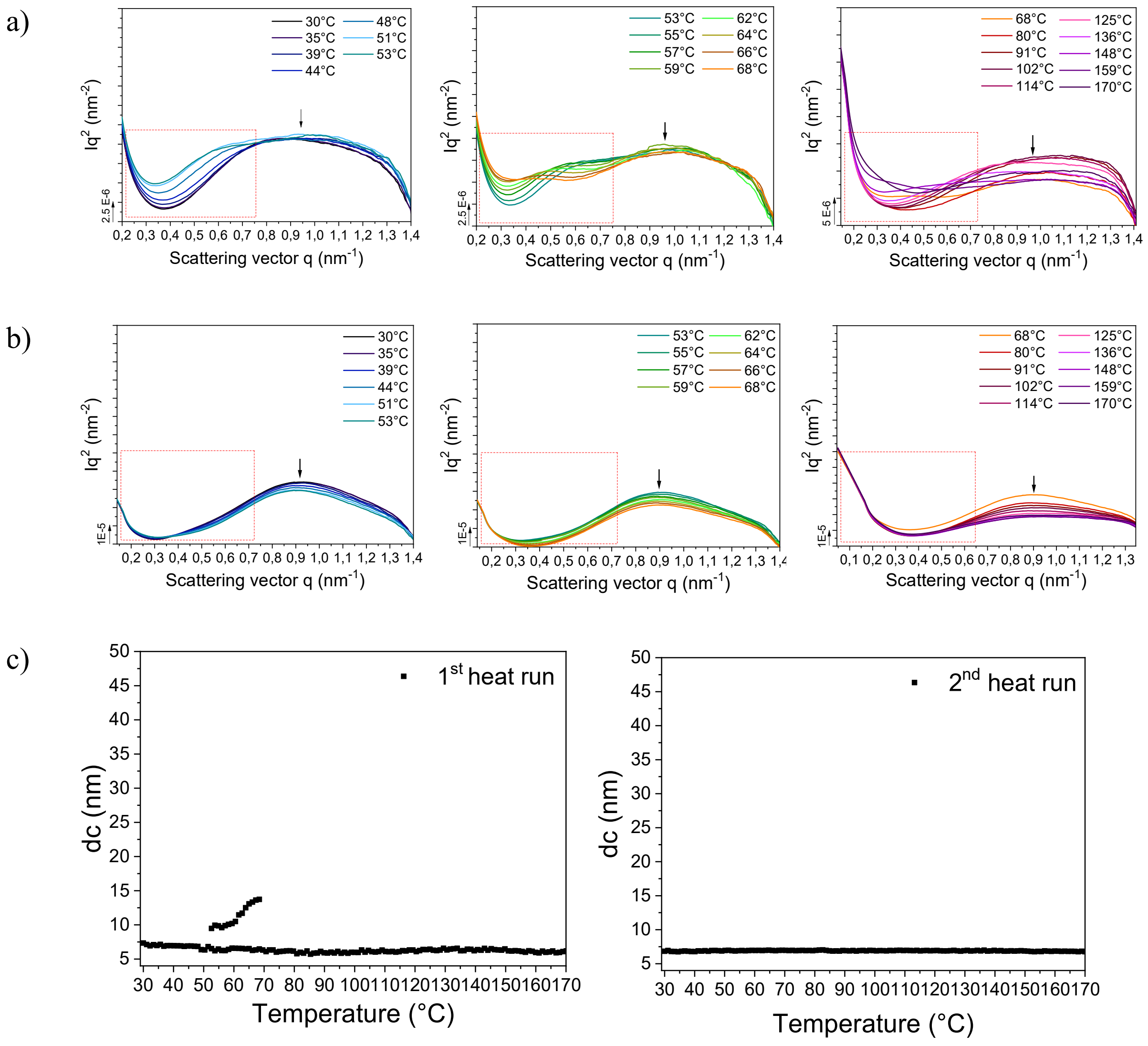

Figure VII-5: SAXS patterns of DC-NR thin film (OF) upon heating. a) First heat run. b) Second heat run. c) Average interdomain spacing within DC-NR thin film (OF) upon a) First heat run. b) Second heat run.

From the first raised temperature, the presence of two apparent contributions are observed. One obvious contribution at low q values, is currently shifted from its first scattering peak position into lower values upon heating (dotted red rectangle). Concurrently, the relative intensity decreases until disappearance from 68°C. The second contribution at high q values seems to be large to define a scattering peak q_{max} position due to the relatively poor structural organization.

However, this position is fixed upon heating that is why an average value was chosen to be follow.

From the observed scattering peak q_{max}, the correlation distance ($dc = 2\pi/q_{max}$) is calculated and reported versus temperature in Figure VII-6c. From 30°C until 50°C, two overlaid signatures dc_1 and dc_2 are underlined. When temperature is ranged from 50°C until 68°C, the interdomain spacing dc_1 increases while dc_2 is constant. From 69°C, only dc_2 is present with a constant value to 170°C.

The behavior of dc_1 is associated to the increase of PEB long period with temperature (as reported in Chapter V) until the crystals melting (T_m = 68.7°C previously measured by DSC). Whereas, dc_2 is constant despite temperature raise up with an average spacing of 6-7 nm. It seems that dc_2 is associated to the presence of hydrogen bonding.

Surprisingly, during the second heating, the contribution at low q is missing as depicted through the dotted red rectangle (Figure VII-5b) and induces the absence of dc_1. The exhibited single scattering maximum is invariant upon heating (Figure VII-5b). The dc_2 corresponding to the average interdomain spacing of 7 nm keeps constant.

It is important to note that PEB blocks are crystallizable owing to L_p spacing regardless the presence or not of DTE-UPy (upon the first heat run). This can be explained by the structural flexibility of OF isomers that will not leads to supramolecular assemblies. Consequently, their existence within the assembly will not only disrupting L_p spacing the but also will apparently reduce crystallinity. Upon the second heating run, it was expected to observe the L_p periodicity but surprisingly its absence suggests the heating highly affected the orderness that prevent crystallizability.

The absence of periodicity related to dc_1 suggests that the cooling influence the formation of PEB crystals and their rearrangement. Indeed, as observed by DSC (Figure VII-1) on the 2nd heating ramp, PEB crystals are present even if the crystallinity degree is reduced (Table VI-2). However, the presence of DTE-UPy prevent a periodic organization with a well define long period because of hydrogen bonding.

The correlation distance dc_2 unchangeable upon heating was also pointed out in the case of PEB-UPy ($d_c \approx 10.2$ nm). The distance differences between UPy-domains seems associated to the presence of DTE-UPy that are aggregated into PEB-UPy. The exact reason for this observed phenomenon is still unclear. One tentative explanation may be attributed to the developed strain by low aggregated DTE-UPy. Such features need to be investigated further later when the photogenerated CF-isomer within DTE-UPy is involved.

VII.1.3.4.2. DC-NR thin film (CF)

The photogenerated non reflexed CF-assembly shows a principal scattering q_{max} that exhibits higher order at 30°C (Figure VII-7).

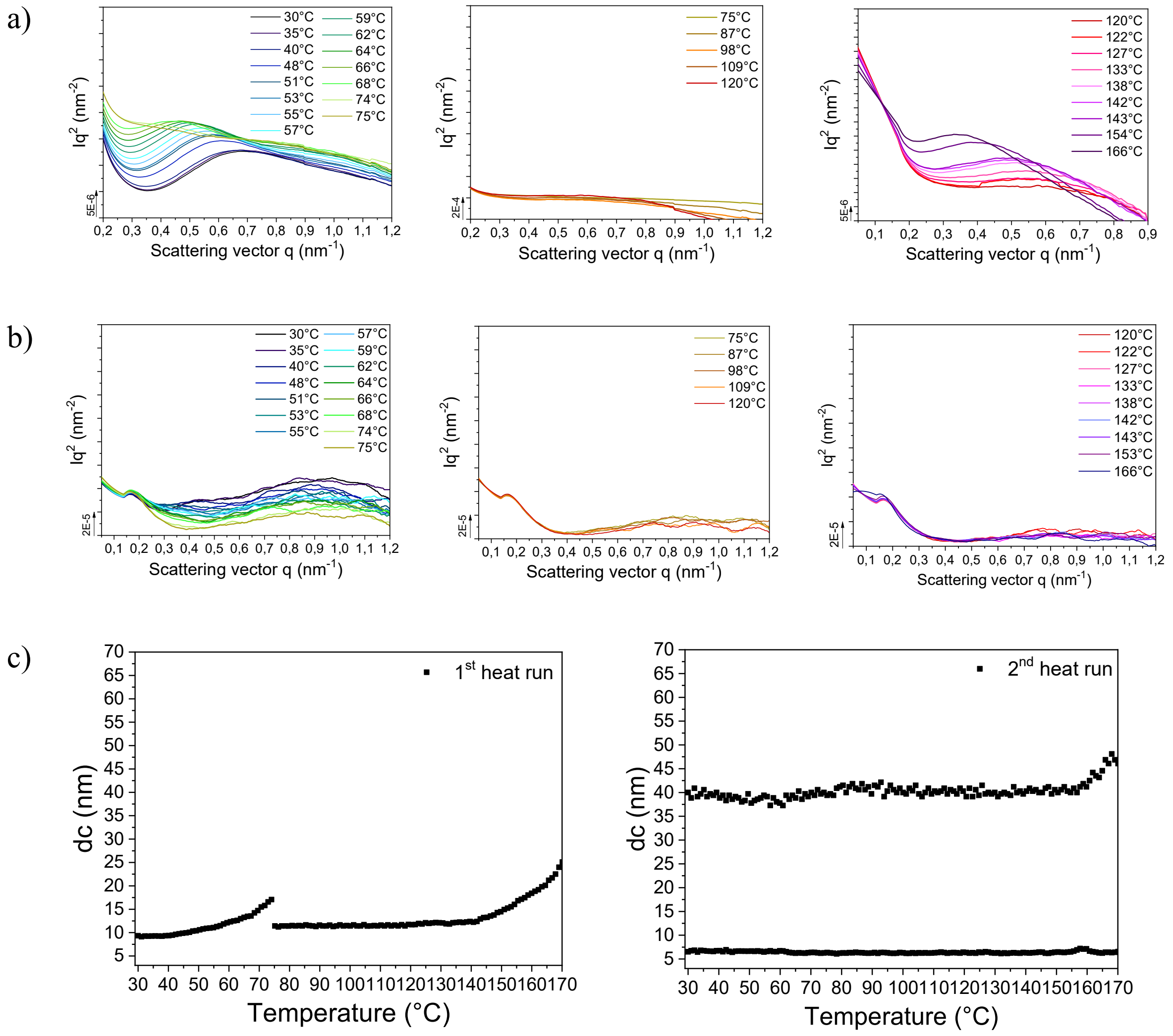

Figure VII-7: SAXS intensity profile of DC-NR thin film (CF) upon heating. a) First heat run. b) Second heat run. c) Average interdomain spacings within DC-NR thin film (CF) upon a) First heat run. b) Second heat run.

The temperature arise induced the peak shift to lower scattering values. The disappearance of the followed peak in remarkably as noticed from approximately 70°C to 125°C. Whereas, a less broaden peak with better-defined positions rise up above 125°C. The calculated correlation distances are consistent with the described observations and revealed three behaviors ranges.

The phenomenon is assessed upon the second heat run of the sample. Surprisingly, two contributions within the SAXS pattern are obtained at 30°C. Moreover, from the mentioned temperature to the end of experiment, the position of the principal scattering q_{max} peaks are noticeably unchangeable as depicted in Figure VII-7b. The positions of maxima are used to calculate spacing between the existent domains (Figure VII-7c).

As previously observed, dc_1 associated to the PEB long period increases with temperature until the melt of crystals (Tm = 74.5°C measured by DSC). The dc_2 associated to the presence of hydrogen bonding is constant with an average spacing of 9 nm. However, dc_2 increases from 140-145°C and corresponds to the glass transition temperature of DTE-UPy.

During the 2nd heating, dc_1 is not visible while two different d-spacing corresponding to two average interdomain distances of 7 nm (dc_2) and 40 nm (called dc_3) are observed on the full temperature range. Once PEB blocks melt, the absence of dc_1 may be attributed to the possible high mobility between UPy-end groups within the specimen that depresses the interdomain rearrangements. As previously described, dc_2 is associated to the presence of hydrogen bonding while dc_3 has the same behavior than dc_2 but with higher value. dc_3 can be attributed to long ranged hydrogen bonds.

VII.1.3.4.3. DC-R thin film (CF)

The CF-cast structure when reflexed displays a single scattering maximum associated to the existance of nano-scaled arrangement at 30°C (Figure VII-8a). Further progession in temperature induces slowly shifts from its first scattering peak q_{max} position into lower values until a full disappearance above 158°C. The Bragg spacing d_c determination confirmed the observed shifts as illustrated in Figure VII-8a.

From the other hand, the undercooled specimen show two principal scattering peaks maxima at 30°C (Figure VII-8b). The evolution of the SAXS profile upon the second heat run reveals that both signals positions seem unchangeable regardless the proceeded temperature. Moreover, the calculated average interdomain spacing is seemingly indicating two well-defined periodicities of $dc_2 = 7$ nm and $dc_3 = 30$ nm, respectively.

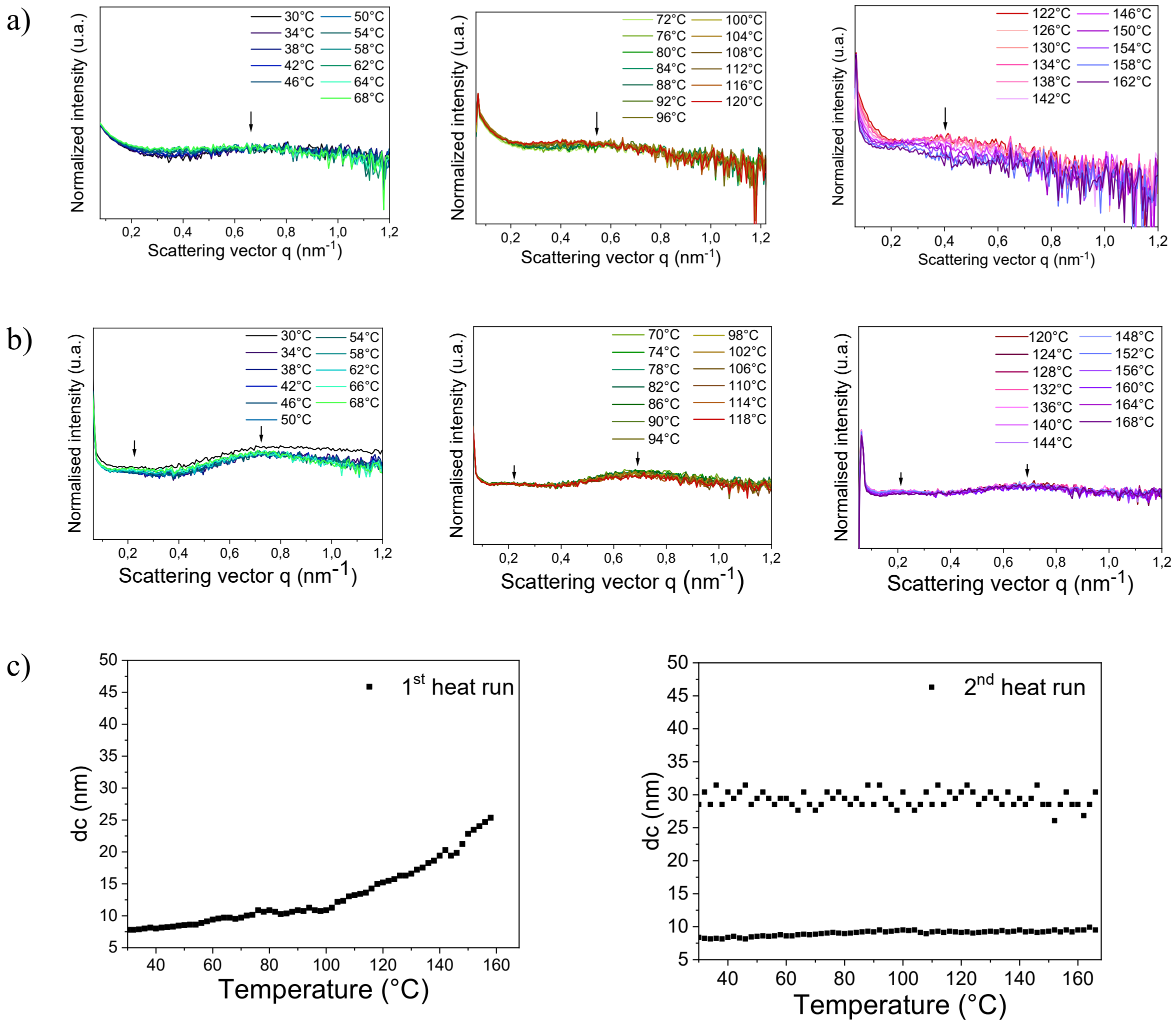

Figure VII-8: Average interdomain spacing within DC-R thin film (CF) upon: a) First heat run. b) Second heat run. c) Average interdomain spacings within DC-R thin film (CF) upon a) First heat run. b) Second heat run.

Taken together, DC-R thin film (CF) demonstrates the absence of the periodic stacking L_p between crystalline and amorphous domains, characteristic of PEB melting signature upon the first and the second heat run. Thus, this observation allows reliable estimation about different aggregation rearrangements within the reflexed supramolecular assembly that suppresses the PEB lamellas organization. From one hand, nano-scaled segregation phase raises progressively due to possible UPy-rearrangements upon the first heat run preparing for phase segregation. From the other hand, the noticed tendencies at dc_2 = 7 nm (observed already within the OF-assemblies) and dc_3 = 30 nm are seemingly associated to different sizes of nano-domains spacing upon the second heat run.

VII.1.3.4.4. MM-NR thin films (CF)

The analysis of SAXS pattern have revealed a broaden principal scattering peak indicating the formation of an equidistanced ordering of about 9 nm at 30°C (Figure VII-9). It is important to note that due to temperature raise up, the position of the scattering peak was seemingly increased until 66°C and then slighlty decressed up to 82°C. Upon further heating, no decernible scattering peak was observed. While a broaden peak is detected attributed to a principal scattering peak beginning from 153°C.

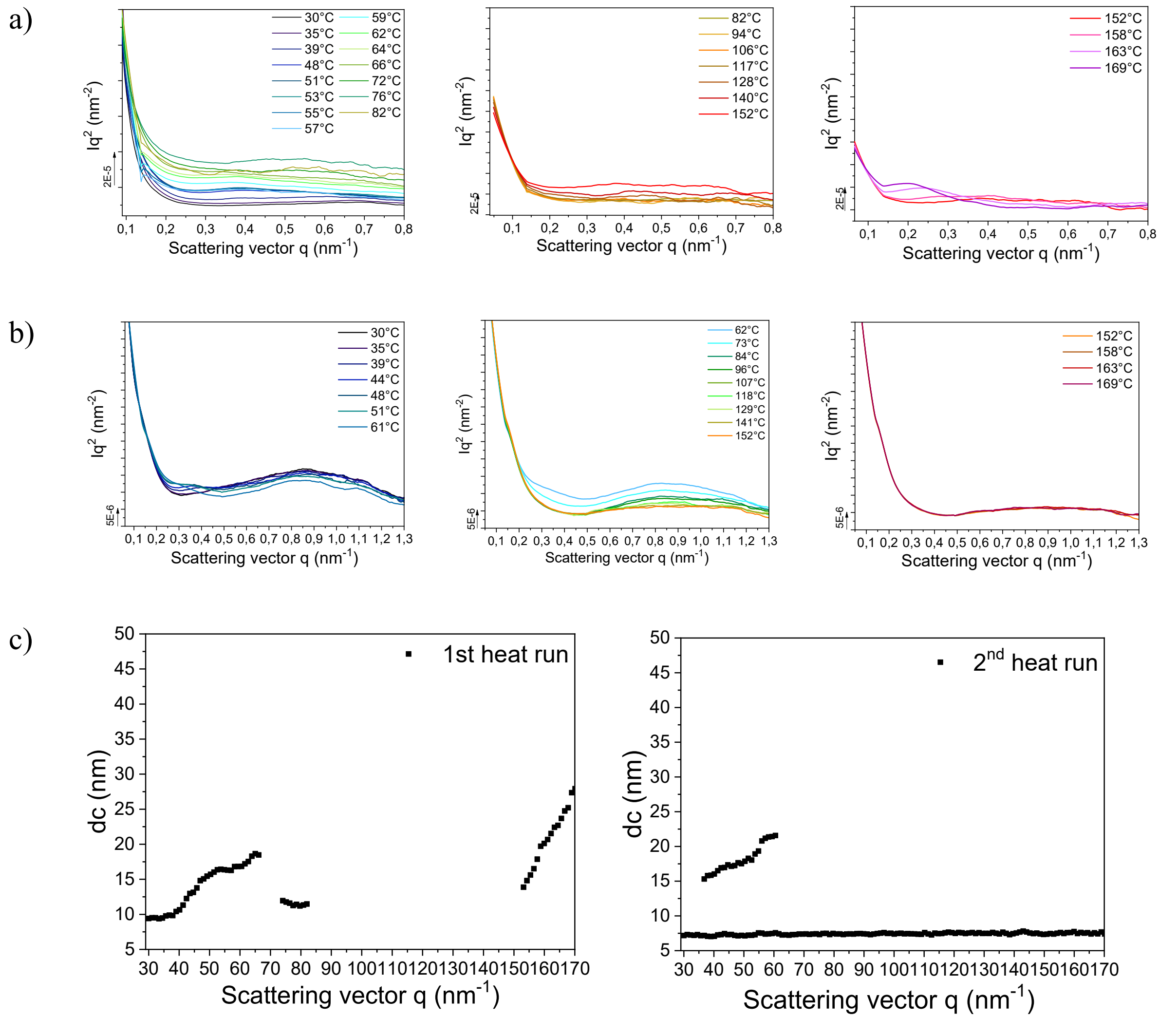

Figure VII-9: Average interdomain spacing within MM-NR thin film (CF) upon a) First heat run. b) Second heat run. c) Average interdomain spacing within MM-NR thin film (CF) upon a) First heat run. b) Second heat run.

On the basis of these q$_{max}$ positions, the average spacing was calculated by means of Bragg law. As depicted in Figure VII-9, the observed average spacing evolution up to approximatly 70°C is associated to L$_p$ of PEB. It seems that this signature overlaid a second signature from below appearing once the PEB crystals melt up to 82°C. Since no scattering peak was observed upon further heating of specimen, the d_c absence is ranged from 82°C until 152°C. Furthermore, the reappearence of the d_c is noticed at 153°C. Meanwhile, an increase within interdomains distance is observed till the end of experiment.

However, the described tendency seems suggesting the existence of proof about supramolecular assembly as the studied SAXS temperature-dependency of PEB-UPy exhibits different behavior. The presence of L_p seems indicating that, even with the melt molded sample, the crystallization driving force is stronger than UPy signals. However, the melting of PEB crystals revealed the hidden d_c. Whilst, the reasons explaining the absence of such signal beginning from 84°C are still unclear. Surprisingly, the reappearance of d_c above the glass transition of DTE-UPy seems indicating information about the beared mobility through DTE-UPy which may lead to increase probability about phase segragation.

After undercooling the MM-NR (CF) thin film, the SAXS pattern of the sample showed broaden scattering peak (q= 0.87 nm^{-1}) at 30°C (Figure 9b). Upon subsequent heating, a shoulder seems to appear beginning from 36°C up to 60°C. The determination of spacing between domains indicates an increase within this mentioned range associated into L_p staking between crystalline and amorphous phases. Once the re-melting of PEB crystals is achieved, the large scattering peak is maintained invariant during temperature raise up. In other word, the correlation distance between UPy-domains is apparently constant at about 7 nm.

After the first heat run and mainly when the d_c increased above T_g, it was expected to observe a phase separation upon the subsequent heat run. Surprisingly, instead of finding two UPy-signatures, only a single UPy-signature is found. Such result is not consistent with the earlier observations with the DC-NR (CF) thin film. Such disagreement lay on the question of MM effect and particularly the effectiveness of rearrangements within the sample.

VII.1.3.4.5. Structure discussion

In order to summarize the behavior previously described, the SAXS results are reported in Table VII-4.

Table VII-4: Evolution of the correlation distance with temperature for the different thin films.

	1^{st} heating	**2^{nd} heating**
DC-NR thin film (OF)	$dc_1 = Lp$ ↑ dc_2 = 6-7 nm cst	dc_2 = 6-7 nm cst
DC-NR thin film (CF)	$dc_1 = Lp$ ↑ dc_2 = 9 nm cst and ↑ (Tg)	dc_2 = 7 nm cst dc_3 = 40 nm cst
DC-R thin film (CF)	dc_2 = 9 nm cst and ↑ (Tg)	dc_2 = 7 nm cst dc_3 = 30 nm cst
MM-NR thin film (CF)	$dc_1 = Lp$ ↑ dc_2 = 7 nm cst and ↑ (Tg)	$dc_1 = Lp$ ↑ dc_2 = 7 nm cst

The long period (L_p) associated to dc_1 corresponds to the regular repartition of stacking between amorphous and crystalline fractions in PEB. The L_p increases with the temperature until the melt of PE crystals. This distance is not observed for the DC thin film made by refluxing the photogenerated CF-assembly for one hour at 55°C. The precipitation of CF-isomers is prevented and PEB Lp is disturbed.

For all the thin films, the correlation distance $dc_2 \approx 7\text{-}9$ nm exists and is observed during the 1st and the 2nd heating. This characteristic distance can be associated to the distance between UPy-domains and is lower compared to the distance dc = 10.2 nm in PEB-UPy. This is possibly due to the characteristic correlation distance in DTE-UPy. The dc_2 is influenced by the glass transition of DTE-UPy when DTE is in its CF isomer and then forms a supramolecular assembly.

The cooling from a temperature set higher than Tg of DTE-UPy induces a rearrangement of the assembly and then the appearance of a long-range hydrogen bonding (dc_3) for DC thin films or the PEB long period ($Lp = dc_1$) for MM thin films.

Based on the elaboration process and taking into account the different correlation distances and the behavior after heating previously reported, it seems PEB-UPy and DTE-UPy self-assemblies could be segregated into (nano)domains whithin the thin films.

VII.2. Surface topography of thin film supramolecular polymers

The structural analysis arises our interest to investigate the thin film morphology at microscale. From the experiments about photo-induced morphological changes in Chapter VI, it was observed that the surface texture of the thin films is different under wild-field microscopy with in-situ irradiation.

The photoinduced behaviors of thin films based on supramolecular polymers seem crucially dependent on the photoactive layer morphology. It is important to obtain information on assemblies under various conditions. For instance, Scanning Electron Microscopy (SEM) is a well-established materials characterization tool providing topographical features in assessing material performance.

Thereby deposing thin films on carbon substrate, the SEM topographic examination was carried out directly on sample after being coated with a transparent thin layer of carbon in order to improve its imaging. Taking into account this created conductive layer of carbon on samples, such carbon coating is expected to reduce thermal damage and is expected to improve the secondary electron signal required for SEM photographs.

VII.2.1. Process effect on self-assemblies

VII.2.1.1.First insights about surface morphology

The surface of PEB-UPy thin films observed by SEM are compared to the surface of DTE-UPy/PEB-UPy assembled thin films using different elaboration procedures (Figure VII-10).

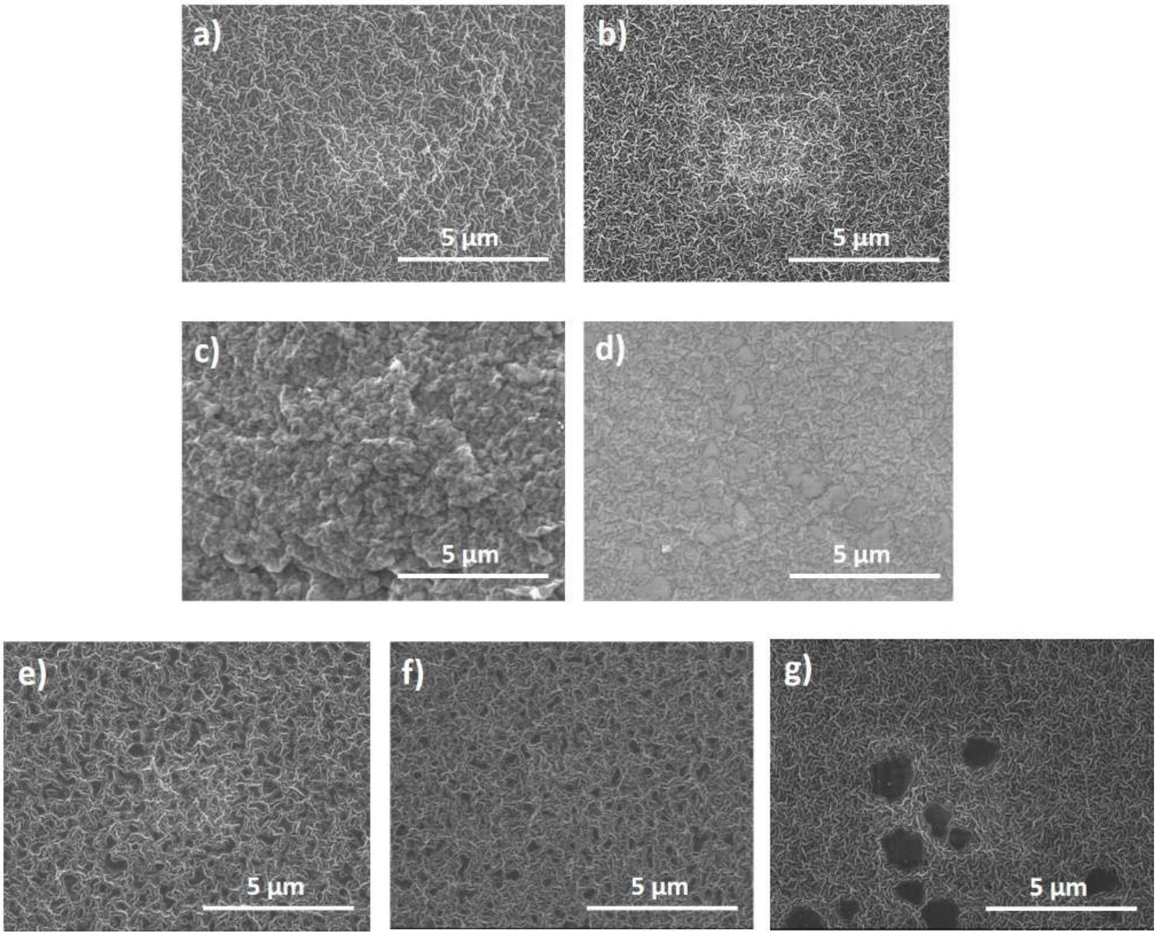

Figure VII-10: SEM surfaces of a) DC and b) MM thin film of PEB-UPy, c) DC-NR thin film (OF), d) MM-NR thin film (OF), e) DC-NR thin film (CF), f) DC-R thin film (CF) and g) MM-NR thin film (CF).

As depicted in Figure VII-10a and Figure VII-10b, the surface of PEB-UPy clearly shows homogeneous texture despite the thin film process (DC or MM). After the incorporation of DTE-UPy photoactive molecules, the surface appears inhomogeneous, many domains with different sizes are underlined. From one hand, MM-NR thin films exhibit random distribution of domains with average diameter of 1.7 ±0.4 µm as shown in Figure VII-10d (OF-assembly) and Figure VII-10g (CF-assembly). From the other hand, the domain size is smaller in the case of DC thin films. However, regularly distributions with average diameter size about 0.5 ± 0.1 µm for DC-NR (Figure VII-10c and Figure VII-10e) and 0.4 ±0.1 µm for DC-R (Figure VII-10f) respectively are underlined. The difference of domains size deliver insight on the thin film elaboration dependence.

VII.2.1.2.Surface analysis

In order to identify the domains and to assess the effect of the process, the chemical analysis of the surfaces is possible by an energy dispersive X-ray spectrometer (EDX) coupled with SEM images. Therefore SEM-EDX mapping follows distribution of chemical element throughout the sample surface. Thus, great care is taken into account when selecting the elemental content owing likely differences of assemblies.

In DTE-UPy/PEB-UPy self-assemblies, the photo-reactive DTE possesses characteristic elements which are not present in PEB such as Sulfur (S) on the thiophene ring and Fluorine (F) on cyclopentane ring.

Experimentally, every thin film is composed of the same elements: Carbon (C), Oxygen (O), Nitrogen (N), Fluorine (F) and Sulfur (S). A supplementary attention was directed toward other specific elements such as Silicon (Si), Chlorine (Cl), Sodium (Na) and Potassium (K) in order to presume whenever environment or synthesis residues may influence the expected self-assemblies and the materials performance.

VII.2.1.2.1. MM-NR thin film (OF) surface topography

SEM images of MM thin film has revealed domains on the surface. Figure VII-11a shows the chemical mapping of OF-MM thin film surface. Uniform element distribution of Si, Na, K and Cl on the surface has been underlined indicating no contamination effect. Whereas, domains with higher-density of O, S and F-elements appears randomly distributed. By following the S-element, it seems that some S-rich areas match with the observed well-defined domains. Whilst the others undefined S-rich areas are qualitatively dispersed within the examined surface.

In Figure VII-11b, the quantitative EDX analysis illustrates the characteristic spectra of abundant elements on four different areas. Taking into account S-element signals, quantitative measurements show different distributions: 7.9 at% (spectrum 1), 4 at% (spectrum 2), 10.7 at% (spectrum 3) and 4.5 at% of S (spectrum 4). Areas related to spectrum 1 and spectrum 3 exhibits denser domains of DTE-UPy. Whereas the darkest zones associated to spectrum 2 and spectrum 4 give insight about the presence of both DTE-UPy and PEB-UPy.

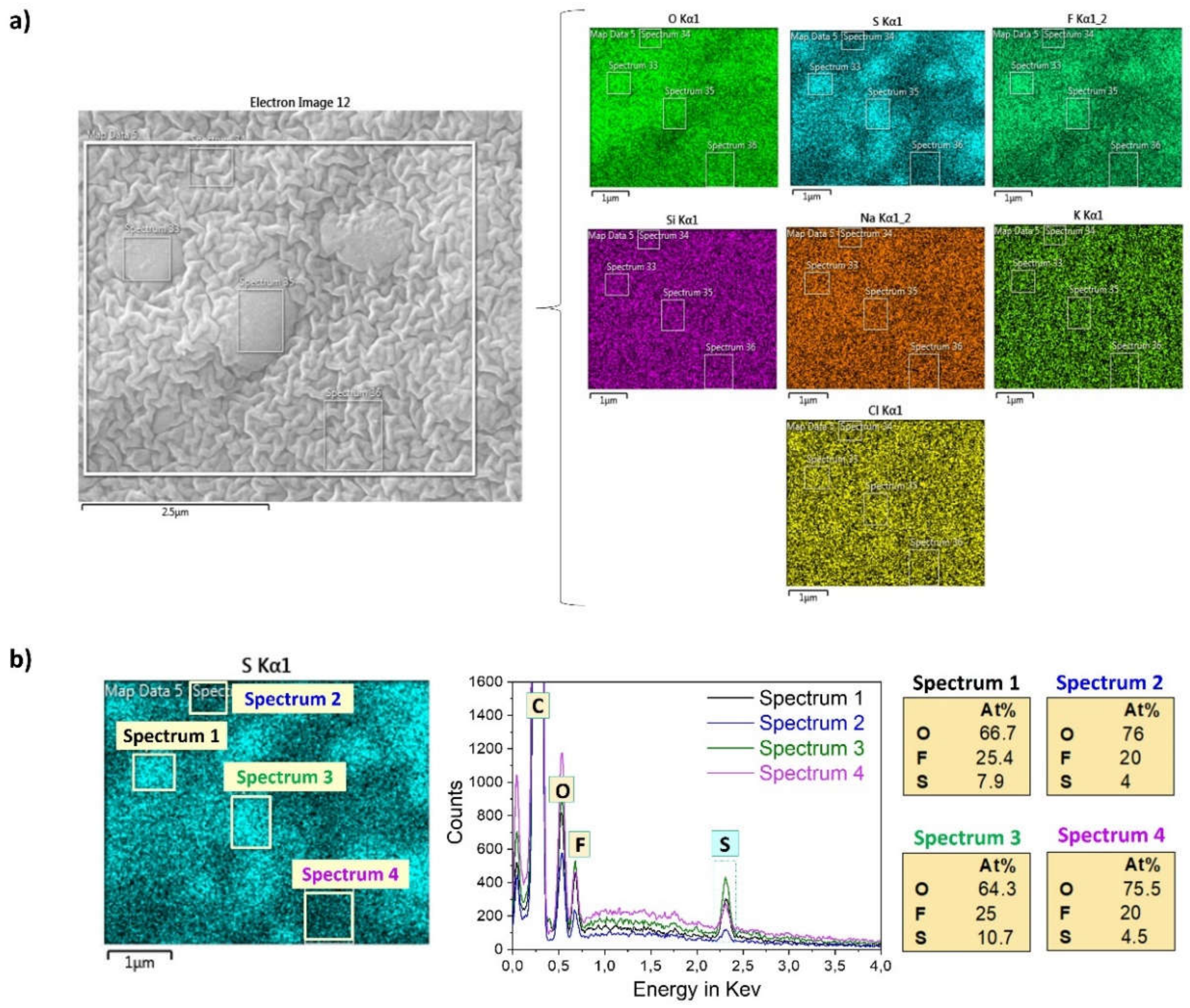

Figure VII-11: Visualization of chemical elements in the MM-NR thin film (OF). a) Micrographs presented along with the SEM–EDX signal mapping for O, N, S, F, Si, Cl, Na and K. Scale bars are 1µm. b) EDX spectra taken within different area.

VII.2.1.2.2. MM-NR thin film (CF)

The chemical analysis of the MM thin film surface with CF-assembly is reported in Figure VII-12a. The map of N, O, F and S-elements exhibit circular domains with higher density. Concurrently, uniform distributions of Si, Cl, Na and K elements is underlined. S-element considered as the main signature of DTE-UPy molecules is highly present in the observed domains. Outside these S-rich domains, uniform dark zones are observed all over the sample. EDX spectra demonstrates a detectable increase of S intensity within domains (spectrum 5, spectrum 6) for thin films with CF-assembly by comparison to MM thin film with OF-assembly as illustrated in Figure VII-12b. Whereas, a lack of S-element (spectrum 7) displays the abundance of PEB-UPy outside the observed domains. Therefore, DTE-UPy (CF) are more agglomerated and embedded within a PEB-UPy matrix.

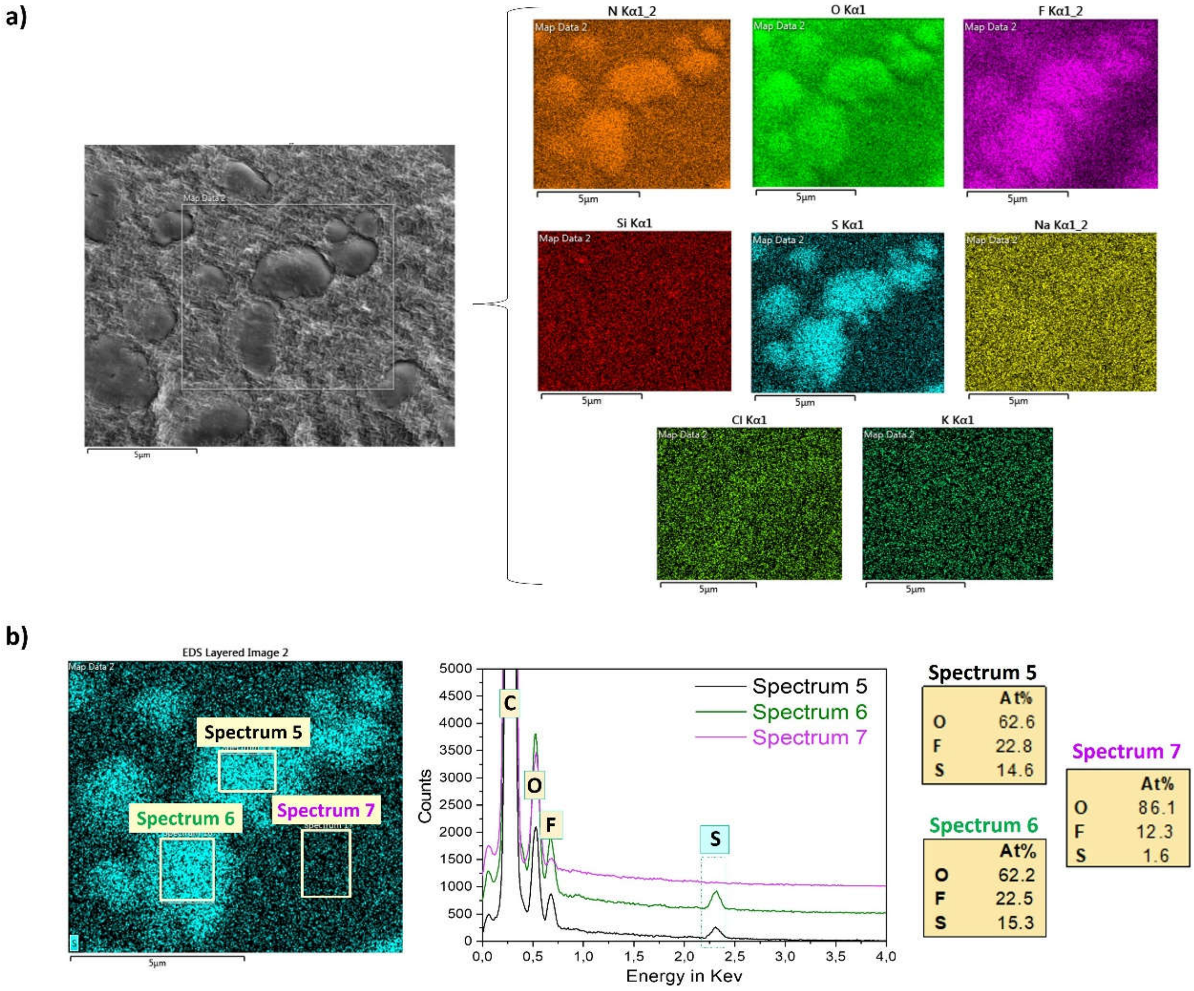

Figure VII-12: Visualization of chemical elements in the MM-NR thin film (CF). a) Micrographs resented along with the SEM–EDX signal mapping for O, N, S, F, Si, Cl, Na and K. Scale bars are 1µm. b) EDX spectra taken within different area.

VII.2.1.2.3. DC-NR thin film (OF) surface topography

The investigation of DC-NR thin film with OF-assembly is reported in Figure VII-13a. In DC thin film, the non-flatness of surface is induced by the solvent evaporation. Despite this, the chemical mapping of surface morphology seems indicating the absence of trends and consequently, the homogeneous repartition within the thin film surface. For this propose, the element distribution was probed in order to confirm this statement.

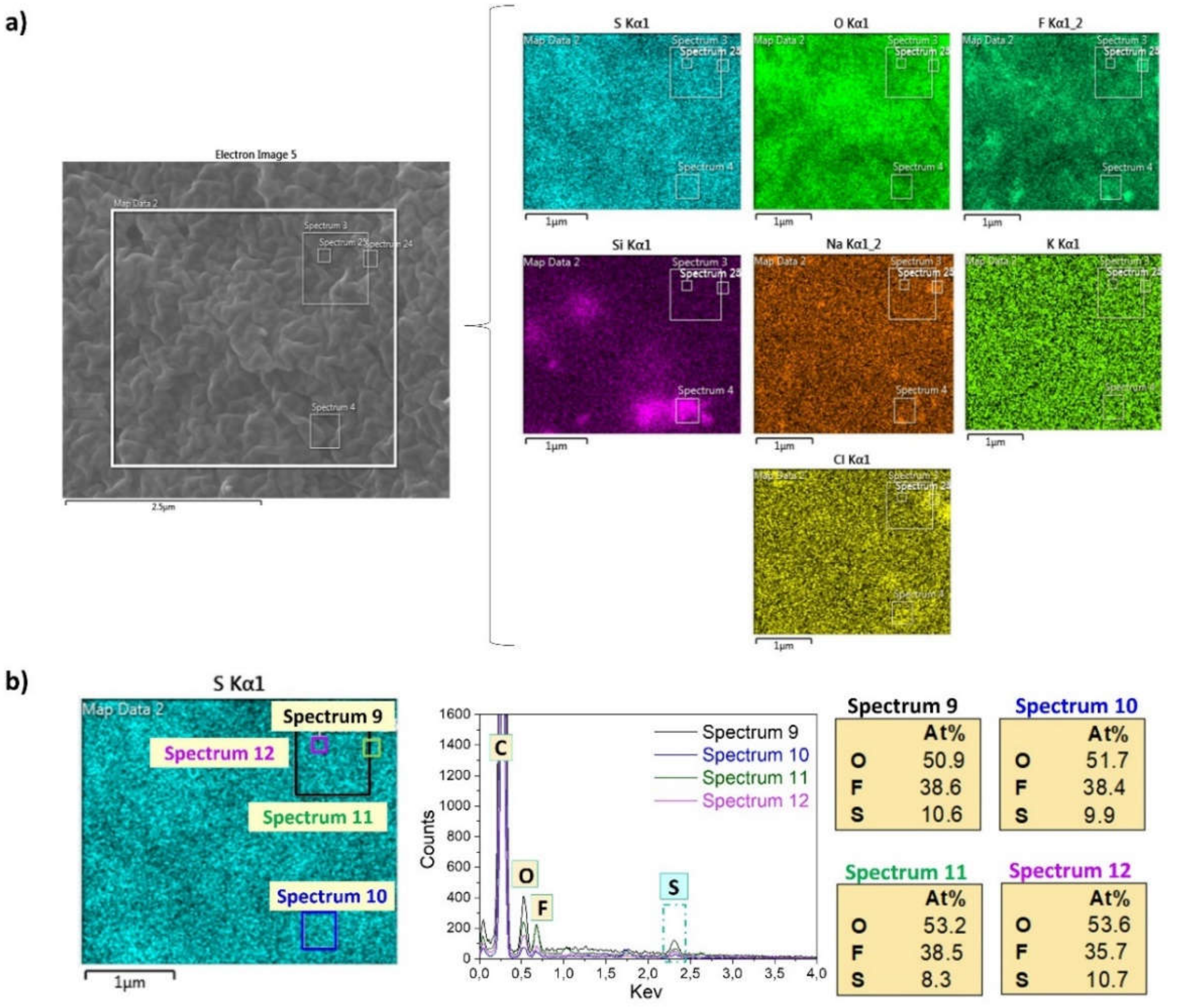

Figure VII-13: Visualization of chemical elements in the DC-NR thin film (OF). a) Micrographs resented along with the SEM–EDX signal mapping for O, N, S, F, Si, Cl, Na and K. Scale bars are 1µm. b) EDX spectra taken within different area.

The S, F and O-elements images indicate heterogeneous distributions with inequitable repartition areas. Note the heterogeneous distribution of Si, Na and Cl which could be due to a contamination of the sample during the casting on PTFE plates at room temperature.

In addition, EDX image of the S-element is illustrated in Figure VII-13b with four quantification regions denoted spectrum 9 to 12. From these spectra, it appears that the lowest fraction of S-element is about 8.3 at% and the highest one is about 10.7 at%. Regions with different fraction of DTE-UPy exists but without defined borders.

VII.2.1.2.4. DC-NR thin film (CF)

Figure VII-14a depicts the surface of DC-NR thin film (CF) where many domains are observed. The domain size seems to be smaller and described as embossed from the surface. The SEM images clearly show a homogeneous surface.

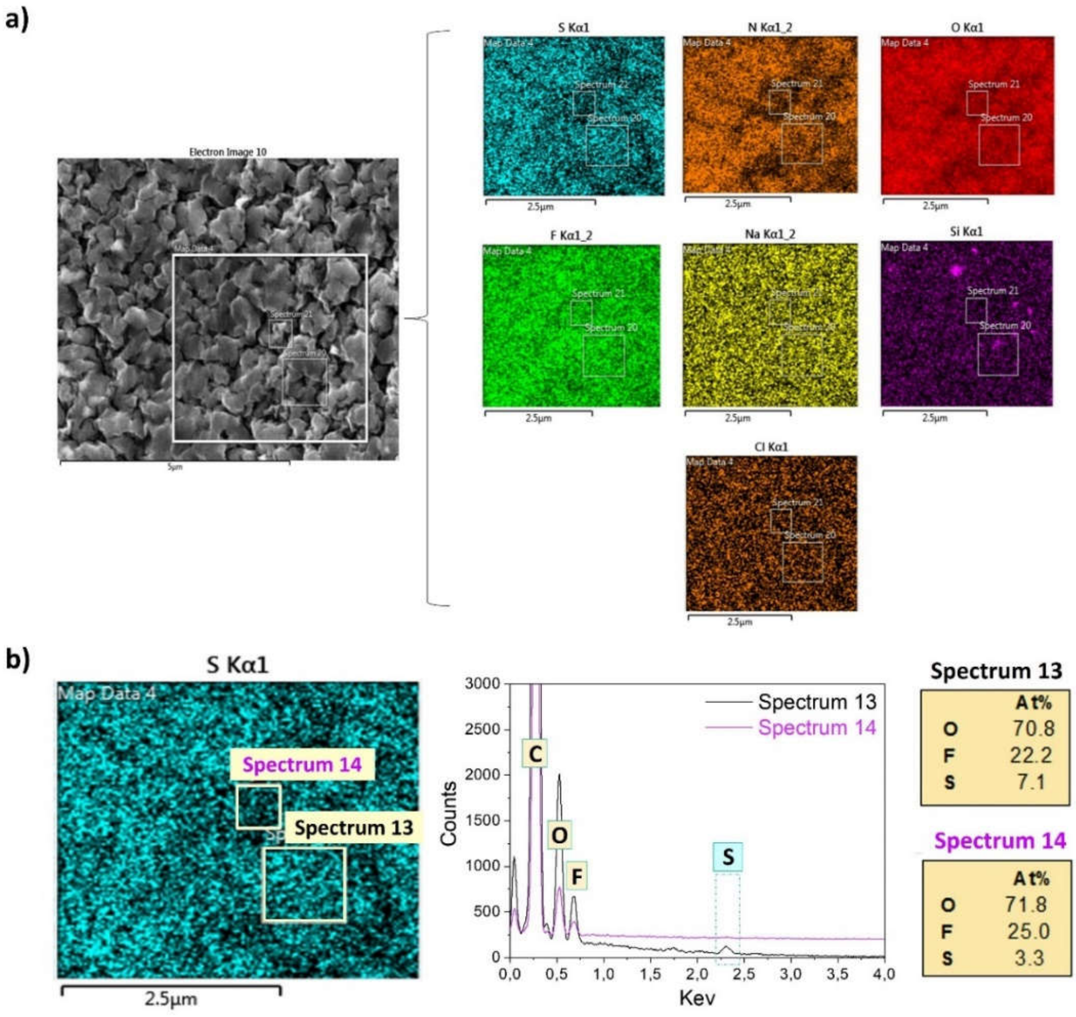

Figure VII-14: Visualization of chemical elements in the DC-NR thin film (CF). a) Micrographs resented along with the SEM–EDX signal mapping for O, N, S, F, Si, Cl, Na and K. Scale bars are 1µm. b) EDX spectra taken within different area.

The SEM–EDX mapping is illustrated in Figure VII-14a. The S, N, O and F-elements present a heterogeneous distribution. Note that as mentioned above, some trends are observed in the Si-map that can be associated to contamination. Two quantification areas associated to spectrum 13 and spectrum 14 are illustrated in Figure VII-14b. The region corresponding to spectrum 13 shows a higher-intensity of S-element in comparison to the spectrum 14.

VII.2.1.2.5. DC-R thin film (CF)

Investigations of the DC-NR thin film (CF) surface is described in Figure VII-15. The surface clearly shows small domains embedded within the surface matrix. Moreover, these beads seem to be homogeneously distributed all over the sample.

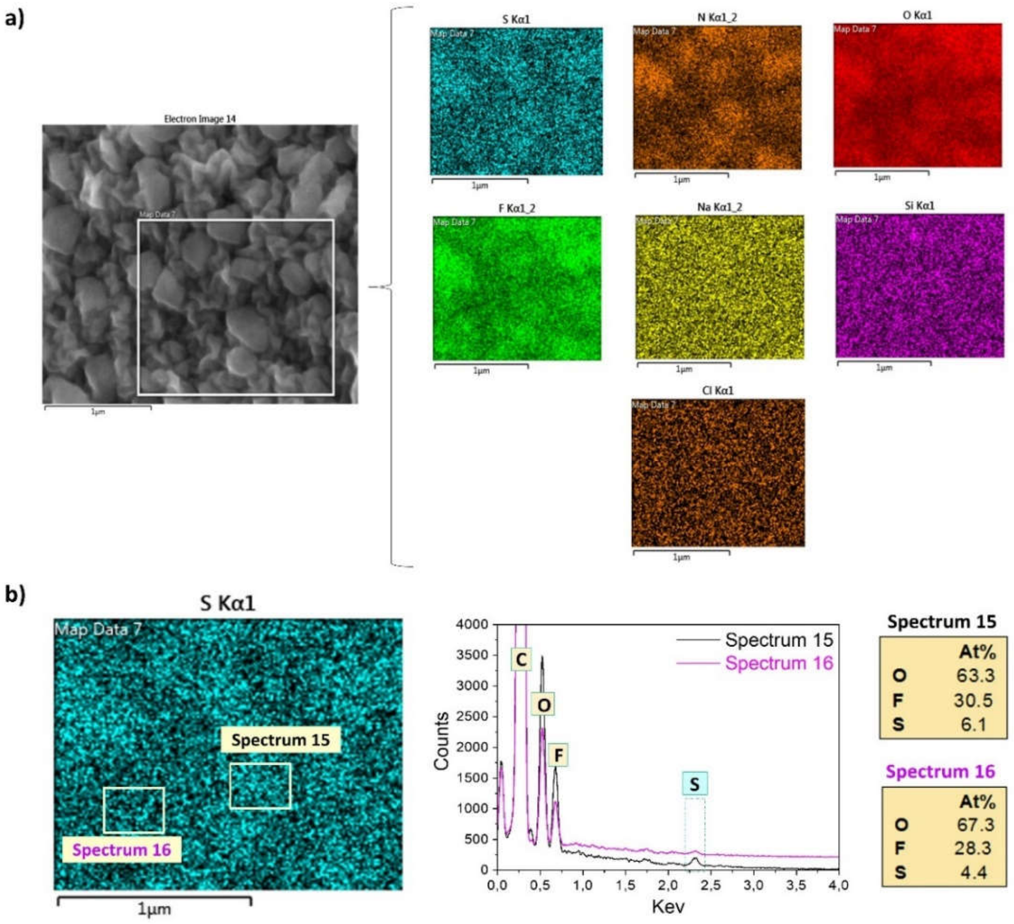

Figure VII-15: Visualization of chemical elements in the DC-R thin film (CF). a) Micrographs resented along with the SEM–EDX signal mapping for O, N, S, F, Si, Cl, Na and K. Scale bars are 1µm. b) EDX spectra taken within different area.

As demonstrated in Figure VII-15a, each map of S, N, O and F elements exhibited correlations where circular domains matching the areas detected on the SEM micrographs. It is important to note that these beads correspond to DTE-UPy assemblies, identified by EDX as sulfur-rich areas. Note that elaboration conditions seem to produce no contaminant signal as homogenous distributions are seen within Si, Na and Cl maps.

Two areas are investigated, the first one in the S-richer region (spectrum 15) and the second one in the S-poorer region (spectrum 16). Both EDX spectra present a value very close (6.1 for spectrum 15 and 4.4 at% for spectrum 16) of S demonstrating the presence of DTE-UPy all over the surface with some small difference of fraction depending the regions.

VII.2.1.2.6. Summary about morphology

In order to compare the S-element distribution in the different thin films, the maximum and minimum values of atomic fraction of S-element is reported in Table VII-5. The average diameter of the domains is as well presented.

Table VII-5: Atomic fraction of S-element.

	SEM-EDX image	max at% of S	min at% of S	Average diameter (µm)
MM-NR thin film (OF)	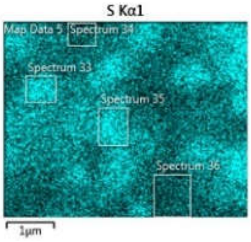	10.7	4.0	0.9 ±0.2
MM-NR thin film (CF)	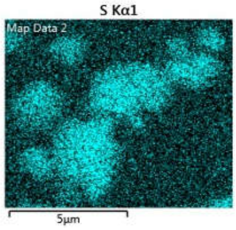	15.3	1.6	1.7 ±0.4
DC-NR thin film (OF)	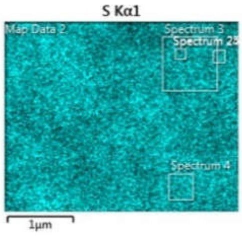	10.7	8.3	-
DC-NR thin film (CF)	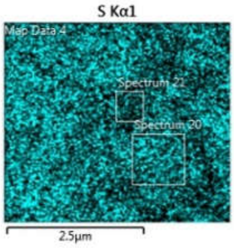	7.1	3.3	0.5 ± 0.1
DC-R thin film (CF)	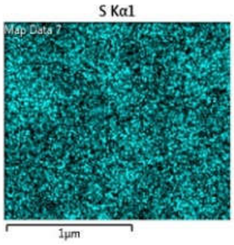	6.1	4.4	0.4 ± 0.1

The sulfur distribution within the MM-NR thin film is heterogeneous compared to those in the DC-NR thin film. This variability demonstrates that inevitably different arrangement may occurring: (i) domains of self-assembled DTE-UPy, (ii) domains of assembled PEB-UPy and DTE-UPy. The DC-R thin film is highly homogeneous with a homogeneous distribution of S-element. The reflux of the photogenerated CF-assembly which prevents the precipitation of CF-isomers improves the homogeneity. Conversely, the MM thin film is heterogeneous with clearly identify micrometric domains.

VII.2.2. Morphology discussion

Combining DTE-UPy with PEB-UPy tend to self-aggregate through quadruple hydrogen bonds. The self-assembled systems seem to be sensitive to external stimuli such as elaboration process and chemical composition as mentioned above.

Since OF-isomer from DTE-UPy displays probable low aggregations through hydrogen bending interactions in solution. This characteristic lends further support to explain the exhibited self-assembling process when associated into PEB-UPy. However, two kinds of diarylethene assembly can exist in the examined thin films: first ones are associated to small supramolecules (lower than 10 nm - DLS measurements) and the second ones are more surrounded with PEB-UPy. The melt molding method may induce agglomeration of small supramolecules of DTE-UPy implying the appearance of visual agglomerations. While the DTE-UPy surrounded with more PEB-UPy will seemingly create individual small supramolecules.

When the solution of the OF-isomer is irradiated with UV light, the photo-cyclization reaction occurs. The photo-generated CF-isomer leads to higher aggregation compared to its OF-assembly. If the solution concentration is higher than $2\,10^{-4}$M, DTE-UPy aggregates increase gradually. Up to certain degree of aggregation, it precipitates while forming large CF-particles (about 650 nm - DLS measurements). The DC-solution on PTFE plates leads to differentiate two types of assembled DTE-UPy: the first diarylethene signature is attributed to large supramolecules of 0.5 ± 0.1 μm creating small visually clusters and the second diarylethene signature are more surrounded with PEB-UPy.

In order to evaluate the key role played by the generated precipitate, the refluxed DC thin film is investigated. The refluxed CF-solution disrupts the development of the precipitate. After subsequent drop casting of this preparation on PTFE plate, the examined surface exhibits DTE-UPy distribution comparable to those of the non-refluxed solution. The only difference concerns the domain size with smaller domains $(0.4 \pm 0.1\ \mu\text{m})$ suggesting preferential DTE-UPy assembling during solvent evaporation.

From the other hand, it is worthwhile to investigate the melt molded thin film resulting from the non-refluxed DC-film. The surface examination revealed the existence of domains of $530 \pm 100\ nm$ in diameter. It is expected that the existed DTE-UPy surrounded with PEB-UPy aggregate while melting (hot pressing). After cooling, domains of 1.70 ± 0.4 µm are observed in the PEB-UPy matrix. The melting and pressing times can play crucial role on the domain size.

When the DTE-UPy content is low in the thin film, the missing of clusters has been noticed despite the melt molding followed procedure. Taking into account the abundancy of PEB-UPy content, this means that the existed DTE-UPy will be dispersed all over the thin film and more surrounded with PEB-UPy.

The powerful SEM/EDX tool has revealed different organization of the photosensitive self-assembled systems. Depending on the elaboration method and the chemical composition, phase separations occur from nano- to micrometric size domains. In view of absence of any indication about UPy-end group signature, it is important to probe whether the quadruple hydrogen bonds alter their contribution while different elaboration processes.

VII.3. First insight to explain photomechanical effect

VII.3.1. Effect of light on structure

The DC thin film (CF) was illuminated with UV light on two different zones. The resulting diffractograms are presented in Figure VII-16. The exposure time was about 1h.

Although the thin film undergoes photochromic reaction from OF isomer to the CF isomer upon UV exposure, the diffractogram of DC thin film (CF) is identical to the diffractogram of the resulted DC thin film (OF). Such observation is confirmed by analyzing two different areas on the same thin film.

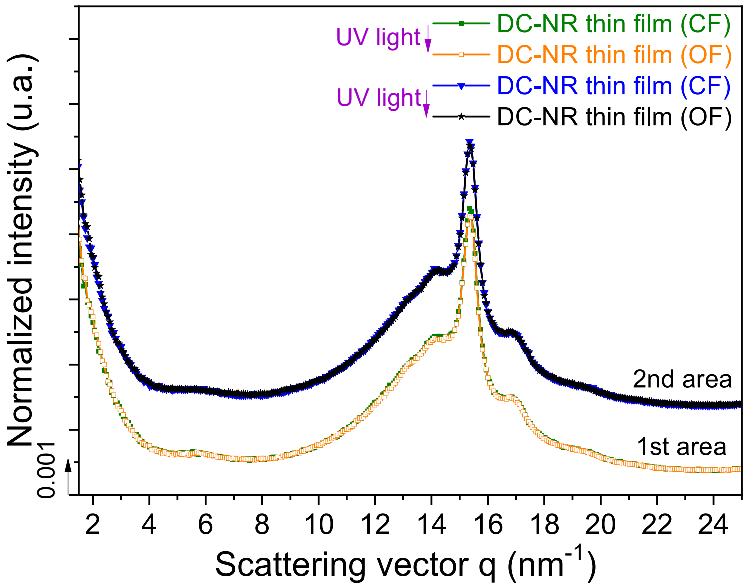

Figure VII-16: WAXS patterns of DC (CF) thin film upon UV irradiations.

Compared to crystalline DTE-pwd where WAXS diffractograms of OF and CF isomers show few differences (Figure III-5), DTE-UPy is herein amorphous. As previously reported in Chapter IV, the illumination does not affect the structural signature of DTE-UPy. In the case of DTE-UPy/PEB-UPy thin film, the crystallinity is related to PEB-UPy explaining why we have not photoinduced changes on diffractograms.

VII.3.2. Correlation morphology/structure with photoactuation

VII.3.2.1.Importance of DTE-UPy domains

Within this Chapter VI, DC thin film displays a more pronounced response compared to MM thin film within macroscopic scale. Whereas, the situation is reversed for MM thin film case. These observations are gathered in Table VII-6.

Table VII-6: Photoinduced changes at micro/macroscopic scales.

	DC thin film	**MM thin film**
Microscopic scale	Weak response	Strong response
Macroscopic scale	Strong response	Weak response

The morphology investigated through SEM revealed that DC thin films present a good distribution between DTE-UPy and PEB-UPy. In other word, small domains of DTE-UPy are present within the thin film surface, with a typical average diameter of 0.5 ± 0.1 µm compared to larger domains of 1.7 ± 0.4 µm for MM thin film (approximately three time bigger). Furthermore, these small domains are well-distributed within the surface compared to MM thin film case.

We have already proved the photoactivity of the DTE-UPy domains in Chapter IV, when the photoinduced response of DTE-UPy$_{\mathrm{prp}}$ is investigated. Such domains are expected to be cooperative thanks to the hydrogen bonds. In the case of DTE-UPy/PEB-UPy thin films, the domains of DTE-UPy photoswtich are also expected to induce cooperative effects due to the presence of hydrogen bondings.

With these statements, we can rationalize MM thin film videos at microscopic scale (Chapter VI) where very strong response is justified by the importance of domain size. The large domains of DTE-UPy are expected to be more cooperative from the local viewpoint. The local photogenerated force $\overrightarrow{f_{MM}}$ is then very high. At macroscopic scale, the DTE-UPy domains are separated by large area, the cooperativity is lessened. The resulting photogenerated force $\overrightarrow{F_{MM}}$ is then weak. A schematic representation related to microscopic and macroscopic changes of MM thin film is illustrated in Figure VII-17.

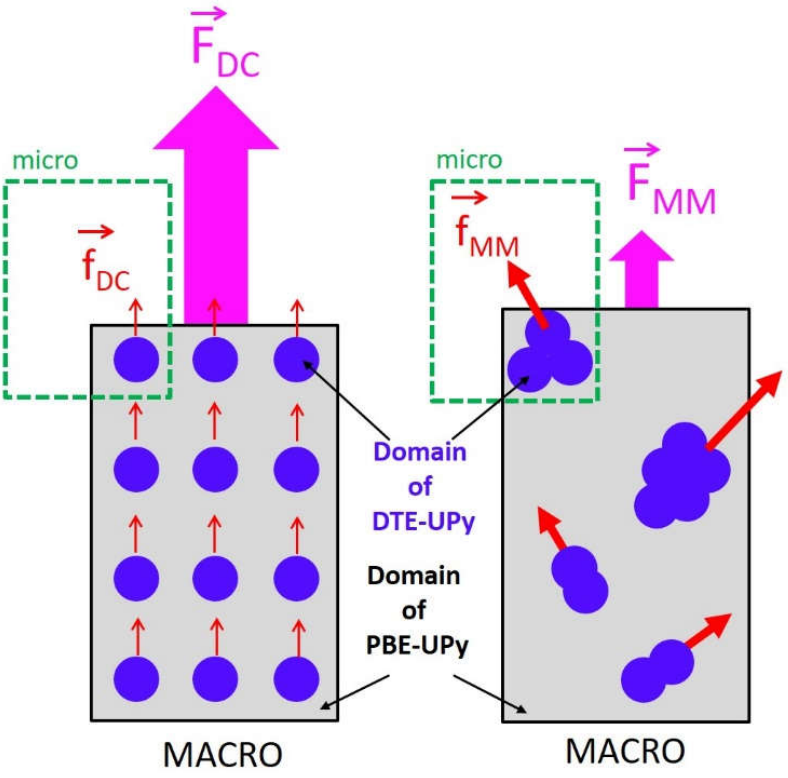

Figure VII-17: Schematic illustration at micro- and macro- scales of the photoinduced changes.

The DC thin film present smaller domains which induce a weaker response upon irradiation at microscopic scale. The photogenerated force $\overrightarrow{f_{DC}}$ is lower compared to those of MM thin film. As the domain distribution is more homogeneous, the small domains are expected to be more cooperative at macroscopic scale. The photogenerated force $\overrightarrow{F_{DC}}$ is then higher as observed in Figure VII-17.

VII.3.2.2.Importance of long period (Lp)

Thin film elaborations lead to different organizations between DTE-UPy and PEB-UPy. From the structural point of view and as mentioned in Table VII-4, DC-NR and DC-R thin films are different due to the presence of PEB long period L_p in the case of DC-NR. Despite the quasi-similar crystallinity, the absence of L_p for DC-R implies that amorphous DTE-UPy in the PEB amorphous phases (L_a) disturb the L_p arrangements as shown Figure VII-18.

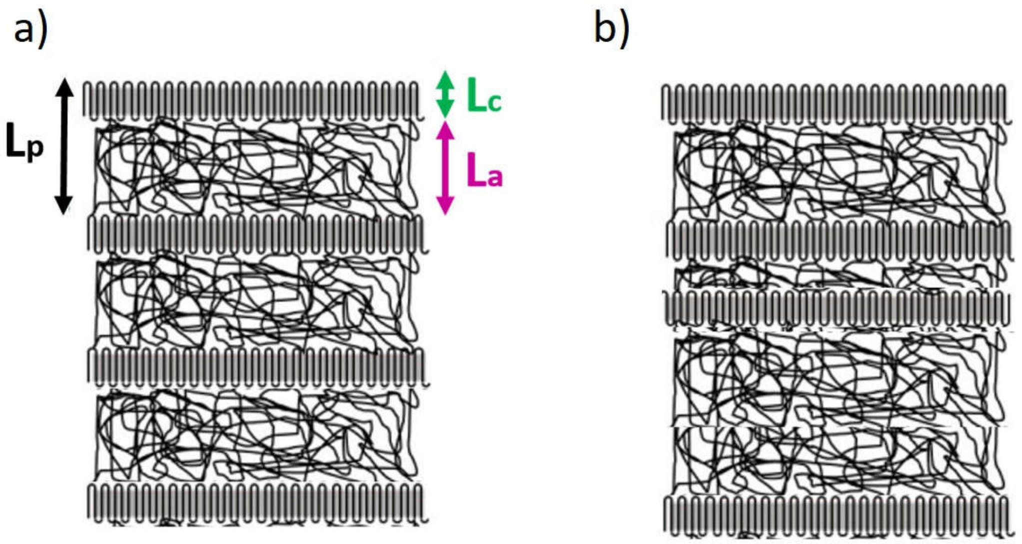

Figure VII-18: Schematic illustration of arrangements within a) DC-NR (presence of L_p) and b) DC-R (absence of L_p).

Moreover, DC-NR thin film presents a more pronounced photomechanical effect compared to DC-R. This difference in macroscopic videos can be rationalized if the DTE-UPy molecules interact with crystalline areas without disturbing it. This suggests that L_p arrangements and then the ordered crystalline regions may play a key role in amplifying the photomechanical effect of DTE-UPy upon irradiation.

VII.4. Conclusion

In Chapter VII, structural and morphological study of DTE-UPy/PEB-UPy systems were elucidated by means of various technics under different thin film elaboration conditions. The Table VII- summarizes the obtained results.

Table VII-7: summary about thin films properties at room temperature.

	Isomer	SEM	DSC	SAXS
DC-NR Thin film	OF	no DTE-UPy domains	χ(%)=24.6	dc_1 = Lp ↑ dc_2 = 6-7 nm cst
	CF	DTE-UPy domains with average diameter of 0.5±0.1 µm	χ(%)=23.2	dc_1 = Lp ↑ dc_2 = 9 nm cst and ↑ (Tg)
DC-R Thin film	CF	DTE-UPy domains with average diameter of 0.4±0.1 µm	-	dc_2 = 9 nm cst and ↑ (Tg)
MM-NR Thin film	OF	small DTE-UPy domains	χ(%)=24.4	-
	CF	DTE-UPy domains with average diameter of 1.7±0.4 µm	χ(%)=21.9	dc_1 = Lp ↑ dc_2 = 7 nm cst and ↑ (Tg)

The DTE-UPy/PEB-UPy system is expected to have three structural signatures: (1) DTE-UPy signature, (2) PEB-UPy signature and (3) DTE-UPy/PEB-UPy system signature.

The investigation of the structure shows that the signature of pristine DTE-UPy photoswitch is associated to long-range organizations (peak-1 and peak-2). Such peaks were attributed in Chapter IV. In other word, peak-1 was related to the intermolecular distances between neighboring molecules. The peak-2 was associated to the distance between two successive stacked molecules.

Moreover, PEB-UPy also presents two characteristic distances described in Chapter V. The slightly lower values of the correlation distances for the DTE-UPy/PEB-UPy systems compared to PEB-UPy is caused by the presence of DTE-UPy, which induces a strain on UPy-network. Note, the incorporation of amorphous DTE-UPy does not affect neither the crystallinity nor the crystal phases of PEB-UPy in the DTE-UPy/PEB-UPy system.

Upon temperature raise up, we reported successfully different signatures (Table VII-7) depending on the elaboration thin film. The first long-range distance dc_1 is associated to the long period (L_p) corresponding to the regular repartition of stacking between amorphous and crystalline fractions in PEB increases with the temperature until the melt of PE crystals. The second characteristic distance dc_2 corresponds to the distance between UPy domains. It adds further proof for existent arrangements within DTE-UPy/PEB-UPy system.

By the analysis of the morphology, we observe the method of thin film elaboration leads to different distribution of DTE-UPy and PEB-UPy molecules. As expected, the reflexed thin film presents the more homogeneous morphology. By comparing DC or MM thin films, the non-reflexed sample exhibits more inhomogeneous surfaces with pronounced domains.

The photomechanical effect of thin film issued from supramolecular assembly and described in Chapter VI was successfully correlated to structural/morphological statements. Two key parameters are found to be responsible for photoactive responsiveness a multi-scale approach. The first parameter is assigned to the cooperativity of small DTE-UPy domains networking induced by the hydrogen bonds. The second parameter is related to the cooperativity associated to the presence of crystalline arrangements (L_p) and their role in amplifying the photoinduced changes.

General Conclusion

This PhD thesis aimed to improve the existing DTE-UPy/PEB-UPy system developed by Pr Takeshita and to give first insights about photomechanical effects by applying a multiscale approach based on material science. There is a need to rationalize the effect of the primary morphological/structural features responsible for the light sensitive behavior.

The photoswitch DTE-UPy. First, the photomechanical potentiality of DTEcore photoswitch (before UPy-functionalization) was explored under UV/visible illuminations. Interestingly, these molecules were found to exhibit two types of photomechanical motions upon UV and visible excitations: bending and jumping behaviors. Such result justifies the choice of the photoactive DTEcore for the photoactuator DTE-UPy/PEB-UPy system. Surprisingly, the amorphous DTEcore obtained from the melt state leads to the same motions despite its non-ordered structure. In the same vain, the impact of the functionalization of DTEcore with UPy-units was unexpected. Indeed DTE-UPy is amorphous (due to lateral alkyl chain) and presents reversible bending for either small (OF) or large (CF) assemblies. To our knowledge, these unexpected results are not reported in the literature since the key parameters explaining the photomechanical effect is the crystallinity of DTEs. Finally, it was found that the precipitate of DTE-UPy in CF displays light emission for a visible excitation only (such effects not observed for UV excitation). In fact, this unexpected process probably due to AIE process (that is a collective process) should be further investigated in the future in order to elucidate whether emissive process can occur in competition with photomechanical effect.

The elastomer PEB-UPy. In literature, the amorphous state of thermoplastic elastomer PEB-UPy has widely been reported. Herein, the synthesized PEB-UPy is crystalline because of the high fraction of polyethylene. The different proportions of orthorhombic and monoclinic crystal phases depend on the thin film elaboration (drop casting or melt molding).

The photomechanical effects of DTE-UPy/PEB-UPy thin films. The main objective is to understand the photomechanical behavior of DTE-UPy/PEB-UPy system by elaborating thin films and examining its photoactive responsiveness under UV or Visible irradiations. This work represents the first study highlighting the photoresponsiveness of DTE-UPy/PEB-UPy supramolecular assembly. For this propose, distinct elaboration methods were tested based on drop casting and melt molding. To reach these objectives, a multiscale approach of the photomechanical effect was performed in-situ upon illumination at two different scales, microscopic (wild-field microscope) and macroscopic scales (camera). Reversibility and relaxation were concurrently examined.

The microscopic scale investigation revealed that the thin films exhibit not only one expected motion (from DTEs monocrystals) but also two different consecutive motions:

1. First motion: fast expansion motion (in few seconds) perpendicularly to the incident light particularly upon visible light.
2. Second motion: bending motions (in hundreds of seconds) toward or away to the incident light for both UV and visible light illuminations.

The macroscopic scale investigation demonstrated that the fast expansion motion reported at microscopic scale was absent (or at least not detectable with present set up). Contrarily, thin film exhibits only one bending motion (analogy with the second motion) for both UV and visible lights within twenty minutes. Such bending behavior depends on the initial shape of thin film and/or on the structure of sample.

To our knowledge the first microscopic motion, i.e. expansion behavior has never been reported in the literature. The second motion observed for both microscopic and macroscopic scales relies on the photomechanical effect of DTEs crystals and the presence of OF/CF gradient within the thin film bulk. Future works could concern the prediction of the bending efficiency by using the bimetallic model and the Timoshenko's equation on thin films with different thicknesses.

From the multiscale investigation, it has been found that:

1. The macroscopic responsiveness to light excitation has the highest magnitude for DC-NR thin film in comparison to DC-R and MM-NR thin films.
2. This microscopic responsiveness to light excitation is higher for MM-NR thin film.

In both cases, reversible motions were achieved for at least two cycles of alternate UV/visible lights. These results highlight the importance of thin film elaboration method and the choice of the process according to the industrial needs. Moreover, it was demonstrated from structure and morphology investigations that the elaboration method leads to differences in self-assembling between DTE-UPy and PEB-UPy molecules.

The DTE-UPy/PEB-UPy system mainly conserves its crystalline character despite the incorporation of amorphous DTE-UPy. Such crystallinity seems to answer to one of our first question related to the key role played by crystalline PEB-UPy. Indeed, the crystals cooperatively amplify (through L_p) the photomechanical effect. Moreover, the presence of DTE-UPy domains with different sizes leads to conclude their key role within the photoresponsiveness of system.

Perspectives. Photochemical, structural and morphological properties of thin films were not fully investigated under illumination within the scope of this thesis. In fact, knowing the impact of supramolecular assembly within DTE-UPy/PEB-UPy system, these aspects need to be further studied as it will be helpful regarding the responsiveness of thin films.

The mentioned video (https://www.youtube.com/watch?v=IVrt9k7rLOQ) in the introduction of this thesis presents the photo-responsiveness of a spin coated thin film due to light sensitive behavior. In fact, two mechanical effects were observed. Upon visible irradiation, the initially bent blue film (CF) is instantaneously flattened and as long as light penetrates into the material. A second motion i.e. slow bending back motion follows this first observed motion. Upon UV irradiation, only moderate flattening is reported. The described first and second motions match with the reported microscopic changes in MM-NR thin film upon visible light. Those statements arise the question about the thin film elaboration process influence on photomechanical effect efficiency.

First insights about quantitative evaluation of the thin film photoactuation was displayed via a set-up monitored through dynamical mechanical analysis (DMA). Light sensitive behaviors were followed through the evolution of the mechanical modulus. Accordingly, these experiments have successfully confirmed the existence of motions depending on the irradiation time. Future works should continue this investigation taking into account the thin film elaboration process.

An additional outlook could be related to the actual control of the matter. For this purpose, it will be undertaken a multi-scale and multi-physics modeling: starting from molecular parameters (UPy distances …etc) and photochemical quantities, it will be interesting to predict from the mechanical modeling the macroscopic curvature of the film.

Appendices

Appendix IV: Full WAXS spectrum of DTE-UPyprp (CF)

WAXS and SAXS measurements were performed via diffractometer with a Micro-source source Genix Collimated Cu (Xenocs). The used radiation was the copper K_{α} line ($\lambda = 1.54$ Å). The dectector-distance was different compared to the described diffractograms presented in chapter IV. The obtained 2θ range was from 0.08° until 56°.

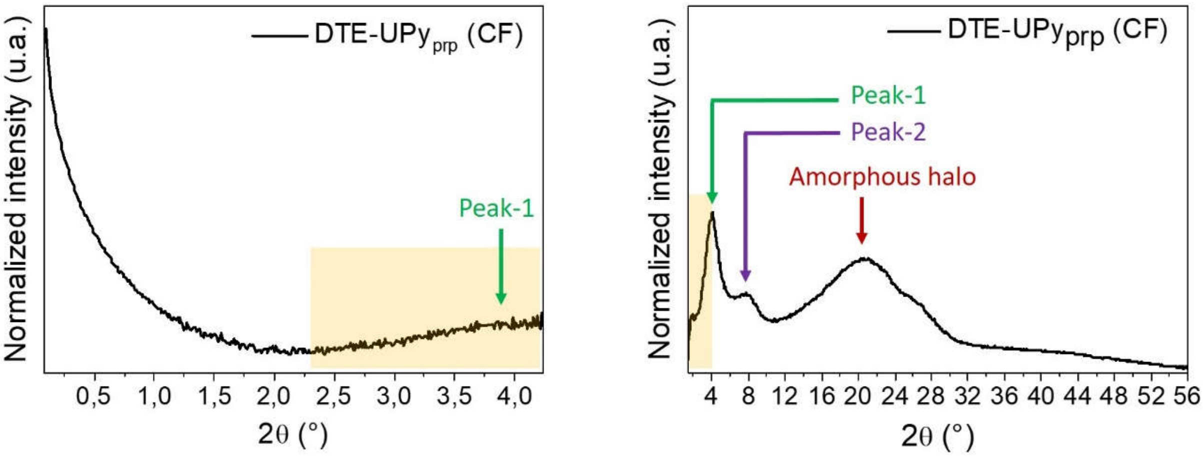

Figure A-1: SAXS pattern at room temperature ranged 0.08° until 56°.

In order to confirm that medium q range [1.4 nm^{-1}-2 nm^{-1}] (equivalent to 2θ range in [1°-1.4°]) does not add new peaks. At room temperature, full covered 2θ-range for CF precipitate sample was carried out via SAXS and WAXS.

Two scattering peaks (noted peak-1 and peak-2) and amorphous halo are present at high 2θ values. While, the beginning of a scattering peak belonging to peak-1 appears on the smaller angle range without any noticeable additional peaks.

Appendix VI: Microscopic photo-induced changes: PEB-UPy thin film

Because photochromic molecules should play a key role in inducing the photo-responsiveness of thin films, the PEB-UPy thin film is explored in order to confirm the proposed statement. For this propose, the MM sample was fixed between two glasses as illustrated within Figure A-2a and exposed to UV and visible lights, accordingly.

As mentioned in Figure A-2b and Figure A-2c, no photoinduced changes have been occurred during UV light exposure and upon a consecutive visible light exposure, over the course of 60, 120, and 180 seconds.

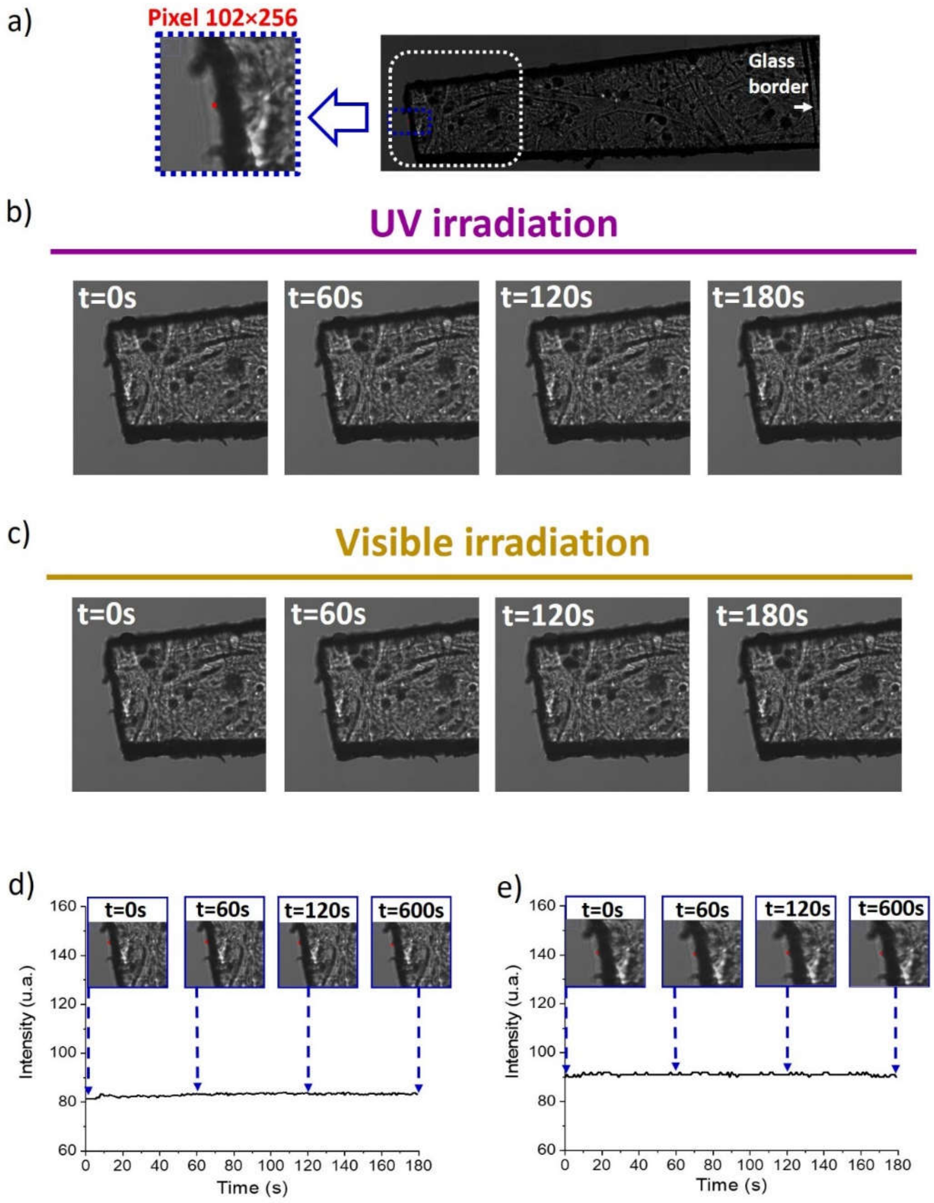

Figure A-2: Photoinduced changes within MM thin film of PEB-UPy upon irradiation process. a) PEB-UPy thin film attached from one side. b) UV light irradiation. c) Visible light irradiation. Thickness of the film: 65µm. d) Kinetic photoinduced follow under UV light irradiation. e) Kinetic photoinduced follow under visible light irradiation.

In order to confirm such observations, a kinetic slice within a pixel from the optical microscopic photograph has been chosen as zoomed within figure A-2a (doted white square) and then followed upon exposure time.

Figure A-2d and Figure A-2e show that the optical signal remains constant regardless the applied light, which is consistent with the earlier observations.

Multiscale approach of photo-mechanical thin films based on the supramolecular assembly of bistable photoswitch and thermoplastic elastomer

Abstract:

An increasing attention has been paid to photo-deformable polymeric materials that can convert light energy into mechanical energy without contact or electrical wires, using photo-responsive molecules. Dithienylethenes known for their thermal stability and their fatigue resistance are one of the best studied compounds that exhibit photomechanical response. Upon alternating irradiation with UV and visible light, a variation of the molecular volume occurs between open- and close-ring of the molecules during the photochromic reaction (carbon-carbon electrocyclization) which induces photomechanical motions. In order to develop a light-driven polymer actuator, we investigate a novel system based on the mixture of a derivative dithienylethenes (ureidopyrimidinone-functionalized dithienylethenes denoted DTE-UPy) and a thermoplastic elastomer (ureidopyrimidinone -functionalized poly(ethylene-co-butylene) denoted PEB-UPy). In solution, the DTE-UPy/PEB-UPy system leads to a supramolecular assembly where the subunits are connected to each other via quadrupole hydrogen bonding. The thin films are elaborated using different techniques such as drop casting or melt molding. Under illumination, a photomechanical response of the film is observed. The objective of this study is to establish a correlation between the photophysical, structural, morphological and mechanical properties responsible for the drastic micro- and macroscopic deformations.

Keywords: Photochromism, Dithienylethenes, thermoplastic elastomer, supramolecular assembly, hydrogen bonding, photomechanical effect, thin film elaboration.

Étude multi-échelle de films minces photomécaniques basés sur l'assemblage supramoléculaire de photochromes bistables et d'élastomère thermoplastique

Résumé :

Le domaine des matériaux polymères mécaniquement déformable sous illumination est à l'heure actuelle en pleine expansion. Ces matériaux à base de molécules photochromiques sont capables de restituer sous forme de travail mécanique l'énergie lumineuse en l'absence de tout contact avec l'environnement. Les dithiényléthènes, connus pour leur stabilité thermique et leur résistance à la fatigue, sont parmi les molécules présentant une réponse photomécanique, les plus intéressantes. Lors d'une irradiation alternée entre les lumières UV et visible, une variation de volume moléculaire induit par un changement de forme ouverte à forme fermée de la molécule au cours de la réaction photochromique (électrocyclisation carbone-carbone) donne lieu à des effets photomécaniques. Afin de développer des actionneurs polymères sensible à lumière, notre étude concerne de nouveaux systèmes basés sur le mélange d'un dérivé de dithiényléthène (dithiényléthènes fonctionnalisés par des groupements uréidopyrimidinones notés DTE-UPy) et d'un élastomère thermoplastique (poly (éthylène-co-butylène) fonctionnalisé par les mêmes groupements ureidopyrimidinones noté PEB-UPy). En solution, le système DTE-UPy/PEB-UPy conduit à un assemblage supramoléculaire où les sous-unités (UPy) sont reliées entre elles par des liaisons hydrogènes quadripolaires. Les films minces sont élaborés en utilisant différentes techniques telles que le « drop casting » ou le « melt molding ». Sous illumination, une réponse photomécanique du film est observée. L'objectif de cette étude est d'établir une corrélation entre les propriétés photophysiques, structurales, morphologiques et mécaniques responsables des déformations micro- et macroscopiques.

Mots clés: photochromisme, dithiényléthènes, élastomère thermoplastique, assemblage supramoléculaire, liaison hydrogène, effet photomécanique, élaboration de films minces.